MINISTRY OF EDUCATION

THE ANNALS OF "DUNAREA DE JOS" UNIVERSITY OF GALATI

Fascicle IX
METALLURGY AND MATERIALS SCIENCE

YEAR XL (XLV)
December 2022, no. 4

ISSN 2668-4748; e-ISSN 2668-4756

2022
GALATI UNIVERSITY PRESS

EDITORIAL BOARD

THE ANNALS OF "DUNAREA DE JOS" UNIVERSITY OF GALATI
FASCICLE IX. METALLURGY AND MATERIALS SCIENCE
Nº. 4 - 2022, ISSN 2668-4748; e-ISSN 2668-4756
Volume DOI: https://doi.org/10.35219/mms.2022.4

Table of Contents

THE ANNALS OF "DUNAREA DE JOS" UNIVERSITY OF GALATI
FASCICLE IX. METALLURGY AND MATERIALS SCIENCE
N°. 4 - 2022, ISSN 2668-4748; e-ISSN 2668-4756
Article DOI: https://doi.org/10.35219/mms.2022.4.01

CONSOLIDATION OF CENTRAL COLUMNS OF CIVIL MULTISTORY STRUCTURES TO INCREASE THE CRITICAL BUCKLING FORCE

Marius BOTIȘ, Costel PLEȘCAN
Transilvania University of Brașov, Department of Civil Engineering, Romania
e-mail: mbotis@unitbv.ro

ABSTRACT

Civil multi-story structures are used as office buildings or residential buildings. The central pillars on the ground floor of the civil structures will have the largest gravitational load and implicitly will be the pillars most stressed in compression. In this paper, the authors propose to increase the critical buckling load of the central pillars on the ground floor in the event that it is necessary to strengthen these pillars, due to the change in the purpose of the building and the modification of the loads on the floors. To increase the buckling load in the case of these columns, it is proposed to increase the moment of inertia of the columns on the base region. To highlight how the critical loss of stability load changes, a theoretical model is made for the column with constant section and another for the column with variable section in steps. Finally, the results obtained for the critical load will be compared and it will be highlighted what is the increase in buckling load for the pole with variable section in relation to the pole with constant section.

KEYWORDS: buckling force, multistory structures, moment of inertia

1. Introduction

Gravitational loads in the case of these structures are permanent loads (self-weight of the floor), quasi-permanent loads (self-levelling piles) and useful loads. The gravity loads collected from the floors through the beams drain through the pillars to the foundations and finally to the good foundation ground. For regular structures in plan and elevation we encounter 3 types of pillars in terms of gravity loads flowing through them. Corner columns that take the load from ¼ of the area of a slab mesh, marginal columns that take the load from ½ of the area of a slab mesh and central columns that take the load from the surface of a slab mesh. From fig.1 it can be seen that the pillars on the ground floor have the largest gravitational effect. The most stressed columns in compression will be the central columns that collect the gravitational load from all the floors above it. Central columns on the ground floor are loaded with the highest compression forces, therefore in their case the increase of the critical force of loss of stability is justified. If the loads with compressive forces become high and at marginal posts, the cross-section at the base can also be increased in their case as well. In general, central columns have high compressive loads due to gravity loads, and marginal columns are loaded with high axial forces due to seismic actions that load and unload marginal columns with compressive forces. The solution proposed in the paper aims to increase the cross-section of the pillars only at the base. In this case, the foundation that will take over the capable moment of the pole must also be checked. In the case of the consolidation of a multi-story civil structure where the incarnation on the floors has been modified, the degree of compression stress on the pillars on the ground floor is different. That's why the area on which the section is died is done according to the type of pillar, the degree of loading with axial forces and the action to which the structure is subjected. If the section enlargement were to be done along the entire length of the pillars, then the space on the ground floor would be considerably reduced. Hence the need to increase the section of the pillars depending on their position within the ground floor and the degree of loading with the axial compression force. The article presents the case of a pillar whose cross-section is increased by half the length of the pillar. Obviously, the civil structures to which the consolidation is done can be metal or concrete. In the case of metal structures, the consolidation is done by welding additional elements and in the case of concrete structures by adding perimeter concrete.

THE ANNALS OF "DUNAREA DE JOS" UNIVERSITY OF GALATI
FASCICLE IX. METALLURGY AND MATERIALS SCIENCE
N°. 4 - 2022, ISSN 2668-4748; e-ISSN 2668-4756
Article DOI: https://doi.org/10.35219/mms.2022.4.01

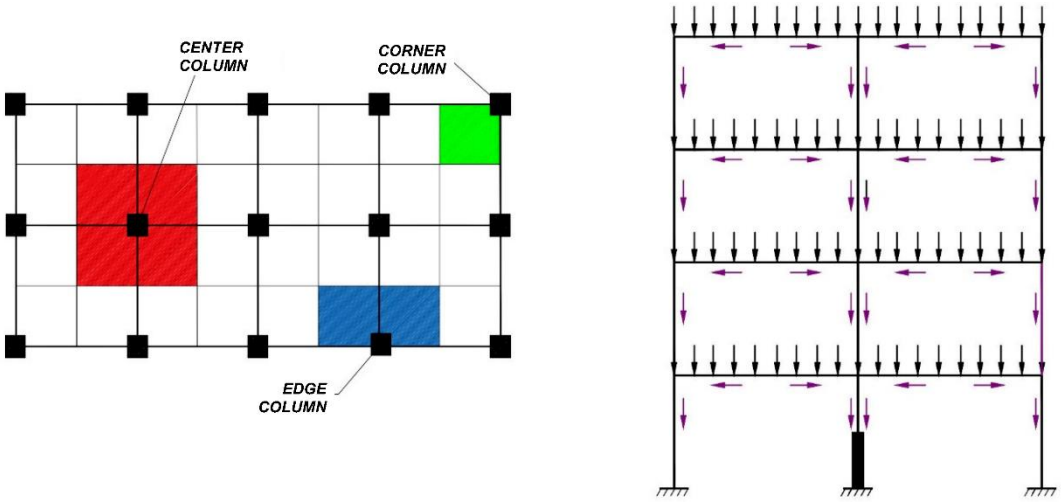

Fig. 1. *Gravitational afferents on the columns*

2. Theoretical calculation model for sliding embedded-recessed bar with constant section and with variable section in steps

We first consider the case of the bar with constant section at which the critical loss of stability force is determined.

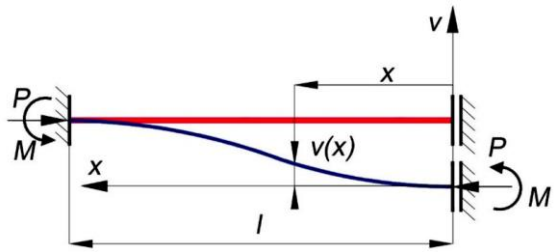

Fig. 2. *The deformed shape of the bar with constant section*

For the bar in Fig. 2, write the equation of the average deformed fiber on the deformed shape of the bar to determine the critical load [1].

For a current section the bending moment variation expression is:

$$M(x) = P \cdot v - M \tag{1}$$

From the approximate deformed mean fiber differential equation, it follows:

$$\frac{d^2v}{dx^2} = -\frac{M(x)}{EI}$$
$$\frac{d^2v}{dx^2} + \frac{P \cdot v}{EI} = \frac{M}{EI} \tag{2}$$

$$k^2 = \frac{P}{EI}$$

The solution of the inhomogeneous second-order differential equation with constant coefficients is:

$$\begin{gathered} v(x) = v_o(\mathrm{x}) + v_p(\mathrm{x}); \\ v(x) = C_1 \sin(kx) + C_2 \cos(kx); \\ v_p(x) = C; \\ \frac{P \cdot v_p}{EI} = \frac{M}{EI}; \\ v_p = \frac{M}{P} \end{gathered} \tag{3}$$

The general solution of the differential equation and its derivative are:

$$\begin{gathered} v(x) = C_1 \sin(kx) + C_2 \cos(kx) + \frac{M}{P}; \\ v'(x) = C_1 k \cos(kx) - C_2 k \sin(kx). \end{gathered} \tag{4}$$

The integration constants are determined from the existence conditions of the deformed shape as an equilibrium configuration:

$$\begin{gathered} x = 0; \\ v(0) = 0; \\ v'(0) = 0; \\ x = l; \\ v'(l) = 0. \end{gathered} \tag{5}$$

By applying the boundary conditions, the homogeneous system of equations results:

THE ANNALS OF "DUNAREA DE JOS" UNIVERSITY OF GALATI
FASCICLE IX. METALLURGY AND MATERIALS SCIENCE
No. 4 - 2022, ISSN 2668-4748; e-ISSN 2668-4756
Article DOI: https://doi.org/10.35219/mms.2022.4.01

$$\begin{cases} C_2 + \dfrac{M}{P} = 0 \rightarrow C_2 = -\dfrac{M}{P}; \\ kC_1 = 0; \\ C_2 k \sin(kl) = 0. \end{cases} \quad (6)$$

The critical force of loss of stability results from the condition that the determinant of the homogeneous system of equations is zero.

$$\begin{gathered} C_2 k \sin(kl) = 0; \\ (kl) = n\pi; n = 1,2,3 \ldots \end{gathered} \quad (7)$$

The first 3 values for critical instability forces are:

for n=1

$$\begin{gathered} k_1 l = \pi; \\ k_1^2 = \frac{P_{cr1}}{EI}; \\ P_{cr1} = \frac{\pi^2 EI}{l^2}. \end{gathered} \quad (8)$$

for n=2

$$\begin{gathered} k_2 l = 2\pi; \\ k_2^2 = \frac{P_{cr2}}{EI}; \\ P_{cr1} = \frac{4\pi^2 EI}{l^2}. \end{gathered} \quad (9)$$

for n=3

$$\begin{gathered} k_3 l = 3\pi; \\ k_3^2 = \frac{P_{cr3}}{EI}; \\ P_{cr3} = \frac{9\pi^2 EI}{l^2}. \end{gathered} \quad (10)$$

For the bar with variable section in steps in Fig. 3, the critical load for loss of stability is determined using the equation of the average deformed fiber, and the balance is written on the deformed shape of the bar [1].

The sectional bending stresses on the section with stiffness module EI and on the section with stiffness module 4EI are:

$$\begin{gathered} M_{EI}(x) = P \cdot v_1 - M; \\ M_{4EI}(x) = P \cdot v_2 - M. \end{gathered} \quad (11)$$

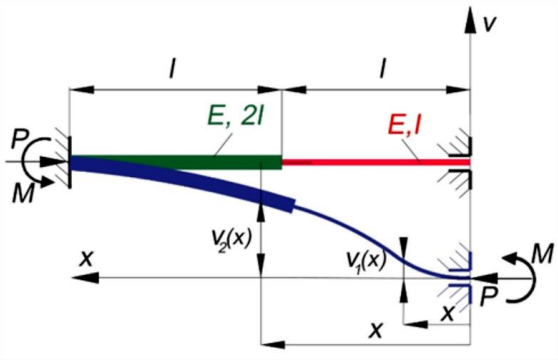

Fig. 3. *The deformed shape of the bar with variable section*

Using the stress variation expressions, the differential equations of the average fiber deformed on the 2 sections result:

$$\begin{gathered} \frac{d^2 v_1}{dx^2} = -\frac{M_{12}(x)}{EI}; \\ \frac{d^2 v_1}{dx^2} + \frac{P \cdot v_1}{EI} = \frac{M}{EI}; \\ \frac{d^2 v_2}{dx^2} = -\frac{M_{23}(x)}{4EI}; \\ \frac{d^2 v_2}{dx^2} + \frac{P \cdot v_2}{4EI} = \frac{M}{4EI}. \end{gathered} \quad (12)$$

If the notations are made,

$$\begin{gathered} \frac{P}{4EI} = \alpha^2; \\ \frac{P}{EI} = (2\alpha)^2. \end{gathered} \quad (13)$$

then the differential equations of the two sections become:

$$\begin{gathered} \frac{d^2 v_1}{dx^2} + (2\alpha)^2 v_1 = \frac{M}{EI}; \\ \frac{d^2 v_2}{dx^2} + \alpha^2 v_2 = \frac{M}{EI}. \end{gathered} \quad (14)$$

The solutions of the differential equations and their derivatives are:

$$\begin{gathered} v_1(x) = C_1 \sin(2\alpha x) + C_2 \cos(2\alpha x) + \frac{M}{P}; \\ v_2(x) = C_3 \sin(\alpha x) + C_4 \cos(\alpha x) + \frac{M}{P}; \\ v_1'(x) = 2\alpha C_1 \cos(2\alpha x) - 2\alpha C_2 \sin(2\alpha x); \\ v_2'(x) = \alpha C_3 \cos(\alpha x) - \alpha C_4 \sin(\alpha x). \end{gathered} \quad (15)$$

Applying the boundary conditions yields:

THE ANNALS OF "DUNAREA DE JOS" UNIVERSITY OF GALATI
FASCICLE IX. METALLURGY AND MATERIALS SCIENCE
N°. 4 - 2022, ISSN 2668-4748; e-ISSN 2668-4756
Article DOI: https://doi.org/10.35219/mms.2022.4.01

$$x = 0 \rightarrow v_1(0) = 0;$$
$$C_2 + \frac{M}{P} = 0 \rightarrow C_2 = -\frac{M}{P};$$
$$x = 0 \rightarrow v_1'(0) = 0;$$
$$2\alpha C_1 = 0 \rightarrow C_1 = 0;$$
$$x = l; v_1(l) = v_2(l);$$
$$C_2\cos(2\alpha x) - C_3\sin(\alpha x) - C_4\cos(\alpha x) = 0;$$
$$x = l; v_1'(l) = v_2'(l);$$
$$2\alpha C_2\sin(2\alpha l) + \alpha C_3\cos(\alpha l) - \alpha C_4\sin(\alpha l) = 0;$$
$$x = 2l; v_2'(2l) = 0;$$
$$\alpha C_3\cos(2\alpha l) - \alpha C_4\sin(2\alpha l) = 0. \quad (16)$$

If αl=x is written, the system of equations (16) becomes:

$$\begin{cases} -C_3 sinx - C_4 cosx - \frac{M}{P} cos2x = 0; \\ -C_3 cosx + C_4 sinx + 2sin2x = 0; \\ C_3 cos2x - C_4 sin2x = 0. \end{cases} \quad (17)$$

The system of equations (17) admits nontrivial solutions if the determinant of the coefficients is zero. Applying this condition results:

$$\begin{vmatrix} -sinx & -cosx & -cos2x \\ -cosx & sinx & 2sin2x \\ cos2x & -sin2x & 0 \end{vmatrix} = 0. \quad (18)$$

After solving the transcendental equation above in the Matlab program [2], the solutions are obtained:

x1= 0
x2=-acos((2^(1/2)*3^(1/2))/6)=-1.1503
x3=acos((2^(1/2)*3^(1/2))/6) =1.1503

The lowest critical force is obtained for x=1.1503, and is determined with the relation:

$$x = \alpha l; \alpha = \frac{x}{l};$$
$$\frac{P_{cr}}{4EI} = \alpha^2 = \left(\frac{x}{l}\right)^2 \quad (19)$$

$$P_{cr} = \frac{4EI \cdot 1{,}32}{l^2} = \frac{5{,}292EI}{l^2} = 2{,}14\frac{\pi^2 EI}{(2l)^2};$$

3. Results and conclusions

From the analysis of the results obtained for the critical force of loss of stability in the case of the bar with constant section and the bar with variable section in steps, it follows:

- the critical force for a bar of length 2l, embedded at one end and sliding embedded at the other end is:

$$P_{cr\_ct} = \frac{\pi^2 EI}{(2l)^2}$$

- the critical force for a step-variable bar of length 2l embedded at one end and sliding embedded at the other end is:

$$P_{cr\_var} = 2{,}14\frac{\pi^2 EI}{(2l)^2}$$

- the ratio between the critical forces in the case of the bar with constant section and the bar with variable section in steps is:

$$\frac{P_{cr\_var}}{P_{cr\_ct}} = 2{,}14$$

In conclusion, an increase in the critical loss of stability force for the central columns on the ground floor can be obtained by increasing the section of the columns at the base.

References

[1]. Bănuț V., Teodorescu M. E., *Calculul geometric neliniar al structurilor de rezistență*, București, Conspress, 2010.
[2]. ***, MathWorks Inc. MATLAB, Math. Graphics. Programming., [Interactiv]. Available: https://www.mathworks.com/products/matlab.html, accessed in 23.07.2022.

THE ANNALS OF "DUNAREA DE JOS" UNIVERSITY OF GALATI
FASCICLE IX. METALLURGY AND MATERIALS SCIENCE
No. 4 - 2022, ISSN 2668-4748; e-ISSN 2668-4756
Article DOI: https://doi.org/10.35219/mms.2022.4.02

RESEARCH ON HEAT TREATMENT APPLIED TO HIGH STRENGTH CONSTRUCTION STEELS

Marian-Iulian NEACȘU
"Dunarea de Jos" University of Galati, Romania
e-mail: marian.neacsu@ugal.ro

ABSTRACT

The paper presents the research carried out on a laboratory scale in order to establish the heat treatment parameters for the thick sheets used for naval constructions (welded joints). Investigations were carried out on steel sheets with two different chemical compositions.

In the same cooling conditions, returns were made at different times and temperatures. For the different sheet thicknesses of 15, 20, 22 and 24 mm, various heat treatment options were performed, by changing the cooling conditions of the sheets, respectively the cooling speeds, conditions that can be achieved in the industry.

The laboratory results showed that the required values for the mechanical characteristics are obtained only by cooling in water under pressure followed by a return at temperatures equal to or greater than 650 °C, a time greater than 70 min.

KEYWORDS: heat treatments, thick sheet metal, metal constructions, mechanical properties

1. Introduction

For high-responsibility metal constructions made by welding, such as ship hulls, the rules recommend the use of thick steel sheets with high mechanical property values [1, 2].

Obtaining these materials is done by adding alloying elements within the limits of weldable steel classes, by heat treatment [3, 4] if the technical conditions are ensured, by controlled lamination or by other methods.

Theoretically, the possibilities of improving the values of the mechanical characteristics for thick weldable steel sheets are multiple and depend on the technical endowment of the metallurgical industry, the experience and the possibilities of welding, which ensure at least equal values in the area where the sheets are joined with those of the base material for the properties of plasticity, toughness, mechanical strength and corrosion resistance [5].

For any of the methods by which it is possible to improve the values of the mechanical and technological characteristics, the specialty literature gives a series of data and principle indications regarding the brands of steels and the conditions in which the set of required properties is obtained [5].

In most cases, the mechanical transposition of data from specialized literature, without a verification of them in concrete manufacturing conditions, does not allow the systematic obtaining of satisfactory results in mass production [6]. For these reasons, it was first necessary to carry out some laboratory experiments, which take into account the possibilities created in the metallurgical industry for improving the values of the mechanical and technological characteristics of thick sheets through heat treatment [7]. The laboratory results were verified industrially to determine the thermal treatment (quenching and tempering) of the thick plates intended for the construction of ship hulls, with the joint by welding.

When establishing the quenching and tempering technology, it was aimed to ensure the obtaining of some physical-mechanical and technological characteristics corresponding to the quality prescriptions, on an economically advantageous scheme [7].

2. Experimental conditions

The studied materials were those provided by the norms [2] for the construction of ship hulls with welding. The recommended steels are produced in electric furnaces. The composition of the two steels

THE ANNALS OF "DUNAREA DE JOS" UNIVERSITY OF GALATI
FASCICLE IX. METALLURGY AND MATERIALS SCIENCE
No. 4 - 2022, ISSN 2668-4748; e-ISSN 2668-4756
Article DOI: https://doi.org/10.35219/mms.2022.4.02

on which the experiments were carried out is shown in Table 1.

Copper is prescribed as mandatory to improve corrosion behavior. The minimum 0.020% Al content is prescribed to ensure the austenitic grain equal to or finer than the one corresponding to score 5.

The behavior of steel during heating and cooling was studied in laboratory conditions by dilatometric determination of critical points at different heating and cooling rates. The Ms point was also determined for the two steels on several chemical compositions.

Table 1. *Chemical composition of the investigated materials*

Steel	Chemical composition, %								
	C max.	Si	Mn	S max.	P max.	Cr max.	Ni max.	Cu	Al min.
1	0.12	0.80... 1.10	1.30... 1.65	0.035	0.035	0.30	0.30	0.15-0.30	0.020
2	0.12	0.80... 1.10	0.50... 0.80	0.035	0.035	0.60... 0.90	0.50... 0.80	0.40... 0.65	0.020

For the different sheet thicknesses of 15, 20, 22 and 24 mm, various heat treatment options were performed, by changing the cooling conditions of the sheets, respectively the cooling speeds, conditions that are possible to achieve in the industry, namely: cooling in still air or in pressurized air, total or interrupted cooling by spraying water under pressure of 2.5 and 6 at on both sides of the plate in the laboratory installation sketched in Figure 1.

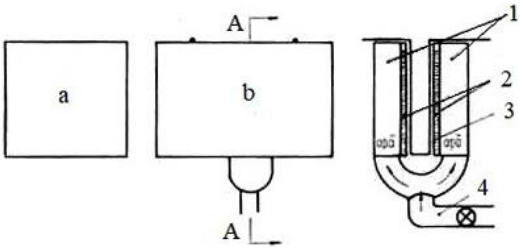

Fig. 1. *The laboratory installation for the treatment of flat samples (sheets) of different thicknesses: a - oven; b - controlled cooling device; 1 - water caisson; 2 - nozzles; 3 - centering support; 4 - water or air supply pipe under pressure*

For the same cooling conditions, returns were made at different times and temperatures. The conditions in which the optimal values of the mechanical characteristics were achieved in the laboratory were verified and completed in the experiments on an industrial scale.

In industry, due to large cooling surfaces [(1.4...3.15 m) x (8…15 m)] the panels deform slightly during cooling and therefore it was necessary to achieve the planning of the board at the temperature of return, when the remaining voltages in the board are also eliminated after planning.

The values of the mechanical characteristics imposed by the norms for the two brands of steels are presented in Table 2.

Table 2*. The values of the mechanical characteristics imposed by the norms for the studied steels*

Steel	Sheet thickness [mm]		The values of the mechanical characteristics					
		Delivery status	R MPa	R_c MPa	A_5 % min	Z, % min.	KCU_2 at – 40 °C kgf.m/cm^2	Bending
1	10...32	Tempering + recovery	540...660	min. 40	19	50	min. 5	180°, 2 a
2	10...32	Tempering + recovery	540...660	min. 40	19	50	min. 5	180°, 2 a

THE ANNALS OF "DUNAREA DE JOS" UNIVERSITY OF GALATI
FASCICLE IX. METALLURGY AND MATERIALS SCIENCE
No. 4 - 2022, ISSN 2668-4748; e-ISSN 2668-4756
Article DOI: https://doi.org/10.35219/mms.2022.4.02

3. Experimental results

The values of the transformation points over a wide range of chemical composition, covering the prescribed chemical composition and ensuring the values of the mechanical characteristics, are presented in Table 3.

Table 3. *values of transformation points over a wide range of chemical composition*

	Heating and cooling at 2.5 °C/min.				**Heating and cooling at 100 °C/min.**				**Ms °C**
Steel	Ac_1	Ac_3	A_{23}	A_{21}	Ac_1	Ac_3	Ar_3	Ar_1	
1	715... 735	890... 910	880... 827	693... 714	720... 756	906... 917	717... 770	477... 568	387... 400
2	750... 760	900... 910	800	678	760... 778	910... 918	700... 730	420... 520	390... 423

This results in a variation of the critical points in relation to the heating and cooling speeds and for each speed the transformation temperature has minimum and maximum values depending on the chemical composition of the shot.

Based on these experiences, it was established that for the thermal treatment of thick sheets, the optimal austenitizing temperature in industrial conditions is between 920…930 °C (plate temperature equal to 920 °C), and the austenitization time (heating and temperature maintenance) is 2…2.5 min/mm with the introduction of the plate directly at a temperature of 930 °C.

Under these conditions, a real fine and homogeneous austenitic grain results (Fig. 2) on the basis of which the tempering structure is formed (Fig. 3). These conditions ensure the systematic reproducibility of the characteristic values depending on the austenitic grain size (R, Rc, Z, A5, KCU.).

The level of the values of the mechanical characteristics varied depending on: the applied cooling speeds, the temperature up to which the cooling was done at speeds higher than the critical speed, therefore depending on the structures resulting from the decomposition of the undercooled austenite.

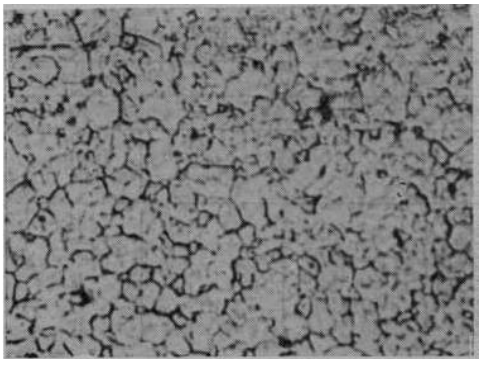

Fig. 2. *Actual austenitic grain size (x100, Nital attack)*

The laboratory results showed that the values imposed for the mechanical characteristics are obtained only by cooling in water under a pressure of 60 MPa for a time equal to or greater than 20 s, followed by a return to temperatures equal to or greater than 650 °C, a time greater than 70 min.

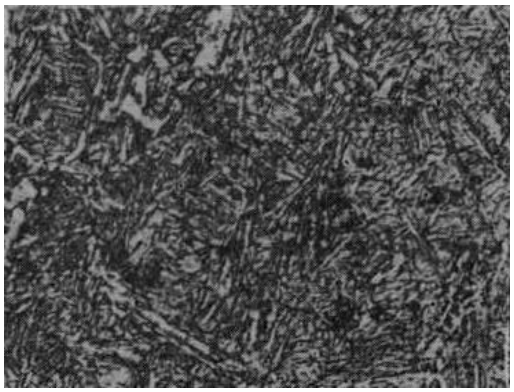

Fig. 3. *Structure of hardened and unhardened plates (x100, Nital attack)*

The laboratory simulation of the possible treatment conditions to be achieved in the industry allowed the establishment of the minimum technological parameters for achieving the values of mechanical characteristics on an industrial scale.

Taking into account the fact that industrially the amount of metal is different, respectively the heating and cooling speeds can be different than those realized in the laboratory, the experiments led to the establishment of the limits in which the technological treatment process can be carried out to ensure the assembly optimal properties, as well as chemical composition limits.

For the coldest thicknesses (20 and 24 mm), the optimal chemical compositions are indicated in Table 4.

THE ANNALS OF "DUNAREA DE JOS" UNIVERSITY OF GALATI
FASCICLE IX. METALLURGY AND MATERIALS SCIENCE
No. 4 - 2022, ISSN 2668-4748; e-ISSN 2668-4756
Article DOI: https://doi.org/10.35219/mms.2022.4.02

Table 4. *Optimal chemical composition for the most common thicknesses*

Steel	Sheet thickness [mm]	Chemical composition, %								
		C	Si	Mn	S max.	P max.	Al min.	Cr max.	Ni max.	Cu min.
1	20	0.09... 0.12	0.85... 1.10	1.40... 1.65	0.035	0.035	0.020	0.30	0.30	0.15... 0.30
	24	0.09... 0.12	0.90... 1.10	1.45... 1.65	0.035	0.035	0.020	0.30	0.30	0.15... 0.30
2	22	0.09... 0.12	0.80... 1.00	0.50... 0.80	0.035	0.035	0.020	0.60... 0.90	0.5... 0.8	0.4... 0.65

Industrially, both the austenitization conditions and the tempering and tempering conditions were verified. The range of tests done covered a wide area. The cooling time with water under pressure was 90s until the complete cooling of the sheet.

After tempering, a lower bainite structure is obtained (Fig. 4) with a greater stability when returning. Very wide annealing conditions were experimented: annealing temperature between 650…725 °C, and the recovery time for certain temperatures between 80 and 140 min.

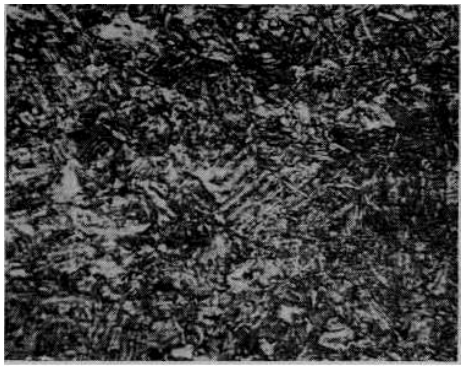

Fig. 4. *The structure of the board after a single comeback (x100, Nital attack)*

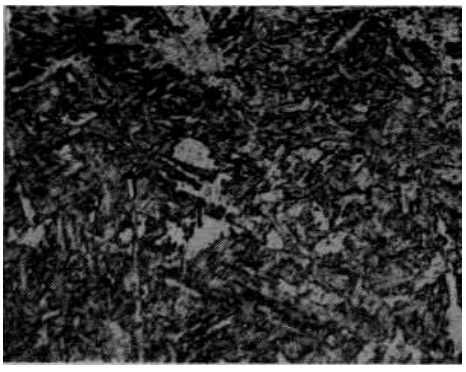

Fig. 5. *The bainite structure of the sheet after double tempering (x 100, Nital attack)*

Table 5 shows the limits of the values of the mechanical characteristics for the sheet with a thickness of 20 mm for a representative number of batches that were subjected to a tempering heat treatment with a holding time of 80 min at a temperature of 700 °C (furnace temperature), compared to the values obtained after the second heating for recovery, (at 690 °C) for 60 min, the results being presented in Table 6.

It follows that the technological parameters of heat treatment established ensure the values of the mechanical characteristics within a small gap.

The bainitic structure, which is formed by cooling with water at a pressure of 60 MPa for 20...90 s, gives after tempering a set of appropriate properties, stable even when the material is reheated either for a double tempering, or the heating during welding in the thermal influence zone where the temperature did not exceed Ac1.

It should be noted that this structure is influenced not only by the cooling conditions, but also by the specific chemical composition of the steel indicated for large-scale metal constructions (ship hulls) with welded joints.

The changes in the values of the mechanical characteristics after the second heating for recovery are very small, which shows that the bainitic structure is resistant to repeated heating (Fig. 5).

Due to the degree of dispersion and uniformity in the distribution of the carbide particles formed in the lower bainites, a high resistance (especially Rc) results, as well as a good plasticity, which are maintained during repeated heating at temperatures lower than Ac1.

The fact that through the cooling conditions of the filler material, used in the welded joints of the respective steel, a bainitic structure is also obtained, means that the material will behave better in corrosion compared to a welded joint where the structure is different from that of the base material.

THE ANNALS OF "DUNAREA DE JOS" UNIVERSITY OF GALATI
FASCICLE IX. METALLURGY AND MATERIALS SCIENCE
N°. 4 - 2022, ISSN 2668-4748; e-ISSN 2668-4756
Article DOI: https://doi.org/10.35219/mms.2022.4.02

Table 5. *Values of the mechanical characteristics for the sheet with a thickness of 20 mm after a single recovery*

No. the test batch	After cooling in water and tempering at 700 °C, 80 min with planning from the tempering temperature				
	R **MPa**	***Rc*** **MPa**	A_5 **%**	***Z*** **%**	***KCU*****, at -40 °C MPa**
1	605...635	47...49	23...24	56...57	89...110 ..11,0
2	615...66,0	43...49	21...24	50...59	63...95 .. 9,5
3	550...56,5	42...50	20...24	55...58	63...79 .. 7,9
4	610...620	47...49	20...22	50...53	70...83 .. 8,3
5	560...590*	45...49	21...24	58...61	68...84 .. 8,4

Table 6. *Values of the mechanical characteristics for the sheet with a thickness of 20 mm after a double recovery*

No. the test batch	After the second heating to return to 690 °C, 60 min and a replanning at the return temperature				
	R MPa	**Rc MPa**	A_5 **%**	**Z %**	**KCU at - 40 °C, MPa**
1	610...620 62,0	468...475 .47,5	23...25	58...61 .61	95...102 10,2
2	620...645 64,5	500...525 .52,5	21...24	59...61 .61	69...81 8,1
3	550...555 55,5	415...435 .43,5	25...27	55...59 .59	64...75 7,5
4	590...610 61,0	460...480 .48,0	21...23	56...57 .57	68...81 8,1
5	550...600 .60,0	405...470 .47,0	25...26	62...65 .65	68...78 7,8

4. Conclusions

The technological parameters of heat treatment of thick sheets in an industrial environment were established by modeling in the laboratory the industrial conditions of heat treatment.

The verification on an industrial scale led to obtaining sheet metal production with an optimal set of mechanical properties, the values of which fall within a small gap.

The temperature of the furnace was divided into zones: at the entrance, on 1/2 of the length of the furnace, the maximum temperature allowed in the furnace (930 °C) is ensured, and on the next length, the temperature prescribed for austenite (920 °C). The total maintenance time is: 2...2.5 min/mm of sheet thickness.

Heating at high speeds by introducing the sheets into the furnace at temperatures higher than the austenitizing temperature and maintaining in this area until the temperature of the sheet reaches the austenitizing temperature, then introducing and maintaining the sheet at the prescribed austenitizing temperature for the respective steel, ensures an austenitic grain really fine and homogeneous on the background of which the final structure is formed that gives high properties to the steel.

The bainitic structure, which is formed during cooling, confers after annealing a set of appropriate

properties, stable even under the conditions in which the steel is subjected to reheating either for a double annealing or due to the thermal influence during welding.

In order to ensure the flatness of the sheets, with a smaller arrow or a maximum of 5 mm per linear meter, it is necessary to carry out planning at the return temperature, with an appropriately sized machine.

References

[1]. Vermesan H., Vermesan G., *et al.*, *Bazele tratamentelor termice*, Editura Universitatii din Oradea, 2002.

[2]. Catana D., *Influence of the heat treatments on the wear-resistant steels properties*, Bullettin of the Transilvania University of Brasov, vol. 8 (57), no. 2, Series I Engineering Sciences, ISSN 2065-2119 (print), ISSN 2065-2127 (CD-ROM), 2015.

[3]. Catana D., *Thermomechanical treatment influence on the high-speed steel hardness and wear*, Universal Journal of Materials Science, vol. 3 (3), ISSN 2331-6691 print, ISSN 2331-6705 online, DOI: 10.13189/ujms.2015.030302, 2015.

[4]. Dulamita I., Vermesan G., *et al.*, *Tehnologia tratamentelor termice*, Edit. Did. Pedag., 1987.

[5]. Cheşa I., *Alegerea şi utilizarea oţelurilor*, Editura Tehnică, Bucureşti, 1984.

[6]. Popescu N., Dumitrescu C., Munteanu A., *Tratamente termice si prelucrari la cald*, Edit. Did. Pedag., 1987.

[7]. Dulamita T., Florian E., *Tratamente termice si termochimice*, Edit. Did. Pedag., 1982.

THE ANNALS OF "DUNAREA DE JOS" UNIVERSITY OF GALATI
FASCICLE IX. METALLURGY AND MATERIALS SCIENCE
Nº. 4 - 2022, ISSN 2668-4748; e-ISSN 2668-4756
Article DOI: https://doi.org/10.35219/mms.2022.4.03

STUDIES ON THE USE OF ELECTRICITY TO REDUCE THE CONSUMPTION OF COKE IN THE DEVELOPMENT OF CAST IRON IN THE FURNACE

Marian-Iulian NEACȘU
"Dunarea de Jos" University of Galati, Romania
e-mail: mneacsu@ugal.ro

ABSTRACT

The paper presents the studies carried out in order to reduce the consumption of the volume of coke required for the production of pig iron in the furnace. Reducing coke consumption is necessary because it is an increasingly expensive material that increases the production cost of pig iron. Internationally, for the partial replacement of coke, auxiliary fuels were generally used in the form of gas or in liquid form, and the most used turned out to be methane. This process is limited by the fact that the temperature in the furnace is difficult to ensure.

The studies carried out have demonstrated that, under the given conditions, it is possible to directly introduce electricity into the crucible, the charge of the crucible presenting properties of electrical resistance that allow the application of additional electrical heating.

KEYWORDS: cast iron, furnace, coke, electrical current, methane gas

1. Introduction

In recent years, numerous improvements have been made to the technology of producing pig iron in smokestacks in order to reduce the specific consumption of coke.

Very good results in industrial practice have been obtained by using auxiliary fuels blown through the wind mouths mixed with hot air, the temperature of which has increased in a controlled and purposeful way in order to compensate for the thermal deficit caused by the combustion of carbon monoxide, carbon and H_2, in the conditions in the furnace crucible, of these fuels.

Worldwide, the use of auxiliary fuels made of gaseous hydrocarbons has become widespread: methane, coke oven gas; of diluted hydrocarbons: fuel oil, tar; of coal in the form of dust or mixture with liquid hydrocarbons. The type of replacement fuel used is dependent on local economic conditions. Of these, the most used is methane [1].

In the present state of the art, the amount of coke that can be replaced in the aforementioned manner with other fuels more economically advantageous than coke is limited primarily because of the temperature to which the air in the furnace can be heated [2, 3].

Starting from the finding that the replacement of coke with other fuels blown through the vents is limited by the impossibility of ensuring by known means the surplus heat necessary to maintain the thermal level in the furnace crucible, the problem of using electrical energy for this purpose was raised.

The use of electric energy in the manner shown, aims to maintain the furnace in its operating parameters and is thus fundamentally different from the other electrothermal aggregates known for the elaboration of cast iron, such as electric furnaces or electric furnaces with a short vat [1, 3].

Although the main source of energy for carrying out the processes in the furnace remains coke, the use of electrical energy in the chimneys as addressed in the present work, has the role of replacing more coke with methane blown in at the vents. The electricity input is a maximum of 100 kWh/t cast iron [1].

Several technological options can be considered for the introduction of heat of electrical origin into the flue:

- the introduction of electricity into the furnace by means of wall electrodes, in the area of the wind mouths or at the base of the display;
- additional heating by electrical induction of the crucible;
- electrical superheating of the air blown into the vents, which can be carried out with the help of the

THE ANNALS OF "DUNAREA DE JOS" UNIVERSITY OF GALATI
FASCICLE IX. METALLURGY AND MATERIALS SCIENCE
No. 4 - 2022, ISSN 2668-4748; e-ISSN 2668-4756
Article DOI: https://doi.org/10.35219/mms.2022.4.03

high-voltage electric arc, jet plasma or high-frequency plasma, the use of resistors, electrical induction with intermediate heat transmitters etc. [4].

2. Theoretical considerations

If it is provided that the thermal regime in the crucible of the furnace does not change when an additional quantity of methane is introduced, by compensating by electricity for the thermal deficit caused by the combustion of methane at CO and H_2 in the presence of coke, the theoretical amount of methane can be determined using the relationship [1, 4]:

$$m = \frac{860}{q_2 - q_1}, Nm^3\, CH_4/kWh \quad (1)$$

in which:

m - quantity of methane (CH_4);

860 is the caloric equivalent of kWh in kcal;

q_1 - the caloric content of methane combustion products under the given conditions, without taking into account the additional heat input, kcal/Nm^3 CH_4;

q_2 - the caloric content of the methane combustion products considered at the theoretical temperature corresponding to the normal operation of the furnace, kcal/Nm^3 CH4.

The combustion reaction of methane in the presence of carbon from coke is [2, 5]:

$$CH_4 + l/2O_2 = CO + 2H_2$$

In the case of air with 1% moisture that has the composition: O_2 = 20.79%; N_2 = 78.21%; $H_2O_{(V)}$ = 1.00%, by burning 1 Nm^3CH_4 results: CO = 1.000 Nm^3; H_2 = 2.0234 Nm^3; N_2 = 1.8368 Nm^3, that is, a total volume of combustion products V_g = 4.8602 Nm^3 [4].

The caloric content of the combustion products is [5]:

$$q_1 = 396 + Qv + Q_{CH_4} - Q_{H_2O}, \text{ kcal/Nm}^3\ CH_4 \quad (2)$$

in which:

396 is the amount of heat resulting from the combustion of methane at CO and H_2, kcal/Nm^3 CH4;

Q_V - combustion air enthalpy;

Q_{CH_4} - enthalpy of methane, kcal/Nm^3 CH_4;

Q_{H_2O} - the heat of dissociation of water vapor from the combustion air.

The calculation shall be carried out for t_{air} = 1000 °C; 1100 °C; 1200 °C; 1300 °C and t_{CH_4} = 0 °C and 600 °C, with the results listed in Table 1 [1].

The table shows that methane combustion products have caloric content that increases with the temperature of preheat of air and methane.

By burning carbon from the coke in front of the air vents with a humidity of 1% results per 1 kg C: CO = 1.867 Nm^3; H_2 = 0.044 Nm^3; N_2 = 3.429 Nm^3, respectively a volume of combustion products V_g = 5.340 Nm^3.

Table 1. *Caloric content of methane-burning products* [1]

Temperature, °C		kcal/Nm^3 CH_4
Air	**Methane**	
1 000	0	1 127.44
1 100	0	1 213.75
1 200	0	1 301.09
1 300	0	1 389.09
1 000	600	1 454.24
1 100	600	1 538.55
1 200	600	1 637.79
1 300	600	1 713.89

Calculation of the theoretical carbon-burning temperature of the coke at the window holes is done with the relation [4]:

$$2340 + Q_v + Q_c - Q_{H2O} = C_0 \cdot V_g \cdot t \quad (3)$$

in which:

2340 is the heat resulting from the combustion of carbon at CO, kcal/kg C;

Q_v - combustion air enthalpy, kcal/Nm^3 CH_4;

Q_c - carbon enthalpy that gets in front of the wind, kcal/kg C;

Q_{H_2O} - the heat of dissociation of water vapor from the combustion air, kcal/kg C;

C_o - the average specific heat of diatomic gases, kcal/Nm^3 °C.

The normal combustion temperature, which results in the use of pre-heated air at 600 °C, without the insufflation of methane, is t = 1952 °C.

The enthalpy of CO and H_2 air methane combustion products, considered at temperature t = 1952 °C, is [4]:

$$q_2 = V_g \cdot C_o \cdot t, \text{ kcal/Nm}^3\ CH_4$$
$$q_2 = 3336.6 \text{ kcal/Nm}^3\ CH_4$$

If the value of enthalpy q_2 is entered in relation (1), it follows [1, 4]:

$$m = \frac{860}{3336{,}6 - q_1} \text{Nm}^3\text{CH}_4\text{/kWh} \quad (4)$$

THE ANNALS OF "DUNAREA DE JOS" UNIVERSITY OF GALATI
FASCICLE IX. METALLURGY AND MATERIALS SCIENCE
No. 4 - 2022, ISSN 2668-4748; e-ISSN 2668-4756
Article DOI: https://doi.org/10.35219/mms.2022.4.03

By entering in the relation (4) the values in Table 1, the variation in the theoretical amount of methane possible to be introduced into the furnace due to electricity is obtained (Fig. 1).

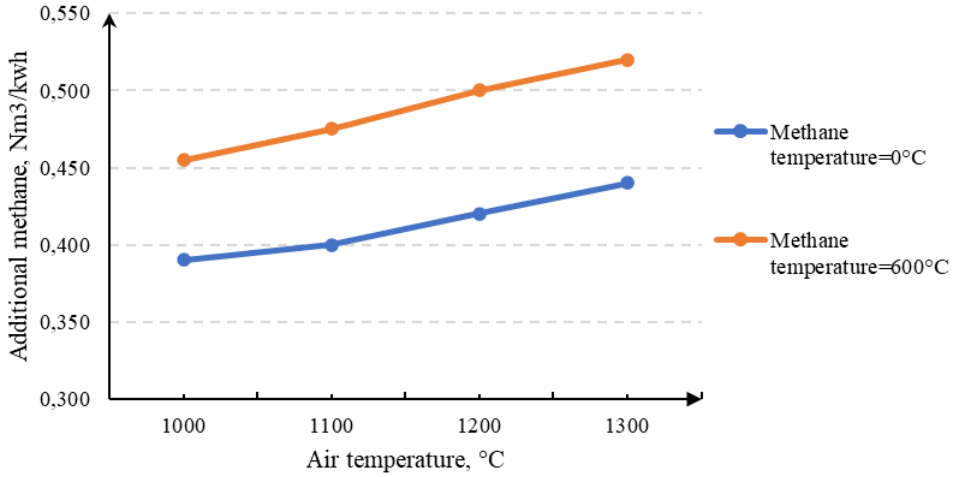

Fig. 1. *Variation in the theoretical amount of methane possible to insert into the furnace due to electricity* [1]

Figure 1 shows that the efficiency of the use of electricity in smoke increases with the temperature of air and methane. This is explained by the increased enthalpy of methane combustion products, which leads to a reduction in the need for electric heat for the introduction of an equal amount of extra methane into the furnace.

For the conditions of the calculation, it follows that for methane at a temperature of 0 °C, an additional 0.389 to 0.442 Nm^3 CH_4/kWh and for methane preheated at 600 °C, between 0.457 and 0.530 Nm^3 CH_4/kWh may be introduced.

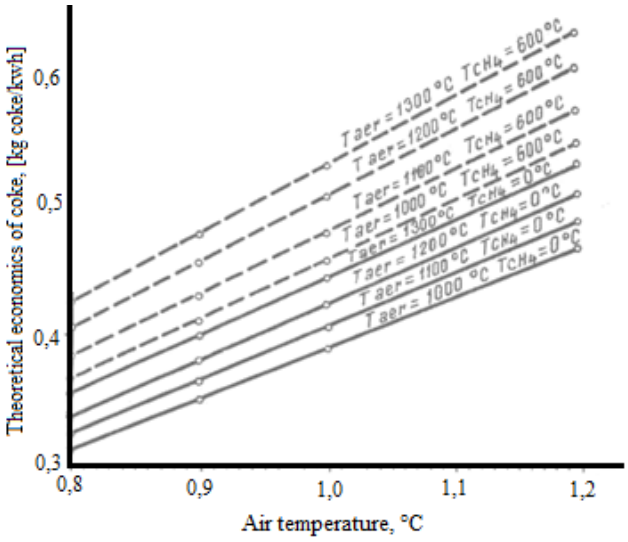

Fig. 2. *The variation in the theoretical coke economy, which can be obtained in kg/kWh, depending on the methane substitution index of coke, for different air and methane temperature values* [2]

The theoretical coke economy that can be obtained by using electricity in smoke is determined by the relation [5]:

$$k = i \cdot m, \text{ Kg/kWh} \quad (5)$$

in which:

i - is the acceptable replacement ratio of 0.8 to 1.2 kg/Nm^3 CH_4;

m - additional introduced methane, Nm^3/kWh;

k - quantity of coke, kg.

THE ANNALS OF "DUNAREA DE JOS" UNIVERSITY OF GALATI
FASCICLE IX. METALLURGY AND MATERIALS SCIENCE
No. 4 - 2022, ISSN 2668-4748; e-ISSN 2668-4756
Article DOI: https://doi.org/10.35219/mms.2022.4.03

When determining the actual electricity consumption (from the grid), account shall be taken of the electricity efficiency used.

Figure 2 shows the additional theoretical economic variation of coke that can be obtained, in kg/kWh, depending on the replacement index.

The additional methane consumption depends on the replacement index between 1.25 and 0.83 Nm^3 CH_4/kg of saved coke.

The additional heat that can be obtained by Joule effect in the wind-mouth area is thermally equivalent to overheating of the insufflation air. The equivalent temperature increase is determined with the relation [1, 4]:

$$t = \frac{860 \cdot E \cdot \eta}{C_i \cdot V} \quad (6)$$

in which:

η is the efficiency of the electrical installation (0.8 to 0.9);

E - specific electricity consumption in kWh/t cast iron, which is determined with the relation [2, 5]:

$$E = \frac{k}{\eta \cdot i \cdot m} \quad (7)$$

C_i - the average specific heat of the air at the insufflation temperature, kcal/Nm^3·°C;

V - the amount of air in cast iron Nm^3/t, which is calculated with the relation [2, 5]:

$$V = 4{,}300 \cdot \left(a \cdot \frac{K}{100} - C_{df}\right) + 2{,}348 \cdot M \quad (8)$$

in which:

K is the specific consumption of technical coke under the studied regimes, kg/t cast iron;

a - fixed carbon content in coke, %;

C_{df} - carbon from coke to be consumed for direct reduction and carburizing of cast iron, kg/t cast iron;

M - specific consumption of additional methane at the studied regime Nm^3/t cast iron.

It is preferable that before the application of the electric intensification of the operation of the furnaces, the classical ways of reducing the specific consumption of coke are practically exhausted, while raising the temperature of the hot air regime to the maximum value compatible with the construction of the capers and the normal operation of the furnace.

3. Experimental part

Due to the lack of experimental data on the introduction of electrical energy through wall electrodes into vertical-melting-vats furnaces, as well as the electrical characteristics of the charge in the crucible of the furnace, the experimental approach to the problem was made in this direction. The studies were done at a 250 m^3 furnace, where the possibility of introducing electricity through the body of the window holes and the mass of liquid cast iron from the crucible of the furnace was investigated.

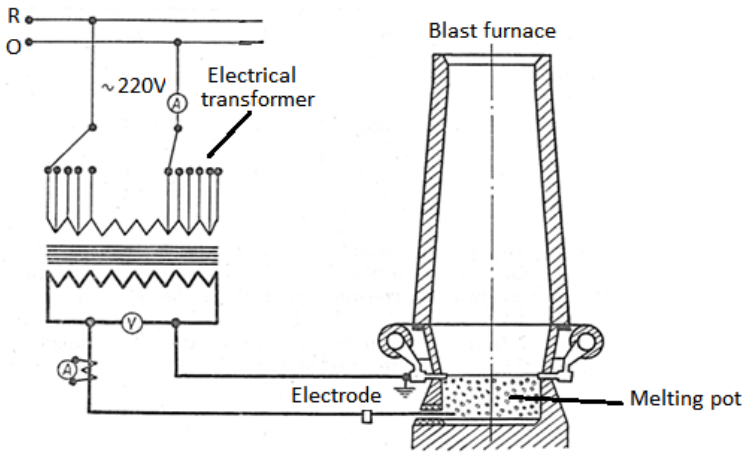

Fig. 3. *Experimental installation scheme*

Prior to the installation of the electrical energy installation, experiments were carried out that did not require any significant technological changes. It was investigated the possibility of passing electric current through the crucible material between the plane of the windpipe and the cast iron bath, respectively an electrode in contact with it, inserted through the cast iron outlet. The electrode was made up of a steel bar

THE ANNALS OF "DUNAREA DE JOS" UNIVERSITY OF GALATI
FASCICLE IX. METALLURGY AND MATERIALS SCIENCE
N°. 4 - 2022, ISSN 2668-4748; e-ISSN 2668-4756
Article DOI: https://doi.org/10.35219/mms.2022.4.03

of 25 mm and 3 m long inserted through the plug of the cast iron outlet and located about 25 cm in length in contact with liquid cast iron.

The scheme of the installation is shown in Figure 3.

Electrical measurements have shown that the plug mass has sufficient electro-insulating characteristics so that short-circuit current losses between the metal electrode and the furnace mantle through the plug mass are very small.

After the discharge of the cast iron from the furnace, the metal electrode was knocked through the centre of the outlet plug of the cast iron, until it entered the cast iron bath. The transformer was then connected to the grid and by adjusting the voltage stages the current intensity and the power output in the system varied. The measurements tracked the current in the primary circuit of the transformer and the voltage and current in the transformer secondary.

The results are shown in Table 2, which refers to the phase of gradual voltage reduction.

According to the data in Table 2 recorded after the experiments, under the conditions given at the furnace it can be said that it is possible to directly introduce electricity into the crucible, the crucible load having electrical resistance properties that allow the application of an additional electric heating.

Table 2. *Experiments to introduce electrical energy into the crucible*

Voltage stage of transformer	Intensity (A)		Secondary voltage U_2 (V)	Electrical power (kW) I_2 U_2 (pt.cos φ=1)	Electrical resistance of the load in the crucible of the furnace
	Primary I_1	Secondary I_2			
8/8	190	1440	25	36.0	0.017
8/0	135	1120	21	23.5	0.018
7/0	70	850	17	14.6	0.020
6/0	50	720	14	10.5	0.019
5/0	10	580	11	6.4	0.019
4/0	-	500	10	5.0	0.020
3/0	-	448	9	4.1	0.020
1/0	-	408	8	3.3	0.020

4. Conclusions

The electric intensification of the operation of the furnace keeps unchanged the basic characteristic of this steel aggregate to use mainly heat energy obtained by burning coke.

The use of electricity is limited, up to consumption of the order of 100 kWh/t cast iron and aims only at a reduction in the specific consumption of coke on account of the increase in the amount of auxiliary fuel inked through the window wings.

The calculations show that when using methane as an auxiliary fuel it is possible to achieve a coke saving of the order of 0.3 to 0.6 kg/kWh, depending on the temperature of the air and the methane-inspired blast furnace and the methane-coke replacement ratio.

The experiments carried out indicated that at the furnace where the research was carried out, the crucible's load has properties that allow the application of electric overheating by Joule effect.

Economically, large fluctuations in the price of coke on the world market, with price fluctuations sometimes reaching very high values, ensure a sufficient margin of profitability of the studied process and justify the research carried out in this direction.

References

[1]. Riposan I., Chisamera M., *Tehnologia elaborarii si turnarii fontei*, Editura didactica si pedagogica, Bucuresti, 1985.
[2]. Cojocaru-Filipiuc V., *Pregatirea încărcaturii pentru elaborarea fontei în cuptoare cu inducţie*, Editura "Samia" Iaşi, 2006.
[3]. Riposan I., Sofroni L., Chisamera M., *Fonta bainitica*, Editura: Tehnica, 1988.
[4]. Gâdea S., Rău A., Oprea F., Tripşa I., Geru N., *Manualul inginerului metalurg*, vol. I, Editura Tehnica, Bucureşti, 1978.
[5]. Carcea I., Roman C., Chelariu R., *Ingineria proceselor metalurgice*, Editura Performantica, Iaşi, 2006.

THE ANNALS OF "DUNAREA DE JOS" UNIVERSITY OF GALATI
FASCICLE IX. METALLURGY AND MATERIALS SCIENCE
N°. 4 - 2022, ISSN 2668-4748; e-ISSN 2668-4756
Article DOI: https://doi.org/10.35219/mms.2022.4.04

VIBRO-ACOUSTIC ANALYSIS OF A SPHERICAL JOINT USING FEM

Doina BOAZU
"Dunarea de Jos" University of Galati, Department of Mechanical Engineering, Romania
e-mail: doina.boazu@ugal.ro

ABSTRACT

Vibro-Acoustic analysis gives the possibility of obtaining the level of sound pressure depending on the frequency, as well as the evaluation of the acoustic pressure in a point of interest.

The monitoring can be done using a microphone placed in an area of acoustic sensitivity.

This paper highlights the possibility of monitoring the level of acoustic pressure in the vicinity of some structural elements that can vibrate under the action of external excitations.

The studied assembly is a spherical joint. All the changes in the acoustic pressure level on the control direction of this assembly can indicate structural changes at the level of the monitored joint, thus highlighting possible defects.

KEYWORDS: vibro-acoustics using FEM, spherical joint, dynamic response

1. Introduction

Acoustics is the study of generation, propagation, absorption, reflection of the sound pressure waves in a fluid medium, and some applications for this analysis include [8-10]:

- design of spikers, acoustic filters;
- underwater acoustics;
- machinery.

Vibro-acoustic analysis is used in:

- noise reduction in machinery;
- noise reduction in buildings;
- noise reduction in vehicles;
- acoustic filters.

Typical quantities of interest in vibro-acoustic analysis are:

- the pressure distribution in a fluid (air) at different frequencies - sound pressure level;
- transmission, attenuation and dispersion of acoustic waves.

A coupled acoustics analysis takes into account the interaction fluid-structure [2, 5-7].

This is the case of vibro-acoustic analysis.

The 3D vibro-acoustic calculus using Ansys Workbench requires [1]:

- define acoustics properties;
- apply acoustic boundary conditions and specific loads;
- assigning acoustic-mechanics structure interfaces;
- post-process acoustic results.

Fluid-structure interaction (FSI) is a term for acoustic and structural body interacts via boundary conditions that couples them.

The formation of coupled equation of motion for FSI is shown below [3].

The finite element equation of motion for acoustic pressure is:

$$[M_f]\{\ddot{p}\} + [K_f]\{p\} = \{F_f\} \quad (1)$$

$[M_f]$: Equivalent fluid mass matrix;
$\{\ddot{p}\}$: Vector of the second derivative of acoustic pressure with respect to time;
$[K_f]$: Equivalent fluid stiffness matrix;
$\{p\}$: Vector of unknown nodal acoustic pressures;
$\{F_f\}$: Vector of applied fluid loads.

The finite element equation of motion for structural elements is:

$$[M_s]\{\ddot{U}\} + [K_s]\{U\} = \{F_s\} \quad (2)$$

$[M_s]$: Equivalent structural mass matrix;
$\{\ddot{U}\}$: Vector of the second derivative of displacements with respect to time;
$[K_s]$: Equivalent structural stiffness matrix;
$\{U\}$: Vector of unknown nodal displacements;
$\{F_s\}$: Vector of applied structural loads.

THE ANNALS OF "DUNAREA DE JOS" UNIVERSITY OF GALATI
FASCICLE IX. METALLURGY AND MATERIALS SCIENCE
N°. 4 - 2022, ISSN 2668-4748; e-ISSN 2668-4756
Article DOI: https://doi.org/10.35219/mms.2022.4.04

Additional terms and coupling matrix, [R] are added to equation (1) and (2) to account for the coupling of structure and fluid.

$$[M_f]\{\ddot{p}\} + [K_f]\{p\} = \{F_f\} + \rho_0[R]^T\{U\} \quad (3)$$

$$[M_s]\{\ddot{U}\} + [K_s]\{U\} = \{F_s\} + [R]\{p\} \quad (4)$$

Matrix equation is then formed from equation (3) and (4) with added structural damping, [C_s] and acoustic damping, [C_f] effects.

$$\begin{bmatrix} M_s & 0 \\ \rho_0 R^T & M_f \end{bmatrix}\begin{Bmatrix} \ddot{U} \\ \ddot{p} \end{Bmatrix} + \begin{bmatrix} C_s & 0 \\ 0 & C_f \end{bmatrix}\begin{Bmatrix} \dot{U} \\ \dot{p} \end{Bmatrix} + \begin{bmatrix} K_s & -R \\ 0 & K_f \end{bmatrix}\begin{Bmatrix} U \\ p \end{Bmatrix} = \begin{Bmatrix} F_s \\ F_f \end{Bmatrix} \quad (5)$$

Sound Pressure Level or SPL is defined as follows:

$$L_p = 20\, log\left(\frac{p_{rms}}{p_{ref}}\right)$$

$$p_{ref} = 20 \times 10^{-6}(Pa)$$

2. Vibro-acoustic modeling of spherical joint using fem

The paper highlights the possibility of monitoring the acoustic pressure level in the vicinity of some structural elements that can vibrate under the action of external excitations.

The change in the acoustic pressure in the control direction of the assembly can indicate structural changes at the level of the monitored joint, thus highlighting possible defects (gaps of inadmissible sizes).

Monitoring can be done with the help of a microphone placed in an area of acoustic sensitivity.

Vibro-Acoustic analysis gives the possibility of obtaining the distribution of the acoustic pressure depending on the frequency, as well as the evaluation of the acoustic pressure in a point of interest.

The structure whose vibrations are of interest is a spherical joint presented in reference [4]; the spherical head of a steel rod is made of Structural Steel and the bearing is made of Teflon / HDPE polyethylene.

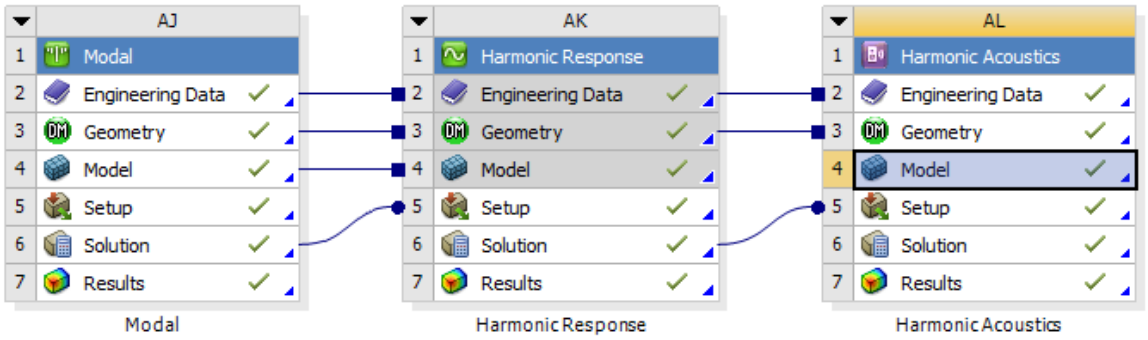

Fig. 1. *Calculation modules for Vibro-Acoustics analysis in Ansys Workbench*

The stages of work with the related modules and the results of each module are presented in the diagram from Fig. 2; the chaining of modules in Ansys Workbench with the sharing of submodules is shown in Fig. 1.

For this purpose, the frequencies and modes of vibration are calculated in a determined range 0-10000 Hz (using MODAL module of Ansys Workbench), then with the help of the Harmonic Response module, the dynamic response of the structure to the external excitation is determined, and finally with the help of the Harmonic acoustics module the pressure distribution is obtained in the considered air enclosure.

In the Geometry submodule, the structure whose vibration is of interest is created and an area of suitable shape and size is defined around the structure, an enclosure that will be considered full of air and will become active only in the HARMONIC ACOUSTICS module (Fig. 3a).

For enclosure, a non-uniform cushion box with the dimensions given in the Fig. 3b is used.

The properties of the materials for the forced vibration analysis are given in Table 1, and the properties for the acoustic simulation (for air) are given in Table 2.

In the MODAL module, in the Model submodule, the boundary conditions for the free vibrations of the structure are imposed, obtaining the natural frequencies and natural modes in the chosen frequency range 0-10000 Hz (Fig. 4).

These results are transferred to the HARMONIC RESPONSE Module; in order to obtain the forced

THE ANNALS OF "DUNAREA DE JOS" UNIVERSITY OF GALATI
FASCICLE IX. METALLURGY AND MATERIALS SCIENCE
N°. 4 - 2022, ISSN 2668-4748; e-ISSN 2668-4756
Article DOI: https://doi.org/10.35219/mms.2022.4.04

vibration, a constant force excitation on the X control direction and 5% damping are imposed.

As results, the speeds and accelerations depending on the frequency can be obtained, results that will be imported into the Acoustic Region in the HARMONIC ACOUSTICS module, the only mode in which the Air Enclosure becomes active, delimited in this module by the Radiation Boundary.

The air enclosure mesh is Adaptive with resolution 7.

Boundary conditions for the MODAL analysis are represented in Fig. 5; the horizontal arm is fixed at the end and the vertical arm has imposed frictionless support at its end.

Harmonic response corresponds to a constant force excitation applied on the steel head of the spherical joint on the command direction (Fig. 6).

Table 1. *Properties for Vibro simulation*

Materials	Mass density (kg/m^3)	Young modulus in compression (Pa)	Poisson ratio
Structural Steel (for structure)	7850	2.1e^11	0.3
Teflon (for structure)	2160	482e^6	0.42

Table 2. *Properties for Acoustic simulation*

Material	Mass density (kg/m^3)	Sound speed (m/s)
Air (for enclosure)	1.2	343

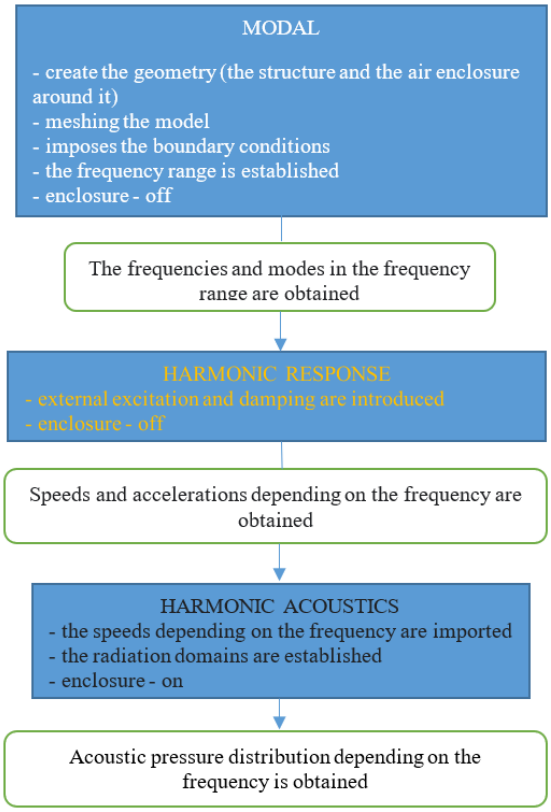

Fig. 2. *The working stages in vibro-acoustic analysis and the results obtained in each stage*

The type of element used in discretization of the structure is SOLID187 [12] (number of nodes 7485, number of elements being 1981).

SOLID187 element is a higher order 3-D, 10-node element. SOLID187 has a quadratic displacement behavior and is well suited to modeling irregular meshes (such as those produced from

THE ANNALS OF "DUNAREA DE JOS" UNIVERSITY OF GALATI
FASCICLE IX. METALLURGY AND MATERIALS SCIENCE
Nº. 4 - 2022, ISSN 2668-4748; e-ISSN 2668-4756
Article DOI: https://doi.org/10.35219/mms.2022.4.04

various CAD/CAM systems). The element is defined by 10 nodes having three degrees of freedom at each node: translations in the nodal x, y, and z directions. The element has plasticity, hyper-elasticity, creep, stress stiffening, large deflection, and large strain capabilities. It also has mixed formulation capability for simulating deformations of nearly incompressible elastoplastic materials, and fully incompressible hyper-elastic materials [12].

The enclosure was discretized in 100808 elements of FLUID221 type - see reference [7].

FLUID221 is a higher order 3-D 10-node solid element that exhibits quadratic pressure behavior. This type of element is used for modeling the fluid medium and the interface in fluid-structure interaction problems.

Meshing of simulation model for acoustic analysis should be sufficiently fine to capture the mode shapes of the model.

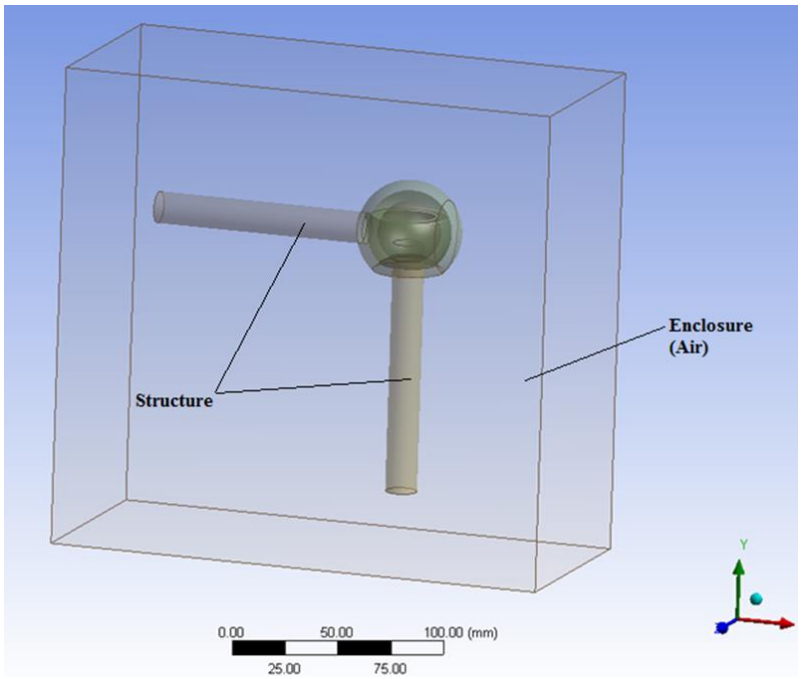

Fig. 3a. *Geometry of the system*

Details of Enclosure1	
Enclosure	Enclosure1
Shape	Box
Number of Planes	0
Cushion	Non-Uniform
FD1, Cushion +X value (>0)	30 mm
FD2, Cushion +Y value (>0)	50 mm
FD3, Cushion +Z value (>0)	30 mm
FD4, Cushion -X value (>0)	30 mm
FD5, Cushion -Y value (>0)	30 mm
FD6, Cushion -Z value (>0)	30 mm
Target Bodies	All Bodies
Export Enclosure	Yes

Fig. 3b. *The dimensions of the enclosure*

THE ANNALS OF "DUNAREA DE JOS" UNIVERSITY OF GALATI
FASCICLE IX. METALLURGY AND MATERIALS SCIENCE
Nº. 4 - 2022, ISSN 2668-4748; e-ISSN 2668-4756
Article DOI: https://doi.org/10.35219/mms.2022.4.04

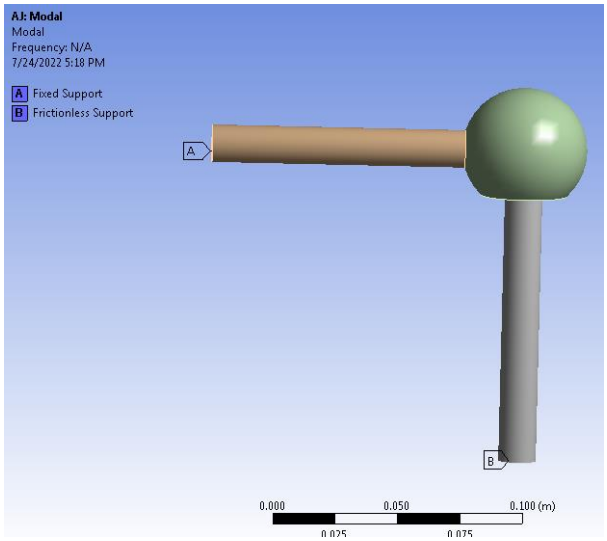

Fig. 4. *Boundary conditions*

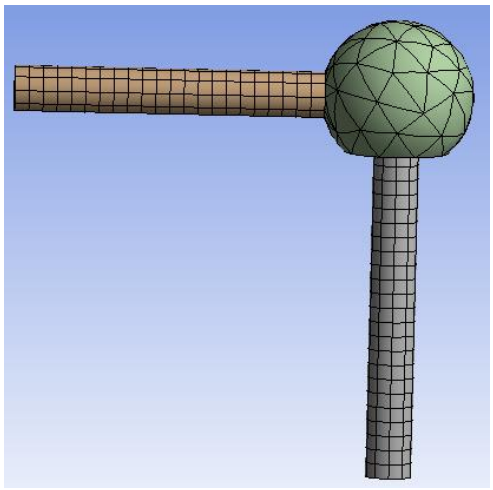

Fig. 5. *The mesh of structure*

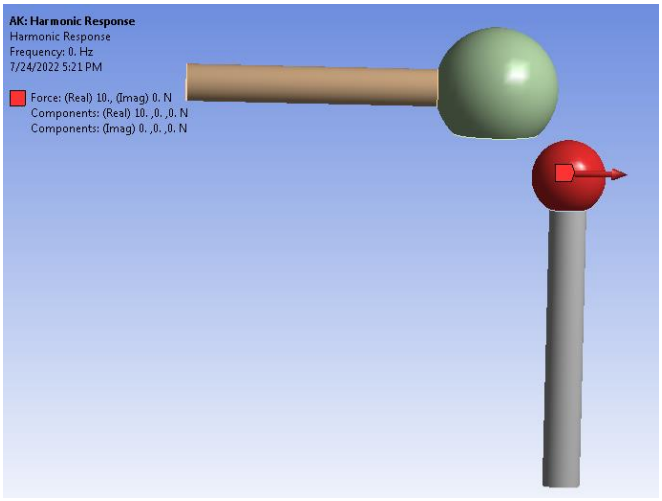

Fig. 6. *Harmonic excitation*

THE ANNALS OF "DUNAREA DE JOS" UNIVERSITY OF GALATI
FASCICLE IX. METALLURGY AND MATERIALS SCIENCE
N°. 4 - 2022, ISSN 2668-4748; e-ISSN 2668-4756
Article DOI: https://doi.org/10.35219/mms.2022.4.04

3. Results and discussions

In Fig. 7 and Fig. 8 are the representations of the speed amplitudes as functions of the frequency, respectively of the accelerations as functions of the frequency (Bode diagrams).

These diagrams show the frequency of 2000 Hz and the corresponding sweeping phase angle for speeds and accelerations.

Fig. 9 shows the distribution of imported speeds at the frequency of 186 Hz.

Fig. 10 gives the sound pressure level distribution (for excitation Force = 10 N) in a section; in the Fig. 11 the distribution of sound pressure level corresponds to the excitation Force = 100 N.

In Fig. 12 is given the Microphone position (-50 mm, -50 mm, 0 mm) for Far field SPL Mic evaluation.

In Fig. 13 is represented comparatively SPL Mic vs Frequency for excitation force of 10 N and of 100 N; the SPL (sound pressure level) charts are similar, only the sound pressure level is different. The position of the Microphone is -50 mm, -50 mm, 0 mm.

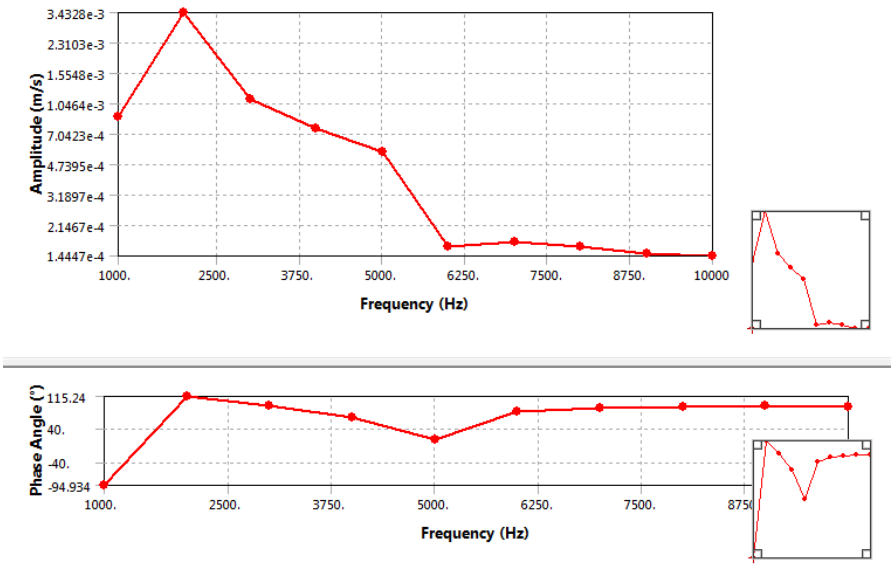

Fig. 7. *Velocities vs frequencies*

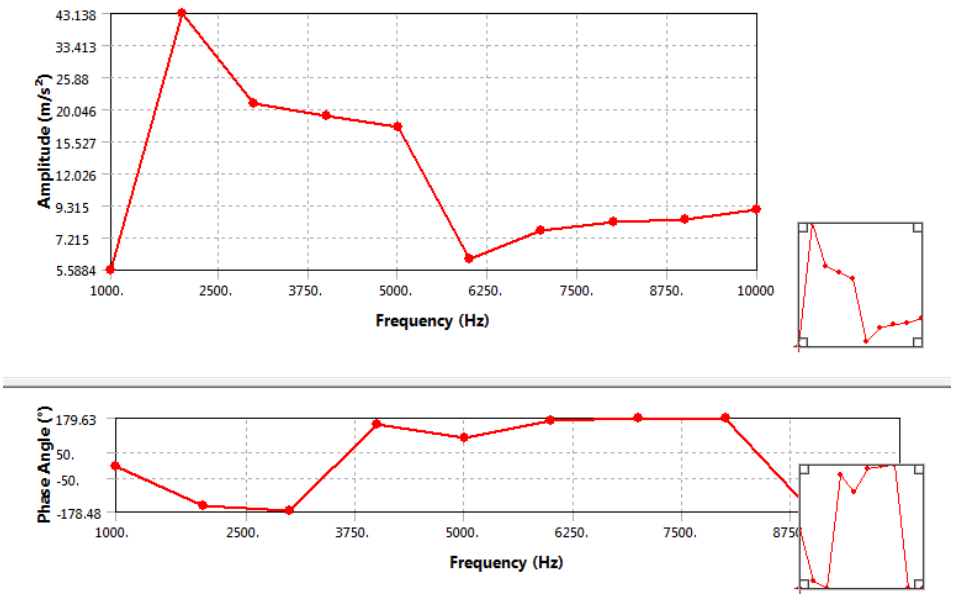

Fig. 8. *Accelerations vs frequencies*

THE ANNALS OF "DUNAREA DE JOS" UNIVERSITY OF GALATI
FASCICLE IX. METALLURGY AND MATERIALS SCIENCE
No. 4 - 2022, ISSN 2668-4748; e-ISSN 2668-4756
Article DOI: https://doi.org/10.35219/mms.2022.4.04

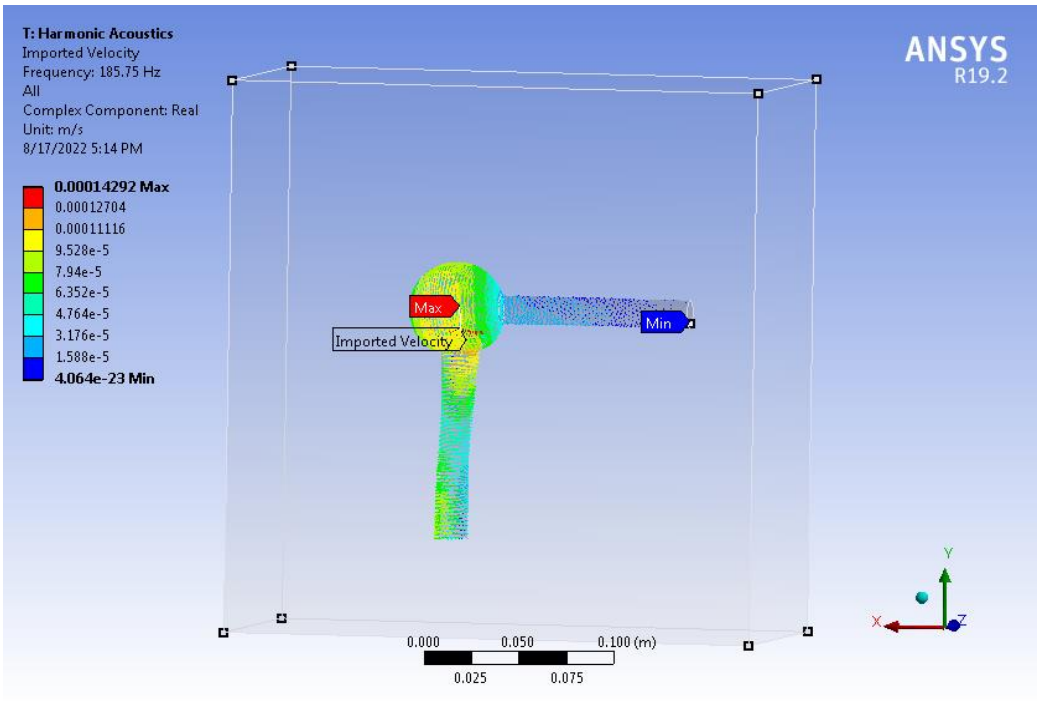

Fig. 9. *Distribution of imported velocity*

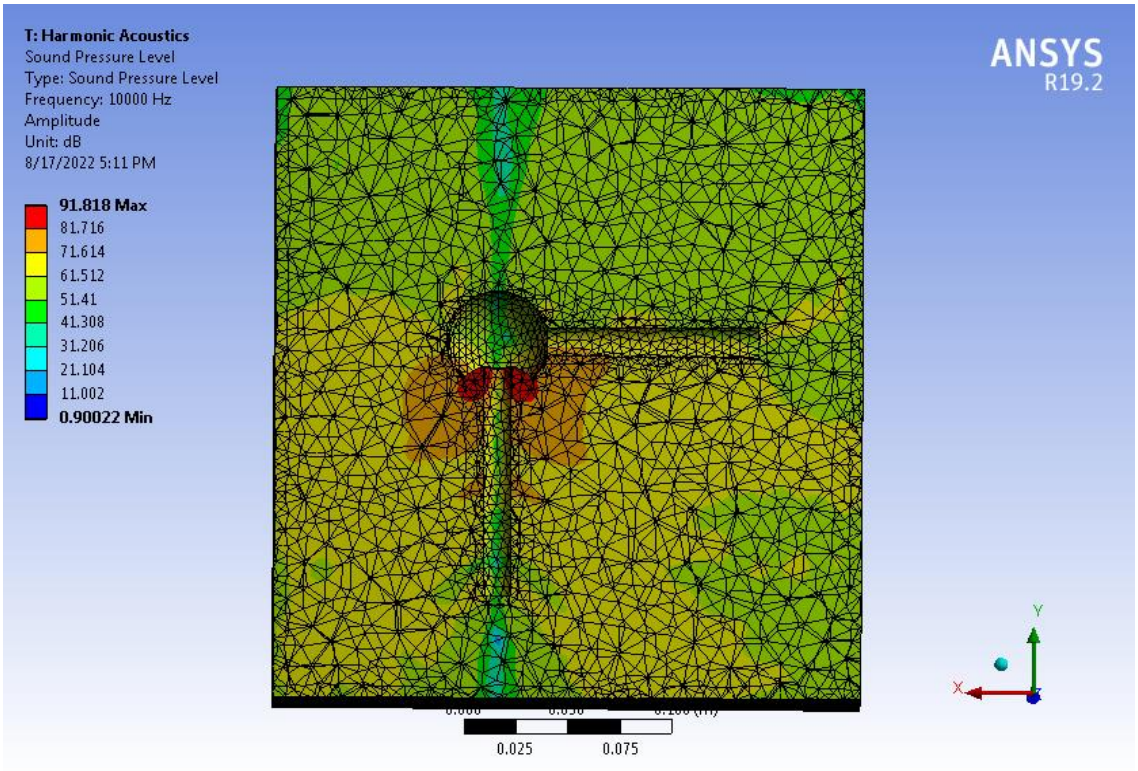

Fig. 10. *Sound pressure level (excitation Force = 10 N) - section in the middle of the enclosure*

THE ANNALS OF "DUNAREA DE JOS" UNIVERSITY OF GALATI
FASCICLE IX. METALLURGY AND MATERIALS SCIENCE
Nº. 4 - 2022, ISSN 2668-4748; e-ISSN 2668-4756
Article DOI: https://doi.org/10.35219/mms.2022.4.04

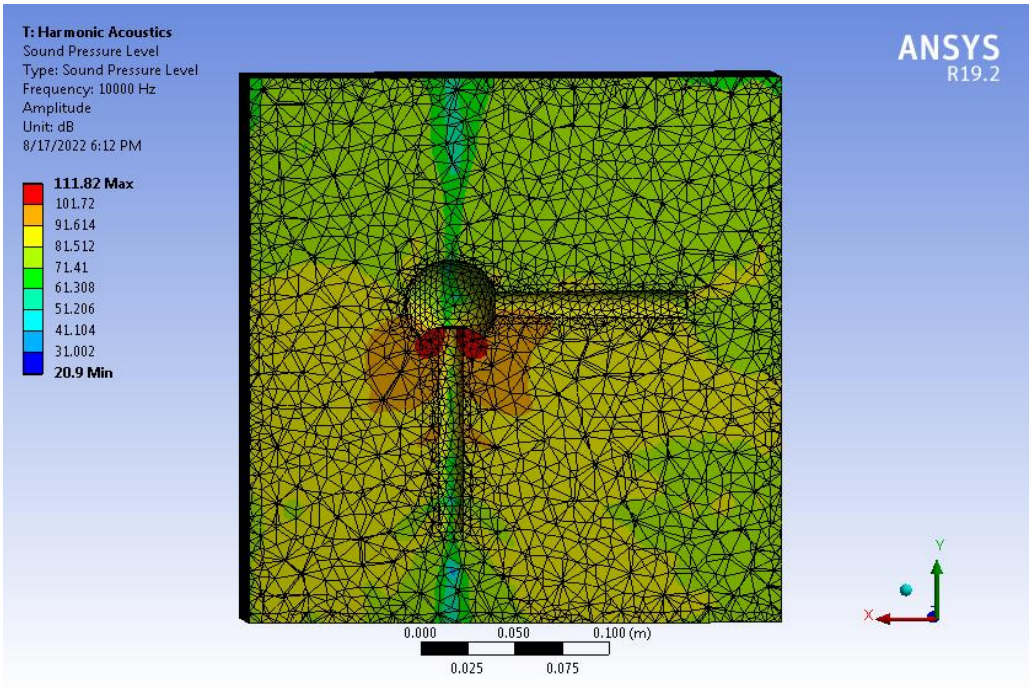

Fig. 11. *Sound pressure level (excitation Force = 100 N) - section in the middle of the enclosure*

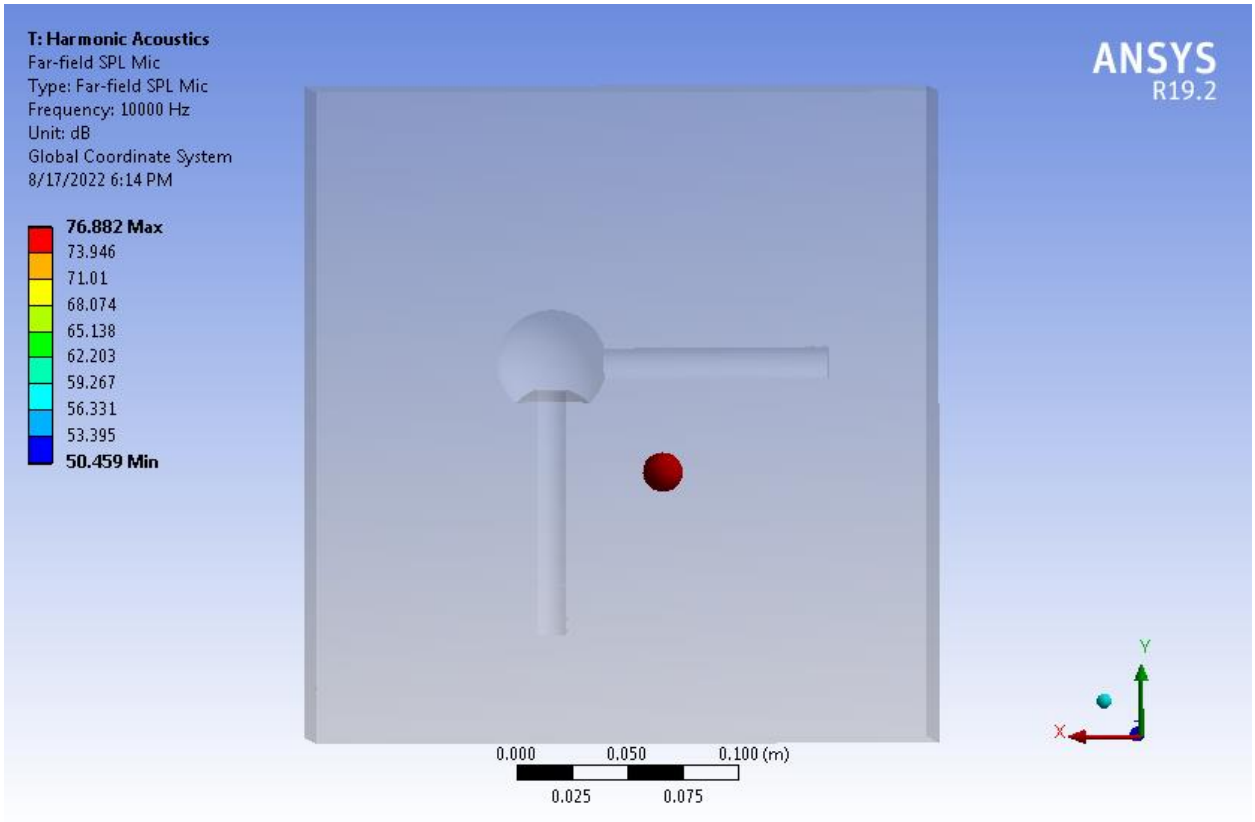

Fig. 12. *Microphone position -50 mm, -50 mm, 0 mm*

THE ANNALS OF "DUNAREA DE JOS" UNIVERSITY OF GALATI
FASCICLE IX. METALLURGY AND MATERIALS SCIENCE
Nº. 4 - 2022, ISSN 2668-4748; e-ISSN 2668-4756
Article DOI: https://doi.org/10.35219/mms.2022.4.04

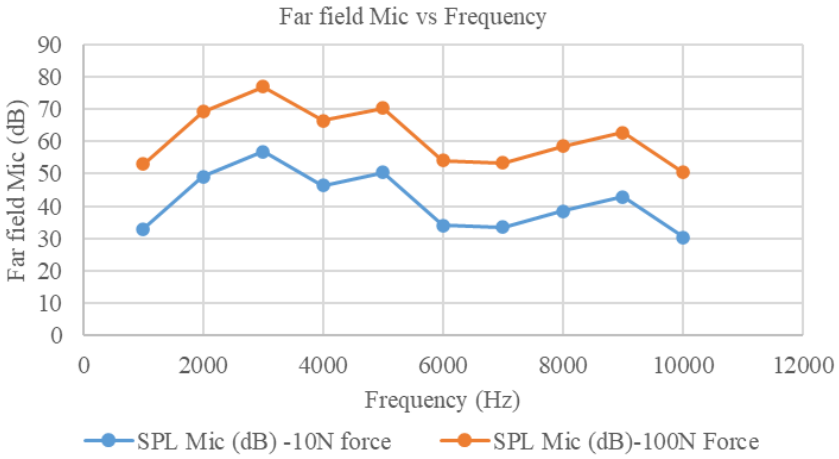

Fig. 13. *SPL Mic for Excitation in the position -50 mm, -50 mm, 0 mm for excitation force 10 N and 100 N*

4. Conclusions

Figures 10 and 11 show that the acoustic pressure level depends on the excitation intensity; in Fig. 10 the acoustic pressure level corresponds to the exciting force F = 10 N, and in Fig. 11 the acoustic pressure level corresponds to the exciting force F = 100 N.

For a certain position of the microphone and different excitations, the variation curves of the SPL are similar, but the acoustic pressure level depends on the intensity of the excitation force (Fig. 13).

References

[1]. ***, *ANSYS, Acoustic and Fluid-Structure Interaction*, A Revision 5.0 Tutorial, ANSYS, Inc., June 1992.
[2]. Aussal M., Alouges F., Bakry M., Serre G., *FEM-BEM applications in vibro-acoustics using GYPSLAB*, Proceedings of the 23rd International Congress on Acoustics, Aachen, Germany, 9-13 September 2019.
[3]. Muhammad Aliff, *AZIZI, Simulation of Acoustic Pressure Field Generated by Ultrasonic Transducer*, University of Queensland, 30 May 2019.
[4]. Boazu D., *The Influence of Small Clearances in the Spherical Joints of the Systems on their Dynamic Response*, The Annals of "Dunarea de Jos" University of Galati Fascicle V, Technologies in Machine Building, ISSN 2668-4829 (Print) 2668-4888 (Online), p. 11-18.
[5]. Jhabindra Prasad Ghimire, *Numerical investigation of noise generation and radiation from modular bridge expansion joint*, Doctoral thesis, Department of Civil and Environmental Engineering, Graduate School of Science and Engineering, Saitama University September, 2008.
[6]. Khan M. S., Cai C., Hung K. C., *Acoustics Field and Active Structural Acoustic Control Modeling in ANSYS*, https://citeseerx.ist.psu.edu/viewdoc/download?doi=10.1.1.470.9406&rep=rep1&type=pdf.
[7]. Carl Q. Howard, Benjamin S. Cazzolato, *Acoustic Analyses Using MATLAB® and ANSYS*, CRC Press, Taylor and Francis Group, International Standard Book Number-13: 978-1-4822-2327-9 (eBook - PDF).
[8]. Timo Ojanen, *Aero-vibro acoustic simulation of an ultrahigh-speed elevator*, Master of Science thesis, Tampere University, Faculty of Engineering Sciences on 12th August 2015.
[9]. Marco Oswald, Sandeep Sovani, *Aero-Vibro-Acoustics for Wind Noise Application*, DAGA 2015, Nurnberg.
[10]. Raffaele Panzella, *Advanced Finite Element Method for the Vibro-Acoustic Response of Plate-cavity Systems*, Master degree thesis, Politecnico di Torino, Department of Mechanical and Aerospace Engineering, April 2020.
[11]. ***, *Acoustics User's Guide*, Siemens Company. https://docs.plm.automation.siemens.com/data_services/resources/scnastran/2019_1/help/tdoc/en_US/pdf/acoustic.pdf.
[12]. ***, *Ansys Workbench*, version 19.2 documentation.

THE ANNALS OF "DUNAREA DE JOS" UNIVERSITY OF GALATI
FASCICLE IX. METALLURGY AND MATERIALS SCIENCE
Nº. 4 - 2022, ISSN 2668-4748; e-ISSN 2668-4756
Article DOI: https://doi.org/10.35219/mms.2022.4.05

A SENSITIVITY STUDY OF THE MAXIMUM STRESS IN A RUBBER CIRCULAR RING TO THE COEFFICIENT OF FRICTION USING FEM

Doina BOAZU
"Dunarea de Jos" University of Galati, Department of Mechanical Engineering, Romania
e-mail: doina.boazu@ugal.ro

ABSTRACT

The paper presents a sensitivity study of a rubber circular ring (O-Ring) depending on the value of the coefficient of friction (design parameter) between the ring and the surfaces between which it is mounted. The response value is the maximum von Mises stress in the rubber ring. The influence of temperature was not taken into account.

Through this sensitivity nonlinear analysis using finite element modeling, the correlation between Equivalent maximum Von Mises Stress and Friction coefficient can be established, determining a maximum stress level of the rubber ring to the friction coefficient. This relationship is important for the preload stage of the gasket functioning.

KEYWORDS: nonlinear analysis, rubber, contact, axisymmetric PLANE2D, friction

1. Introduction

O-rings are one of the most widely used seals today in industries like automotive, shipping, machinery, energy. They have simple design, easy to manufacture [5]. In the preload stage of functioning, O-ring follows the principle: when compressing an elastomer material between two surfaces, it changes its shape. During this procedure, the material is forced to restore its original shape and as a result, contact pressure is developing [5].

György Szabó and Károly Váradi in [5] investigated the behavior of an O-ring made of NBR rubber under extreme conditions. The effect of the extreme initial compression, operating pressure and extreme temperature conditions were examined.

The stresses in the O-rings made of elastomers have been investigated in recent years, the studies containing both simulations with finite elements and experimental determinations.

George A. F., Strozzi A. and Rich I. in reference [2] developed a finite element stress analysis computer program, FEMALES (an acronym for Finite Element Mechanical Analysis of Large Elastic Strain), at the University of Bologna, Italy. This program was developed specifically for the analysis of large deformations in elastomeric materials.

In [3] the authors studied the stresses and deformations of the compressed elastomeric O-rings, and Jeong-Hwan Nam, Jai-Sug Hawong, Dong-Chul Shin and Bruno R. Mose studied the stresses of O-rings using transparent type photo-elastic experiment [4].

The most common materials used for gaskets are Graphite, Rubber, Teflon, PTFE, and Compressed Non-Asbestos Fiber (CNAF). These are soft gaskets. It can be full face or inside bolt circle type [6, 7].

Non-Metallic gaskets can easily compress with low tension bolting.

These types of gaskets are used with low-pressure and also in low-temperature. However, graphite gasket can be used up to 500 Degree centigrade.

Rubber and elastomer gaskets are not used in hydrocarbon services but used in utility lines.

Non-Metallic gaskets are the cheapest and most easily available.

There are many different types of gaskets and each are classified by material, function, and fields of application. Typically, a gasket is manufactured with a soft, hyper-elastic material and placed between two separate surfaces.

The main types of Rubber Gasket Materials used are:

- Neoprene;

THE ANNALS OF "DUNAREA DE JOS" UNIVERSITY OF GALATI
FASCICLE IX. METALLURGY AND MATERIALS SCIENCE
Nº. 4 - 2022, ISSN 2668-4748; e-ISSN 2668-4756
Article DOI: https://doi.org/10.35219/mms.2022.4.05

- Nitrile (Buna-N);
- Ethylene Propylene Diene Monomer (EPDM);
- Silicone Rubber;
- Viton®;
- Styrene Butadiene Rubber (SBR).

2. Material properties of the structural elements

The structural elements and their dimensions are shown in Fig. 1a (according to a scheme presented in [9]). The circular rubber ring of the type shown in Fig. 1b is crushed between the two steel plates.

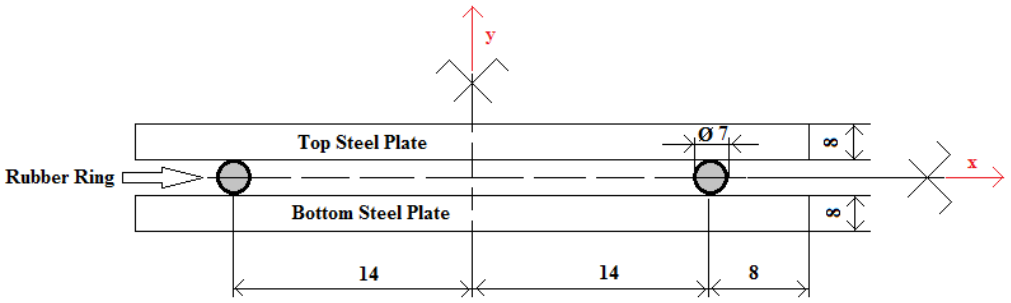

Fig. 1a. *Structural elements of the system* [9]

Fig. 1b. *Neoprene O-ring*

In the non-linear analysis, which involves frictional contact between the steel plates and the rubber ring, the behavior of the material of the steel plates was considered linear elastic (Structural Steel), while for the rubber ring the Neoprene Rubber having Neo-Hookean material model from the library of Ansys Workbench program was chosen (*Initial Shear Modulus Mu = 27104 (Pa) and Incompressibility Parameter D1 = 1.4429E-7 (Pa^-1)*); the Stress-Strain curves for this Neopren rubber is represented in Fig. 2.

The mechanical properties for the material of the Structural Steel plates are:

- Young Modulus 2.1e11 N/m^2;
- Poisson ratio 0.3.

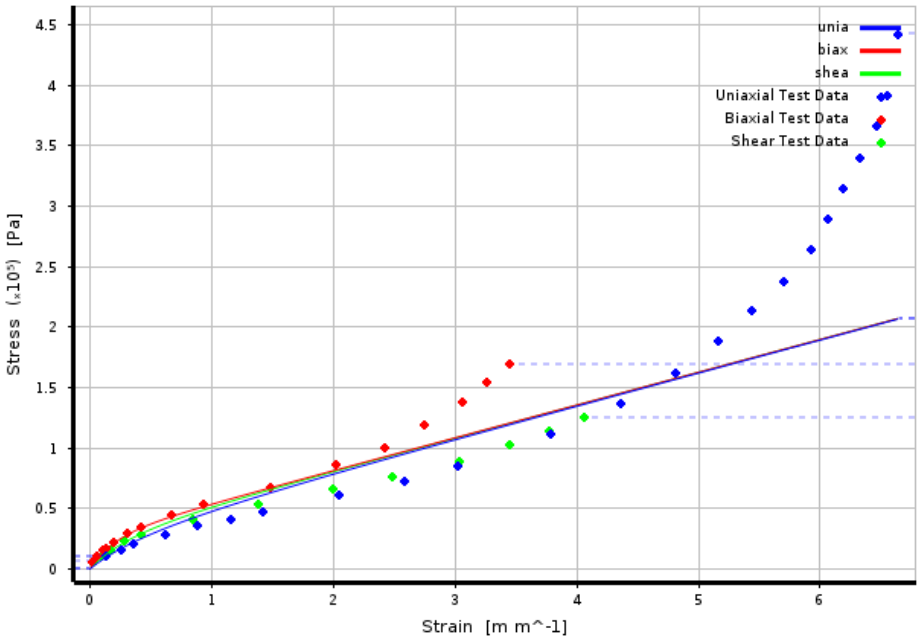

Fig. 2. *Stress-strain curves for Neoprene Rubber* [8]

THE ANNALS OF "DUNAREA DE JOS" UNIVERSITY OF GALATI
FASCICLE IX. METALLURGY AND MATERIALS SCIENCE
Nº. 4 - 2022, ISSN 2668-4748; e-ISSN 2668-4756
Article DOI: https://doi.org/10.35219/mms.2022.4.05

3. Finite element model and parametrization

The nonlinear model was created in the Ansys Workbench version 19.2 program in the Static Structural module.

In this study of sensitivity of circular ring response to the friction coefficient value, the friction coefficient was considered the design variable and the maximum von Mises stress in the rubber ring was considered the response quantity.

The elements of the structure are shown in Fig. 1a. The rubber ring is placed between the two circular steel plates. Due to the double symmetry, the model with finite elements can only be made on a quarter, imposing specific conditions in the planes of symmetry (zero displacements outside the planes of symmetry).

The model can therefore be made on a quarter with axisymmetric 2D elements, imposing *asymmetric* contact conditions with friction between the circular surface of the rubber ring (*Contact*) and the steel plate (*Target*) Fig. 3. Since the contact is made in 2D, it is between a circle and a line and for the non-linear calculation, the option *Interface treatment* > *Adjust to Touch* is activated. For the non-linear calculation, the incremental calculation and large displacement calculation options are activated.

The finite element discretization is presented in Fig. 4.

The finite element used in the discretization is PLANE183 with axisymmetric option (Fig. 5) [8].

Plane183 is a higher order 2D, 8-node per element with has quadratic displacement behavior. This element is more accurate in modeling curved boundaries. The element Plane183 has two DOF – displacement in x and y direction.

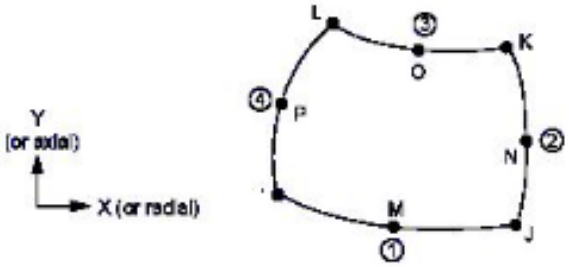

Fig. 5. *The element PLANE183 with axisymmetric option* [8]

For the nonlinear analysis, it is advantageous to apply the load in the form of prescribed displacement (a half of the O-ring radius), the corresponding force being evaluated as a reaction in the imposed boundary.

The boundary conditions are presented in Fig. 6. These boundary conditions are:

- A - Displacement on X direction (radial) – Free and Displacement on Y direction (axial) – Zero;
- B - Displacement on X direction (radial) – Zero and Displacement on Y direction (axial) – Free;
- C - Prescribed displacement on Y direction – 1.5 mm and Displacement on X direction (radial) – Zero.

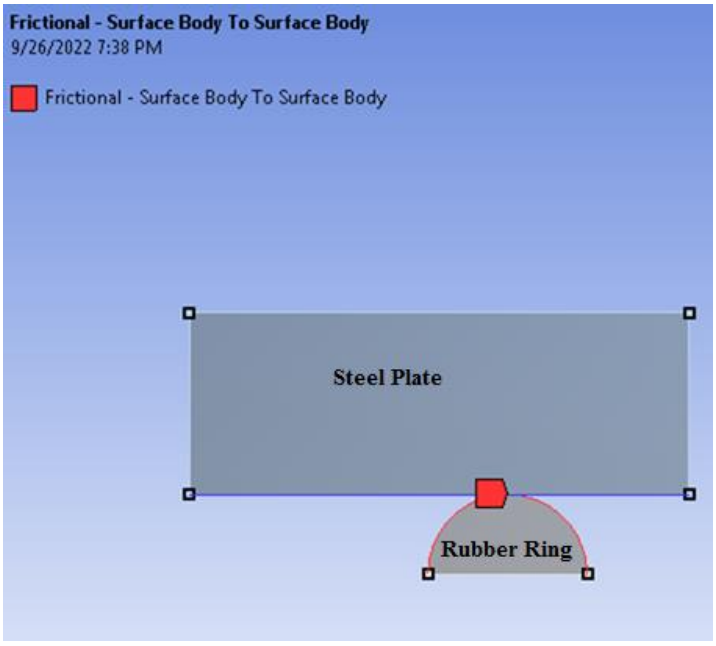

Fig. 3. *Contact surfaces*

THE ANNALS OF "DUNAREA DE JOS" UNIVERSITY OF GALATI
FASCICLE IX. METALLURGY AND MATERIALS SCIENCE
Nº. 4 - 2022, ISSN 2668-4748; e-ISSN 2668-4756
Article DOI: https://doi.org/10.35219/mms.2022.4.05

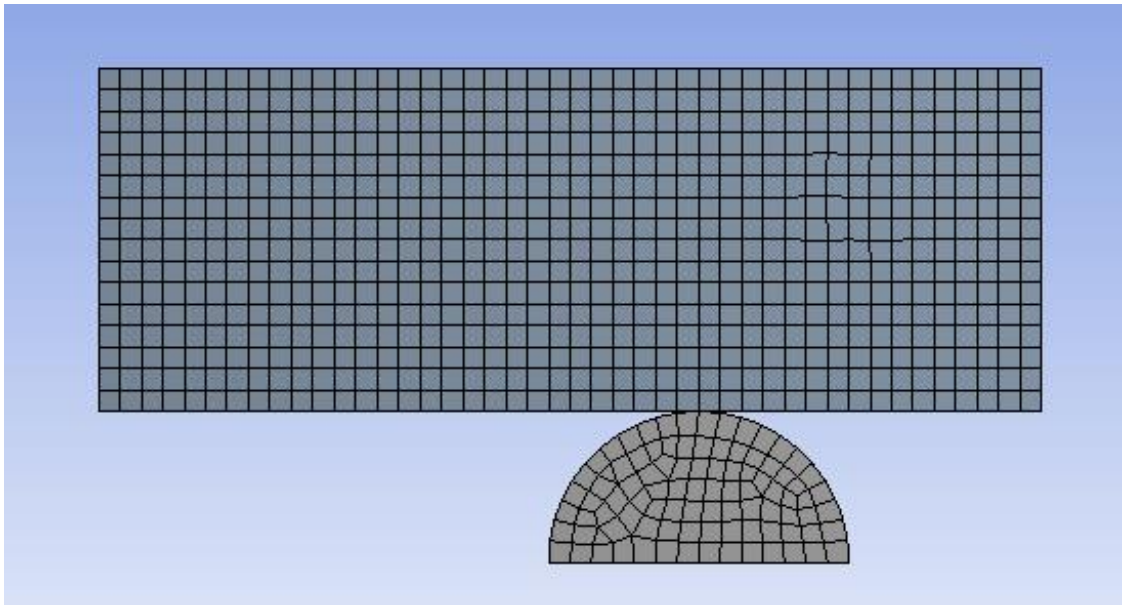

Fig. 5. *Mesh using PLANE183 (size of element 0.5 mm)*

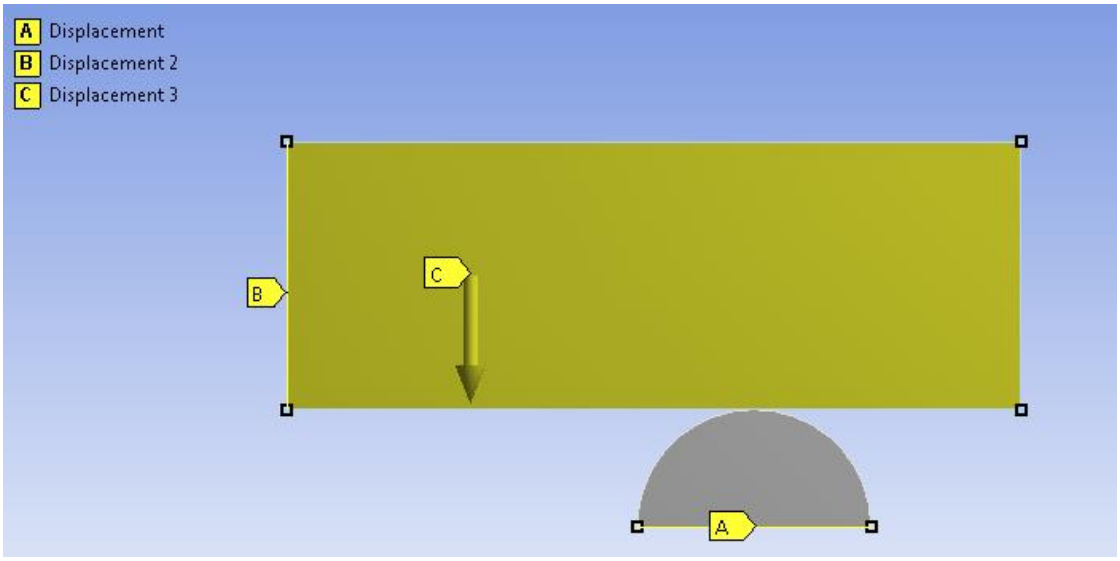

Fig. 6. *Boundary conditions*

4. Results and discutions

The results obtained for the friction coefficient value of 0.01 are presented in Fig. 7 and Fig. 8.

The distribution of total displacements is given in Fig. 7, and the von Mises stress distribution is given in Fig. 8. The maximum stress appears in the centre of the rubber ring.

Schematic Project in the Ansys Workbench analysis program is presented in Fig. 9.

In the sensitivity study, the value of the friction coefficient as a parameter varies between 0.01 and 0.25 (Fig. 10). In Fig. 10 - Design of experiments, both the values of the friction coefficient (variable design) and the corresponding response values of the maximum von Mises stress can be found.

To obtain the Response Surface, the Response Surface Optimization Module was used, and then to obtain the correlation of the parameters, the Parameters Correlations module was used (Fig. 9).

The graphic representation of Equivalent maximum Von Mises Stress vs Friction coefficient is given in the Fig. 11.

The correlation between Equivalent Maximum Von Mises Stress vs Friction coefficient for the linear and quadratic trends has the graphic representation in the Fig. 12, with the correlation functions and the correlation coefficients in Table 1.

THE ANNALS OF "DUNAREA DE JOS" UNIVERSITY OF GALATI
FASCICLE IX. METALLURGY AND MATERIALS SCIENCE
No. 4 - 2022, ISSN 2668-4748; e-ISSN 2668-4756
Article DOI: https://doi.org/10.35219/mms.2022.4.05

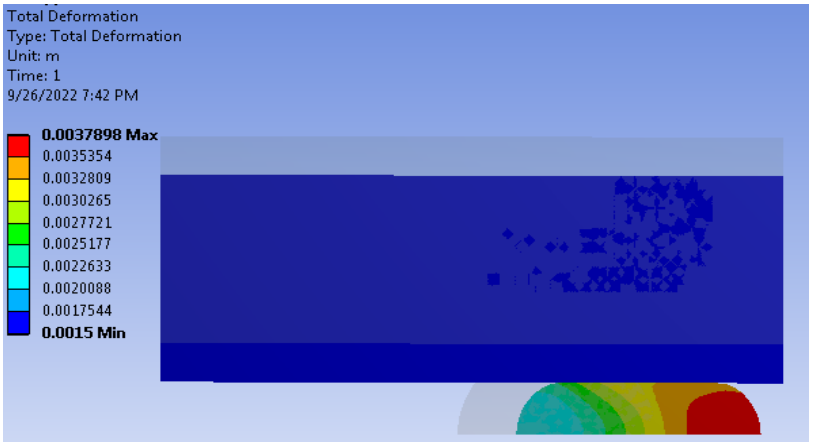

Fig. 7. *Total Deformation distribution (over the initial position)*

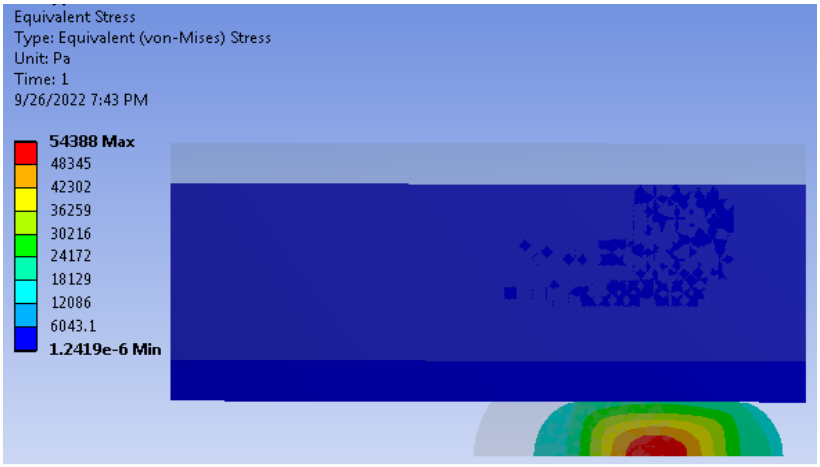

Fig. 8. *Distribution of von Mises stress (over the initial position)*

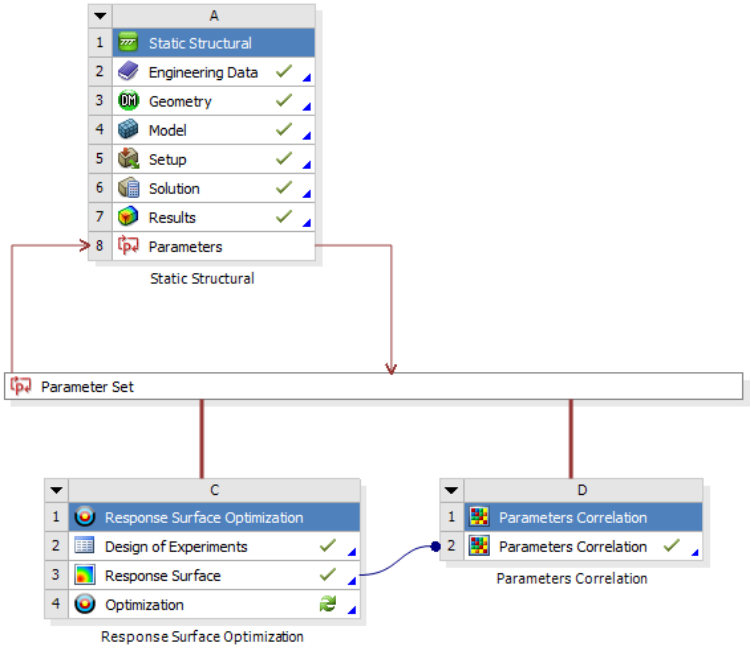

Fig. 9. *Project schematic*

THE ANNALS OF "DUNAREA DE JOS" UNIVERSITY OF GALATI
FASCICLE IX. METALLURGY AND MATERIALS SCIENCE
Nº. 4 - 2022, ISSN 2668-4748; e-ISSN 2668-4756
Article DOI: https://doi.org/10.35219/mms.2022.4.05

Table of Outline A2: Design Points of Design of Experiments

	A	B	C
1	Name	P1 - Frictional - Surface Body To Surface Body Friction Coefficient	P2 - Equivalent Stress 2 Maximum (Pa)
2	1 DP 0	0.01	54388
3	2 DP 1	0.05	64085
4	3 DP 2	0.09	79608
5	4 DP 3	0.13	90890
6	5 DP 4	0.17	99057
7	6 DP 5	0.21	1.0493E+05
8	7 DP 6	0.25	1.0783E+05
*	New Design Point		

Fig. 10. *Design of experiments*

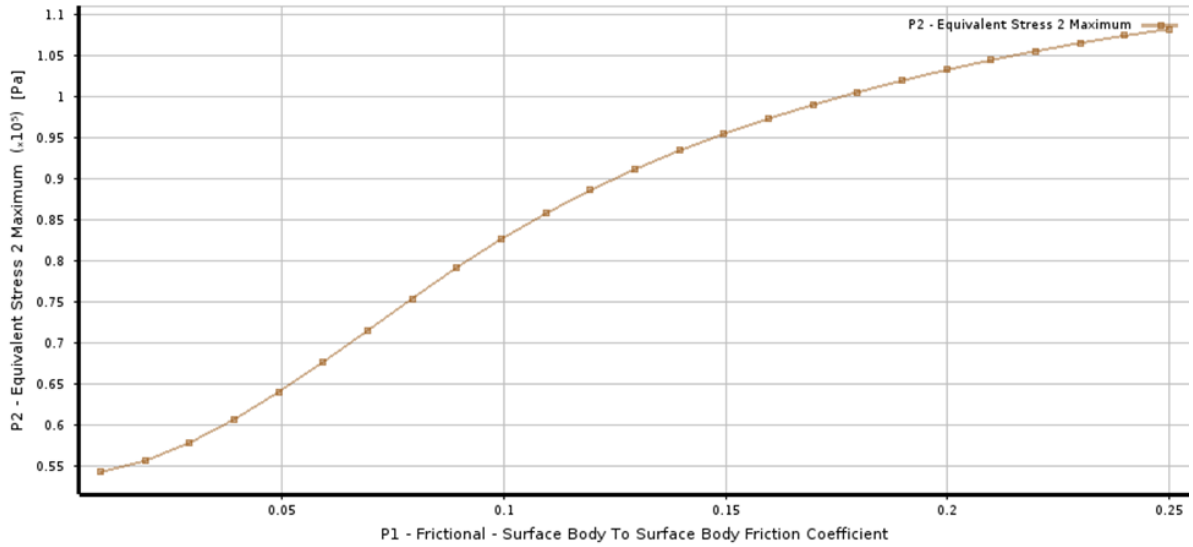

Fig. 11. *Equivalent maximum Von Mises Stress vs Friction coefficient*

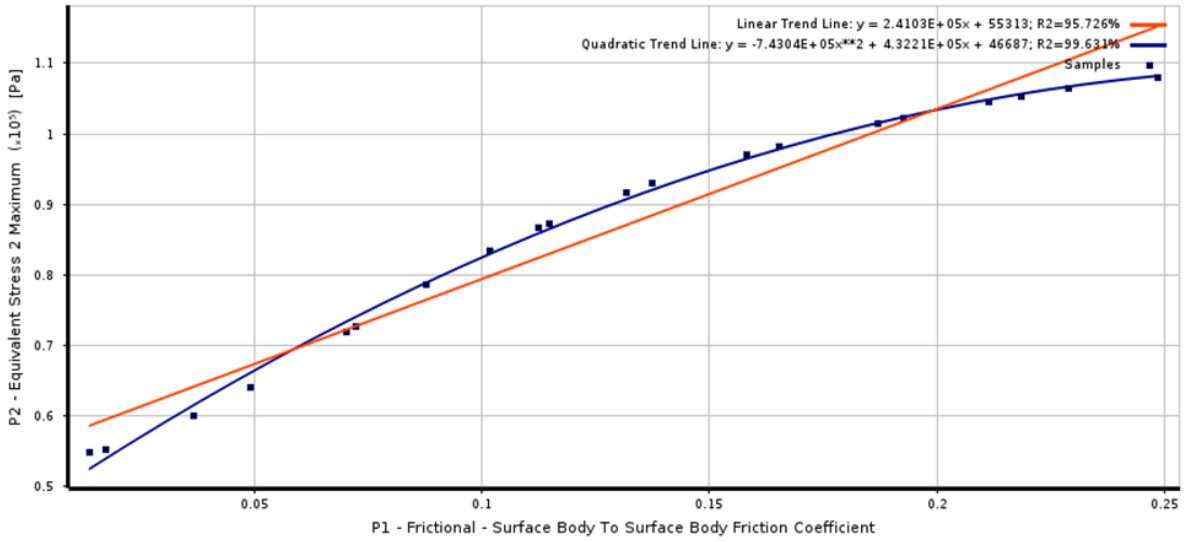

Fig. 12. *Correlation Equivalent maximum Von Mises Stress "y" vs Friction coefficient "x" for linear and quadratic trends*

THE ANNALS OF "DUNAREA DE JOS" UNIVERSITY OF GALATI
FASCICLE IX. METALLURGY AND MATERIALS SCIENCE
N°. 4 - 2022, ISSN 2668-4748; e-ISSN 2668-4756
Article DOI: https://doi.org/10.35219/mms.2022.4.05

Table 1. *Trend lines for sensitivity study*

Trend Lines	Function	Correlation
Linear	$y = 2.41e5 * x + 55313$	R = 95.726%
Quadratic	$y = -7.43e4 * x^2 + 4.322e5 * x + 46687$	R = 99.631%

5. Conclusions

If the material curves for the O-ring are known, the dependence curves of Equivalent maximum Von Mises Stress vs Friction coefficient can be obtained from the sensitivity analysis with finite elements.

Having the dimensions of the elements of the system and the value of the coefficient of friction between the O-ring and the steel surface and performing a sensitivity analysis, the maximum von Mises stresses in the centre of the O-ring can be established.

A better correlation function between Equivalent maximum Von Mises Stress and the Friction coefficient is that corresponding to quadratic trend (Table 1) and this relationship is very important for the preload stage of the O-ring loading.

The maximum von Mises stress for this preload stage of loading of the O-ring should be below the value of 25 MPa.

References

[1]. Brice N., Cassenti Alexander Staroselsky, *Deformation and stability of compressible rubber O-rings*, International Journal of Mechanical and Materials Engineering, vol. 12, article number: 5, 2017.
[2]. George A. F., Strozzi J. A., Rich I., *Stress fields in a compressed unconstrained elastomeric O-ring seal and a comparison of computer predictions and experimental results*, Tribology International, vol. 20, issue 5, p. 237-247, October 1987.
[3]. Itzhak Green, Capel English, *Stresses and deformation of compressed elastomeric O-ring seals*, 14th International Conference on Fluid Sealing, Firenze, Italy, 6-8 April 1994.
[4]. Jeong-Hwan Nam, Jai-Sug Hawong, Dong-Chul Shin, Bruno R. Mose, *A study on the behaviors and stresses of O-ring under uniform squeeze rates and internal pressure by transparent type photoelastic experiment*, Journal of Mechanical Science and Technology, 25 (9), DOI: 10.1007/s12206-011-0713-4, 2011.
[5]. György Szabó, Károly Váradi, *Failure Mechanism of O-Ring Seals under Extreme Operating Conditions*, Modern Mechanical Engineering, vol. 8, no. 1, February 2018.
[6]. ***, https://www.linkedin.com/pulse/main-causes-failure-o-ring-seals-permanent-lisa.
[7]. ***, https://www.callapg.com/blog-the-9-most-common-types-of-gaskets.
[8]. ***, *Ansys Workbench*, version 19.2 documentation.
[9]. ***, Cosmos/M, version 2.7 documentation.

THE ANNALS OF "DUNAREA DE JOS" UNIVERSITY OF GALATI
FASCICLE IX. METALLURGY AND MATERIALS SCIENCE
N°. 4 - 2022, ISSN 2668-4748; e-ISSN 2668-4756
Article DOI: https://doi.org/10.35219/mms.2022.4.06

RESEARCH ON THE IMPROVEMENT OF THE MECHANICAL PROPERTIES OF ALUMINUM ALLOYS OF THE SERIES Al-Zn-Mg-Cu BY HEAT PROCESSING

Marian-Iulian NEACȘU
"Dunarea de Jos" University of Galati, Romania
e-mail: mneacsu@ugal.ro

ABSTRACT

The paper presents the results of the research carried out on an Al alloy from the 7000 series. The material was subjected to several variants of thermal and thermomechanical processing. Research has been conducted on various artificial aging temperatures of the material in combination with various aging time values. Some samples were also subjected to plastic deformation, between quenching and artificial aging, in order to determine the influence of this deformation on the values of the final mechanical properties.

KEYWORDS: aluminum alloy, solution hardening, artificial aging, plastic deformation

1. Introduction

The high mechanical properties, which characterize the Al-Zn-Mg-Cu system alloys, are obtained by plastic deformation and hardening thermal treatment, the last operation being performed under conditions similar to those applied to the other light alloys that can be hardened by precipitation, respectively putting in solution, quenching in water and artificial aging [1].

Establishing the technological elements that determine the heat treatment of Al-Zn-Mg-Cu type alloys required a large volume of experiments, the working conditions having a direct influence on the material's resistance to stress cracking corrosion [2].

In parallel with the classical processes, the application possibilities of thermo-mechanical treatment, isothermal treatment and thermal treatment in steps to these alloys were studied, on the one hand, and on the other hand, the mechanical properties that could be obtained in each case.

During the thermal treatment of aluminum alloys, supersaturation of the solid solution (putting in solution), maintenance of the supersaturated solid solution at ambient temperature (quenching), precipitation, in the mass of the supersaturated solid solution, of the excess phases, in the form of fine and uniformly distributed particles (aging), which ensure the hardening of the alloy [2].

The solution temperature Ts must be close to the melting temperature Tt of the alloy; practically it is accepted: Ts = Tt - 30 °C. The duration of the operation is variable depending on the type of alloy, the casting conditions, the geometry of the part and the thickness of its walls. During the solvation operation there is a substantial increase in the number of vacancies (from 10^{-4} to 10^{-3}), due to the rise in temperature [3].

The effect of quenching depends on the type of alloy and the rate of quenching; the last parameter is conditioned by the thickness of the part walls and the cooling medium used. Tempering allows, at normal temperature, to maintain the number of vacancies from the solution temperature.

Since the transition of the alloy from the hardened state to the aged state is not instantaneous, intermediate, metastable states appear in the material during the operation.

If the temperature does not exceed the ambient one, in the hardened material there is a monophasic, sub microscopic separation of atoms of the phase dissolved in excess in the form of coherent precipitates, which are deposited in the material of the basic solid solution recipe, as agglomerations; sites enriched in separate atoms form the GUINIER-PRESTON zones [4, 5].

The changes that occur because of this in the arrangement of the atoms in the network of the basic solid solution produce a hardening of it called cold hardening.

At slightly higher temperatures, metastable precipitates of an intermediate phase appear, which

THE ANNALS OF "DUNAREA DE JOS" UNIVERSITY OF GALATI
FASCICLE IX. METALLURGY AND MATERIALS SCIENCE
No. 4 - 2022, ISSN 2668-4748; e-ISSN 2668-4756
Article DOI: https://doi.org/10.35219/mms.2022.4.06

differ, from the point of view of the crystalline recipe, both from that of the basic solid solution and from that of the stable precipitation phase [6, 7].

Along with the appearance of this precipitation process, a significant increase in hardness is also manifested, called hot hardening.

If the temperature continues to rise, the stable precipitation phase is finally reached. The decrease in hardness, which is often found at the end of this process, is known as over aging.

Cold hardening can take place either before or simultaneously with heat hardening.

There are aluminum alloys, such as those of the Al-Cu-Mg type, in which the introduction of dislocations, through the cold plastic deformation of the hardened material, increases the aging speed and ensures obtaining higher quality figures than those in which it would have arrived through aging, under similar conditions of the undeformed witness; the phenomenon is explained by the nucleating action of dislocations on the hardening phases.

In other types of alloys, including those in the Al-Zn-Mg-Cu group, the effect of the cold deformation of the hardened material, on the mechanical properties obtained after aging, is practically nil or even negative [4, 8].

The explanation of this different behavior lies in the fact that the hardening of the alloys is essentially due to the formation of the Guinier-Preston zones during the artificial aging heat treatment and not due to the reduction of dislocation mobility.

2. Experimental conditions

The samples subjected to research were made from the alloy of chemical composition presented in Table 1.

Table 1. *Chemical composition of the studied alloy*

The chemical element	**Zn**	**Mg**	**Cu**	**Mn**	**Cr**	**Ti**	**Fe**	**Si**	**Al**
%	6	2	1	0.15	0.5	0.10	0.4	0.4	rest

The minimum mechanical properties of the material, which had to be obtained after heat treatment, are those shown in Table 2.

Table 2. *The imposed mechanical properties*

Rm, MPa	**$R_{p0,2}$, MPa**	**HB, MPa**	**A_5, %**
500	400	160	8

The alloy was developed in electric furnaces. The alloying was done in induction furnaces, casting in metal shells or by the semi-continuous method, and the homogenization of the cast bars in electrically heated furnaces, part of the semi-continuously cast bars were extruded from Φ135 mm to Φ 80 mm.

The heat treatment of the samples and parts was done in electric resistance furnaces with temperature regulation between the limits: ±10 °C at around 550 °C and ±2 °C at around 170 °C.

Due to the large number of alloying elements, it contains, the investigated alloy has a complex structure, which from the point of view of the way of presentation in the microscopic examination depends on its condition. The phases that can be found at ambient temperature in Al-Zn-Mg-Cu type alloys can be synthesized as follows:

- complex solid solution α of Zn, Mg and Cu in Al and solid solution β (Zn-Mg);
- defined binary or ternary compounds: Al_2Cu, Al_3Fe and $T(Al_2Mg_3Zn_3)$;
- binary eutectic: (α + Al_2Cu), (α + T) and (α + Al_3Fe).

Figure 1 shows the microstructure, at room temperature, of a sample taken from a semi-continuously cast bar.

If the cast raw alloy is heated to about 460 °C, so close to its melting point, only Al, α solid solution and β compound (Zn Mg) exist in its structure.

In the specialized literature, the prescriptions for the heat treatment of Al-Zn-Mg-Cu type alloys are as follows [4, 5]:

- the solution temperature is in the range of 450-470 °C;
- the heating duration, which depends on the geometry and size of the piece, must be chosen so that the entire metal mass has a uniform temperature;
- the tempering of the piece must be done within 15 s maximum after leaving the mouth of the furnace; in practice, sheets and profiles are quenched in water at room temperature, while forged parts are quenched in warm water (50-70 °C), in order to reduce the stresses generated by too energetic cooling. Before artificial aging, the hardened parts are left to rest for about 16 h; if this term is not respected, the parts hardened by heat treatment have about 10% lower mechanical properties;

THE ANNALS OF "DUNAREA DE JOS" UNIVERSITY OF GALATI
FASCICLE IX. METALLURGY AND MATERIALS SCIENCE
Nº. 4 - 2022, ISSN 2668-4748; e-ISSN 2668-4756
Article DOI: https://doi.org/10.35219/mms.2022.4.06

- working parameters, in the case of artificial aging, depend on the chemical composition of the alloy; generally, the temperature varies between 105 °C and 200 °C, and the duration between 4 and 24 h;
- in order to reduce the duration of the artificial aging process, step aging is sometimes applied.

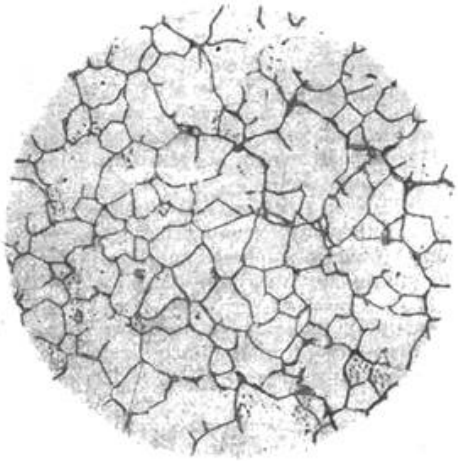

Fig. 1. *Microstructure of a cast bar; Magnification x250, Attack: 0.5 HF* [4]

Figures 2, 3 and 4 show diagrams given in the literature regarding the variation of the mechanical properties of some semi-finished products from Al-Zn-Mg-Cu type alloys used in the USA and Switzerland, depending on heat treatment parameters.

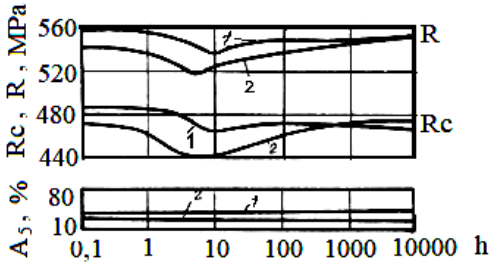

Fig. 2. *The influence of time between solution quenching and artificial aging of 7075 alloy sheets, on the mechanical properties aged at 120 ºC/24 hours (curves 1) and at 135 ºC/12 hours (curves 2)* [4]

For the thermal treatment of the studied alloy, furnaces with electric resistances were used, equipped with devices for automatic temperature regulation and internal air recirculation and with tempering tanks that allow the water to be heated to about 50 °C.

In the framework of the research, samples taken from extruded bars with cores 4 and 8 were used; the chemical composition of the alloy being within the prescribed limits.

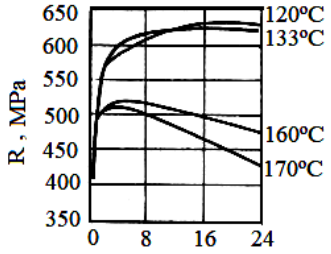

Fig. 3. *The influence of artificial aging parameters on mechanical strength for the Swiss alloy PERUNAL* [4]

The experimental researches were carried out after 6 variants of thermal processing according to the schemes in Figures 4, 5, 6, and 7. In all cases, the placing in the solution was carried out at 460 ± 5 °C/8 h, and the final cooling in the open air.

Within the six variants studied, the artificial aging was done in classical conditions (I_A and I_B), isothermal (II), in two stages (III and IV) and in three stages (V).

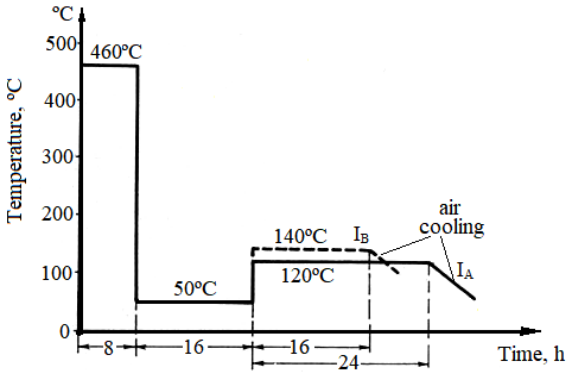

Fig. 4. *Treatment scheme according to variants I_A and I_B*

Treatment parameters for variants I_A and I_B were:

- putting in solution at 460 °C/8 hours;
- quenching in water at a temperature of 50 °C;
- artificial aging at 120 °C/24 hours (I_A);
- artificial aging at 140 °C/16 hours (I_B);
- air cooling.

THE ANNALS OF "DUNAREA DE JOS" UNIVERSITY OF GALATI
FASCICLE IX. METALLURGY AND MATERIALS SCIENCE
No. 4 - 2022, ISSN 2668-4748; e-ISSN 2668-4756
Article DOI: https://doi.org/10.35219/mms.2022.4.06

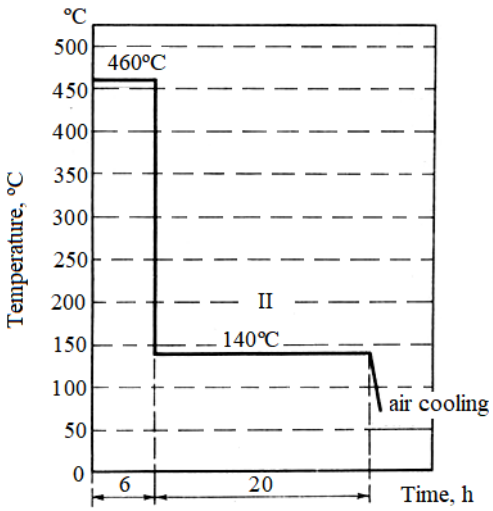

Fig. 5. *Isothermal treatment scheme according to variant II*

Treatment technological parameters for variant II were:

- putting in solution at 460 °C;
- quenching in water at a temperature of 50 °C;
- artificial aging at 140 °C/20 hours;
- cooling in the air.

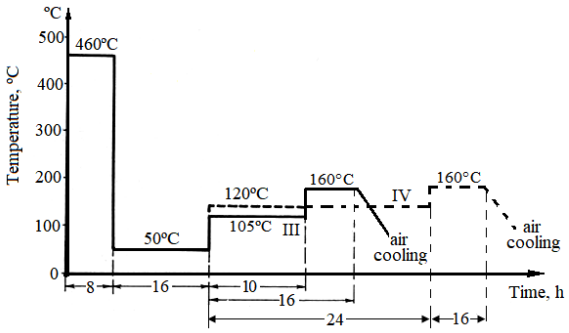

Fig. 6. *Stepwise treatment scheme according to variants III and IV*

For variants III and IV, the research consisted of the following:

- putting in solution at 460 °C/8 hours;
- quenching in water at a temperature of 50 °C;
- artificial aging at 120 °C/24 hours (I_A);
- artificial aging at 140 °C/16 hours (I_B);
- air cooling.

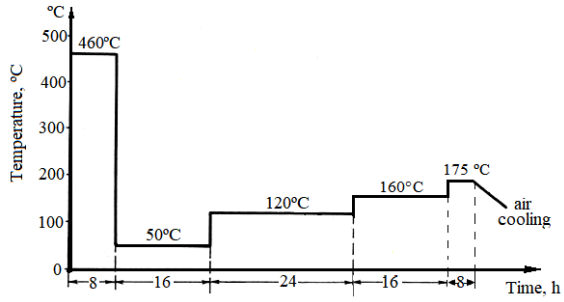

Fig. 7. *The two-stage treatment scheme according to the V variant*

Variant of treatment consisted of the following sequence of specific technological operations:

- placing in solution 460 ± 5 °C/8 hours;
- water quenching at 50 °C;
- artificial aging 120 °C/24 hours +160 °C/16 hours + 175 °C/6 hours;
- air cooling.

The results obtained following the application of these treatment variants are illustrated in Figures 8 for Mechanical Strength and Yield Strength, 9 for Brinell hardness and 10 for Elongation at break.

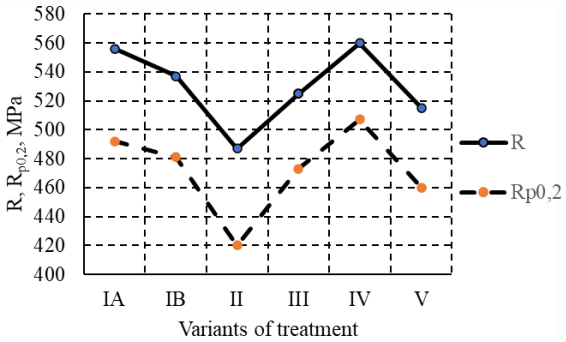

Fig. 8. *Variation of mechanical strength and yield strength depending on the treatment option adopted*

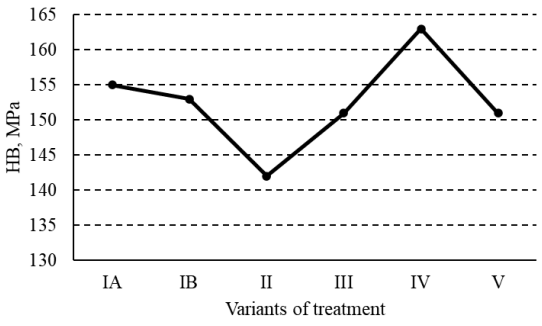

Fig. 9. *Brinell hardness variation depending on the treatment option adopted*

THE ANNALS OF "DUNAREA DE JOS" UNIVERSITY OF GALATI
FASCICLE IX. METALLURGY AND MATERIALS SCIENCE
No. 4 - 2022, ISSN 2668-4748; e-ISSN 2668-4756
Article DOI: https://doi.org/10.35219/mms.2022.4.06

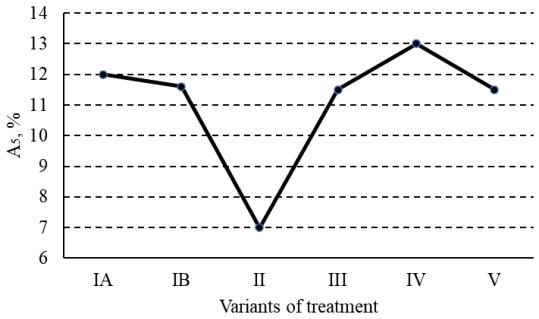

Fig. 10. *The variation of elongation at break depending on the treatment option adopted*

From these images it can be seen that the best properties are obtained in the case of thermal processing according to variants IA and IV.

During the tests, the influence of the cold plastic deformation of the hardened alloy, as well as the amount of time between the end of the quenching operation and the start of the aging process, on the mechanical properties of the artificially aged material was also monitored.

In the samples that in the hardened state had been cold forged (plastically deformed) at cores 4 and 8, mechanical properties were obtained, after artificial aging, about 10% lower compared to those found in the samples that did not undergo this deformation intermediate plastic.

It was thus practically verified that the hardening by heat treatment of Al-Zn-Mg-Cu type alloys is mainly due to the formation of Guinier-Preston zones.

A similar reduction in the mechanical properties of the artificially aged material is also found in the case when the duration of keeping the material in the hardened state is less than 16 h.

3. Conclusions

The factors that condition the obtaining of high mechanical properties of the studied Al-Zn-Mg-Cu alloy, after the thermal hardening treatment, can be concretized as follows:

- strict compliance with the prescribed heating temperatures and durations, a tempering carried out in max. 15 s from removing the part from the oven and starting the artificial aging only after the time interval indicated above (16 h);
- the use of precise furnaces in terms of working temperature tolerances.

In the case of the studied alloy, the optimal heat treatment parameters resulting from the tests performed are:

- solution tempering at a temperature of 460 °C with a holding time of 8 h;
- cooling (quenching) in hot water at 50 °C;
- artificial aging in stages: the first stage was carried out at a temperature of 105 °C with a holding time of 10 h followed by a second stage at a temperature of 160 °C and an aging time of 6 h.

Cold plastic deformation of Al-Zn-Mg-Cu quenched alloy was found not to improve the mechanical properties after artificial aging.

References

[1]. Alexandru I., *Ştiinţa materialelor metalice*, Editura Didactică şi Pedagogică, Bucureşti, 1996.
[2]. Aloman A., *Fazele şi compoziţia chimică a materialelor*, Editura Bren Bucureşti, 2001.
[3]. Aloman A., *Structura materialelor*, Editura AGIR Bucureşti, 2000.
[4]. Stoicănescu M., Giacomelli I., *Influenţa tratamentului termomagnetic asupra proprietăţilor aliajelor de aluminiu plasticizabile şi de turnare*, Revista de turnătorie, 4/2001.
[5]. M. H. Jakobs, *TALAT–Aluminiums Materials Technology, Aluminium Metallurgy*, 1204 Precipitation Hardening, University of Birmingham, 1999.
[6]. Bane M., *et al.*, *Analiza structurii materialelor metalice*, Editura Tehnică, Bucureşti, 1991.
[7]. Ceylan M., *et al.*, *The influence of the cooling rate on the microstructure of Al- Cu- Si, Al- Si and Al-Zn alloys*, Journal of Materials Processing Technology 65, p. 41-51, 1997.
[8]. Zheng J. B., Shu X. D., Zhang S., Lu Q. Y., *Effect of process parameters on forming quality of Mg alloy(MZ21)-Al alloy(7075) composite pipe*, Metalurgija 61, no. 3-4, 2022.

THE ANNALS OF "DUNAREA DE JOS" UNIVERSITY OF GALATI
FASCICLE IX. METALLURGY AND MATERIALS SCIENCE
Nº. 4 - 2022, ISSN 2668-4748; e-ISSN 2668-4756
Article DOI: https://doi.org/10.35219/mms.2022.4.07

THE INFLUENCE OF THE WEAR OF THE REFRACTORY LINING, OF THE TUNDISH, ON THE QUALITY OF THE STEEL

Beatrice Daniela TUDOR
"Dunarea de Jos" University of Galati, Romania
e-mail: beatrice.tudor@ugal.ro

ABSTRACT

The quality of steel and continuously cast semi-finished products largely depend on the degree and control of the interaction between slag, gas, and refractories, with the steel melt. In this work, through the analysis of some samples from a used refractory lining of a tundish, with the help of optical microscopy, the wear of the refractory layer was highlighted, due to the erosion and infiltration of steel microparticles into the pores of the lining. The examination of the samples was carried out in the interface area, metal-shotcrete, shotcrete-concrete, and the area with refractory concrete.

KEYWORDS: tundish, erosion, infiltration, refractory lining

1. Introduction

The tundish represents the link between the steel production, in the converter and its continuous casting process. The quality of steel and continuously cast semi-finished products largely depend on the degree and control of the interaction between slag, gas, and refractories, with the steel melt.

The elimination of impurity of the steel, with the atmosphere, or with particles from the refractory lining, as well as the technologies for making the refractory lining of the distributor, have led to an increase in the resistance of the refractory lining, at the number of castings, and an increase in the purity of the steel, from the point of view of the inclusions [1, 3].

In the last decade, alumina-graphite (ALG) refractories have emerged as a standard solution, for operations from the tundish. Alumina-graphite refractories offer good resistance to thermal shock and increased resistance to contact with metal and slag.

To prevent melt suction through the pores of the tundish walls, a good thickness and density of the refractory, as well as a low permeability, are required. Oxidation is controlled by applying glazes to the interior and exterior surfaces. The tundish lining is important in the technological process. The lining should be inert and not contribute to the growth of exogenous inclusions in the steel [2, 8].

2. The refractory lining of the tundish

The refractory materials used to line the tundish are often overlooked, in the importance of the technological flow. The realization of the refractory lining must take into account the following considerations:

- refractory materials are materials that wear out, and the user must take into account all the factors that influence the quality of the refractory material, in order to increase their lifespan, and the impact on costs;
- the chemical composition of the refractory material can be variable, because it is composed of multicomponent raw materials, therefore it should be tested;
- the quality of the refractory lining is of particular importance and is also influenced by the fixing method and the additives used;
- the temperature variation causes cracks for the refractory material too, lose its resistance, break and thus contribute to shortening the life of the tundish;
- failures of the refractory lining must be evaluated, taking into account all the data related to materials, operations, maintenance and the use of consumables, such as fluxes and alloys, to determine the true cause, which leads to the appearance of the defect.

Typically, the tundish liner is composed of three layers. The working liner is made of high MgO

THE ANNALS OF "DUNAREA DE JOS" UNIVERSITY OF GALATI
FASCICLE IX. METALLURGY AND MATERIALS SCIENCE
Nº. 4 - 2022, ISSN 2668-4748; e-ISSN 2668-4756
Article DOI: https://doi.org/10.35219/mms.2022.4.07

material and is exposed to direct contact with the steel [4, 7].

The emergence of the technology of applying the refractory lining, by spraying, led to an increase in the life of the tundish. The thickness of the layer of sprayed material is 40-50 mm, but an additional 10-15 mm can be applied to the area of contact with the slag. (Fig. 1).

Areas subject to a strong erosive flow require refractories based on magnesite.

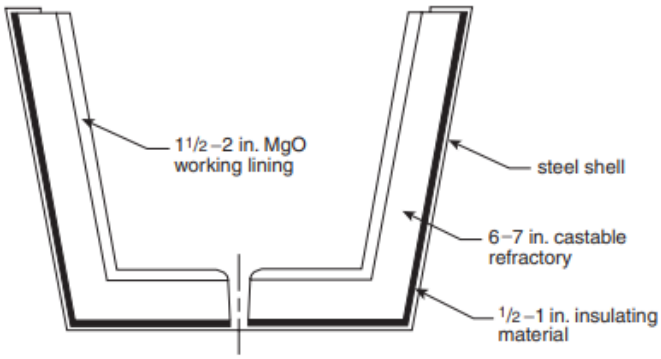

Fig. 1. *Cross-sectional view of a tundish liner*

At the distributor from the continuous casting machine, the refractory lining is made of shotcrete TUNDEX, with the following physical and chemical characteristics: - 50-75 % magnesium oxide; - 1-5% glass, oxide and chemicals.

Table 1. *Physical and chemical properties of the refractory lining*

Physical state	Color	Odor	pH	Density	Solubility
solid (powder)	grey	odorless	alkaline	1.5 - 1.8 g/cm³ [20 °C]	partially soluble in the following materials: cold water and warm water

Table 2. *Standard values of the TUNDEX 175 CS layer composition*

MgO%	SiO_2%	CaO%	Fe_2O_3%	Al_2O_3%	C%	Bulk density g/cm³
73-78	15-20	1-2	0.6-1.2	<1	2-4	1.5-1.7

3. Optical microscopy of the samples, from the tundish lining

Optical microscopy, is a method of analysing the quality of concrete samples, the purpose of the control being the determination of the existence of degradation due to corrosion.

In optical microscopy, non-oxidized steel strongly reflects light, and corrosion products, reflect the light more attenuated, than steel, with a stronger intensity, than aggregates and cement stone.

Steel and corrosion products are opaque in light transmission. Aggregates are generally transparent in light transmission.

The aggregate particle, in the upper and middle portion of the image is subject to the chemical reactions and thermal shocks that occur. The aggregate particle is more porous inside, and denser at the contact surface with the cement stone.

Alternating layers of ceramic material, silica gel and corrosion products, deposited on the side faces of the crack, can be seen in the images below (Fig. 2-5).

The examination of the samples was done with an Olympus BX51M optical microscope, the samples being taken from the used refractory lining, of a distributor from the continuous casting machine.

Through microscopy, the wear of the layer due to the erosion and infiltration of steel microparticles into the pores of the lining was highlighted.

The impact zone of the melt with the blasted surface of the distributor was highlighted, at 100X magnification.

Examined:

- the area from interface 1, respectively shotcrete - metal;
- the area at interface 2, respectively shotcrete-concrete;
- the area with refractory concrete.

THE ANNALS OF "DUNAREA DE JOS" UNIVERSITY OF GALATI
FASCICLE IX. METALLURGY AND MATERIALS SCIENCE
N°. 4 - 2022, ISSN 2668-4748; e-ISSN 2668-4756
Article DOI: https://doi.org/10.35219/mms.2022.4.07

It can be observed a surface wear, highlighted by the roughness of the contact surface. Also, the steel particles penetrated the capillaries of the shotcrete layer (Fig. 3).

It can be noted that both the shotcrete layer and a good part of the concrete layer have been damaged. The liquid alloy particles penetrated the capillaries, due to the porosity of the material, as well as due to the microcracks, which appear due to the temperature gradient, and the pressure exerted on the walls of the distributor.

Analysing the multitude of causes that lead to the deterioration of concrete elements, it is noted that most of them evolve, depending on a very important characteristic of hardened concrete – permeability (STAS 3518-89).

Permeability can be defined as the property (of a material with a porous structure), which quantitatively characterizes the ease with which a fluid or vapor passes through it, under the action of a pressure difference.

For concrete constructions, which are located in environments exposed to wear, and in areas of intense exploitation, obtaining concretes with a low degree of permeability is essential.

Fig. 2. *The appearance of the sample, in the area at the shotcrete -metal interface*

Fig. 3. *Penetration of the liquid alloy into the capillaries of the ceramic material*

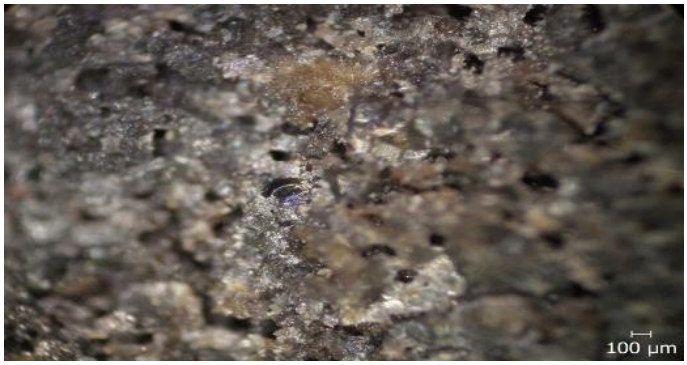

Fig. 4. *The appearance of the sample, in the area at the shotcrete-refractory concrete interface*

THE ANNALS OF "DUNAREA DE JOS" UNIVERSITY OF GALATI
FASCICLE IX. METALLURGY AND MATERIALS SCIENCE
No. 4 - 2022, ISSN 2668-4748; e-ISSN 2668-4756
Article DOI: https://doi.org/10.35219/mms.2022.4.07

Fig. 5. *The appearance of the sample, in the area of the refractory concrete wall*

4. Phenomenon of pores production

Pores represent any space in the concrete structure (spherical or cylindrical), which is filled with air or water, and which can have a winding route, through the section of the concrete element.

In order to understand the complexity of the concrete formation mechanism, as compact as possible, it should be remembered that each of its components (binder and aggregate) has its own permeability, and that the products obtained as a result of the reactions between them will influence, in a certain way measure, the general permeability of the mass [5, 6].

The dehydration of the hardened binder gels, and its weak adhesion to the aggregate granules, makes the concrete always represent a microporous, with a microcracked system - gel pores. Thus, it can be found that the permeability of the cement paste varies over time, depending on the progress of the cement hydration process.

Spherical pores appear due to the resettlement of cement granules, according to their weight, immediately after the preparation, transport, and placing of the concrete. The excess water is collected on top, from which the air included in the mixing is separated in bubbles. The pores under the aggregates (spheres), are finer than those created by the inclusion of mixing air, and are not visible to the naked eye [7].

Capillary pores in concrete appear due to the loss of excess water through evaporation (Fig. 6).

Fig. 6. *The image obtained by optical microscopy of a pore that appeared in the lay of ceramic material*

Analysing the aspects presented, we can highlight several factors that influence the permeability of concrete of the tundish following corrosion:

- fineness of cement grinding (the finer the cement, the lower the permeability);
- cement dosage (increasing the cement dosage reduces permeability);
- the type of cement (cements with additions, require a larger amount of water, which can increase permeability);
- concrete treatment after putting into work (keeping fresh concrete in a humid environment for as long as possible, it decreases permeability);
- the use of additives in concrete compositions (use correctly, they considerably reduce permeability);

THE ANNALS OF "DUNAREA DE JOS" UNIVERSITY OF GALATI
FASCICLE IX. METALLURGY AND MATERIALS SCIENCE
Nº. 4 - 2022, ISSN 2668-4748; e-ISSN 2668-4756
Article DOI: https://doi.org/10.35219/mms.2022.4.07

- the existence of tensile stresses and compressive stresses above the cracking limit (increase permeability).

Corrosion can also continue in compact and thick layers. In this case, the film of reaction products does not adhere at the metal, but detaches as it forms and falls. This detachment can occur for the following reasons:

- the volume of the formed oxide is greater than the volume of the original metal, and this increase in volume, caused by oxidation, can produce internal stresses that exceed the adhesion between the corrosion layer and the metal. These efforts are all the greater, as the ratio between the volume of the oxide, and the volume of the metal from which the oxide originates, is higher;
- the formed oxide layer has a different coefficient of thermal expansion than that of the base metal and when the temperature of the surrounding environment varies, internal stresses arise due to unequal expansions.

The porosity of the layer of ceramic material is an important factor that leads to the degradation of the refractory lining of the tundish and is influenced by a multitude of phenomena that were highlighted previously.

5. Conclusions

The quality of the refractory lining is of particular importance and is also influenced by the fixing method and the additives used.

The variation in temperature causes the refractory material to crack, lose its strength, break and thus contribute to shortening the life of the tundish.

The tundish lining is composed of three layers. The working liner is made of high MgO material and is exposed to direct contact with the steel.

Areas subject to a strong erosive flow require refractories based on magnesite. At the tundish, from the continuous casting machine, the refractory lining is made of shotcrete TUNDEX.

The samples taken from a used tundish, from the continuous steel casting machine were also examined by optical microscopy.

Optical microscopy is a method of analysing the quality of concrete samples, the purpose of the control being to determine the existence of degradations due to corrosion.

We highlighted through microscopy the wear of the layer due to the erosion and infiltration of steel microparticles into the pores of the lining.

We examined: the area at the metal-shotcrete interface, the area at the shotcrete-concrete interface, the area with refractory concrete.

Both the shotcrete layer and a good part of the concrete layer were damaged. The liquid alloy particles entered the capillaries, due to the porosity given by the material, as well as due to the microcracks that appear due to the temperature gradient, and the pressure exerted on the walls of the distributor.

Analysing the multitude of causes that lead to the deterioration of concrete elements, it is noted that most of them evolve according to a very important characteristic - permeability.

For concrete constructions that are located in harmful exposure and exploitation environments, obtaining concretes with a low degree of permeability is essential.

The durability of concrete decreases through the degradation of the intimate structure due to the phenomena of dissolution, expansion, cracking or exfoliation.

The porosity of the ceramic material layer is an important factor that leads to the degradation of the refractory lining of the tundish and is influenced by a multitude of phenomena that have been highlighted.

References

[1]. McLean A., *The Turbulent Tundish-Contaminator or Refiner*, Proc. Steelmaking Conf., Iron and Steel Society, 71, p. 3-23, 1988.
[2]. Van der Stel J., *et al.*, *Tundish Metallurgy: A Solution or a Limitation to Clean Steel*, Development in Ladle Steelmaking and Continuous Casting, edited by G.D. Lawson, Montreal: The Canadian Institute of Mining and Metallurgy, p. 218-223, 1990.
[3]. Lowry M. L., Sahai Y., *Thermal Effects on the Flow of Liquid Steel in Continuous Casting Tundishes*, Iron and Steelmaker, 19:3, p. 81-88, J. Schade. Lecture Notes, ISS Short Course on Ladle and Tundish Metallurgy for Clean Steels, 314-321, 1992.
[4]. ***, *Refractories, Manufactured Carbon and Graphite Products, Activated Carbon, and Advanced Ceramics*, Annual Book of ASTM Standards, vol. 15.01 (Index), 1998.
[5]. Daussan A., Martin J., Roziere J., *Steel Purity in Continuous Casting Tundishes*, Proc. Steelmaking Conf., 78, p. 471-477, 1995.
[6]. Melville S. D., Brinkmeyer L., *Evaluating Steelmaking and Casting Practices Which Affect Quality*, Proc. Steelmaking Conf., 78, p. 563-569, 1995.
[7]. ***, https://www.holcim.ro/sites/romania/files/documents/Manual_de_utilizare_a_betoanelor_5.pdf.
[8]. ***, https://www.creeaza.com/tehnologie/constructii/Proprietatile-betonului-intari669.php.
[9]. ***. https://materialedeconstructie.files.wordpress.com/2010/03/28246437-controlul-calitatii-betoanelor.pdf.
[10]. ***, https://www.revistaconstructiilor.eu/wpcontent/uploads/2011/09/nr_72_iulie_2011.pdf.

THE ANNALS OF "DUNAREA DE JOS" UNIVERSITY OF GALATI
FASCICLE IX. METALLURGY AND MATERIALS SCIENCE
N°. 4 - 2022, ISSN 2668-4748; e-ISSN 2668-4756
Article DOI: https://doi.org/10.35219/mms.2022.4.08

INVESTIGATION OF STRUCTURAL CHARACTERISTICS BY FTIR SPECTROSCOPY OF CHITOSAN DERIVATIVE WITH N HETEROCYCLIC COMPOUND

Iuliana Florina COSTEA (NOUR)[1], Florentina ȘORCARU[2], Geta CÂRÂC[1,*]

[1]"Dunarea de Jos" University of Galati, Faculty of Science and Environment, Department of Chemistry, Physics and Environment, Domneasca Street 47, Galati, 80008, Romania
[2]Compa SA-Automotive Components Company, Sibiu, Romania, Henri Coandă Street 8, Sibiu 550234, Romania
e-mail: iulianaflorinanour@gmail.com; *geta.carac@ugal.ro

ABSTRACT

Chitosan and chitosan derivatives are biomaterials of great scientific interest for biomedical applications although some of the properties are limited as their solubility in the aqueous medium. N-heterocyclic compounds are of interest for chitosan alkylation and new derivatives can be obtained by modification of his structure resulting thus new structures of biomedical interest Chitosan samples from two sources were analysed, in which the dissociation is favoured in the aqueous medium by the presence of a bipyridine salt, N,N'-bis(phenacyl)-4,4'-bipyridinium dibromide. The synthesis of chitosan' derivate was conducted in aqueous medium at 60 °C, by magnetic stirring for 24 hours. The dissociation is better and reduced the pH, to values lower than pH 6, which suggests the achievement of favourable structural arrangements between chitosan and dibromide bipyridinium. The FTIR spectra parameters indicate the presence of characteristic bands of the bipyridinium salt in the chitosan derivates structures, with structural differences in their composition.

KEYWORDS: functionalized chitosan, bipyridinium salt, structure, FTIR spectrometry

1. Introduction

Chitosan is a biomaterial with a very similar structure to cellulose, which ensures the structural integrity and protection of plants and animals, but it is also useful in the medical field in formulations with different functions and properties [1-6]. The only difference between the chitosan and cellulose structure is the amine group (NH_2) in the C-2 position of the chitosan structure instead of the hydroxyl group (-OH), present in the cellulose structure [4].

Chitosan, the most widespread biomaterial is considered a biopolymer that consists of N-acetyl-2-amino-2-deoxy-D-glucopyranose and 2-amino-2-deoxy-D-glucopyranose and is a compound that is easily alkylated with several chemical compounds. After purification, chitosan has a rigid crystalline structure, through intermolecular bonding and intramolecular hydrogen bonding, showing polymorphism. However, unlike plant fiber, chitosan possesses net positive ionic charges, which enable it to chemically bond with negatively charged substances such as fats, lipids, cholesterol, metal ions, proteins and macromolecules etc., making it a biomaterial of wide interest [7-13].

By alkylation with chemical compounds (Schiff bases, N-heterocyclic compounds) at the functional groups in the structure formed by N-acetyl-2-amino-2-deoxy-D-glucopyranose and 2-amino-2-deoxy-D-glucopyranose, many reports have been made structures of new derivatives of chitosan with relevant properties and functions in medical and biomedical applications, as well as in pharmaceutical and industrial applications [6-7, 10, 13-16].

N-heterocyclic compounds are studied with the aim to obtain new structures with chitosan, each new compound confirming properties of biomedical or pharmaceutical interest [18].

In this work we propose the informal structural exploration in the obtaining of new derivative by

THE ANNALS OF "DUNAREA DE JOS" UNIVERSITY OF GALATI
FASCICLE IX. METALLURGY AND MATERIALS SCIENCE
Nº. 4 - 2022, ISSN 2668-4748; e-ISSN 2668-4756
Article DOI: https://doi.org/10.35219/mms.2022.4.08

synthesis between chitosan from two sources and an organic compound, N-heterocyclic salt, from the class of bipyridinium. The Fourier Transform Infrared Spectroscopy (FTIR) has been performed for analysis samples. The structure of chitosan is differentiated, depending on the manufacturer, from which materials it is obtained, and what degree of alkylation the final product has, characteristics that can greatly influence the structure and properties of new chitosan derivatives.

2. Materials, synthesis and method of structural analysis

In the synthesis to obtain new chitosan derivatives, two different chitosan samples were used, a commercial one marked CH_c (Sigma Aldrich Chemie GmbH; flakes, 85% degree of deacetylation) and a pharmaceutical product CH_f (capsules, with a content of 1.5 g chitosan (93% degree of deacetylation, obtained from the chitin of crustacean shells), cellulose (filling agent), magnesium stearate and silicon dioxide) (Figure 1.a). The schematic structure of chitosan of N-acetyl-2-amino-2-deoxy-D-glucopyranose and 2-amino-2-deoxy-D-glucopyranose is shown below:

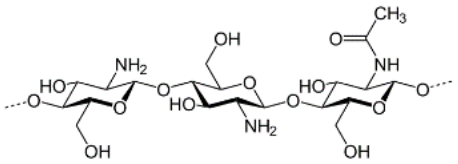

Chemical analysis of CH_c chitosan (fine grated) by fluorescence spectrophotometry (XRF Niton) indicates the presence of chemical elements such as: Ca (1875 ppm), K (450 ppm) Cr (139 ppm), As (2.5 ppm) and Zn, Ni, Cu, Fe, Mn, Se etc., as proof of the origin of chitosan from seaweed, chitosan being known as a biopolymer with a high degree of inhomogeneity [7].

(a) (b)

Fig. 1. *Chitosan 'samples (a) and Bruker Alpha-P ATR FTIR equipment (b)*

The bipyridinium salt (S) used in the synthesis is N,N'-bis(phenacyl)-4,4'-bipyridinium dibromide (M = 554 g/mol) obtained in our laboratory according to the reference [19], the molecular structure being reproduced below:

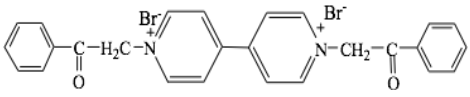

- 0.2 g of chitosan (CH_c and CH_f respectively) were weighed in two glasses and 50 mL of distilled water was added. The procedure was followed by heated samples to 60 °C, by mechanical stirring (700 rpm) for 2 h, in duplicated samples for each type of chitosan. It was observed that the chitosan from both types of samples does not completely dissolve, and the pH analysed in the samples was 7.42 ± 0.04. Chitosan solutions were evaluated conductometric and pH-metrically, but also at 24 h and after 72 h, and there are no essential changes.
- 25 mL were measured from the clear chitosan CH_c solution, 0.01 g of the chemical compound, N,N'-bis(phenacyl)-4,4'-bipyridinium dibromide salt was added (ratio between chitosan: salt of 10:1) and the mixture was heated to 60 °C, by mechanical stirring (700 rpm), for 2 h. The resulting samples were made in duplicates and marked CH_cS_1. The pH and electrical conductivity for solutions are measured using the Constant C862 multiparametric analyser.
- at each remaining CH_c chitosan solution, of 25 mL hydrogel (with undissolved chitosan) was added 0.01 g of bipyridinium salt, obtaining the solution/sample marked CH_cS_2. The samples are heated to 60 °C, by stirring at 700 rpm, for 2 h. The pH and electrical conductivity of the solutions are measured also.

After the addition of the bipyridinium salt, the solutions showed an intensive red colour, as an effect of the protonation reaction of the N-heterocyclic salt,

THE ANNALS OF "DUNAREA DE JOS" UNIVERSITY OF GALATI
FASCICLE IX. METALLURGY AND MATERIALS SCIENCE
Nº. 4 - 2022, ISSN 2668-4748; e-ISSN 2668-4756
Article DOI: https://doi.org/10.35219/mms.2022.4.08

but colour disappears after 40 minutes of stirring, and the pH change over time is obtained (value of 5.35 ± 0.02 at sample CH_cS_1, and respectively of 6.70 ± 0.01 at CH_cS_2).

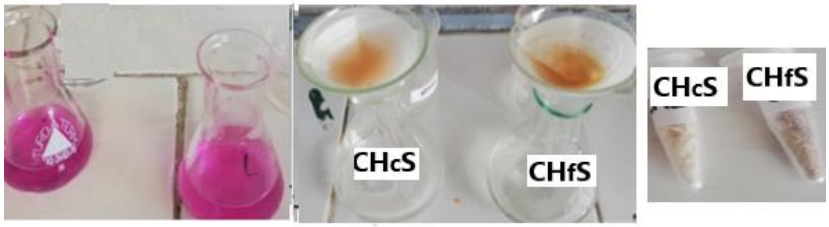

- the same synthesis procedure is followed for the sample of the pharmaceutical product and the samples were marked CH_f, obtaining the chitosan derivative with the bipyridinium salt, in the sample marked CH_fS_1, respectively CH_fS_2. The solutions have a pH of 5.70 ± 0.02 at sample CH_fS_1 and respectively of 6.50 ± 0.02 at sample CH_fS_2.

The samples synthesised marked CHcS2 and CH_fS_2 were filtered, resulting solid contents dried in the oven at 100 ºC, weighed and the overage masses were: m_{CHcS2} = 1.2566 g (η = 62.5%), m_{CHfS2} = 1.1555 g (η = 57.5%).

Fourier transform infrared (FTIR) spectra of the chitosan powder, salt and chitosan derivates were recorded using a Bruker Alpha-P ATR (Germany) with a Diamond Crystal ATR (Attenuated Total internal Reflectance) accessory, over the range between 4000 and 400 cm^{-1} with a spectra resolution of 4 cm^{-1} (Figure 1.b).

3. Results and discussion

Synthesis experiments regarding the absorption of N-heterocyclic salt, N,N'-bis(phenacyl)-4,4'-bipyridinium dibromide (S) were carried out in chitosan solutions, in aqueous medium, samples purchased from two sources. The new compounds obtained were analysed physic-chemical and the investigation of structural characteristics was provided. The chitosan, samples of CH_c and CH_f in aqueous medium indicate a pH value higher than 6.3, with average values of 7.40 ± 0.04 being obtained, a pH that does not favour total solubilization of them, because the positive charge of the amino groups is lost and thus chitosan becomes insoluble in water [20-21]. Most of the characteristic properties for chitosan are due to the primary amino groups that at pK_a of 6.3 are found in large numbers in the polymer chain, for a lower pH, the ions of the NH_3^+ group transform chitosan into a water-soluble cationic polyelectrolyte [21-22].

Through the heating process at 60 °C, between chitosan and salt (ratio of 10:1) with mechanical stirring, after 2 h, pH values of 5.35 ± 0.02 are obtained for samples with CH_cS_1, which suggests that through the addition of bipyridine salt, bridges are created with the functional groups of the chitosan, the derived compound being a new structure. The pH value favours the solubility of chitosan in the aqueous medium. The synthesis procedure in this medium indicates a yield obtained of over 55%, with a higher value for samples with CH_c. There is possible that at temperatures over 60 °C there is also a deterioration of some properties.

Regarding the electrical conductivity analysis in solutions, CH_c shows values λ of 110 ± 10 $\mu S \cdot cm^{-1}$, and the CH_f solution indicates a less dissociation (52 ± 8 $\mu S \cdot cm^{-1}$), due to their excipients in structure. When adding an equal amount (0.01 g) of bipyridinium salt, in both types of samples, dissociation is favoured in aqueous solutions, the electrical conductivity value increases, with a greater tendency for samples with CH_c (780 ± 21 $\mu S \cdot cm^{-1}$), compared to samples with CH_f (530 ± 12 $\mu S \cdot cm^{-1}$), the explanation being the resistance of the excipients.

The samples of chitosan derivatives obtained were dried at 100 °C and structurally characterised, by using FTIR spectrophotometry, to identify the structural chemical characteristics, obtaining useful information regarding the spectral parameters, the vibration's characteristics associations of the various types of bonds in structures, the existence and the strength of the chemical bonds between chitosan and the salt [23-24].

In Figure 2, the FTIR spectra of the chitosan showed different bonds, indicating some structural changes between the chitosan powders (CH_c, CH_f). The resulting spectra were compared with standard chitosan taken as a reference to confirm the structure, the results being consistent with the data reported by Puvvada *et al.* [22]. There are structural differences in the chitosan composition, the sample marked CH_f (with the excipients), suggests also the possibility of different structural arrangements, which are not found in the chitosan marked CH_c. This similarity of the spectra confirms the basic structure of the chemically chitosan extracted from a different source.

THE ANNALS OF "DUNAREA DE JOS" UNIVERSITY OF GALATI
FASCICLE IX. METALLURGY AND MATERIALS SCIENCE
Nº. 4 - 2022, ISSN 2668-4748; e-ISSN 2668-4756
Article DOI: https://doi.org/10.35219/mms.2022.4.08

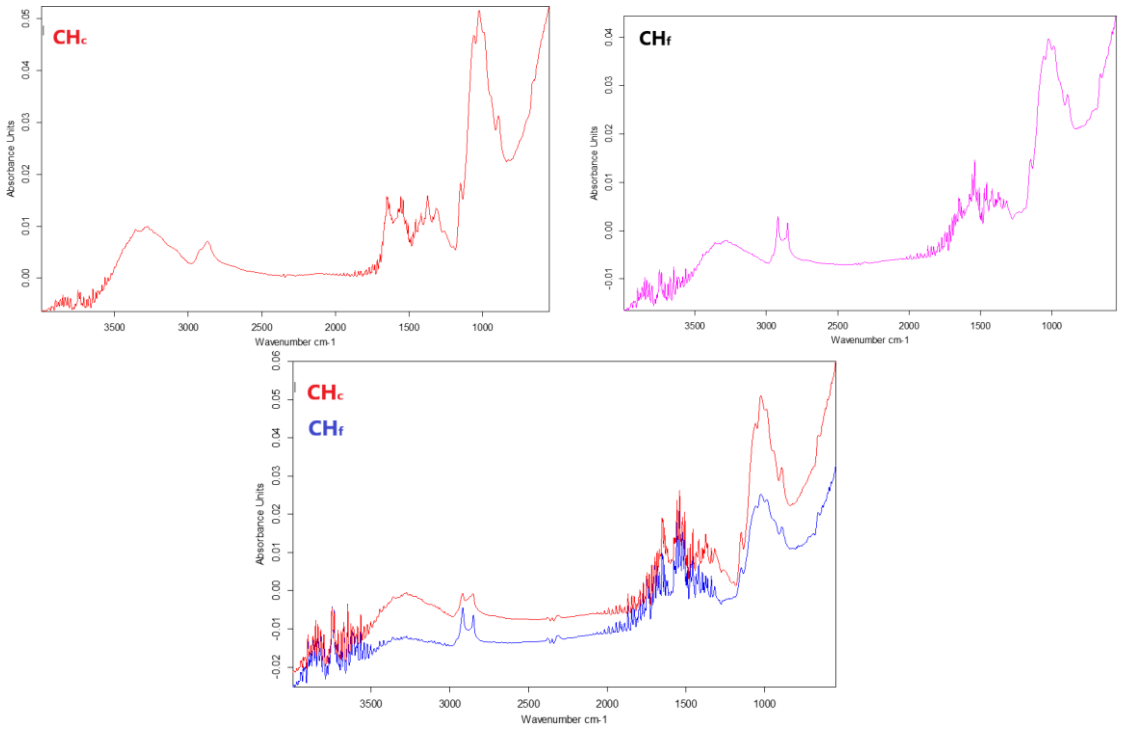

Fig. 2. *FT-IR spectra for chitosan powder and in aqueous medium (CH_c CH_f), at 60 °C, 700 rpm*

In the chitosan derivatives samples obtained with the N-heterocyclic salt, N,N'-bis(phenacyl)-4,4'-bipyridinium dibromide (S) (Figures 3-6), FTIR spectra indicate essential changes for the higher frequency area, up to 3500 cm^{-1} and around 1500 cm^{-1}.

The representative peaks for the chitosan samples and for the new compounds are mainly grouped in three regions. In the area of 3500-3300 cm^{-1}, the existence of absorption bands confirms the presence of hydroxyl groups (-OH), from the chitosan structure. The broadband aspect of absorption indicates association through hydrogen bonds. Sample CH_c, for example, showing a high absorption capacity of water molecules (WA_{24} = 355.29 %) (Figure 4). The broad-band aspect of the absorption for the chitosan derivative CH_cS_1 (Figure 5) indicates a somewhat more favourable association through hydrogen bonds compared to the sample CH_fS_2 (Figure 6).

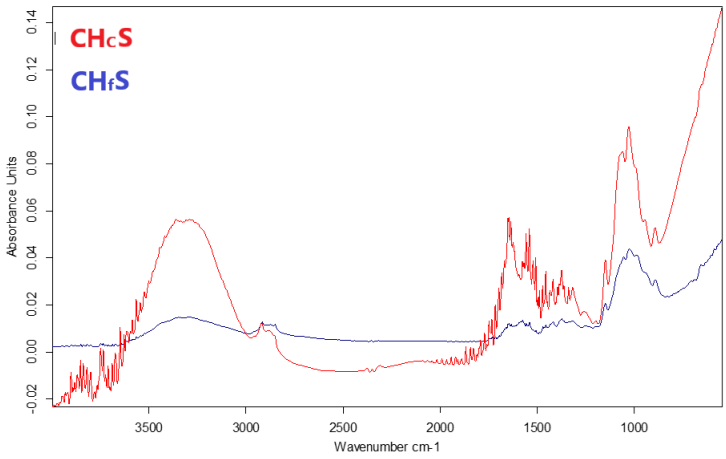

Fig. 3. *FT-IR spectra for chitosan solutions with addition of 0.01 g of N,N'-bis(phenacyl)-4,4'-bipyridinium dibromide (S), in aqueous medium, at 60 °C, 700 rpm*

THE ANNALS OF "DUNAREA DE JOS" UNIVERSITY OF GALATI
FASCICLE IX. METALLURGY AND MATERIALS SCIENCE
Nº. 4 - 2022, ISSN 2668-4748; e-ISSN 2668-4756
Article DOI: https://doi.org/10.35219/mms.2022.4.08

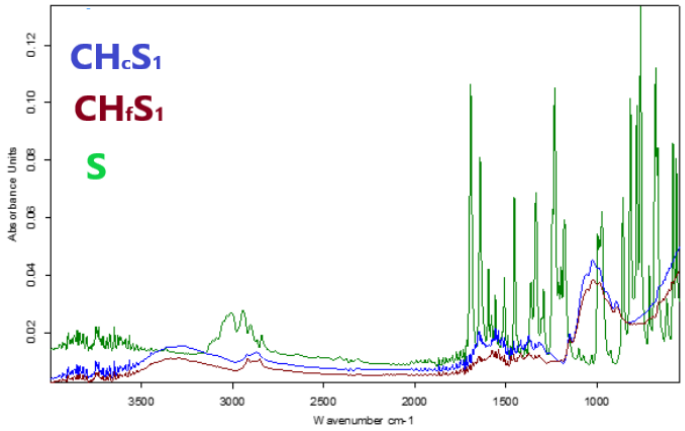

Fig. 4. *Comparative FT-IR spectra of clear chitosan solutions, with addition of 0.01 g of N,N'-bis(phenacyl)-4,4'-bipyridinium dibromide (S), in aqueous medium, at 60 °C, 700 rpm*

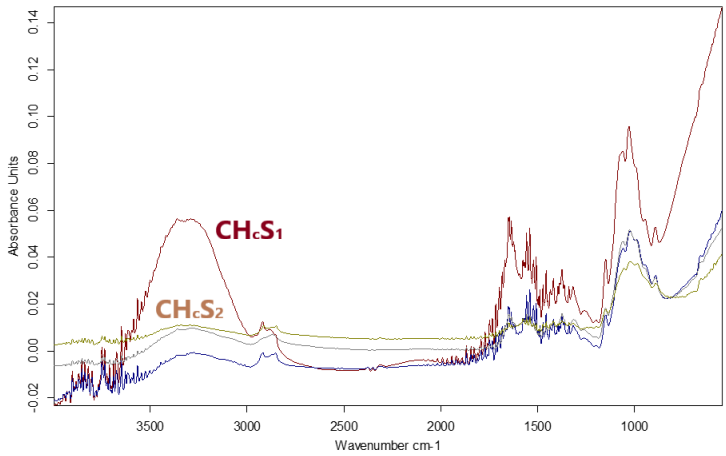

Fig. 5. *Comparative FT-IR spectra of the chitosan' derivate CH_cS_1 and CH_cS_2, in aqueous medium, at 60 °C, 700 rpm*

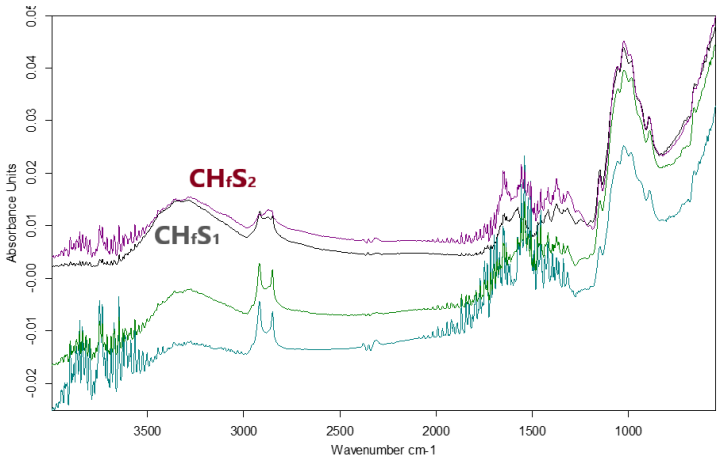

Fig. 6. *Comparative FT-IR spectra of the chitosan' derivate CH_fS_1 and CH_fS_2, in aqueous medium, at 60 °C, 700 rpm*

The FTIR analysis of samples proved the presence of N,N'-bis(phenacyl)-4,4'-bipyridinium dibromide in structure of the new chitosan compounds (Figure 4) by the ν_{CHarom} absorption bands

THE ANNALS OF "DUNAREA DE JOS" UNIVERSITY OF GALATI
FASCICLE IX. METALLURGY AND MATERIALS SCIENCE
Nº. 4 - 2022, ISSN 2668-4748; e-ISSN 2668-4756
Article DOI: https://doi.org/10.35219/mms.2022.4.08

positioned at 3054-3061 cm^{-1}, with a slight shift to the left (2 cm^{-1}) compared to those find in the spectrum of the bipyridinium salt (Figure 7). The FT-IR spectra at N,N'-bis(phenacyl)-4,4'-bipyridinium dibromide (S) were made on solid samples (crystals) and is a confirmation a series of characteristic bands: 3040-3000 cm^{-1} (C-H_{arom}), 1730-1722 cm^{-1} (C-O_{ester}), 1700-1670 cm^{-1} (C=O), 1640-1630 cm^{-1} (C=N), 1200 and 1100 cm^{-1} (C-O-C) [24].

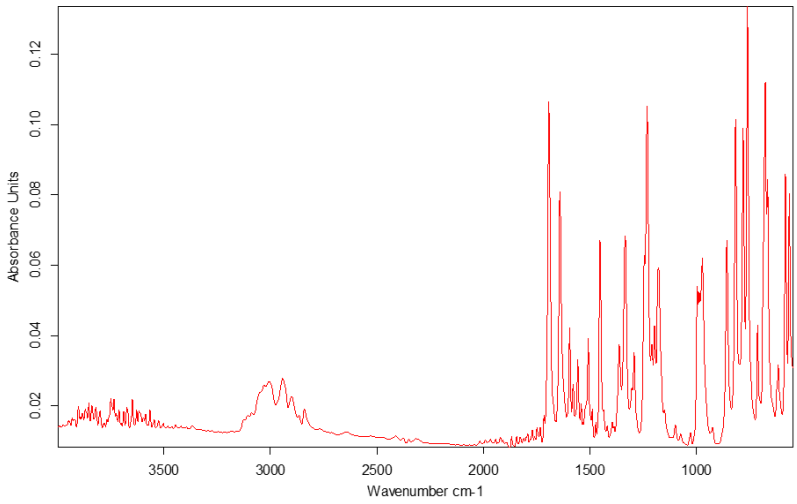

Fig. 7. *FT-IR spectra of N,N'-bis(phenacyl)-4,4'-bipyridinium dibromide (S)*

Of interest in the FTIR spectra is the region at 1650 cm^{-1}, as an effect of the intense absorption due in particular to the valence vibration of the heterogeneous double bond C=O, component part of the bipyridinium salt structure, position for samples and derivatives. And the peak position at 1646 cm^{-1} supports new positions for amide bonds forming δ_{N-H}.

The FT-IR spectral analysis highlights the fact that, for the same functional group in the spectral range at 1400-1490 cm^{-1}, the characteristic peaks are more numerous in the chitosan derivatives spectra, compared to the spectrum of the bipyridinium salt [20]. At the same time, small shifts of these peak positions to the right are highlighted, compared to the FTIR spectrum of the salt, as a result of the complex steric effects that appear in the new structures of the chitosan derivatives.

More intense peaks appear in the chitosan derivatives spectra, at 1191 cm^{-1}, 1085 cm^{-1}, 1049 cm^{-1} and 1014 cm^{-1}. The spectra also indicate the positions of the absorption band, at 1100-1050 cm^{-1}, which characterizes the molecular structure as a whole and can be attributed to C-O or C-N bonds, the peak position confirming the structure of the salt in the chitosan derivative, by comparing it with the spectrum of chitosan, when the position is shifted from 1162 cm^{-1} for ν_{C-0}, towards lower values. The position at 1029 cm^{-1}, assigned for ν_{C-0}, is similar in all spectra with chitosan and its derivatives, with a shift of 3-5 cm^{-1} to the left in samples with CH_f.

Spectra proved the presence of amino and carbonyl functional groups on derivates, available for binding with biological compounds. Chitosan CH_f, although it indicates links with the bipyridinium salt, presenting a higher degree of deacetylation, is not recommended for the continuation of our study, due to the presence of excipients in the structure, which affects the properties. Chitosan CH_c, although it has a lower degree of acetylation, structurally confirms a chitosan derivative, with bipyridinium salt, promising new properties, but there are studies that recommend much higher degrees of deacetylation. Derivates of chitosan are interesting biomaterials which could promise a potential in the biomedical applications [16, 18, 25-26].

4. Conclusions

The chitosan samples, from two sources, show dissociation in aqueous medium, for weak basic pH, which indicates less solubilization of their structure. The dissociation is favoured by the presence of the bipyridinium salt in the synthesis process for new derivates, with notable differences between the two samples of different origin. In the synthesis solutions, for new chitosan derivates, the pH is reduced when bipyridinium salt is added, which suggests the achievement of favourable structural arrangements between chitosan and N heterocyclic salt, in the aqueous medium, the values pH reaching 6.3. The FT-IR spectrum confirms the presence of the characteristic bands for the bipyridinium salt in the new structures, but indicates structural differences that appear in their composition, and excipients

influence the data. The mechanism study of the reaction between chitosan with bipyridinium salt is of interest, the nature/type of chitosan samples is important and the degree of deacetylation of chitosan has a decisive role in the synthesis process. Results justify the usefulness of FTIR spectroscopy for chitosan derivates structural investigation.

References

[1]. Shigemasa Y., Minami S., *Applications of Chitin and Chitosan for Biomaterials*, J Genet Eng Biotechnol, 13, p. 383-420, doi:10.1080/02648725.1996.10647935, 1996.
[2]. Borchard G., Junginger H. E., *Modern drug delivery applications of chitosan*, Adv. Drug Deliv. Rev, 52, p. 103-150, doi:10.1016/s0169-409x(01)00188-0, 2001.
[3]. Dutta P. K., Ravikumar M. N. V., Dutta J., *Chitin and chitosan for versatile applications*, J. Macromol. Sci. Phys., 42:3, p. 307-354, doi:10.1081/MC-120006451, 2002.
[4]. Yuan Y., Chestnutt B. M., Haggard W. O., Bumgardner J. D., Muzzarelli R. A. A., *In Chitin and chitosan in biomaterial science*, edited by R. Jayakumar & A. Prabaharan, Trivandrum, India: Research Signpost, 2008.
[5]. Muzzarelli R. A. A., *Chitins and chitosan's for the repair of wounded skin, nerve, cartilage and bone*, Carbohydr Polym, 76(2), p. 167-182, 0144-8617, doi.org/10.1016/j.carbpol.2008.11.002, 2009.
[6]. Bansal V., Sharma P. K., Sharma N., Pal O. P., Malviya R., *Applications of Chitosan and Chitosan Derivatives in Drug Delivery*, Adv. Biol. Res., 5, 1, p. 28-37, ISSN 1992-0067, doi:360101108, 2011.
[7]. Puvvada Y. S., Vankayalapati S., Sukhavasi S., *Extraction of chitin from chitosan from exoskeleton of shrimp for application in the pharmaceutical industry*, Int. Curr. Pharm. J., 1(9), p. 258-263, doi.org/10.3329/icpj.v1i9.11616, 2012.
[8]. Irom B. C., Kavitha K., Rupeshkumar M., Jagadeesh Singh S. D., *Applications of Natural Polymer Chitosan and Chitosan Derivatives in Drug Delivery: A Review*, RJPBCS, 3, 4, p. 309-316, 2012.
[9]. Ahmad S., Ikram S., *Chitosan & its derivatives: a review in recent innovations*, Inter J Pharmaceutical, 6(1), p. 14-30, doi: 10.13040, 2015.
[10]. Muzzarelli R. A. A., Boudrant J., Meyer D., Manno N., Demarchis M., *Current views on fungal chitin/chitosan, human chitinases, food reservation, glucans, pectins and inulin: A tribute to Henri Braconnot, precursor of the carbohydrate polymers science, on the chitin bicentennial*, Carbohydr Polym, 8, 7995-1012, doi: 10.1016/j.carbpol.2011.09.063, 2012.
[11]. Gibot L., Chabaud S., Bouhout S., Bolduc S., Auger F. A., Moulin V. J., *Anticancer properties of chitosan on human melanoma are cell line dependent*, Int J Biol Macromol, 72, p. 370-379, doi:10.1016/j.ijbiomac.2014.08.033, 2015.
[12]. Cheung R. C. F, Ng T. B., Wong J. H., Chan W. Y., *Chitosan: An Update on Potential Biomedical and Pharmaceutical Applications*, Mar Drugs, 13(8), p. 5156-5186. doi:10.3390/md13085156, 2015.
[13]. Singh R., Shitiz K., Singh A., *Chitin and chitosan: biopolymers for wound management*, Int. Wound J., 14(6), p. 1276-1289, doi:10.1111/iwj.12797, 2017.
[14]. Elson C. M., *Covalently linked N,O-carboxymethyl chitosan*, Patent US 5888988, 2000, US5888988A - Covalently linked N,O-carboxymethylchitosan and uses thereof - Google Patents.
[15]. Cho J., Heuzey M. C., Begin A., Carreau J. P., *Gelation study of chitosan/b-glycerophosphate solutions by rheological measurements*, In Proceedings of the XIVth international congress on rheology (FB09), Seoul, Korea, web, 2004.
[16]. Mouryaa V. K., Nazma N. Inamdara, Ashutosh T., *Carboxymethyl chitosan and its applications*, Zair./J. Soc. Mater. Sci. Jpn., 1(1), p. 11-33, doi: 10.5185/amlett.2010.3108, 2010.
[17]. Pokhrel S., Yadav P. N., *Functionalization of chitosan polymer and their applications*, J. Macromol. Sci., Part A, 56:5, p. 450-475, doi: 10.1080/10601325.2019.1581576, 2019.
[18]. El-Gharably A. A., Kenawy E. R. S., Safaan A. A., *et al.*, *Synthesis, characterization and application of chitosan conjugated heterocyclic compounds*, J, Polym Res, 29, 141, doi.org/10.1007/s10965-021-02672-1, 2022.
[19]. Dinica R. M., Marchetti F., Pettinari C., Skelton B. W., White A. H., *Synthesis, spectroscopic and structural characterization of the reaction products of quaternary cationic 2,20-bipyridylium ligand bromide salts with metal halides*, Inorg. Chim. Acta, 360, 2609, doi:10.1016/j.ica.2006.12.037, 2007.
[20]. Sinha V. R., Singla A. K., Wadhawan S., Kaushik R., Bansal R., Dhawan S., *Chitosan microspheres as a potential carrier for drugs*, Int. J. Pharm., 274, p. 1-33, doi:10.1016/j.ijpharm.2003.12.026, 2004.
[21]. Pillai C. K. S., Paul W., Sharma C. P., *Chitin and Chitosan Polymers: Chemistry, Solubility and Fiber Formation*, Prog. Polym. Sci., 34, 7, p. 641-678, doi.org/10.1016/j.progpolymsci.2009.04.001, 2009.
[22]. Puvvada Y. S., Vankayalapati S., Sukhavasi S., *Extraction of chitin from chitosan from exoskeleton of shrimp for application in the pharmaceutical industry*, Int. Curr. Pharm. J., 1(9), p. 258-263, doi.org/10.3329/icpj.v1i9.11616, 2012.
[23]. Mustafa A., *Studii fizico-chimice pentru realizarea și caracterizarea unor forme farmaceutice pe bază de chitosan*, Rezumat teza, Univ. „Carol Davila", Buc, 2018.
[24]. Cârâc A., Boscencu R., Dinică R. M., Guerreiro J. F., Silva F., Marques F., Cabral Campello M. P., Moise C., Brîncoveanu O., Enăchescu M., Cârâc G., Tăbăcaru A., *Synthesis, characterization and antitumor activity of two new dipyridinium ylide based lanthanide (III) complexes*, Inorg. Chim. Acta, 480, p. 83-90, doi: 10.1016/j.ica.2018.05.003, 2018.
[25]. Wang W., Meng Q., Li Q., Liu J., Zhou M., Jin Z., Zhao K., *Chitosan Derivatives and Their Application in Biomedicine*, Int J Mol Sci., 21(2):487, PMID: 31940963, PMCID: PMC7014278, doi:10.3390/ijms21020487, 2020.
[26]. Hsieh W. C., Chang C. P., Lin S. M., *Morphology and characterization of 3D micro-porous structured chitosan scaffolds for tissue engineering*, Colloids Surf B Biointerfaces, 57(2), p. 250-255, PMID: 17363229, doi: 10.1016/j.colsurfb.2007.02.004, 2007.

THE ANNALS OF "DUNAREA DE JOS" UNIVERSITY OF GALATI
FASCICLE IX. METALLURGY AND MATERIALS SCIENCE
N°. 4 - 2022, ISSN 2668-4748; e-ISSN 2668-4756
Article DOI: https://doi.org/10.35219/mms.2022.4.09

MATHEMATICAL MODELING OF THE CASTING PROCESS OF THE SECOND MERGER

Marian-Iulian NEACȘU
"Dunarea de Jos" University of Galati, Romania
e-mail: mneacsu@ugal.ro

ABSTRACT

The paper shows the method of making the equations of the mathematical model that describes the dependence of several mechanical and casting properties on the chemical composition of the cast irons of the second fusion and on the casting conditions.

The chemical composition taken into account refers to the contents of C, Si and Mn and the casting conditions analysed were: casting temperature, superheating time and superheating temperature.

After performing the specific mathematical calculations, the specific mathematical equations were obtained that describe the dependence of the studied properties according to the parameters of the casting process taken into account.

KEYWORDS: casting temperature, fluidity, gray cast iron, mathematical model

1. Introduction

The global energy crisis determines the use of material resources that include low manufacturing, processing and exploitation costs. Thus, the existence and accessibility on the market of materials with increasingly high mechanical performances is taken into account.

The development and casting of cast iron is not a simple but a complex process. This process depends on many factors that have an important influence on the mechanical properties of the cast iron parts thus made [1, 2].

Cast irons are second fusion cast irons usually produced in arc furnaces or induction furnaces. These cast irons, if they are developed according to the standards in force and if they are subsequently applied to certain specific treatments, can compete in properties even with some steels [2].

For the most precise management of the elaboration and casting processes, it is useful to resort to the establishment of mathematical models based on which to find the most efficient agreement between the values of the parameters of the two processes and the values of the properties that these pieces must achieve [3].

The construction of a mathematical model for any process is conditioned by the fulfilment of some contrary requirements that must be met in the most balanced way possible. On the one hand, the developed mathematical model must be quite simple, be a representation of the real system with a certain degree of abstraction, and on the other hand, it must be a fairly faithful representation of the system it models [4].

In the complete understanding of reality, it is often necessary to know, understand and master the connections between two or more phenomena, quantified by variables.

This actually requires being able to build and then use for forecasting, the so-called statistical models or regression models, these being models that describe the existing correlation between any two variables and, in particular, between a variable and time [5].

Most of the time, the foundation of these models is based on a large volume of data and this is where the software packages designed to assist the forecast calculations prove their usefulness.

In regression modeling we start from the following situation: given two variables X and Y, studied in a population A, the question arises whether between the two variables, respectively between the phenomena described by them, there is a certain dependence called correlation [4, 5].

A rigorous substantiation of the existence of a correlation and then of the model that describes the correlation, also called a regression model, can be

THE ANNALS OF "DUNAREA DE JOS" UNIVERSITY OF GALATI
FASCICLE IX. METALLURGY AND MATERIALS SCIENCE
No. 4 - 2022, ISSN 2668-4748; e-ISSN 2668-4756
Article DOI: https://doi.org/10.35219/mms.2022.4.09

done based on the calculation and interpretation of some statistical indicators [5, 6].

In the case of some regression model, the forecast based on the model is the more truthful, the better the model is chosen to fit the data and the smaller the forecast horizon.

Regression models are part of the category of stochastic (statistical) models, in which all explanatory factors of a phenomenon, which do not find their place directly in the model, appear accumulated in the form of a random variable called error.

A variable Y (the output parameter) that quantifies the studied phenomenon can be explained by regression on one or more explanatory factors X (input parameters). If we have two or more explanatory (predictive) factors, X_1, X_2, ..., X_p, then the regression is called multiple and the corresponding model will be [4, 6]:

$$Y = f(X_1, X_2, ..., X_p) \quad (1)$$

2. Experimental conditions

The casting properties and mechanical properties of some cast irons produced in electric induction furnaces were investigated as a function of chemical composition and casting conditions.

The cast iron was developed in the induction furnace having as raw materials carbon steel waste, superheated to 1550 ºC. The modification process was done in the silicocalcium pot.

The mathematical model that was proposed to create is based on the active experiment method that uses a number of data obtained by performing programmed experiments.

The equation of the mathematical model is of the form of equation (1) and written unfolded has the form:

$$Y=b_0+x_1 \cdot b_1+x_2 \cdot b_2+ x_3 \cdot b_3+x_4 \cdot b_4+ x_5 \cdot b_5 + x_6 \cdot b_6, \quad (2)$$

The independent variables of the proposed mathematical model are the following:

x_1 - carbon content, in %;
x_2 - silicon content, in %;
x_3 - manganese content, in %;
x_4 - casting temperature, in ºC;
x_5 - overheating time, in ºC;
x_6 - overheating temperature, in ºC.

The dependent variables of the proposed mathematical model are:

Y_1 - fluidity, in mm;
Y_2 - linear contraction, in %;
Y_3 - initial expansion, in %;
Y_4 - tendency of hot crack formation, in %;
Y_5 - bleaching tendency, in %;
Y_6 - HB type hardness, in MPa;
Y_7 - tensile strength, in MPa.

The chemical composition, the content of C, Si and Mn, of the cast irons subjected to the experiments is shown in Table 1.

Table 1. *C, Si and Mn content of the cast irons under investigation*

	%C	**%Si**	**%Mn**
Min	2.5	1.5	0.2
Max	3.5	2.5	0.6

The experimental conditions (pouring temperature, superheating temperature and superheating time) are those from Table 2.

Table 2. *Experimental conditions*

Nr. crt.	**Pouring temperature, ºC**	**Overheating time, in min.**	**Overheating temperature, in ºC**
1	1450	40	1580
2	1400	30	1530
3	1350	20	1480

After conducting the experiments, the basic level, the upper level, the lower level and the range of variation of the values for the six parameters considered in order to create the equations of the mathematical model for the researched process were established. The upper level was denoted by (+1), the lower level by (-1), the base level by (0), and the variation range by △xi. Table 3 illustrates these notations with their associated values.

Table 3. *Initial calculation data*

The level of variation	**X_1**	**X_2**	**X_3**	**X_4**	**X_5**	**X_6**
Top Level (+1)	3.5	2.5	0.6	1450	40	1580
Base Level (0)	3.0	2.0	0.4	1400	30	1530
Lower Level (-1)	2.5	1.5	0.2	1350	20	1480
The range of variation △xi	0.5	0.5	0.2	50	10	50

THE ANNALS OF "DUNAREA DE JOS" UNIVERSITY OF GALATI
FASCICLE IX. METALLURGY AND MATERIALS SCIENCE
N°. 4 - 2022, ISSN 2668-4748; e-ISSN 2668-4756
Article DOI: https://doi.org/10.35219/mms.2022.4.09

Since k (the number of variables) is equal to six, 2^6 = 64 experiments should be performed, but since the values of six coefficients have to be calculated, I made a fractional program with a replica of 1/8 of 64, namely 8 experiments with the conditions: 1 = $x_1 x_3 x_5 = x_1 x_4 x_6 = x_2 x_3 x_6 = x_2 x_4 x_5 = x_1 x_2 x_3 x_4 = x_1 x_2 x_5 x_6 = x_3 x_4 x_5 x_6$, (3).

The experimental matrix for the 8 experiments is shown in Table 4.

The values of the coefficients resulting from the calculations are presented in Table 5.

Table 4. *Matrix of the experiment*

Nr. exp.	X_0	X_1	X_2	X_3	X_4	X_5	X_6	Y_1	Y_2	Y_3	Y_4	Y_5	Y_6	Y_7
1	+1	-1	-1	-1	-1	-1	-1	163	1.8	0.015	83	100	429	35.0
2	+1	+1	-1	+1	-1	-1	+1	573	1.4	0.057	31.5	48	235	23.5
3	+1	+1	-1	-1	+1	+1	-1	1210	1.0	0.170	7.0	60	248	18.3
4	+1	-1	+1	+1	-1	+1	-1	450	1.5	0.050	52.5	100	415	29.4
5	+1	-1	+1	-1	+1	-1	+1	540	1.5	0.015	33.5	74	277	30.0
6	+1	+1	+1	+1	+1	-1	-1	1033	1.0	0.015	2.0	59	235	15.0
7	+1	+1	+1	-1	-1	+1	+1	840	1.5	0.040	15.0	54	212	13.6
8	+1	-1	-1	+1	+1	+1	+1	455	2.8	0.030	55.5	100	415	14.4

Table 5. *Values of regression coefficients*

Property	b_0	b_1	b_2	b_3	b_4	b_5	b_6
Y_1	645.5	256	57.75	-30.25	151.5	80.75	-56
Y_2	1.56	-0.34	-0.19	0.11	0.01	0.14	0.24
Y_3	0.045	0.025	-0.015	0.015	0.005	0.02	-0.017
Y_4	35	-21.25	-9.25	-0.4	-10.5	-3.5	-1.1
Y_5	74.3	-19.1	-2.62	2.37	-1.12	4.12	-5.37
Y_6	308.3	-75.8	-23.5	16.8	-14.5	14.3	-23.5
Y_6	22.9	-5.3	-0.9	-2.3	-3.5	-4.0	-2.5

The equations of the mathematical model whose coefficients were calculated are:

$$Y_1 = 645{,}5 + 256 \cdot X_1 + 57{,}75 \cdot X_2 - 30{,}25 \cdot X_3 + 151{,}5 \cdot X_4 + 80{,}75 \cdot X_5 - 56 \cdot X_6 \quad (4)$$

$$Y_2 = 1{,}56 - 0{,}34 \cdot X_1 - 0{,}19 \cdot X_2 + 0{,}11 \cdot X_3 + 0{,}01 \cdot X_4 + 0{,}14 \cdot X_5 + 0{,}24 \cdot X_6 \quad (5)$$

$$Y_3 = 0{,}045 + 0{,}025 \cdot X_1 - 0{,}015 \cdot X_2 + 0{,}015 \cdot X_3 + 0{,}005 \cdot X_4 + 0{,}020 \cdot X_5 - 0{,}017 \cdot X_6 \quad (6)$$

$$Y_4 = 35 - 21{,}25 \cdot X_1 - 9{,}25 \cdot X_2 - 0{,}4 \cdot X_3 - 10{,}5 \cdot X_4 - 3{,}5 \cdot X_5 - 1{,}1 \cdot X_6 \quad (7)$$

$$Y_5 = 74{,}3 - 19{,}1 \cdot X_1 - 2{,}62 \cdot X_2 + 2{,}37 \cdot X_3 - 1{,}12 \cdot X_4 + 4{,}12 \cdot X_5 - 5{,}37 \cdot X_6 \quad (8)$$

$$Y_6 = 308{,}3 - 75{,}8 \cdot X_1 - 23{,}5 \cdot X_2 + 16{,}8 \cdot X_3 - 14{,}5 \cdot X_4 + 14{,}3 \cdot X_5 - -23{,}5 \cdot X_6 \quad (9)$$

$$Y_7 = 22{,}9 - 5{,}3 \cdot X_1 - 0{,}9 \cdot X_2 - 2{,}3 \cdot X_3 - 3{,}5 \cdot X_4 - 4{,}0 \cdot X_5 - 2{,}5 \cdot X_6 \quad (10)$$

where: $x_1 = \frac{C-3{,}0}{0{,}5}$, $x_2 = \frac{Si-2{,}0}{0{,}5}$, $x_3 = \frac{Mn-0{,}4}{0{,}2}$, $x_4 = \frac{T_t-1400}{50}$, $x_5 = \frac{\tau_{supr}-30}{10}$, $x_6 = \frac{T_{supr}-1530}{50}$

3. Conclusions

From the analysis of the equations of the developed mathematical model, the following conclusions result:

- with the increase of carbon and silicon content, the fluidity of the alloy increases and the linear contraction, the tendency to form hot cracks and the tendency to bleach decrease;

THE ANNALS OF "DUNAREA DE JOS" UNIVERSITY OF GALATI
FASCICLE IX. METALLURGY AND MATERIALS SCIENCE
No. 4 - 2022, ISSN 2668-4748; e-ISSN 2668-4756
Article DOI: https://doi.org/10.35219/mms.2022.4.09

- hardness and tensile strength decrease as the carbon and silicon content increases;

- from equation (4) it can be seen that the casting temperature and the overheating temperature have a strong influence on the fluidity of the alloy, being directly proportional to it;

- the longer the overheating time, the more it leads to a decrease in the strength characteristics of the cast alloy, according to equations (9) and (10);

- the superheating temperature has a not very big but similar influence to the superheating time on the mechanical characteristics (mechanical strength and hardness) as shown by equations (9) and (10).

References

[1]. Riposan I., Chisamera M., *Tehnologia elaborarii si turnarii fontei*, Editura didactica si pedagogica, Bucuresti, 1985.
[2]. Cojocaru-Filipiuc V., *Pregatirea încărcaturii pentru elaborarea fontei în cuptoare cu inducţie*, Editura "Samia" Iaşi, 2006.
[3]. Taloi D., *et al.*, *Optimizarea proceselor tehnologice-aplicaţii în metalurgie*, Editura Academiei, Bucureşti, 1987.
[4]. Popescu D., Ionescu F., Dobrescu R., Stefanoiu D., *Modelare in ingineria proceselor industriale*, Editura AGIR, Bucuresti, 2011.
[5]. Ciuca I., Dumitriu S., *Modelarea si Optimizarea proceselor metalurgice de deformare plastica si tratamente termice*, Ed. Didactica si Pedagogica, Bucuresti, 1998.
[6]. Baron T., *et al.*, *Statistică teoretică şi economică*, Editura Didactică şi Pedagogică, Bucureşti, 1995.

THE ANNALS OF "DUNAREA DE JOS" UNIVERSITY OF GALATI
FASCICLE IX. METALLURGY AND MATERIALS SCIENCE
Nº. 4 - 2022, ISSN 2668-4748; e-ISSN 2668-4756
Article DOI: https://doi.org/10.35219/mms.2022.4.10

PHYSICO-CHEMICAL ANALYSIS OF DRINKING WATER FROM THE TOWN OF BÂRLAD, VASLUI COUNTY

Gina Genoveva ISTRATE, Irina-Nicoleta PENIȘOARĂ
"Dunarea de Jos" University of Galati, Romania
e-mail: gina.istrate@ugal.ro

ABSTRACT

The quality of drinking water was investigated in two localities from Vaslui county (Bârlad and Văleni) by comparison with a sample from Galați county. A number of parameters such as pH, turbidity, conductivity, nitrates, nitrites, temporary hardness, dissolved oxygen were analysed for each water sample collected during the month of May. The obtained values of each parameter were compared with the standard values set by the local standards, Law no. 458/2002 regarding the quality of drinking water.

KEYWORDS: drinking water, physico-chemical analysis, nitrate, pH value, hardness

1. Introduction

Water is an essential constituent of living matter, having a role in the development of vital processes. For the adult human body, water represents approximately 60% of its body weight. Drinking water is important to public health, whether it is used for domestic use, recreational purposes, or food production. Improved water supply and sanitation and better management of water resources can boost countries' economic growth and contribute greatly to poverty reduction [1].

The water quality of Romania is monitored according to the methodological structures and principles of the *Sistemului de Monitoring Integrat al Apelor din România* - S.M.I.A.R. (Integrated Water Monitoring System in Romania), restructured according to the European Directives' requirements.

A number of scientific procedures and tools have been developed to assess drinking water contaminants. These procedures include the analysis of various parameters such as pH, turbidity, conductivity, total suspended solids (TSS), total dissolved solids (TDS), temporary and total hardness, dissolved oxygen. These parameters can affect the quality of drinking water, if their values are in concentrations higher than those of the safety limits established by the World Health Organization (WHO) and other regulatory bodies. Therefore, drinking water quality survey by researchers and government departments has been regularly conducted all over the world [2-4].

Nitrates are a common pollutant of drinking water, with a major source being the use of fertilizers in agricultural activities, and in some countries nitrate levels in drinking water supplies have increased due to more intensive agriculture and animal husbandry. Nitrates in water are dangerous because they turn into nitrites, either by boiling or in the body, and nitrites affect haemoglobin and metabolism. The exposure limit for nitrate in drinking water set by the World Health Organisation (WHO) and adopted by many countries, is 50 mg/L NO_3^- (nitrate ion). Several epidemiological studies have investigated the possible association between chronic exposure to nitrates in drinking water and the risk of bladder, colon or rectal cancer [5-6].

The determination of microplastics or antibiotics in drinking water is also very topical. The number of scientific publications on microplastics in surface water and in drinking water has increased exponentially. These indicated that microplastics are frequently found in drinking water sources. The effects on human health are not yet known, but plastic often contains additives such as stabilizers or flame retardants, as well as other toxic chemicals that can be harmful to animals or humans who ingest them [7, 8].

In order to carry out the water quality study, four samples of drinking water were collected from different areas: one sample of well water and one tap water from the town of Văleni – Vaslui county; one sample from the tap of the public supply system in the town of Bârlad and one sample from the tap of the public supply system in the town of Galați. The water samples from Galați and Văleni, Vaslui county, were

THE ANNALS OF "DUNAREA DE JOS" UNIVERSITY OF GALATI
FASCICLE IX. METALLURGY AND MATERIALS SCIENCE
Nº. 4 - 2022, ISSN 2668-4748; e-ISSN 2668-4756
Article DOI: https://doi.org/10.35219/mms.2022.4.10

analysed in order to compare the tap water of the public supply system of Bârlad.

2. Experimental results

2.1. Determination of water turbidity

The turbidity of the water is due to the presence in water of very fine particles (organic and inorganic) that are in suspension and that do not settle over time. Turbid water is an epidemiological danger because suspended particles can constitute a support for pathogenic germs.

Turbidity represents the optical scattering effect of a light flux when passing through a fluid medium that contains particles in suspension or in a colloidal state.

The quantitative determination of the turbidity is done in the laboratory with the turbidimeter (Figure 1). The determination of turbidity is based on the Tyndall effect, according to which turbid water becomes bright if a light beam passes through it, due to the fact that the suspended particles laterally scatter some of the light rays [9].

Fig. 1. *Turbidimeter HACH*

The measure unit used in measuring turbidity is the Formazin Nephelometric Unit (FNU). Figure 2 shows the results obtained after the turbidity determination.

From the chart it can be seen that the water sample that has the highest turbidity value is the Văleni well water - 1.2 FNU, while the other samples have values close to 0.4 FNU. From the analysed samples, none of them exceeded the maximum value allowed by the legislation in force, according to Law 458/2002 including subsequent amendments and additions. The maximum admitted valued is 5 FNU. Therefore, all analysed samples are within the maximum limit allowed by the law in force.

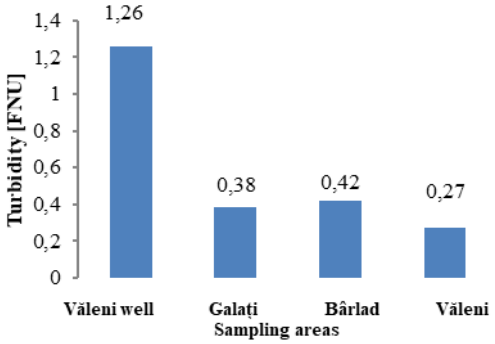

Fig. 2. *Results obtained from the determination of turbidity*

2.2. Determination of water pH

The water's pH is one of the most important factors when it comes to water quality, irrespective of whether it is well water or drinking water from the public supply system. Law no. 458/2002 regarding the quality of drinking water stipulates a pH between 6.5-9.5. Water that has a pH between 0-7 is considered acid, the pH 7 of the water shows that the water is neutral, and above the level of 7 pH units the water has a basic character, it is alkaline.

The pH determination for this article was carried out with the HACH multiparameter with the special pH probe. Figure 3 shows the results obtained after the pH determination.

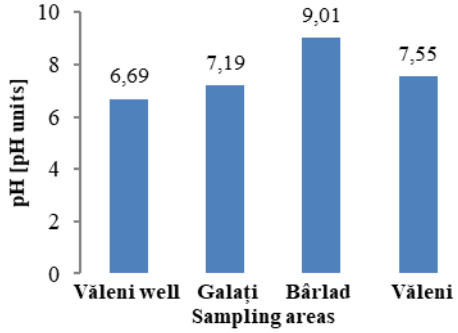

Fig. 3. *Results obtained from the determination of pH*

From the above chart, it can be seen that the water sample with the highest pH is the one collected from the public supply system of Bârlad with a value of 9 pH units that has an alkaline character, while the other analysed water samples have close pH values between 6.69 to 7.55.

According to Law no. 458/2002 regarding the quality of drinking water, the pH value of the

THE ANNALS OF "DUNAREA DE JOS" UNIVERSITY OF GALATI
FASCICLE IX. METALLURGY AND MATERIALS SCIENCE
N°. 4 - 2022, ISSN 2668-4748; e-ISSN 2668-4756
Article DOI: https://doi.org/10.35219/mms.2022.4.10

drinking water must be between 6.5 and 9.5 pH units. All analysed water samples do not exceed the maximum value allowed by the legislation in force.

2.3. Determination of water conductivity

Conductivity is a measure of the water's ability to conduct an electrical current. Conductivity in water is affected by the presence of dissolved inorganic solids, like chloride, nitrate, sulphate, and phosphate anions (ions that carry a negative charge) or sodium, magnesium, calcium, iron, and aluminium cations (ions that carry a positive charge).

The basic unit of conductivity is the siemens. Conductivity is measured in micro siemens per centimetre (µs/cm).

Conductivity is measured with the HACH multiparameter and a probe for determining conductivity. The voltage is applied between two electrodes in a probe immersed in the water sample. The voltage drop caused by water resistance is used to calculate the conductivity per centimetre. The indicator converts the probe measurement in micro siemens per centimetre and displays the result to the user.

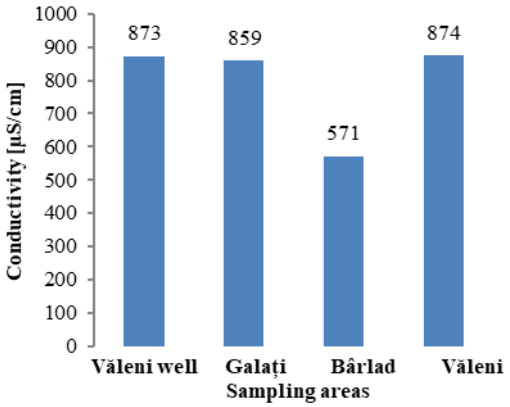

Fig. 4. *Results obtained from the determination of water conductivity*

From the data presented in figure 4, it can be seen that the highest value of conductivity is the Văleni tap sample, i.e., 874 µS/cm, and the lowest conductivity was obtained by the drinking water from the public supply system of Bârlad.

According to the legislation of Romania, the admitted value for the water's electrical conductivity is 1000 µS/cm, which indicates that the analysed samples are within the limits imposed by the legislation.

2.4. Determination of hardness

The water hardness is the total concentration of calcium and magnesium ions from a water sample and is indicated as calcium carbonate concentration. Temporary hardness is a part of the total hardness that disappears on boiling.

The main natural sources of hardness in water are polyvalent metallic dissolved ions from sedimentary rocks, seepage and leaks from soils. Calcium and magnesium, the two main ions, are present in many sedimentary rocks, the most common being limestone and chalk.

Water hardness is measured in hardness degrees (German - °dH, French - °TH, English - °e, American) and in mE/L (milliequivalents/liter of water). In Romania the German hardness degree is used (°dH).

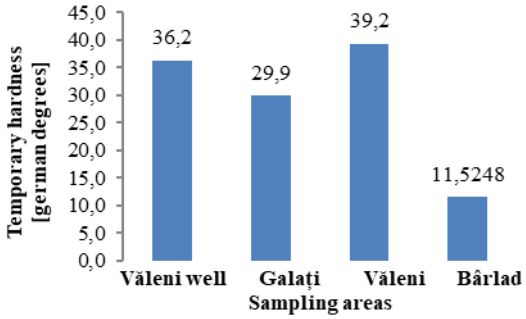

Fig. 5. *Results obtained from the determination of temporary hardness*

After determining the temporary hardness of the analysed water samples, it was observed that the lowest value was obtained for the water sample collected from the public supply system of Bârlad, with a value of 11.52 German degrees, and the highest value is from the Văleni tap water, with a value of 39.2 German grades.

2.5. Determination of nitrates

Nitrates are also found naturally at safe and healthy levels in some foods (such as spinach and carrots) and come from natural processes such as plant decomposition. Nitrates are in many fertilizers used on yards, golf courses and crops. Other sources of nitrates include discharge from sewage systems and animal waste.

Natural processes can lower the level of nitrates in drinking water – usually less than 3 mg/L. The health concern is with nitrate levels above 10 mg/L. High level of nitrates in water can be the result of the leak or leaks from fertilized soil, sewage, landfills, animal feedlots, septic systems, or urban drainage. It can be difficult to identify the source of nitrates in

THE ANNALS OF "DUNAREA DE JOS" UNIVERSITY OF GALATI
FASCICLE IX. METALLURGY AND MATERIALS SCIENCE
Nº. 4 - 2022, ISSN 2668-4748; e-ISSN 2668-4756
Article DOI: https://doi.org/10.35219/mms.2022.4.10

drinking water because there are a lot of possibilities [10].

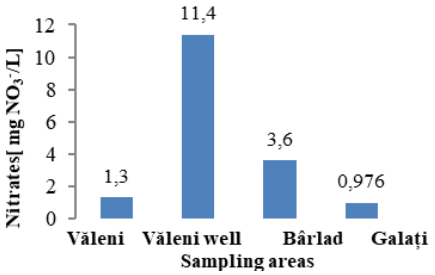

Fig. 6. *Results obtained from the determination of nitrates*

According to the attached chart in figure 6., it can be observed that the highest value for nitrates was obtained by the well water sample from Văleni – Vaslui county, with a higher value than the other samples, i.e., 11.4 mg NO_3^-/L, followed by the other samples with low values. The lowest value was obtained by the sample collected from the public supply system of Galați.

Romanian legislation imposes a maximum admissible limit for nitrates in water of 50 mg NO_3^-/L, which means that no sample exceeded the maximum amount allowed by law.

In Romania, nitrate poisoning is still a problematic reality, especially in the north-eastern region of the country.

2.6. Determination of nitrites

Nitrites are a salt or ester anion of nitric acid that can be naturally or artificially present in groundwater. Nitrites come from fertilizers through water drain, sewage and mineral deposits. Nitrite is used in food production for curing meat products because it inhibits the growth of bacteria. Unfortunately, it can also stimulate bacteria growth when it is introduced in high levels in a body of water.

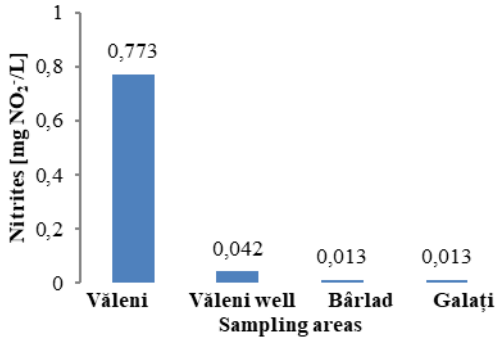

Fig. 7. *Results obtained from the determination of nitrites*

High levels of nitrites are toxic for people and animals, especially for babies. They can enter the body as nitrates, a nutrient that is essential for plant growing and it can be transformed in nitrites that disrupt the ability of haemoglobin to deliver oxygen in the bloodstream [10].

According to the above chart, it can be seen a high difference between the highest and lowest value. The highest value of nitrites can be found in the water from the public supply system of Văleni with a value of 0.773 mg NO_2^-/L, while the other samples have close values. The lowest value was obtained for the water sample from the public supply system of Galați, 0.013 mg NO_2^-/L.

The Romanian legislation provides an admissible maximum limit of 0.5 mg NO_2^-/L. Therefore, it can be observed that the tap water sample from Văleni – Vaslui county, exceeds the maximum concentration allowed by law with a value of 0.22 mg NO_2^-/L.

2.7. Determination of oxygen content in waters

Oxygen is a soluble gas and it is found in water as O_2 molecules. The presence of oxygen in water conditions the existence of the vast majority of aquatic organisms. All waters that are in contact with the atmospheric air contain dissolved oxygen while underground waters are low in oxygen. The solubility of oxygen in water depends on atmospheric pressure, air temperature, water temperature and salinity.

The volumetric (iodometric) method was proposed in order to determine the oxygen.

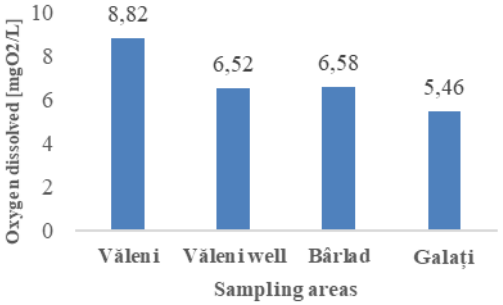

Fig. 8. *Results obtained from the determination of oxygen dissolved*

The concentration of dissolved oxygen is expressed in mg O_2/L or by the degree of water saturation with oxygen. The saturation degree represents the ratio between the quantity of oxygen found in the analysed water sample and the quantity of oxygen dissolved in water under saturation conditions [10].

THE ANNALS OF "DUNAREA DE JOS" UNIVERSITY OF GALATI
FASCICLE IX. METALLURGY AND MATERIALS SCIENCE
Nº. 4 - 2022, ISSN 2668-4748; e-ISSN 2668-4756
Article DOI: https://doi.org/10.35219/mms.2022.4.10

Oxygen dissolved in water oxidizes the manganese hydroxide in manganic hydroxide which in the acidic environment removes iodine from potassium iodide in an amount equivalent to the oxygen dissolved in water and which is titrated with sodium thiosulfate in the presence of starch solution.

In the chart presented in figure 8, it can be seen that the highest value of oxygen content in water was determined for the water sample from the public supply system of Văleni with a value of 8.82 mg O_2/L. The lowest value was obtained by the water sample collected from the public supply system of Galați with a value of 5.46 mg O_2/L.

From the presented data, it can be observed that the highest value for oxygen saturation is obtained for the tap water sample from Văleni – Vaslui county with a value of 99.932%. The well water sample from Văleni and the water sample from the public supply system of Bârlad have close values of 78% and the lowest value was obtained for the public supply system with drinking water of Galați, i.e., 65.179%.

3. Conclusions

Following the determinations made, we can conclude that:

- all analysed water samples do not exceed the maximum value of pH, conductivity, temporary hardness, nitrates and oxygen dissolved allowed by the legislation in force;

- the highest value of nitrites can be found in the water from the public supply system of Văleni with a value of 0.773 mg NO_2^-/L. The Romanian legislation provides an admissible maximum limit of 0.5 mg NO_2^-/L. Therefore, it can be observed that the tap water sample from Văleni – Vaslui county, exceeds the maximum concentration allowed by law with a value of 0.22 mg NO_2^-/L.

References

[1]. World Health Organization, *Guidelines for Drinking-water Quality*, Third Edition, vol. 1, Geneva, 2004.

[2]. Rahmanian N., Ali S. H. B., Homayoonfard M., Ali N. J., Rehan M., Sadef Y., Nizami A. S., *Analysis of physiochemical parameters to evaluate the drinking water quality in the State of Perak*, Malaysia, J. Chem., 716125, 2015.

[3]. Thomas Küpper, Christian Apel, Daniela Bertsch, Michael van der Giet, Simone van der Giet, Maren Graß, Carina Cerfontaine, Miriam Haunolder, Nina Hundt, Christian Kühn, Audry Morrison, Sonja Museo, Lisa Timmermann, Knut Wernitz, Julia Jäger, *Analysis of local drinking water for fecal contamination in Solu-Khumbu / Mt. Everest region*, Nepal, International Journal of Hygiene and Environmental Health, 246, 114043, 2022.

[4]. Poojashree B. P., Peladdy B., Kaveri H., Akkivalli P., Swathi L. A., *Determination of Physio-Chemical Parameters and Water Quality Index (Wqi) of Kundapura Taluk*, Udupi District, Karnataka, India, Pollutants, 2(3), p. 388-406, https://doi.org/10.3390/pollutants2030026, 2022.

[5]. Ahmed Arafa, Ashraf Ewis, Ehab Eshak, *Chronic exposure to nitrate in drinking water and the risk of bladder cancer: a meta-analysis of epidemiological evidence*, Public Health, 203, p. 123-129, 2022.

[6]. Mark Elwood J., Bert van der Werf, *Nitrates in drinking water and cancers of the colon and rectum: a meta-analysis of epidemiological studies*, Cancer Epidemiology, 78, 102148, 2022.

[7]. Patrick S. Bäuerlein, Roberta C. H. M. Hofman-Caris, Eelco N. Pieke, Thomas L. ter Laak, *Fate of microplastics in the drinking water production*, Water Research, 221, 118790, 2022.

[8]. Dan-Yu Huang, Yan Wu, Yan-Jun Jiang, Min-Shan Zhang, Long Cheng, Shu-Hai He, Biao-Juan Chen, *Rapid determination, pollution characteristics and risk evaluations of antibiotics in drinking water sources of Hainan*, China, Chinese Journal of Analytical Chemistry, 50.12, 100164, 2022.

[9]. Carmen Zaharia, *Chimia mediului – teste de laborator și probleme*, Editura Performantica, ISBN: 978-606-685-148-0, 2014.

[10]. Maria Cioroi, *Analize chimice de ape și sol*, Editura Evrika Brăila, ISBN 973-8052-49-1, 2000.

THE ANNALS OF "DUNAREA DE JOS" UNIVERSITY OF GALATI
FASCICLE IX. METALLURGY AND MATERIALS SCIENCE
N°. 4 - 2022, ISSN 2668-4748; e-ISSN 2668-4756
Article DOI: https://doi.org/10.35219/mms.2022.4.11

TRENDS ON REINFORCED POLYMER COMPOSITES – A REVIEW

Tamara APARECI (GÎRNEȚ), Irina DĂNĂILĂ (ȚÎCĂU), Iulian PĂDURARU, Adrian CÎRCIUMARU, Mihaela-Claudia GOROVEI
"Dunarea de Jos" University of Galati, Romania
e-mail: mihaela_gorovei@yahoo.com

ABSTRACT

In recent years, the interest in using fiber reinforced composites (FRC) has increased due to their potential to replace traditional materials in various applications. The advantages of polymer composites from natural fibres are: biodegradability, high performance, market availability and low price. This article is based on a review that discusses both polymer composite materials and typical applications by other authors on fiber reinforced composites (FRCs).

KEYWORDS: polymer, fibres, composites

1. Introduction

The development of composite materials plays a crucial role in the advancement of technology [1-5]. Considering that both industrial and technological requirements are continuously increasing in fields (energy, naval, aerospace and automotive), there is a need for devices based on high-performance materials that can perform more than one function. This frequently involves the ability to respond in a controllable way to a certain physical or chemical stimulus, changing at least one of the material properties in direct correlation with the external stimulus [6].

Fiber reinforced composite materials are used in various industries due to their mechanical strength, modulus and corrosion resistance. Polymer nanocomposites based on carbon nanostructures for strain and temperature self-sensing have been proposed as the next generation of materials that are expected to overcome the well-known problems of inorganic sensors, such as complex processing, brittleness, narrow sensing range, and high sensitivity [7-10]. The polymer blend is the addition of two polymers at the macromolecular level, and the phase-separated morphology will influence the mechanical performance of the blend. Due to the poor reactivity of polymer-based materials with modifiers, poor adhesion between the epoxy and the modifier can result, and that can lead to a reduction in the mechanical properties of the composite. Therefore, the characterization of polymer matrix composites is essential [11].

For the synthesis of polymer-based composites there are, at least, two processes that are governing the formation of polymers and associated composites: direct processing and in situ preparation. The direct mixing method involves synthesizing the desired nanomaterial and then dispersing it into the polymer matrix either by solution or mechanical dispersion. In the case of preparing composites based on in situ polymerization, the polymeric material creates a microenvironment to produce the desired metal/metal oxide from the precursors through series of chemical reactions. This process is of particular interest because the particle size and morphology could be easily controlled [12]. Analysing current trends, it can be seen that fiber reinforced thermosetting composites are among the most important materials. Due to the reliable mechanical performance of fiber reinforced polymer (FRP) composites, they have gained a huge market opening with inherent properties such as high corrosion resistance, high strength and improved fatigue resistance. These properties are superior because they are based on the interfacial bonds and cross-links between the matrix and the fiber. Thermosetting matrices such as epoxy, vinyl ester and polyester are commonly used as polymer matrices. Among them, epoxy resin is commercialized as a structural adhesive and as a polymer matrix for FRP composites [13]. Modification of epoxy resin (EP) with nanofillers has been extensively explored over the past three decades. Nanomaterials including carbon nanotubes, nanofibers (VGCF), organoclay, graphene oxide (GO) and its derivatives, functionalized aramid nanofibers (fANF) have been used in EP modification [14].

THE ANNALS OF "DUNAREA DE JOS" UNIVERSITY OF GALATI
FASCICLE IX. METALLURGY AND MATERIALS SCIENCE
Nº. 4 - 2022, ISSN 2668-4748; e-ISSN 2668-4756
Article DOI: https://doi.org/10.35219/mms.2022.4.11

2. Kevlar fibres

Due to its unique properties, Kevlar fiber has become very popular as reinforcing material in composite materials, and its applications are considerably increasing [15-17]. Composite materials reinforced with synthetic fibres have become significantly popular over the years [18-20]. Among the synthetic fibres, poly-aramid fibres known as Kevlar fibres are mainly used for applications in industrial and advanced technologies such as ballistic armour, helicopter blades, pneumatic fittings, sports goods [21-23]. Their application has become considerably very wide due to its excellent mechanical properties, lighter weight, unique flexibility, corrosion resistance, ease of manufacture, etc. [24-26]. Compared with other synthetic fibres, Kevlar fiber has an elongation of fibres significantly lower and higher tensile strength and modulus [27]. They also exhibit very good properties at high temperatures for a polymeric material [28-30]. The glass transition temperature of Kevlar fiber is around 360 °C and it does not melt like nylon [31-33].

3. Polymer matrix composites (PMCs)

PMCs are promising materials for many engineering applications due to their superior properties such as self-lubricating properties, excellent chemical stability, electrical insulation properties, and wear resistance [34-37]. They have applicability in the aerospace, marine and sports industries. Also, other applications include the toy industry, coal handling equipment in power plants, bearings, transmission pumps, cosmetics and medical devices [38-42]. The advantages of polymer composites from natural fibres are: biodegradability, high performance, availability on the market and low price [43-48]. Hybrid composite is the material made from natural fibres and carbon fibres [49-51]. Interest in fabric-reinforced thermoplastic matrix composites has increased in recent years due to their faster processing possibilities compared to traditional thermo-resistant matrix composites [52, 53]. Textiles pre-impregnated with thermoplastic resins can be heated above the melting point of the matrix in seconds using infrared heaters and can be formed into a three-dimensional (3D) component [54-62], which involves significantly longer cycle times shorter than autoclave processing or resin transfer techniques [63-72]. Advanced fabrication techniques such as local reinforcement by tape placement is also facilitated due to the presence of the thermoplastic matrix [34]. Improved performance, shorter cycle times and reduced density are some features that have made woven thermoplastic composites attractive for the aerospace and automotive industries [73-76]. Polymer matrix composites can be fabricated by various methods such as liquid casting, compression moulding, resin injection, and injection moulding, all of which belong to autoclave manufacturing methods [77-79]. In the field of external strengthening and repair of existing structures made of traditional materials such as concrete and masonry, fiber reinforced polymer (FRP) [80-84], has attracted much attention worldwide due to its ease of application, ability to limit impact aesthetic of repair works to the original structure and its appropriate reversibility for historical or artistic reasons [85-89]. Currently, almost all FRP applications [90-92], involve FRP made with glass fiber (GFRP) [93-96], carbon fiber (CFRP) [97-102], and in a smaller measure aramid fiber (AFRP) [103-117].

4. Epoxy resin

There are different types of epoxy resins, such as bisphenol A diglycidyl ether, cycloaliphatic epoxy resins, trifunctional epoxy resins, and tetrafunctional epoxy resins [118]. The global commercialization of epoxy resins market reached USD 25.8 billion in 2018, and for the year 2022 it is estimated to be around USD 34 billion [119]. Among these, bisphenol A diglycidyl ether is the most widely used in the coating industry due to its low cost and many desirable properties such as hardness, gloss and chemical resistance. Epoxy resin is one of the most common thermoset resins widely used as composite matrix and high-performance coatings due to its excellent characteristics such as: mechanical strength, chemical resistance, low shrinkage and electrical insulating properties [120-122]. Since the 1950s, various reports have appeared in the literature detailing the complex internal nanostructure of epoxy resin [123]. One of the disadvantages of epoxy resin is the brittleness caused by the tight three-dimensional (3D) polymer network. In recent years, efforts have been made to solve the problem of fragility. The hardness of epoxy can be improved by using elastomers, thermoplastic materials, nanofillers [124]. The most common component of epoxy resins is diglycidyl ether bisphenol A (DGEBA). DGEBA is industrially synthesized by reacting bisphenol A (BPA) with a large excess of epichlorohydrin under alkaline conditions [125]. The behavior of the resin depends on certain factors such as time, temperature, curing speed and pressure on the curing process. Characterization of the cure-dependent thermo-mechanical behavior of a fast-curing resin under process-relevant conditions remains a challenge [126-128]. It is known that when properly cured, epoxy resins exhibit a high crosslink density. When used as matrices in polymer composites, brittle resins can

THE ANNALS OF "DUNAREA DE JOS" UNIVERSITY OF GALATI
FASCICLE IX. METALLURGY AND MATERIALS SCIENCE
Nº. 4 - 2022, ISSN 2668-4748; e-ISSN 2668-4756
Article DOI: https://doi.org/10.35219/mms.2022.4.11

produce composites with low damage tolerance [129-131]. Epoxy resins are frequently used as matrix of fiber reinforced composites. Matrix cracking has been shown to occur throughout the fracture process of the composite, particularly under fatigue loading. Brittleness of epoxy resins is the main source of composite failure, which can trigger composite defects such as delamination and debonding [132].

5. General presentation of the applications of composite materials

Cheng Chen *et al.* [133] performed a comparative analysis of natural fiber reinforced polymer and carbon fiber reinforced polymer for the strengthening of reinforced concrete beams. Due to the large amount of impregnated epoxy resin, the cost advantage of natural fibres was offset, and the overall cost efficiency of NFRP laminates ranged from 60% to 160% compared to CFRP laminates.

Sebastian Huayamares *et al.* [134] used unidirectional glass fiber reinforced epoxy, carbon fiber reinforced quasi-isotropic epoxy, and quasi-isotropic glass fiber reinforced epoxy to compare three-point bending and torsion methods to determine the viscoelastic properties of fiber-reinforced epoxy. This study showed that an irregular sample width can result in large dispersions in storage modulus values. Torsion tests, on the other hand, gave results that were consistent for fiber-reinforced composites regardless of specimen length, providing a more suitable method if materials are scarce and specimen length must be limited. Absolute values for viscoelastic properties cannot be directly compared between the three-point bending and torsion methods. At three-point bending, the storage and loss moduli were always higher than those measured in the torsional modulus for all of the studied composites.

This demonstrates that three-point bending measures higher moduli than torsion, regardless of fiber orientation, fiber type, or epoxy resin used for the two devices and test modes specified in this study.

Abdel-Hamid I. Mourad *et al.* [135] investigated the effect of nano additives on the damage resistance of a newly developed Kevlar fabric. Three types of nano additives were investigated: (1) silicon carbide (SiC), (2) aluminium oxide (Al_2O_3), and (3) carbon nanotubes. Damage was mainly observed in and around the impact area. The addition of small amounts of nano additives to Kevlar composites effectively improved the damage propagation resistance and interlaminar shear strength of the fabricated composites. In addition, increasing the nano additive content an improvement in the energy absorption capacity of the composites, especially with SiC and Al_2O_3 is observed, as the number of damaged layers and the percentage of damaged area decreases. Among all the samples examined, the lowest number of damaged layers with the smallest damaged area was obtained with the addition of 0.5% by mass.

Ali Tabatabaeian, and Ahmad Reza Santhosh G. and Rajath N. Rao [136] fabricated polymer hybrid composites based on thermosetting resins using different hybrid fibres/fabrics with and without castor oil. The effect of reinforcements and/or castor oil on mechanical and thermal behaviours were evaluated. The results showed that the tensile, flexural and impact strength of composites with castor oil increases compared to composites without castor oil. The thermal behaviour was evaluated using DMA, the results showed an increase in the damping properties of the composites with castor oil. Lower glass transition temperature for castor oil composites indicated better damping behavior at higher temperatures.

Bo Yang *et al.* [137] analysed the nesting effect on laminates. They found that compared to increasing the length of the main flow channel, decreasing the width is a more significant factor in reducing through-thickness permeability. The results also show that a considerable degree of Nesting can occur due to unidirectional displacement, the total thickness can decrease by up to 5-6%, and the through-thickness permeability reduction can reach up to 80%. Bidirectional fabric displacement leads to a greater degree of Nesting, the total thickness decreases by more than 12%, and the through-thickness permeability decreases by more than two orders of magnitude.

Dhanush Kumar *et al.* [138] analysed the tensile behavior of Kevlar and glass fiber reinforced hybrid polymer composite as a function of cut-out size and position. Based on the experimental results obtained after subjecting the Kevlar and fiberglass reinforced composites to tensile testing, the authors state that the strength of the plates was improved by making the holes further from the centre, where the load carrying capacity was higher and the concentration factor upon request it was smaller. The authors stated that by moving the holes away from the centre a higher load capacity is obtained. It was also observed that the strain hardening coefficient increases linearly from sample 1 to sample 5 indicating higher resistance to necking before fracture. This means that the boards can be stretched longer by moving the holes away from the centre.

Silvio Leonardo Valença *et al.* [139] evaluated the mechanical behavior of epoxy composite reinforced with plain Kevlar fabric and glass/Kevlar hybrid fabric. Thanks to the values obtained after the mechanical tests, it can be seen that the structures developed with Kevlar and glass fiber hybrid fabrics have transferred the highest values of mechanical

THE ANNALS OF "DUNAREA DE JOS" UNIVERSITY OF GALATI
FASCICLE IX. METALLURGY AND MATERIALS SCIENCE
Nº. 4 - 2022, ISSN 2668-4748; e-ISSN 2668-4756
Article DOI: https://doi.org/10.35219/mms.2022.4.11

strength and specific stiffness, becoming a new alternative for use as a structural laminated composite in the industrial market.

Xu W., *et al.* [140] performed experimental and analytical characterizations of finite interlaminar crack growth of 2D woven textile composites. The authors concluded that: the interlaminar static fracture resistance of the woven composite material determined by the double compliance method is consistent with that of the ASTM methods. The relative difference between the average fracture resistance obtained by these methods is less than 3%. The crack growth length can be accurately calculated using the dual compliance method, this advantage will significantly simplify the measurement of the strength at break of woven textile composites. The fracture strength of the unstable crack is given, in this paper, by using the dual compliance method. The fracture strength during unstable crack growth is lower than the initial fracture strength and results in the unstable growth of finite cracks.

Velmurugan V., *et al.* [141] performed an experimental evaluation of the mechanical properties of natural fiber reinforced polymer composites. The authors found that jute reinforcement with nylon fillers exhibits higher flexural strength compared to the combination of nylon and spider silk fillers in the flexural test. Reinforcement of the composite with spider silk and nylon fillers with epoxy matrix achieved higher toughness, and reinforcement with jute and nylon fillers with epoxy matrix achieved higher flexural and tensile strengths.

Murugan R., *et al.* [142] investigated the static and dynamic mechanical properties of glass epoxy composite fabrics and hybrid carbon composite laminates. Carbon laminate has higher mechanical strengths than glass laminate, except impact resistance. The variation in tensile strength and impact strength between the hybrid laminates is minimal, and the H2 hybrid layout has a higher flexural strength than the H1 hybrid laminate. The glass transition temperature, T_g of the H2 laminate has been changed by 5 °C to the glass laminate, which facilitates the higher operating temperature. The hybrid laminate with carbon fiber as the wrap layer, H2, performs better than another hybrid arrangement H1 and proves to be a good alternative for the glass laminate.

Jun Misumia and Toshiyuki Oyama [143] fabricated low-viscosity, high-strength epoxy resin modified by in situ radical polymerization method to improve the mechanical properties of carbon fiber reinforced plastics. In order to obtain both good mechanical properties, including the strength and toughness of the cured resin and the reduced viscosity of the uncured resin composition, the *radical in situ polymerization method* was applied to the epoxy resin for the CFRP matrix. The results demonstrated that the *in situ radical polymerization method* can be effective for improving the fracture strength of CFRP laminates while maintaining the low viscosity of the uncured resin composition.

Mawarnie Ismail, *et al.* [24] studied the mechanical properties of composites made by reinforcing epoxy resin with bidirectional glass fibres and short RH fibres. The total fiber content for each sample was 30% and 70% by mass for the epoxy resin. The mass distributions for the RH fiber were between 5%, 10% and 15% by mass, while 25%, 20% and 15% by mass for the bidirectional glass fiber. It was indicated that its mechanical properties tend to decrease when the RH fiber content exceeds 5% by mass.

Kiran M. D., *et al.* [144] evaluated the breaking strength of carbon fiber and epoxy composite with different carbon fiber thicknesses. The composites were fabricated using hand-stretching technique by infusing 200 gsm, 400 gsm resin and hybrid carbon fabric laminate. The fracture toughness of the hybrid carbon fiber composites was studied using the single-edge notched beam method at room temperature (25 °C). From the experimental results, it was found that the epoxy composites reinforced with 200 gsm carbon fiber resist at breaking better compared to the composites reinforced with other fibres.

Goli E., *et al.* [145] developed a homogenized thermochemical model to simulate the production of unidirectional composites made of carbon fibres embedded in a thermoset dicyclopentadiene (DCPD) matrix using frontal polymerization (FP). The reaction-diffusion model is then solved using the finite element method to investigate the temperature evolution and degree of hardening during the manufacturing process. The results reveal two different processing regimes: At lower fiber volume fractions, the polymerization front speed increases with fiber volume fraction due to the increase in the effective thermal conductivity of the composite. At higher fiber volume fractions, the frontal velocity decreases with increasing fiber content due to the reduced heat source generated by the exothermic reaction.

Dai S., *et al.* [146] fabricated six types of 3D woven composites from carbon fiber and epoxy matrix. They studied the influence of fiber architecture on the tensile, compressive and flexural behavior of 3D woven composites. Four orthogonal weaves and two blocking angles were tested with the primary loading direction parallel to the warp direction. The mechanical performance was found to be affected by the distribution of resin-rich regions and the waviness of the load-bearing fibres, which were determined by the fiber architectures. Bonding points in resin-rich regions were found to be the sites

THE ANNALS OF "DUNAREA DE JOS" UNIVERSITY OF GALATI
FASCICLE IX. METALLURGY AND MATERIALS SCIENCE
Nº. 4 - 2022, ISSN 2668-4748; e-ISSN 2668-4756
Article DOI: https://doi.org/10.35219/mms.2022.4.11

of damage initiation in all fabric types under all loading conditions, which was confirmed with both visual observation and image correlation strain maps.

In [147], the authors investigated a new epoxy resin matrix carbon fiber reinforced composite with viscoelastic sandwich layers by co-reinforcement technology. After testing, it was found that the addition of 0.1 mm thick damping film in laminates could lead to a 1.34% decrease in tensile strength and a 1.30% increase in flexural strength of the composites, reaching up to at 878.5 MPa and 766.3 MPa. However, the bending strength decreased with increasing thickness of the damping layer. The new co-reinforced damping composite exhibited high shear strength. The co-reinforced damping composites studied in this paper exhibited excellent damping properties.

In [148], the authors conducted a study that provides a low-cost solution to improve the mechanical and electrical properties of carbon fiber reinforced polymer composites by incorporating ultra-thin sheets of carbon nanotubes (CNTs) between CFRP layers (laminates). For this purpose, dry carbon fiber fabrics are first sandwiched between CNT sheets. The fabrics are then stacked and infused with epoxy to form a CFRP with interlaminated CNT sheets. Unlike the typical approach where micron-sized long CNTs are randomly distributed in a CFRP for reinforcement, this study uses 100nm-thick CNT sheets made of aligned and ultra-long (0.3 mm) nanotubes. Despite their negligible mass fraction of only 0.016%, interlaminar CNT sheets enhanced CFRP flexural strength by 49%, interlaminar shear strength by 30%, and mode I fracture strength by 30%. X-ray micro-tomography has shown that samples with interlaminar CNTs are significantly resistant to delamination and crack propagation. Moreover, the in-plane electrical conductivity of these composites increased proportionally with the mass fraction of CNTs, giving a maximum improvement of 278% over the reference sample for 0.048 mass% of CNT sheets.

6. Conclusions

- composite materials show a wide interest from researchers who approach a problem that starts from the matrix, reaches the reinforcement and the characterization of the materials;

- a lot of research considers composites with polymer matrix - either thermoset or thermoplastic;

- working models and interpretations of the results are proposed and, within certain limits, they are acceptable;

- many studies are carried out that take into account small variations of the matrix properties to identify the response of the composite;

- many studies refer to the matrix-reinforcement interphase (or other elements immersed in the polymer) to increase the utility value of the composites;

- we did not find bibliographic references regarding the analysis of the properties of polymer junctions, although in the design of the properties of composites a solution is to use layered matrices;

- some studies carried out at CCDCOMT aimed at the analysis of composites with a layered matrix consisting of the same polymer but modified in a different way for certain depths in the composite (the modifications being produced either by the introduction of solvents or by the addition of organic or inorganic agents).

References

[1]. Madra A., Breitkopf P., Raghavan B., Trochu F., *Diffuse manifold learning of the geometry of woven reinforcements in composites*, Comptes Rendus Mécanique, vol. 346, no. 7, p. 532-538, doi: 10.1016/j.crme.2018.04.008, iul. 2018.

[2]. Nair R. G., Sundararajan T., Guruprasad P. J., *A novel framework using point interpolation method with voxels for variational asymptotic method unit cell homogenization of woven composites*, Composite Structures, vol. 202, p. 261-274, doi: 10.1016/j.compstruct.2018.01.072, oct. 2018.

[3]. Vassilopoulos A. P., *The history of fiber-reinforced polymer composite laminate fatigue*, International Journal of Fatigue, vol. 134, p. 105512, doi: 10.1016/j.ijfatigue.2020.105512, mai 2020.

[4]. Kazemi M., Fini E. H., *State of the art in the application of functionalized waste polymers in the built environment*, Resources, Conservation and Recycling, vol. 177, p. 105967, doi: 10.1016/j.resconrec.2021.105967, feb. 2022.

[5]. Das P., Banerjee S., Das N. C., *Polymer-graphene composite in aerospace engineering*, în Polymer Nanocomposites Containing Graphene, Elsevier, p. 683-711, doi: 10.1016/B978-0-12-821639-2.00001-X, 2022.

[6]. Pech-Pisté R., Cen-Puc M., Balam A., May-Pat A., Avilés F., *Multifunctional sensing properties of polymer nanocomposites based on hybrid carbon nanostructures*, Materials Today Communications, vol. 25, p. 101472, doi: 10.1016/j.mtcomm.2020.101472, dec. 2020.

[7]. Shakil U. A., Abu Hassan S. B., Yahya M. Y., Nurhadiyanto D., *A review of properties and fabrication techniques of fiber reinforced polymer nanocomposites subjected to simulated accidental ballistic impact*, Thin-Walled Structures, vol. 158, p. 107150, doi: 10.1016/j.tws.2020.107150, ian. 2021.

[8]. Huang T., Gong Y., *A multiscale analysis for predicting the elastic properties of 3D woven composites containing void defects*, Composite Structures, vol. 185, p. 401-410, doi: 10.1016/j.compstruct.2017.11.046, feb. 2018.

[9]. Karmazin A., Kirillova E., Seemann W., Syromyatnikov P., *Investigation of Lamb elastic waves in anisotropic multilayered composites applying the Green's matrix*, Ultrasonics, vol. 51, no. 1, p. 17-28, doi: 10.1016/j.ultras.2010.05.003, ian. 2011.

[10]. Gupta P., *Polymer-graphene composites as sensing materials*, Polymer Nanocomposites Containing Graphene, Elsevier, p. 401-424, doi: 10.1016/B978-0-12-821639-2.00017-3, 2022.

[11]. Miah M. H., Chand D. S., Rahul B., Malhi G. S., *Mechanical behavior of unsaturated polyester toughened epoxy hybrid polymer network reinforced with glass fibre*, Materials Today: Proceedings, vol. 56, p. 669-674, doi: 10.1016/j.matpr.2022.01.069, 2022.

THE ANNALS OF "DUNAREA DE JOS" UNIVERSITY OF GALATI
FASCICLE IX. METALLURGY AND MATERIALS SCIENCE
Nº. 4 - 2022, ISSN 2668-4748; e-ISSN 2668-4756
Article DOI: https://doi.org/10.35219/mms.2022.4.11

[12]. Yashas S. R., Shahmoradi B., Wantala K., Shivaraju H. P., *Potentiality of polymer nanocomposites for sustainable environmental applications: A review of recent advances*, Polymer, vol. 233, p. 124184, doi: 10.1016/j.polymer.2021.124184, oct. 2021.
[13]. Ganesh Gupta K. B. N. V. S., Hiremath M. M., Ray B. C., Prusty R. K., *Improved mechanical responses of GFRP composites with epoxy-vinyl ester interpenetrating polymer network*, Polymer Testing, vol. 93, p. 107008, doi: 10.1016/j.polymertesting.2020.107008, ian. 2021.
[14]. Wang W., Yu B., Zhang Y., Peng M., *Fully aminated rigid-rod aramid reinforced high strength epoxy resin and its composite with carbon fibers*, Composites Science and Technology, vol. 221, p. 109324, doi: 10.1016/j.compscitech.2022.109324, apr. 2022.
[15]. Bachchan A. A., Das P. P., Chaudhary V., *Effect of moisture absorption on the properties of natural fiber reinforced polymer composites: A review*, Materials Today: Proceedings, p. S2214785321019751, doi: 10.1016/j.matpr.2021.02.812, mar. 2021.
[16]. Zhou J., *et al.*, *Advanced functional Kevlar composite with excellent mechanical properties for thermal management and intelligent safeguarding*, Chemical Engineering Journal, vol. 428, p. 131878, doi: 10.1016/j.cej.2021.131878, ian. 2022.
[17]. Wu Y., *et al.*, *Liquid or solid? a biologically inspired concentrated suspension for protective coating*, Chemical Engineering Journal, vol. 428, p. 131793, doi: 10.1016/j.cej.2021.131793, ian. 2022.
[18]. Koohbor B., Ravindran S., Kidane A., *A multiscale experimental approach for correlating global and local deformation response in woven composites*, Composite Structures, vol. 194, p. 328-334, doi: 10.1016/j.compstruct.2018.04.016, iun. 2018.
[19]. Römelt P., Cunningham P. R., *A multi-scale finite element approach for modelling damage progression in woven composite structures*, Composite Structures, vol. 94, nr. 3, p. 977-986, doi: 10.1016/j.compstruct.2011.10.024, feb. 2012.
[20]. Jiang H., Ren Y., Gao B., Xiang J., *Numerical investigation on links between the stacking sequence and energy absorption characteristics of fabric and unidirectional composite sinusoidal plate*, Composite Structures, vol. 171, p. 382-402, doi: 10.1016/j.compstruct.2017.03.047, iul. 2017.
[21]. Saba N., Jawaid M., *Epoxy resin based hybrid polymer composites*, Hybrid Polymer Composite Materials, Elsevier, p. 57-82, doi: 10.1016/B978-0-08-100787-7.00003-2, 2017.
[22]. Madhavi P., Yadagiri G., Naveen A., Shravan M., Ravi A., Chandra Shekar K., *Flexural strength and inter laminar shear strength of carbon fabric and silk satin fabric reinforced hybrid composites*, Materials Today: Proceedings, vol. 19, p. 322-328, doi: 10.1016/j.matpr.2019.06.763, 2019.
[23]. Isart N., El Said B., Ivanov D. S., Hallett S. R., Mayugo J. A., Blanco N., *Internal geometric modelling of 3D woven composites: A comparison between different approaches*, Composite Structures, vol. 132, p. 1219-1230, doi: 10.1016/j.compstruct.2015.07.007, nov. 2015.
[24]. Ismail M., Rejab M. R. M., Siregar J. P., Mohamad Z., Quanjin M., Mohammed A. A., *Mechanical properties of hybrid glass fiber/rice husk reinforced polymer composite*, Materials Today: Proceedings, vol. 27, p. 1749-1755, doi: 10.1016/j.matpr.2020.03.660, 2020.
[25]. Shamohammadi Maryan M., Ebrahimnezhad-Khaljiri H., Eslami-Farsani R., *The experimental assessment of the various surface modifications on the tensile and fatigue behaviors of laminated aluminum/aramid fibers-epoxy composites*, International Journal of Fatigue, vol. 154, p. 106560, doi: 10.1016/j.ijfatigue.2021.106560, ian. 2022.
[26]. Louwsma J., Carvalho A., Lutz J.-F., Joly S., Chan-Seng D., *Adsorption of phenylalanine-rich sequence-defined oligomers onto Kevlar fibers for fiber-reinforced polyolefin composite materials*, Polymer, vol. 217, p. 123465, doi: 10.1016/j.polymer.2021.123465, mar. 2021.
[27]. Wang B., *et al.*, *Multiscale insights into the stretching behavior of Kevlar fiber*, Computational Materials Science, vol. 185, p. 109957, doi: 10.1016/j.commatsci.2020.109957, dec. 2020.
[28]. Li S., *et al.*, *Synthesis, processing and characterization of impact hardening gel (IHG) reinforced Kevlar fabric composites*, Materials & Design, vol. 195, p. 109039, doi: 10.1016/j.matdes.2020.109039, oct. 2020.
[29]. Chowdhury M. A., *et al.*, *Improvement of interfacial adhesion performance of the kevlar fiber mat by depositing $SiC/TiO_2/Al_2O_3$/graphene nanoparticles*, Arabian Journal of Chemistry, vol. 14, nr. 11, p. 103406, doi: 10.1016/j.arabjc.2021.103406, nov. 2021.
[30]. Lu W., Yu W., Zhang B., Dou X., Han X., Cai H., *Kevlar fibers reinforced straw wastes-polyethylene composites: Combining toughness, strength and self-extinguishing capabilities*, Composites Part B: Engineering, vol. 223, p. 109117, doi: 10.1016/j.compositesb.2021.109117, oct. 2021.
[31]. Singh T. J., Samanta S., *Characterization of Kevlar Fiber and Its Composites: A Review*, Materials Today: Proceedings, vol. 2, no. 4-5, p. 1381-1387, doi: 10.1016/j.matpr.2015.07.057, 2015.
[32]. Rana R. S., Buddi T., Purohit R., *Effect of SiC reinforcement on the mechanical properties of Kevlar fiber based hybrid epoxy composites*, Materials Today: Proceedings, vol. 44, p. 2478-2481, doi: 10.1016/j.matpr.2020.12.542, 2021.
[33]. Tilak S. R., Shuib Pasha S. A., Nayeem Ahmed M., Daniel S., *An experimental investigation of flexural and inter laminar shear stress on hybrid polymer based composites (E glass fibre – Kevlar fibre with Epoxy resin 5052) for different thickness*, Materials Today: Proceedings, vol. 46, p. 8991-8994, doi: 10.1016/j.matpr.2021.05.375, 2021.
[34]. Garoz D., Gilabert F. A., Sevenois R. D. B., Spronk S. W. F., Van Paepegem W., *Consistent application of periodic boundary conditions in implicit and explicit finite element simulations of damage in composites*, Composites Part B: Engineering, vol. 168, p. 254-266, doi: 10.1016/j.compositesb.2018.12.023, iul. 2019.
[35]. Vedrtnam A., Pawar S. J., *Laminated plate theories and fracture of laminated glass plate – A review*, Engineering Fracture Mechanics, vol. 186, p. 316-330, doi: 10.1016/j.engfracmech.2017.10.020, dec. 2017.
[36]. Obert E., Daghia F., Ladevèze P., Ballere L., *Micro and meso modeling of woven composites: Transverse cracking kinetics and homogenization*, Composite Structures, vol. 117, p. 212-221, doi: 10.1016/j.compstruct.2014.06.035, nov. 2014.
[37]. Prabhakar M. N., Naga Kumar C., Dong Woo L., Jung-IL S., *Hybrid approach to improve the flame-retardant and thermal properties of sustainable biocomposites used in outdoor engineering applications*, Composites Part A: Applied Science and Manufacturing, vol. 152, p. 106674, doi: 10.1016/j.compositesa.2021.106674, ian. 2022.
[38]. Pujar V., Devarajaiah R. M., Suresha B., Bharat V., *A review on mechanical and wear properties of fiber-reinforced thermoset composites with ceramic and lubricating fillers*, Materials Today: Proceedings, p. S2214785321012967, doi: 10.1016/j.matpr.2021.02.214, mar. 2021.
[39]. Mahdi E., Hamouda A. M. S., *Energy absorption capability of composite hexagonal ring systems*, Materials & Design, vol. 34, p. 201-210, doi: 10.1016/j.matdes.2011.07.070, feb. 2012.
[40]. Swarup Mohanty S., Kumar Rout A., Kumar Jesthi D., Chandra Routara B., Kumar Nayak R., *Evaluation of mechanical and wear performance of glass/carbon fiber reinforced polymer hybrid composite*, Materials Today: Proceedings, vol. 5, nr. 9, p. 19854-19861, doi: 10.1016/j.matpr.2018.06.350, 2018.
[41]. A. Tabatabaeian, Ghasemi A. R., *Curvature changes and weight loss of polymeric nano-composite plates with consideration of the thermal cycle fatigue effects and different resin types: An experimental approach*, Mechanics of Materials, vol. 131, p. 69-77, doi: 10.1016/j.mechmat.2019.01.017, apr. 2019.
[42]. Hu J., Liu Y., Zhang S., Tang B., *Novel designed core–shell nanofibers constituted by single element-doped $BaTiO_3$ for high-energy–density polymer nanocomposites*, Chemical Engineering

Journal, vol. 428, p. 131046, doi: 10.1016/j.cej.2021.131046, ian. 2022.
[43]. Suhas S., Raju M. J. S., Vijayan D. S., *Natural fibre reinforcement experimental study in polymer composite*, Materials Today: Proceedings, vol. 45, p. 6655-6659, doi: 10.1016/j.matpr.2020.12.051, 2021.
[44]. Sliseris J., Yan L., Kasal B., *Numerical modelling of flax short fibre reinforced and flax fibre fabric reinforced polymer composites*, Composites Part B: Engineering, vol. 89, p. 143-154, doi: 10.1016/j.compositesb.2015.11.038, mar. 2016.
[45]. Oliveira M. S., *et al.*, *Statistical analysis of notch toughness of epoxy matrix composites reinforced with fique fabric*, Journal of Materials Research and Technology, vol. 8, nr. 6, p. 6051-6057, doi: 10.1016/j.jmrt.2019.09.079, nov. 2019.
[46]. Mu B., Yang Y., *Complete separation of colorants from polymeric materials for cost-effective recycling of waste textiles*, Chemical Engineering Journal, vol. 427, p. 131570, doi: 10.1016/j.cej.2021.131570, ian. 2022.
[47]. Singh M. K., Singh A., *Fibers and fiber-forming polymers*, Characterization of Polymers and Fibres, Elsevier, p. 1-27, doi: 10.1016/B978-0-12-823986-5.00002-6, 2022.
[48]. Rizwan K., Rasheed T., Bilal M., *Nano-biodegradation of polymers*, Biodegradation and Biodeterioration at the Nanoscale, Elsevier, p. 213-238, doi: 10.1016/B978-0-12-823970-4.00010-5, 2022.
[49]. Benin S. R., Kannan S., Bright R. J., Jacob Moses A., *A review on mechanical characterization of polymer matrix composites & its effects reinforced with various natural fibres*, Materials Today: Proceedings, vol. 33, p. 798-805, doi: 10.1016/j.matpr.2020.06.259, 2020.
[50]. Chandekar H., Chaudhari V., Waigaonkar S., *A review of jute fiber reinforced polymer composites*, Materials Today: Proceedings, vol. 26, p. 2079-2082, doi: 10.1016/j.matpr.2020.02.449, 2020.
[51]. Miller W., Ren Z., Smith C. W., Evans K. E., *A negative Poisson's ratio carbon fibre composite using a negative Poisson's ratio yarn reinforcement*, Composites Science and Technology, vol. 72, nr. 7, p. 761-766, doi: 10.1016/j.compscitech.2012.01.025, apr. 2012.
[52]. Treutenaere S., Lauro F., Bennani B., Haugou G., Matsumoto T., Mottola E., *Constitutive modelling of the strain-rate dependency of fabric reinforced polymers*, International Journal of Impact Engineering, vol. 108, p. 361-369, doi: 10.1016/j.ijimpeng.2017.04.010, oct. 2017.
[53]. Andrew J. J., Srinivasan S. M., Arockiarajan A., Dhakal H. N., *Parameters influencing the impact response of fiber-reinforced polymer matrix composite materials: A critical review*, Composite Structures, vol. 224, p. 111007, doi: 10.1016/j.compstruct.2019.111007, sep. 2019.
[54]. Koohbor B., Ravindran S., Kidane A., *Experimental determination of Representative Volume Element (RVE) size in woven composites*, Optics and Lasers in Engineering, vol. 90, p. 59-71, doi: 10.1016/j.optlaseng.2016.10.001, mar. 2017.
[55]. Mahadik Y., Hallett S. R., *Finite element modelling of tow geometry in 3D woven fabrics*, Composites Part A: Applied Science and Manufacturing, vol. 41, nr. 9, p. 1192-1200, doi: 10.1016/j.compositesa.2010.05.001, sep. 2010.
[56]. Xu W., Waas A. M., *Fracture toughness of woven textile composites*, Engineering Fracture Mechanics, vol. 169, p. 184-188, doi: 10.1016/j.engfracmech.2016.11.027, ian. 2017.
[57]. Green S. D., Matveev M. Y., Long A. C., Ivanov D., Hallett S. R., *Mechanical modelling of 3D woven composites considering realistic unit cell geometry*, Composite Structures, vol. 118, p. 284-293, doi: 10.1016/j.compstruct.2014.07.005, dec. 2014.
[58]. Saleh M. N., Lubineau G., Potluri P., Withers P. J., Soutis C., *Micro-mechanics based damage mechanics for 3D orthogonal woven composites: Experiment and numerical modelling*, Composite Structures, vol. 156, p. 115-124, doi: 10.1016/j.compstruct.2016.01.021, nov. 2016.
[59]. Ansar M., Xinwei W., Chouwei Z., *Modeling strategies of 3D woven composites: A review*, Composite Structures, vol. 93, no. 8, p. 1947-1963, doi: 10.1016/j.compstruct.2011.03.010, iul. 2011.
[60]. Liu X., Tang T., Yu W., Pipes R. B., *Multiscale modeling of viscoelastic behaviors of textile composites*, International Journal of Engineering Science, vol. 130, p. 175-186, doi: 10.1016/j.ijengsci.2018.06.003, sep. 2018.
[61]. Mulay S. S., Udhayaraman R., *On the constitutive modelling and damage behaviour of plain woven textile composite*, International Journal of Solids and Structures, vol. 156-157, p. 73-86, doi: 10.1016/j.ijsolstr.2018.08.002, ian. 2019.
[62]. Mohd Yusoff N. H., Irene Teo L.-R., Phang S. J., Wong V.-L., Cheah K. H., Lim S.-S., *Recent Advances in Polymer-based 3D Printing for Wastewater Treatment Application: An Overview*, Chemical Engineering Journal, vol. 429, p. 132311, doi: 10.1016/j.cej.2021.132311, feb. 2022.
[63]. Feld N., Coussa F., Delattre B., *A novel approach for the strain rate dependent modelling of woven composites*, Composite Structures, vol. 192, p. 568-576, doi: 10.1016/j.compstruct.2018.03.053, mai 2018.
[64]. Machado M., Fischlschweiger M., Major Z., *A rate-dependent non-orthogonal constitutive model for describing shear behaviour of woven reinforced thermoplastic composites*, Composites Part A: Applied Science and Manufacturing, vol. 80, p. 194-203, doi: 10.1016/j.compositesa.2015.10.028, ian. 2016.
[65]. Pant S., Laliberte J., Martinez M., Rocha B., *Derivation and experimental validation of Lamb wave equations for an n-layered anisotropic composite laminate*, Composite Structures, vol. 111, p. 566-579, doi: 10.1016/j.compstruct.2014.01.034, mai 2014.
[66]. Todor M.-P., Kiss I., Cioata V. G., *Development of fabric-reinforced polymer matrix composites using bio-based components from post-consumer textile waste*, Materials Today: Proceedings, vol. 45, p. 4150-4156, doi: 10.1016/j.matpr.2020.11.927, 2021.
[67]. Pant S., Laliberte J., Martinez M., Rocha B., Ancrum D., *Effects of composite lamina properties on fundamental Lamb wave mode dispersion characteristics*, Composite Structures, vol. 124, p. 236-252, doi: 10.1016/j.compstruct.2015.01.017, iun. 2015.
[68]. Gereke T., Döbrich O., Hübner M., Cherif C., *Experimental and computational composite textile reinforcement forming: A review*, Composites Part A: Applied Science and Manufacturing, vol. 46, p. 1-10, doi: 10.1016/j.compositesa.2012.10.004, mar. 2013.
[69]. Udhayaraman R., Mulay S. S., *Multi-scale approach based constitutive modelling of plain woven textile composites*, Mechanics of Materials, vol. 112, p. 172-192, doi: 10.1016/j.mechmat.2017.06.007, sep. 2017.
[70]. Wang L., *et al.*, *Progressive failure analysis of 2D woven composites at the meso-micro scale*, Composite Structures, vol. 178, p. 395-405, doi: 10.1016/j.compstruct.2017.07.023, oct. 2017.
[71]. Patnaik P. K., Swain P. T. R., Mishra S. K., Purohit A., Biswas S., *Recent developments on characterization of needle-punched nonwoven fabric reinforced polymer composites – A review*, Materials Today: Proceedings, vol. 26, p. 466-470, doi: 10.1016/j.matpr.2019.12.086, 2020.
[72]. Remanan S., Das T. K., Das N. C., *Graphene as a reinforcement in thermoset resins*, Polymer Nanocomposites Containing Graphene, Elsevier, p. 317-341, doi: 10.1016/B978-0-12-821639-2.00012-4, 2022.
[73]. Machado M., Murenu L., Fischlschweiger M., Major Z., *Analysis of the thermomechanical shear behaviour of woven-reinforced thermoplastic-matrix composites during forming*, Composites Part A: Applied Science and Manufacturing, vol. 86, p. 39-48, doi: 10.1016/j.compositesa.2016.03.032, iul. 2016.
[74]. Behera B. K., Dash B. P., *Mechanical behavior of 3D woven composites*, Materials & Design, vol. 67, p. 261-271, doi: 10.1016/j.matdes.2014.11.020, feb. 2015.
[75]. Nishida H., Carvelli V., Fujii T., Okubo K., *Quasi-static and fatigue performance of carbon fibre reinforced highly polymerized thermoplastic epoxy*, Composites Part B: Engineering, vol. 144, p. 163-170, doi: 10.1016/j.compositesb.2018.03.002, iul. 2018.

[76]. Verma D., Sharma M., Jain S., *An introduction to high-performance advanced polymers composites, their types, processing, and applications in automotive industries*, Sustainable Biopolymer Composites, Elsevier, p. 3-26, doi: 10.1016/B978-0-12-822291-1.00004-X, 2022.
[77]. Kulkarni P., Mali K. D., Singh S., *An overview of the formation of fibre waviness and its effect on the mechanical performance of fibre reinforced polymer composites*, Composites Part A: Applied Science and Manufacturing, vol. 137, p. 106013, doi: 10.1016/j.compositesa.2020.106013, oct. 2020.
[78]. Martínez-Hergueta F., Ares D., Ridruejo A., Wiegand J., Petrinic N., *Modelling the in-plane strain rate dependent behaviour of woven composites with special emphasis on the non-linear shear response*, Composite Structures, vol. 210, p. 840-857, doi: 10.1016/j.compstruct.2018.12.002, feb. 2019.
[79]. Kenari M. A., Verma D., *An introduction to self-healing of polymer composite materials and conventional repairing process*, Sustainable Biopolymer Composites, Elsevier, p. 155-172, doi: 10.1016/B978-0-12-822291-1.00003-8, 2022.
[80]. Naser M. Z., Hawileh R. A., Abdalla J. A., *Fiber-reinforced polymer composites in strengthening reinforced concrete structures: A critical review*, Engineering Structures, vol. 198, p. 109542, doi: 10.1016/j.engstruct.2019.109542, nov. 2019.
[81]. Meng W., Khayat K. H., Bao Y., *Flexural behaviors of fiber-reinforced polymer fabric reinforced ultra-high-performance concrete panels*, Cement and Concrete Composites, vol. 93, p. 43-53, doi: 10.1016/j.cemconcomp.2018.06.012, oct. 2018.
[82]. Bal B. C., *Flexural properties, bonding performance and splitting strength of LVL reinforced with woven glass fiber*, Construction and Building Materials, vol. 51, p. 9-14, doi: 10.1016/j.conbuildmat.2013.10.041, ian. 2014.
[83]. Hegemier G., Stewart L., *Application of fiber-reinforced polymers to reinforced concrete bridges*, Innovative Bridge Design Handbook, Elsevier, p. 933-950. doi: 10.1016/B978-0-12-823550-8.00034-2, 2022.
[84]. Wu Y., Li C., Chen T., Qiu R., Liu W., *Photo-curing 3D printing of micro-scale bamboo fibers reinforced palm oil-based thermosets composites*, Composites Part A: Applied Science and Manufacturing, vol. 152, p. 106676, doi: 10.1016/j.compositesa.2021.106676, ian. 2022.
[85]. Kubo G., Matsuda T., Sato Y., *A novel basic cell modeling method for elastic-viscoplastic homogenization analysis of plain-woven laminates with nesting*, International Journal of Mechanical Sciences, vol. 146-147, p. 497-506, doi: 10.1016/j.ijmecsci.2018.01.007, oct. 2018.
[86]. Domun N., *et al.*, *Ballistic impact behaviour of glass fibre reinforced polymer composite with 1D/2D nanomodified epoxy matrices*, Composites Part B: Engineering, vol. 167, p. 497-506, doi: 10.1016/j.compositesb.2019.03.024, iun. 2019.
[87]. Fiore V., Valenza A., *Epoxy resins as a matrix material in advanced fiber-reinforced polymer (FRP) composites*, Advanced Fibre-Reinforced Polymer (FRP) Composites for Structural Applications, Elsevier, p. 88-121. doi: 10.1533/9780857098641.1.88, 2013.
[88]. Ali H. T., *et al.*, *Fiber reinforced polymer composites in bridge industry*, Structures, vol. 30, p. 774-785, doi: 10.1016/j.istruc.2020.12.092, apr. 2021.
[89]. Zhao S., Song Z., Espinosa H. D., *Modelling and Analyses of Fiber Fabric and Fabric-Reinforced Polymers under Hypervelocity Impact Using Smooth Particle Hydrodynamics*, International Journal of Impact Engineering, vol. 144, p. 103586, doi: 10.1016/j.ijimpeng.2020.103586, oct. 2020.
[90]. Shakir Abbood I., aldeen Odaa S., Hasan K. F., Jasim M. A., *Properties evaluation of fiber reinforced polymers and their constituent materials used in structures – A review*, Materials Today: Proceedings, vol. 43, p. 1003-1008, doi: 10.1016/j.matpr.2020.07.636, 2021.
[91]. Luo G., Li X., Zhou Y., Sui L., Chen C., *Replacing steel stirrups with natural fiber reinforced polymer stirrups in reinforced concrete Beam: Structural and environmental performance*, Construction and Building Materials, vol. 275, p. 122172, doi: 10.1016/j.conbuildmat.2020.122172, mar. 2021.
[92]. Cheon J., Lee M., Kim M., *Study on the stab resistance mechanism and performance of the carbon, glass and aramid fiber reinforced polymer and hybrid composites*, Composite Structures, vol. 234, p. 111690, doi: 10.1016/j.compstruct.2019.111690, feb. 2020.
[93]. Forintos N., Czigany T., *Multifunctional application of carbon fiber reinforced polymer composites: Electrical properties of the reinforcing carbon fibers – A short review*, Composites Part B: Engineering, vol. 162, p. 331-343, doi: 10.1016/j.compositesb.2018.10.098, apr. 2019.
[94]. Morampudi P., Namala K. K., Gajjela Y. K., Barath M., Prudhvi G., *Review on glass fiber reinforced polymer composites*, Materials Today: Proceedings, vol. 43, p. 314-319, doi: 10.1016/j.matpr.2020.11.669, 2021.
[95]. Carpenter A. J., Chocron S., Anderson C. E., *Bridging the scales: Continuum-based material constitutive modeling of mechanical and ballistic test data from composites and fabrics*, International Journal of Impact Engineering, vol. 120, p. 31-45, doi: 10.1016/j.ijimpeng.2018.05.005, oct. 2018.
[96]. Beauson J., Schillani G., Van der Schueren L., Goutianos S., *The effect of processing conditions and polymer crystallinity on the mechanical properties of unidirectional self-reinforced PLA composites*, Composites Part A: Applied Science and Manufacturing, vol. 152, p. 106668, doi: 10.1016/j.compositesa.2021.106668, ian. 2022.
[97]. Matsuda T., Goto K., Kubota N., Ohno N., *Negative through-the-thickness Poisson's ratio of elastic–viscoplastic angle-ply carbon fiber-reinforced plastic laminates: Homogenization analysis*, International Journal of Plasticity, vol. 63, p. 152-169, doi: 10.1016/j.ijplas.2014.05.007, dec. 2014.
[98]. Olave M., Vara I., Usabiaga H., Aretxabaleta L., Lomov S. V., Vandepitte D., *Nesting effect on the mode II fracture toughness of woven laminates*, Composites Part A: Applied Science and Manufacturing, vol. 74, p. 174-181, doi: 10.1016/j.compositesa.2015.03.020, iul. 2015.
[99]. Stephen I., Hughes E., Das S., *Reinforced concrete beams strengthened with basalt fibre fabric – A parametric study*, Structures, vol. 27, p. 309-318, doi: 10.1016/j.istruc.2020.05.008, oct. 2020.
[100]. Azimpour-Shishevan F., Akbulut H., Mohtadi-Bonab M. A., *Synergetic effects of carbon nanotube and graphene addition on thermo-mechanical properties and vibrational behavior of twill carbon fiber reinforced polymer composites*, Polymer Testing, vol. 90, p. 106745, doi: 10.1016/j.polymertesting.2020.106745, oct. 2020.
[101]. Hamoutami J. E., Moustachi O. E. K., *The behavior of a reinforced concrete portal frame treated by carbon fiber reinforced polymer (CFRP)*, Materials Today: Proceedings, vol. 45, p. 7697-7705, doi: 10.1016/j.matpr.2021.03.222, 2021.
[102]. Manocha L. M., *Carbon Based Materials*, Encyclopedia of Materials: Metals and Allloys, Elsevier, p. 394-419, doi: 10.1016/B978-0-12-819726-4.00098-3, 2022.
[103]. Ascione F., Lamberti M., Napoli A., Razaqpur G., Realfonzo R., *An experimental investigation on the bond behavior of steel reinforced polymers on concrete substrate*, Composite Structures, vol. 181, p. 58-72, doi: 10.1016/j.compstruct.2017.08.063, dec. 2017.
[104]. Yan L., Kasal B., Huang L., *A review of recent research on the use of cellulosic fibres, their fibre fabric reinforced cementitious, geo-polymer and polymer composites in civil engineering*, Composites Part B: Engineering, vol. 92, p. 94-132, doi: 10.1016/j.compositesb.2016.02.002, mai 2016.
[105]. Sethu Ramalingam P., Mayandi K., Srinivasan T., Jerin Leno I., Ravi R., Suresh G., *A study on E-Glass fiber reinforced interpenetrating polymer network (vinylester/polyurethane) laminate's flexural analysis*, Materials Today: Proceedings, vol. 33, p. 854-858, doi: 10.1016/j.matpr.2020.06.330, 2020.
[106]. Albert Seldon P., Abilash N., *Appraisal on Varied Natural and Artificial Fiber Reinforced Polymeric Composites*, Materials

Today: Proceedings, vol. 22, p. 3213-3219, doi: 10.1016/j.matpr.2020.03.459, 2020.

[107]. Ferreira Batista M., Basso I., de Assis Toti F., Roger Rodrigues A., Ricardo Tarpani J., *Cryogenic drilling of carbon fibre reinforced thermoplastic and thermoset polymers*, Composite Structures, vol. 251, p. 112625, doi: 10.1016/j.compstruct.2020.112625, nov. 2020.

[108]. Zhang C., Zheng D., Song G.-L., Guo Y., Liu M., Kia H., *Influence of microstructure of carbon fibre reinforced polymer on the metal in contact*, Journal of Materials Research and Technology, vol. 9, nr. 1, p. 560-573, doi: 10.1016/j.jmrt.2019.10.085, ian. 2020.

[109]. Miura M., Shindo Y., Narita F., Watanabe S., Suzuki M., *Mode III fatigue delamination growth of glass fiber reinforced polymer woven laminates at cryogenic temperatures*, Cryogenics, vol. 49, nr. 8, p. 407-412, doi: 10.1016/j.cryogenics.2009.05.004, aug. 2009.

[110]. Zhang B., Jia L., Tian M., Ning N., Zhang L., Wang W., *Surface and interface modification of aramid fiber and its reinforcement for polymer composites: A review*, European Polymer Journal, vol. 147, p. 110352, doi: 10.1016/j.eurpolymj.2021.110352, mar. 2021.

[111]. Dong K., Peng X., Zhang J., Gu B., Sun B., *Temperature-dependent thermal expansion behaviors of carbon fiber/epoxy plain woven composites: Experimental and numerical studies*, Composite Structures, vol. 176, p. 329-341, doi: 10.1016/j.compstruct.2017.05.036, sep. 2017.

[112]. Espadas-Escalante J. J., van Dijk N. P., Isaksson P., *The effect of free-edges and layer shifting on intralaminar and interlaminar stresses in woven composites*, Composite Structures, vol. 185, p. 212-220, doi: 10.1016/j.compstruct.2017.11.014, feb. 2018.

[113]. Laffan M. J., Pinho S. T., Robinson P., McMillan A. J., *Translaminar fracture toughness testing of composites: A review*, Polymer Testing, vol. 31, nr. 3, p. 481-489, doi: 10.1016/j.polymertesting.2012.01.002, mai 2012.

[114]. Sacchetti F., Grouve W. J. B., Warnet L. L., Villegas I. F., *Woven fabric composites: Can we peel it?*, Procedia Structural Integrity, vol. 2, p. 245-252, doi: 10.1016/j.prostr.2016.06.032, 2016.

[115]. Tambe P., Tanniru M., Sai B. L. N. K., *Structural/load bearing characteristics of polymer-graphene composites*, Polymer Nanocomposites Containing Graphene, Elsevier, p. 379-400, doi: 10.1016/B978-0-12-821639-2.00005-7, 2022.

[116]. Bhagabati P., Rahaman M., *Structure-property relationship in polymer-graphene composites*, Polymer Nanocomposites Containing Graphene, Elsevier, p. 299-315, doi: 10.1016/B978-0-12-821639-2.00016-1, 2022.

[117]. Pritzkow W. E. C., Wehner F., Koch D., *Oxide Fiber Reinforced Oxide Ceramic Matrix Composite – An Alternative to Metallic Alloys at High Temperature*, Encyclopedia of Materials: Metals and Allloys, Elsevier, p. 425-441, doi: 10.1016/B978-0-12-819726-4.00040-5, 2022.

[118]. Park J. K., Kim M. O., *The effect of different exposure conditions on the pull-off strength of various epoxy resins*, Journal of Building Engineering, vol. 38, p. 102223, doi: 10.1016/j.jobe.2021.102223, iun. 2021.

[119]. da Silva L. R. R., *et al.*, *Bio-based one-component epoxy resin: Novel high-performance anticorrosive coating from agro-industrial byproduct*, Progress in Organic Coatings, vol. 167, p. 106861, doi: 10.1016/j.porgcoat.2022.106861, iun. 2022.

[120]. Liu Z., Xie C., Tuo X., *Laminated aramid nanofiber aerogel reinforced epoxy resin composite*, Materials Today Communications, vol. 31, p. 103376, doi: 10.1016/j.mtcomm.2022.103376, iun. 2022.

[121]. Feng Q.-K., *et al.*, *Particle packing theory guided multiscale alumina filled epoxy resin with excellent thermal and dielectric performances*, Journal of Materiomics, vol. 8, nr. 5, p. 1058-1066, doi: 10.1016/j.jmat.2022.02.008, sep. 2022.

[122]. Ruan K., Zhong X., Shi X., Dang J., Gu J., *Liquid crystal epoxy resins with high intrinsic thermal conductivities and their composites: A mini-review*, Materials Today Physics, vol. 20, p. 100456, doi: 10.1016/j.mtphys.2021.100456, sep. 2021.

[123]. Morsch S., Kefallinou Z., Liu Y., Lyon S. B., Gibbon S. R., *Controlling the nanostructure of epoxy resins: Reaction selectivity and stoichiometry*, Polymer, vol. 143, p. 10-18, doi: 10.1016/j.polymer.2018.03.065, mai 2018.

[124]. Zhao H., Xu S., Guo A., Li J., Liu D., *The Curing Kinetics Analysis of Four Epoxy Resins Using a Diamine Terminated Polyether as Curing Agent*, Thermochimica Acta, vol. 702, p. 178987, doi: 10.1016/j.tca.2021.178987, aug. 2021.

[125]. Wang X., Amason A.-C., Lei Y., Gabbard R., Wieland J. A., Gross R. A., *Bio-based alternative for encapsulating fragrance oils in epoxy resin microcapsules*, Colloids and Surfaces A: Physicochemical and Engineering Aspects, vol. 640, p. 128387, doi: 10.1016/j.colsurfa.2022.128387, mai 2022.

[126]. Lorenz N., *et al.*, *Characterization and modeling cure- and pressure-dependent thermo-mechanical and shrinkage behavior of fast curing epoxy resins*, Polymer Testing, vol. 108, p. 107498, doi: 10.1016/j.polymertesting.2022.107498, apr. 2022.

[127]. Ratna D., *Chemistry and general applications of thermoset resins*, Recent Advances and Applications of Thermoset Resins, Elsevier, p. 1-172, doi: 10.1016/B978-0-323-85664-5.00006-5, 2022.

[128]. Wan X., Demir B., An M., Walsh T. R., Yang N., *Thermal conductivities and mechanical properties of epoxy resin as a function of the degree of cross-linking*, International Journal of Heat and Mass Transfer, vol. 180, p. 121821, doi: 10.1016/j.ijheatmasstransfer.2021.121821, dec. 2021.

[129]. Opelt C. V., Coelho L. A. F., *On the pseudo-ductility of nanostructured epoxy resins*, Polymer Testing, vol. 78, p. 105961, doi: 10.1016/j.polymertesting.2019.105961, sep. 2019.

[130]. Bhadra S., Nair S., *Tailor-made one-part epoxy resin for tire compound to improve ride and handling and reduce rolling resistance*, Materials Today: Proceedings, vol. 62, p. 7002-7006, doi: 10.1016/j.matpr.2021.12.544, 2022.

[131]. Cui M., Qing Y., Yang Y., Long C., Liu C., *Nanofunctionalized composite-crosslinked epoxy resin for eco-friendly and robust superhydrophobic coating against contaminants*, Colloids and Surfaces A: Physicochemical and Engineering Aspects, vol. 633, p. 127914, doi: 10.1016/j.colsurfa.2021.127914, ian. 2022.

[132]. Li Y., Huang K., Yu H., Hao L., Guo L., *Experimentally validated phase-field fracture modeling of epoxy resins*, Composite Structures, vol. 279, p. 114806, doi: 10.1016/j.compstruct.2021.114806, ian. 2022.

[133]. Chen C., *et al.*, *Comparative analysis of natural fiber reinforced polymer and carbon fiber reinforced polymer in strengthening of reinforced concrete beams*, Journal of Cleaner Production, vol. 263, p. 121572, doi: 10.1016/j.jclepro.2020.121572, aug. 2020.

[134]. Huayamares S., Grund D., Taha I., *Comparison between 3-point bending and torsion methods for determining the viscoelastic properties of fiber-reinforced epoxy*, Polymer Testing, vol. 85, p. 106428, doi: 10.1016/j.polymertesting.2020.106428, mai 2020.

[135]. Mourad A.-H. I., Idrisi A. H., Zaaroura N., Sherif M. M., Fouad H., *Damage assessment of nanofiller-reinforced woven kevlar KM2plus/Epoxy resin laminated composites*, Polymer Testing, vol. 86, p. 106501, doi: 10.1016/j.polymertesting.2020.106501, iun. 2020.

[136]. Santhosh G., Rao R. N., *Effect of castor oil on mechanical and thermal behaviours of hybrid fibres reinforced epoxy based polymer composites*, Materials Today: Proceedings, p. S2214785321017417, doi: 10.1016/j.matpr.2021.02.594, mar. 2021.

[137]. Yang B., Wang S., Wang Y., *Effect of Nesting in Laminates on the Through-Thickness Permeability of Woven Fabrics*, Appl Compos Mater, vol. 25, nr. 5, p. 1237-1253, doi: 10.1007/s10443-018-9699-8, oct. 2018.

[138]. Dhanush Kumar K. K., Ashish B. V., Vinod B., *Evaluation of tensile properties of hybrid kevlar-glass reinforced*

epoxy composite for multi holes configuration, Materials Today: Proceedings, vol. 44, p. 1065-1070, doi: 10.1016/j.matpr.2020.11.180, 2021.

[139]. Valença S. L., Griza S., de Oliveira V. G., Sussuchi E. M., de Cunha F. G. C., *Evaluation of the mechanical behavior of epoxy composite reinforced with Kevlar plain fabric and glass/Kevlar hybrid fabric*, Composites Part B: Engineering, vol. 70, p. 1-8, doi: 10.1016/j.compositesb.2014.09.040, mar. 2015.

[140]. Xu W., Guo Z. Z., Yu Y., Xiong J., Gao Y., *Experimental and analytical characterizations of finite interlaminar crack growth of 2D woven textile composites*, Composite Structures, vol. 206, p. 713-721, doi: 10.1016/j.compstruct.2018.08.050, dec. 2018.

[141]. Velmurugan V., Dinesh Kumar D., Thanikaikarasan S., *Experimental evaluation of mechanical properties of natural fibre reinforced polymer composites*, Materials Today: Proceedings, vol. 33, p. 3383-3388, doi: 10.1016/j.matpr.2020.05.190, 2020.

[142]. Murugan R., Ramesh R., Padmanabhan K., *Investigation on Static and Dynamic Mechanical Properties of Epoxy Based Woven Fabric Glass/Carbon Hybrid Composite Laminates*, Procedia Engineering, vol. 97, p. 459-468, doi: 10.1016/j.proeng.2014.12.270, 2014.

[143]. Misumi J., Oyama T., *Low viscosity and high toughness epoxy resin modified by in situ radical polymerization method for improving mechanical properties of carbon fiber reinforced plastics*, Polymer, vol. 156, p. 1-9, doi: 10.1016/j.polymer.2018.09.050, nov. 2018.

[144]. Kiran M. D., Govindaraju H. K., Yadhav B. R. L., Suresha B., Keerthi Kumar N., *Fracture toughness study of epoxy composites reinforced with carbon fibers with various thickness*, Materials Today: Proceedings, p. S2214785321013584, doi: 10.1016/j.matpr.2021.02.271, mar. 2021.

[145]. Goli E., *et al.*, *Frontal polymerization of unidirectional carbon-fiber-reinforced composites*", Composites Part A: Applied Science and Manufacturing, vol. 130, p. 105689, doi: 10.1016/j.compositesa.2019.105689, mar. 2020.

[146]. Dai S., Cunningham P. R., Marshall S., Silva C., *Influence of fibre architecture on the tensile, compressive and flexural behaviour of 3D woven composites*, Composites Part A: Applied Science and Manufacturing, vol. 69, p. 195-207, doi: 10.1016/j.compositesa.2014.11.012, feb. 2015.

[147]. Zheng C., Duan F., Liang S., *Manufacturing and mechanical performance of novel epoxy resin matrix carbon fiber reinforced damping composites*, Composite Structures, vol. 256, p. 113099, doi: 10.1016/j.compstruct.2020.113099, ian. 2021.

[148]. Koirala P., van de Werken N., Lu H., Baughman R. H., Ovalle-Robles R., Tehrani M., *Using ultra-thin interlaminar carbon nanotube sheets to enhance the mechanical and electrical properties of carbon fiber reinforced polymer composites*, Composites Part B: Engineering, vol. 216, p. 108842, doi: 10.1016/j.compositesb.2021.108842, 2021.

THE ANNALS OF "DUNAREA DE JOS" UNIVERSITY OF GALATI
FASCICLE IX. METALLURGY AND MATERIALS SCIENCE
Nº. 4 - 2022, ISSN 2668-4748; e-ISSN 2668-4756
Article DOI: https://doi.org/10.35219/mms.2022.4.12

MODIFIED THERMOSETS – A REVIEW

Sebastian Marian DRĂGHICI, Irina DĂNĂILĂ (ȚÎCĂU), Tamara APARECI (GÎRNEȚ), Gabriel SĂRACU, Iulian PĂDURARU, Vasile BRIA, Adrian CÎRCIUMARU, Mihaela-Claudia GOROVEI
"Dunarea de Jos" University of Galati, Romania
e-mail: mihaela_gorovei@yahoo.com

ABSTRACT

Recent and extensive reports on the development of preparation methods that can lead to obtaining various nanostructured polymeric materials, including the preparation of nanoparticles, nano-capsules, nano-gels, nano-fibres, dendrimers and nano-composites, have been presented in the literature to provide a picture of the complexity of the field, and the diversity of approaching methods. From the data presented by various researchers, it appears that by ensuring a rigorous control of the nano-structuration of polymers and/or by adding nano-particles to the polymer matrices, improvements in structural and functional properties can be achieved in a significant number of polymer systems as a response to the continuous demands of industrial advanced sectors. Until now, most of the studies on polymer blends have been related to the control of their physical and chemical properties, their barrier properties or their electrical conductivity. This paper briefly presents various applications of resins (thermoset polymers) used to synthesize some polymer materials and blends.

KEYWORDS: nano-fibres, thermoset polymers, synthesis

1. Introduction

Miscible polymer blends offer great design capability over shape memory effect (SME) with controllable mechanical properties and stimuli sensitivity by simply changing the constituent compositions. However, understanding the thermodynamics behind those IMMs on miscible polymer blends has not yet been explored [1-3]. For the advancement of polymer science and polymer technologies, the chemical characterization of the polymer mixture remains the fundamental analytical study [4-6]. Mixing polymers and inorganic nano-materials opens new paths for synthesizing flexible composite materials and improves the macroscopic performance of the materials [7-9]. Polymers can be in raw form (filaments, powders, resins and reactive agents) for various categories of use [10].

Recently, increased attention has been imposed on the environment, what causes an impediment to the use of thermosetting resins [11-13]. Thermosetting resins are known to be cheaper in terms of processability compared to thermoplastics, which require high production costs and higher energy consumption [14-16]. Even though thermoplastic resins have advantages such as: recyclability, thermoformability and weldability, they have not yet reached the same technological maturity as thermosetting resins. Thermoplastics have the ability to form liquids during the heating process and become hard when the cooling process takes place [17-21].

2. Epoxy resins (ERs)

Epoxy resin is considered one of the most important thermoset polymers, having in its composition at least epoxy groups in the molecule. It comes in three forms: liquid, solid or viscous [22-24]. According to the latest reports, epoxy resins currently have the highest sales percentage (about 70%) in the thermosets market, the main advantages being excellent mechanical properties, thermal stability, outstanding electrical and chemical insulation and low cost [25-32]. Epoxy resin (EP) is most often used in the electronic and electric field (design of tiny electronic components, generators, motors, voltage distribution networks or electrical insulating materials) [33-37]. Due to the poor weathering resistance and high brittleness of epoxy resin, it is necessary to improve the performance of the EP

THE ANNALS OF "DUNAREA DE JOS" UNIVERSITY OF GALATI
FASCICLE IX. METALLURGY AND MATERIALS SCIENCE
Nº. 4 - 2022, ISSN 2668-4748; e-ISSN 2668-4756
Article DOI: https://doi.org/10.35219/mms.2022.4.12

matrix to meet the requirements of composite materials [38-44]. Epoxy resin can be modified by both chemical and physical methods. According to studies in the literature, chemical modification involves quite high costs and some deficiencies of the complex technology [45-47]. On the other hand, physical modification of EP is the most used method. The main types of modifiers are inorganic nanoparticles, rubber particles and thermoplastics [48-50].

3. Polyurethane resins (PUs)

Polyurethanes are a class of polymers that exhibit three types of behaviour: thermoplastic, thermoset, and elastomer. PUs present versatile properties both thermally and in terms of mechanical and chemical aspects [51]. Compared to epoxy resins, PUs shows better fatigue and damage resistance properties. At the same time, they have the advantage of being synthesized with various vegetable oils to replace petrochemical products with renewable or recycled materials [52-54]. In most cases, polyurethanes are used for sealing, or for protection against condensation [55, 56]. Polyurethanes belong to the category of foaming materials, with high porosity, light weight and good energy absorption capacity, being excellent for packaging and damping sensitive objects [57-59]. Linear polyurethanes have good toughness and re-processability, but have poor solvent resistance [23, 60-62].

4. Vinylester resins (VER)

Vinylester resins (VERs) are used in various commercial applications (automotive parts, coatings, adhesives, military and aerospace applications, moulding compounds) due to their high hardness, low exothermic heat, low volume shrinkage and low cost [39, 63-67]. Nature provides us with a variety of plant biomass that we can use as raw material for the production of precursors and chemical substances (plant oils, tung oil, cashew nut shell liquid (CNSL), lingo-cellulosic, fatty acid dimers) for new VERs [68-72]. Materials containing VE can be used as neutron shielding material for radioactive material transport/storage containers [73]. Fibre reinforced plastic (FRP) manufacturers are using vinylesters because they offer greater resistance to attacks in aggressive chemical environments, or other types of acids and caustics [72, 74, 75].

5. Thermosets and thermoplastics applications

Yan Wang and his collaborators [76], developed a multi-scale simulation scheme by which they generated the atomic structure of epoxy resins. The simulation scheme they proposed provides a reasonable use of the advantages of the DFT method in dealing with systems involving the breaking and formation of chemical bonds. This multi-scale simulation strategy provides a possible investigation scheme to study such an epoxy resin system, which can also be applied to study other similar composite materials with complex network structures.

Ruowen Tu and Henry Sodano [72] fabricated high-performance vinylester resin-based nano-composites by direct ink writing with dual UV-thermal curing. The fracture strength of dual-imprinted and reinforced VER nano-composites was also 16% higher than MEKP-reinforced pure cast VER.

In [77], the authors synthesized the organo-silicon additive-modified epoxy resin RSN-6018 through the condensation reaction between the organo-silicon intermediate (RSN-6018) and the epoxy resin (E-20). The results of mechanical property testing showed that the incorporation of RSN-6018 organo-silicon improved the hardness of the cured ER films.

Apriany Saludung and his collaborators [78] incorporated epoxy resin into the geopolymer matrix. The improvement of mechanical strengths and alkali binding properties of naturally hardened geopolymer by adding epoxy resin can lead to extensive application of geopolymer binder in the construction industry.

In [39], researchers created a high-performance permeable concrete with polyester and epoxy resins. From the tests carried out, they concluded that: increasing the resin content improves the compressive, tensile and flexural strength, while an increase in the size of the coarse aggregate and the use of epoxy resin instead of polyester resin decreases the previously listed strengths.

Valentino R., *et al.* [57], carried out an experimental study on the mechanical behaviour of two polyurethane resins used for geotechnical applications. Experimental measurements showed that resin density and confining pressure are closely related, and for the same type of resin under limited conditions, the mechanical response is constant.

Peng Y.-J., *et al.* [51], designed a composite material consisting of polyurethane and epoxy resin with multi-level structure and high performance. Such a well-established structure–property relationship could further provide guidance for the fabrication of high-performance recyclable material with precisely controllable microstructures and behaviours.

In [32], the authors studied the changes in structure, mechanical and adhesion properties of vinylester resins after aging. Chemical and structural changes were observed in vinylester resins after aging

in a climatic chamber. Most changes occur in the first three days.

Banna M. H., *et al.* [63], analysed the effects of two acidic aqueous solutions on polyester and bisphenol A epoxy vinylester resins. For both resins, the average hardness increased more after two weeks of exposure and then decreased after four weeks of exposure due to a relationship between hardness, micro-hardness indentation depth, and microstructure. Acid exposure affected the polyester resin more than the bisphenol epoxy vinyl ester.

Yang X., *et al.* [80], produced a type of solvent-free epoxy-modified silicone resin transparent coating with high transparency and low volume shrinkage. The silicone layers that were obtained have a transmittance greater than 95% and a hardness of 5H after UV curing with a percentage of 3% by mass for 20 s time interval. It was found that the silicone resin materials obtained have good thermal stability, a good adhesion and a fairly low volume shrinkage.

In [64], researchers improved the thermal, impact and tensile properties of unsaturated thermosetting polyester (UP) by blending with thermosetting vinylester (VE) and methyl methacrylate (MMA). UP blended with 30%VE and 10%MMA had the highest impact strength (an increase of 17.6%), higher tensile strength (an increase of 45.5%) and higher elongation at break (an increase of 26.9%) compared to pure UP. The addition of VE and MMA to UP led to an increase in the toughness of UP as a result of disruption of the chain network links of UP, resulting in a decrease in structural stiffness, and an increase in the plastic strain fraction.

The enhancement of solvent resistance and thermo-mechanical properties of thermoplastic acrylic polymers and composites by reactive hybridization has been studied [81]. Both unreinforced polymer blends and glass fibre reinforced composites have been studied. The authors' findings showed that incorporating reactive PPE into a reactive acrylic resin to produce a hybrid matrix system is a simple and effective strategy for increasing solvent resistance.

Luo D., *et al.* [82], incorporated Fe_3O_4 and SiO_2 nano-particles into epoxy modified silicone resin (ESR) as a coating for soft magnetic composites (SMC) with improved performance. On the one hand, the introduction of Fe_3O_4 reduces the magnetic dilution effect, which is beneficial for magnetization and permeability. On the other hand, the incorporation of SiO_2 prevents the agglomeration of Fe_3O_4 nano-particles and leads to an increased electrical resistivity as well as increased mechanical strength of SMCs.

Wei Y.-Y., *et al.* [83], fabricated both photo-polymerized and thermo-polymerized silicone hydrogels with different surface microstructure and wettability. It was found that the surface of silicone hydrogels prepared by thermal polymerization was significantly more hydrophilic than the surface made by photo-initiation polymerization. ATR-FTIR and SEM as well as XPS analysis indicated that the chemical composition and elemental distribution of the two hydrogels were similar. However, AFM images showed that the silicone hydrogel prepared by photo-polymerization has a lot of tiny pores on the surface, so air bubbles can be stored. Whereas, the surface of silicone hydrogel obtained by thermal polymerization has some tiny slopes.

In [84], researchers devised a method by which they recycled waste thermoset unsaturated polyester resins into oligomers for the synthesis of amphiphilic aerogels. Styrene-maleic acid copolymer (SMC) was obtained by cleavage of ester groups from waste thermoset unsaturated polyester resins (WTUPR). The degradation occurred at 180 °C in glycol with potassium carbonate as a catalyst for 5 h, and the resulting potassium salt of SMC (SMC-K) could be very easily separated by precipitation using ethanol with a yield of 63.8%. Good compressibility and strength of the aerogel were demonstrated.

Zheng C., *et al.* [85], developed a negative ion implantation system to study the surface modification of room temperature vulcanizing silicone rubber (RTV SR) for cell biocompatibility. They concluded that the main reason for the improved hydrophilicity is that the implanted ions result in a new surface atomic bonding state and a new morphology. Based on the XPS and ATR-FTIR results, it can be deduced that ion implantation breaks the hydrophobic functional groups of RTV SR and generates functional groups. SEM demonstrated that cracks appear on the implanted surface of RTV SR.

Sultania M., *et al.* [71], conducted studies on the synthesis and curing of epoxidized novolac vinyl ester resin from materials from renewable resources. It was concluded that the synthesis of low viscosity vinylester resin from renewable resource materials such as cardanol could reduce the use of harmful chemicals such as styrene during curing of such resin. The cure temperature was found to be very close to the cure temperature for VER of epoxidized phenolic novolac resin cured using 40% styrene. The curing time, using 40% styrene, for the CNEVER sample was lower than for the PVER sample. Also, the curing time is the shortest when the CNEVER sample is used without styrene. Undoubtedly, the cost of the resin will be lower than that of already existing VERs.

Malucelli G., *et al.* [54], synthesized adhesives based on polyurethane resins. They investigated the hardening reaction and the influence of surface properties on adhesion. Curing kinetics of the PU

THE ANNALS OF "DUNAREA DE JOS" UNIVERSITY OF GALATI
FASCICLE IX. METALLURGY AND MATERIALS SCIENCE
Nº. 4 - 2022, ISSN 2668-4748; e-ISSN 2668-4756
Article DOI: https://doi.org/10.35219/mms.2022.4.12

resin, evaluated by FTIR spectroscopy, revealed an asymptotic trend, with a reaction completed after approximately 100 h. The results of the adhesion measurements of the PU adhesive on different substrates were in total agreement with the surface properties of both the resin and the substrates.

Cristiana Ittner and Maria Felisberti [65], studied the influence of three silicone-based additives to modify the properties of vinylester resin. The study of the curing kinetics revealed that these additives influenced the curing kinetics. The influence of these additives is directly related to the initiator/catalyst/promoter system used in curing, which can accelerate or delay the reaction depending on the presence or absence of DMA. The use of DMA as a peroxide decomposition promoter in the initial stage of resin curing in the presence of silicone-based additives results in an increase in the reaction enthalpy and a decrease in the activation energy. This suggests that the curing mechanism is modified due to silicone-based additives.

Zhao H., *et al.* [86], analysed the curing kinetics of four epoxy resins using a diamine-terminated polyether as curing agent. It has been shown that a diamine-terminated polyether (DAPE) can enhance the flexibility of epoxy systems, which is attributed to the unique chemical structure. The results showed that the curing reaction can be described by the Sestak-Berggren (SB(m,n)) kinetic model and fits well the experimental curves. According to the tensile test and DMA test results, the strengthening effect of DAPE was successfully achieved on four epoxy systems. The cure is modified due to the silicone-based additives presence.

Pragnesh Dave and Nikul Patel [87], prepared unsaturated poly(ester-amide) resins based on epoxy resins (UPEA). These UPEAs were then treated with acryloyl chloride to obtain acrylated UPEA resin (ie AUPEA). Interacting mixtures of equal proportions of AUPEA and vinyl ester epoxy resin (VE) were prepared. The general advantages of the produced PEA formation are as follows: the intermolecular reaction with bismaleimides formed UPEA with good chemical resistivity and moderate thermal stability. The glass fibre reinforced composites of all PEAs were laminated and exhibited excellent strength properties and good mechanical and electrical properties.

In [88], a silicone-epoxy copolymer was prepared by synergizing the o-allylphenol-modified (UC-233) and methoxy-terminated silicone methylphenyl intermediate (PMPS-S). SEM and DMA revealed that the comb-shaped silicone-epoxy copolymer showed better compatibility due to the pre-chemical grafting reaction. In addition, TGA showed that the thermal stability of the comb-shaped silicone-epoxy copolymer was improved and maintained the excellent mechanical properties of the epoxy resin. TGA-FTIR shows the thermal degradation process that methoxy-terminated methylphenyl silicone intermediate (PMPS-S) and phenyl hydrogen-containing silicone oil (UC-233) could inhibit the degradation of epoxy resin.

In [67], the synthesis and the investigation of a new brominated vinyl ester resin are presented. The DMA results demonstrate that all resin formulations comprising Br-VER exhibit improved mechanical performance compared to the commercial vinylester resin. Rheological studies on the resin compositions showed that, compared to the commercial resin (Derakane 510A-40), the synthesized Br-GVER has a significantly lower viscosity and a longer lifetime (9 hours vs. 2 hours), thereby eliminating the need for an inhibitor when used for applications such as resin infusion.

Studies have been conducted on the preparation and super-hydrophobic surface properties of RTV silicone rubber [89]. The authors concluded that the preparation of the super-hydrophobic surface by physical deposition has the advantages of simple processing, low cost and large surface area preparation. In addition, SR has outstanding high temperature resistance. Therefore, this super-hydrophobic material is suitable to be applied at both room temperature and high temperature, and has wide-scale application prospects.

In [90], a study was conducted on the modification of room temperature vulcanized silicone rubber (RTV) by microencapsulated phase change material (MEPCM). MEPCM blended RTV has been shown to have better thermal insulation than regular silicone rubber. As the mass ratio of MEPCM increases, it takes more time for the modified RTV to cool to 0 °C. The decrease in volume resistivity of the modified RTV can increase the leakage current, which is also a good aspect for anti-icing.

Goram Gohel and his collaborators [91], used epoxy resins and carbon fibres to manufacture sports helmets. Overall, detailed manufacturing and certification tests performed on helmets have shown significant potential for using the composite shell as a viable alternative to conventional helmet material systems in terms of achieving increased safety.

In [92], researchers studied the effects of graphene on various properties and applications of silicone rubber and silicone resin. They found that graphene has high electron mobility, thermal conductivity and mechanical properties at room temperature. As a typical carbon nano-scale filler, graphene added to the polymer matrix can improve the performance of the polymer.

Vincent Joseph and collaborators [93], combined rigid epoxy resins with platinum-catalysed soft silicone rubbers for additive manufacturing of

THE ANNALS OF "DUNAREA DE JOS" UNIVERSITY OF GALATI
FASCICLE IX. METALLURGY AND MATERIALS SCIENCE
Nº. 4 - 2022, ISSN 2668-4748; e-ISSN 2668-4756
Article DOI: https://doi.org/10.35219/mms.2022.4.12

soft robots. By adjusting the composition of the hybrid resins, the elastic modulus can be tuned over an unprecedented ratio of five orders of magnitude (from 20 kPa to 2 GPa) with remarkable interfacial strength (from 1 to 3 kJ m^{-2}). The significance of this new class of hybrid resins is demonstrated by the fabrication of various functional devices relevant to wearables, healthcare and soft robotics. Overall, these hybrid resins open new frontiers for manufacturing the next generation of soft robots using unique continuous additive manufacturing processes.

In [94], researchers synthesized and characterized new room temperature vulcanized (RTV) silicone rubbers using polyhedral oligomeric Vinyl-Silsesquioxanes (POSS) derivatives as crosslinking agents. The results showed improved effects of POSS on thermal stability, mechanical properties, and hardness compared to PDMS polymers prepared with the traditional tetra-functional cross-linkers TMOS and TEOS. The improvements in thermal properties, mechanical properties and hardness could be attributed to the synergistic effect of increasing the dimensionality of the cross-linked networks in new RTV silicone rubbers resulting from the special three-dimensional structure of the new POSS cross-linkers, that are plasticizing self-bonds.

Jitendra Kumar Katiyar and Abdul Samad Mohammed [95], studied the tribological properties of polymer composite coating on silicon wafer. It was concluded that: SU-8/talc/PFPE composite exhibited a hydrophobic surface with higher thermal stability, higher mechanical properties, lower friction coefficient and smaller wear rate, making it a potential candidate to be used in MEMS fabrication. The results of the wetting test showed that the surface of the SU-8 coating changed from hydrophilic to hydrophobic after mixing it with PFPE.

In [96], a new strategy to improve the tribological properties of the polymer by coating with amorphous carbon growing in situ on the surface was realized. The cross-linked structure of the in-situ transition layer served as a barrier to the diffusion of organic polymer chains, followed by the continuous epitaxial growth of the pure aC matrix with continuous carbon plasma treatment. Surface and cross-sectional micrographs showed that the thickness of the in-situ transition layer was about 35nm. The degree of graphitization of aC coatings increased with increasing carbon plasma treatment time. The in-situ transition layer provided strong adhesive strength between the aC coating and the EPC substrates through chemical bonding. The aC segments contributed to the low coefficient of friction and wear rate of EPC substrates with aC surface coating.

Bharadwaja K., *et al.* [97], evaluated the mechanical and tribological performance of epoxy-SiO_2 nano-composites. In order to obtain a high-quality dispersion of epoxy-SiO_2 nano-composites, ultrasonic mixing was used and the results revealed that the bending properties of the epoxy matrix with the introduction of nanoparticles, the hardness and impact resistance, as well as the wear and friction coefficient of the nano-composite were significantly reduced by adding 1% of the volume of SiO_2 nanoparticles to the epoxy matrix. The high mechanical properties of epoxy-SiO_2 nano-composites together with good abrasion, allow the material to normally replace fibres in composites as a partial or full replacement.

The tribological behaviour and mechanical properties of PET and PDMS [98], were evaluated at the nano-scale with respect to environmental conditions. Based on the experimental results, the following conclusions can be drawn: the adhesion force of PET increased near Tg, but showed a similar value at other temperatures. As for PDMS, the adhesion increased steadily with temperature. PET friction was dominated by the deformation mechanism, while PDMS friction is well correlated with adhesion. Despite its softness, PDMS showed no evidence of wear, while significant wear was observed for PET.

A tribological analysis of bulk polymers used in high load applications was carried out in [99]. Four polymers polyetheretherketone (PEEK), polytetrafluoroethylene (PTFE) and aromatic thermosetting polyester (ATSP) were analysed. Researchers have found that high-performance bulk polymers exhibit high tribological properties compared to unfilled polymers. Comparing the four polymers it was concluded that ATSP exhibited better wear resistance while maintaining a moderate COF.

Massimiliano Avalle and Elisa Romanello [100], performed the tribological characterization of modified polymer blends. The results indicated beneficial effects on wear rate. Silicone can be an interesting material for polyurethane and for polyamide, and graphite raised some problems in combination with polyamides. In the case of carbon nanotubes, the harmful influence of polyurethane, CNT caused the formation of residues that prematurely damage the surface.

6. Conclusions

Thermoset resins, as well as thermoplastics, are increasingly used to form composite materials to replace metals. Considerable efforts are being made in all industries to replace metals with composite materials. The main driver of these efforts is low price and improved mechanical properties.

Another benefit of using resins is that the recycled materials can be used to make other objects.

Following the regulations on environmental protection, the management of waste from parts or scrapped vehicles requires that all materials used in engineering be recovered and recycled.

Unfortunately, recycling of thermoset matrix composites is currently limited. Thermoplastic matrix composites offer the potential for recycling or reforming.

Even though epoxy resins are used in a wide range of applications, their poor break strength limits their applicability especially in structural applications.

The hardness of the epoxy could be improved by changing the chemical composition of the resin with a flexible modifier or by reducing the crosslink density.

The toughness of the epoxy resin could be improved, without suffering thermo-mechanical damage, by adding a filler material (rubber, thermoplastic or rigid) as a second phase.

Acknowledgements

This work has been funded by the European Social Fund from the Sectoral Operational Programme Human Capital 2014-2020, through the Financial Agreement with the title "Training of PhD students and postdoctoral researchers in order to acquire applied research skills - SMART", Contract no. 13530/16.06.2022 - SMIS code: 153734.

References

[1]. Wang X., Lu H., Liu X., Hossain M., Fu Y. Q., Xu B. B., *Dynamic coordination of miscible polymer blends towards highly designable shape memory effect*, Polymer, vol. 208, p. 122946, doi: 10.1016/j.polymer.2020.122946, nov. 2020.

[2]. Alsewailem F. D., *Low-temperature synthesis method for the fabrication of efficient polymer-blend systems*, Journal of Materials Research and Technology, vol. 13, p. 1098-1102, doi: 10.1016/j.jmrt.2021.05.020, iul. 2021.

[3]. Mehra N., Mu L., Ji T., Li Y., Zhu J., *Moisture driven thermal conduction in polymer and polymer blends*, Composites Science and Technology, vol. 151, p. 115-123, doi: 10.1016/j.compscitech.2017.08.010, oct. 2017.

[4]. Kato R., Yano T., Tanaka T., *Multi-modal vibrational analysis of blend polymers using mid-infrared photothermal and Raman microscopies*, Vibrational Spectroscopy, vol. 118, p. 103333, doi: 10.1016/j.vibspec.2021.103333, ian. 2022.

[5]. Huang L.-H., Wu C.-H., Hua C.-C., Huang T.-J., *Multiscale simulations of coupled composition-stress-morphology of binary polymer blend*, Polymer, vol. 193, p. 122366, doi: 10.1016/j.polymer.2020.122366, apr. 2020.

[6]. Hu J., Song Y., Ning N., Zhang L., Yu B., Tian M., *An effective strategy for improving the interface adhesion of the immiscible methyl vinyl silicone elastomer/thermoplastic polyurethane blends via developing a hybrid janus particle with amphiphilic brush*, Polymer, vol. 214, p. 123375, doi: 10.1016/j.polymer.2020.123375, feb. 2021.

[7]. Kalita G., Umeno M., Tanemura M., *Blend of Silicon Nanostructures and Conducting Polymers for Solar Cells*, Nanostructured Polymer Blends, Elsevier, p. 495-508, doi: 10.1016/B978-1-4557-3159-6.00014-6, 2014.

[8]. Song S., *et al.*, *Mussel-inspired, self-healing polymer blends*, Polymer, vol. 198, p. 122528, doi: 10.1016/j.polymer.2020.122528, iun. 2020.

[9]. Tipduangta P., Belton P., McAuley W. J., Qi S., *The use of polymer blends to improve stability and performance of electrospun solid dispersions: The role of miscibility and phase separation*, International Journal of Pharmaceutics, vol. 602, p. 120637, doi: 10.1016/j.ijpharm.2021.120637, iun. 2021.

[10]. Keshavamurthy R., Tambrallimath V., Saravanabavan D., *Development of Polymer Composites by Additive Manufacturing Process*, Encyclopedia of Materials: Composites, Elsevier, p. 804-814, doi: 10.1016/B978-0-12-803581-8.11885-5, 2021.

[11]. Shi Y.-C., *et al.*, *Rational design of a functionalized silicone polymer for modifying epoxy-based composites*, Journal of Materials Research and Technology, vol. 19, p. 3867-3876, doi: 10.1016/j.jmrt.2022.06.086, iul. 2022.

[12]. Fu Y., Yao X., *A review on manufacturing defects and their detection of fiber reinforced resin matrix composites*, Composites Part C: Open Access, vol. 8, p. 100276, doi: 10.1016/j.jcomc.2022.100276, iul. 2022.

[13]. Nash N. H., Portela A., Bachour-Sirerol C. I., Manolakis I., Comer A. J., *Effect of environmental conditioning on the properties of thermosetting- and thermoplastic-matrix composite materials by resin infusion for marine applications*, Composites Part B: Engineering, vol. 177, p. 107271, doi: 10.1016/j.compositesb.2019.107271, nov. 2019.

[14]. Voto G., Sequeira L., Skordos A. A., *Formulation based predictive cure kinetics modelling of epoxy resins*, Polymer, vol. 236, p. 124304, doi: 10.1016/j.polymer.2021.124304, nov. 2021.

[15]. Varma I. K., Gupta V. B., Sini N. K., *2.19 Thermosetting Resin – Properties*, Comprehensive Composite Materials II, Elsevier, p. 401-468, doi: 10.1016/B978-0-12-803581-8.03829-7, 2018.

[16]. Ratna D., *Handbook of thermoset resins*, Shawbury: iSmithers, 2009.

[17]. Obande W., Ó Brádaigh C. M., Ray D., *Continuous fibre-reinforced thermoplastic acrylic-matrix composites prepared by liquid resin infusion – A review*, Composites Part B: Engineering, vol. 215, p. 108771, doi: 10.1016/j.compositesb.2021.108771, iun. 2021.

[18]. Shafiei E., Kiasat M. S., *A new viscoplastic model and experimental characterization for thermosetting resins*, Polymer Testing, vol. 84, p. 106389, doi: 10.1016/j.polymertesting.2020.106389, apr. 2020.

[19]. Li J., *et al.*, *A multiscale model for the synthesis of thermosetting resins: From the addition reaction to cross-linked network formation*, Chemical Physics Letters, vol. 720, p. 64-69, doi: 10.1016/j.cplett.2019.02.012, apr. 2019.

[20]. Hu J., *et al.*, *A novel development route for cyano-based high performance thermosetting resins via the strategy of functional group design-dicyanoimidazole resins*, Polymer, vol. 203, p. 122823, doi: 10.1016/j.polymer.2020.122823, aug. 2020.

[21]. Dhinakaran V., Surendar K. V., Hasunfur Riyaz M. S., Ravichandran M., *Review on study of thermosetting and thermoplastic materials in the automated fiber placement process*, Materials Today: Proceedings, vol. 27, p. 812-815, doi: 10.1016/j.matpr.2019.12.355, 2020.

[22]. Memon H., Wei Y., Zhu C., *Recyclable and reformable epoxy resins based on dynamic covalent bonds – Present, past, and future*, Polymer Testing, vol. 105, p. 107420, doi: 10.1016/j.polymertesting.2021.107420, ian. 2022.

[23]. Kudo H., Nishioka S., Jin H., Maekawa H., Nakamura S., Masuda T., *Thermosetting epoxy resin system: Ring-opening by copolymerization of epoxide with D,L-Lactide*, Polymer, vol. 240, p. 124489, doi: 10.1016/j.polymer.2021.124489, feb. 2022.

[24]. Laouchedi D., Bezzazi B., Aribi C., *Elaboration and characterization of composite material based on epoxy resin and clay fillers*, Journal of Applied Research and Technology, vol. 15, nr. 2, p. 190-204, doi: 10.1016/j.jart.2017.01.005, apr. 2017.

[25]. Jeong H., Jang K.-S., *Catalysis of reduced tin oxide in various epoxy resins*, Materials Today Communications, vol. 30, p. 103178, doi: 10.1016/j.mtcomm.2022.103178, mar. 2022.
[26]. Shen Z., Xia Z., Zhang Y., *Characterization and properties of epoxy resin (E-20) modified with silicone intermediate RSN-6018*, Progress in Organic Coatings, vol. 114, p. 115-122, doi: 10.1016/j.porgcoat.2017.10.014, ian. 2018.
[27]. Wang X., Ma B., Chen S., Wei K., Kang X., *Properties of epoxy-resin binders and feasibility of their application in pavement mixtures*, Construction and Building Materials, vol. 295, p. 123531, doi: 10.1016/j.conbuildmat.2021.123531, aug. 2021.
[28]. da Silva L. R. R., *et al.*, *Bio-based one-component epoxy resin: Novel high-performance anticorrosive coating from agro-industrial byproduct*, Progress in Organic Coatings, vol. 167, p. 106861, doi: 10.1016/j.porgcoat.2022.106861, iun. 2022.
[29]. Wang W., Yu B., Zhang Y., Peng M., *Fully aminated rigid-rod aramid reinforced high strength epoxy resin and its composite with carbon fibers*, Composites Science and Technology, vol. 221, p. 109324, doi: 10.1016/j.compscitech.2022.109324, apr. 2022.
[30]. Varganici C., *et al.*, *Semi–interpenetrating networks based on epoxy resin and oligophosphonate: Comparative effect of three hardeners on the thermal and fire properties*, Materials & Design, vol. 212, p. 110237, doi: 10.1016/j.matdes.2021.110237, dec. 2021.
[31]. Abd El-Rahman M., Yassien K. M., Yassene A. A. M., *Effect of gamma irradiation on the optical properties of epoxy resin thin films*, Optik, vol. 183, p. 962-970, doi: 10.1016/j.ijleo.2018.12.182, apr. 2019.
[32]. Kanchanomai C., Thammaruechuc A., *Effects of stress ratio on fatigue crack growth of thermoset epoxy resin*, Polymer Degradation and Stability, vol. 94, nr. 10, p. 1772-1778, doi: 10.1016/j.polymdegradstab.2009.06.012, oct. 2009.
[33]. Ruan K., Zhong X., Shi X., Dang J., Gu J., *Liquid crystal epoxy resins with high intrinsic thermal conductivities and their composites: A mini-review*, Materials Today Physics, vol. 20, p. 100456, doi: 10.1016/j.mtphys.2021.100456, sep. 2021.
[34]. An X., Ding Y., Xu Y., Zhu J., Wei C., Pan X., *Epoxy resin with exchangeable diselenide crosslinks to obtain reprocessable, repairable and recyclable fiber-reinforced thermoset composites*, Reactive and Functional Polymers, vol. 172, p. 105189, doi: 10.1016/j.reactfunctpolym.2022.105189, mar. 2022.
[35]. Wang Y., Wang C., Zhou S., Liu K., *Influence of cationic epoxy resin type on electrophoretic deposition effect on repair of rust-cracked reinforced concrete*, Construction and Building Materials, vol. 324, p. 126714, doi: 10.1016/j.conbuildmat.2022.126714, mar. 2022.
[36]. Cui M., Qing Y., Yang Y., Long C., Liu C., *Nanofunctionalized composite-crosslinked epoxy resin for eco-friendly and robust superhydrophobic coating against contaminants*, Colloids and Surfaces A: Physicochemical and Engineering Aspects, vol. 633, p. 127914, doi: 10.1016/j.colsurfa.2021.127914, ian. 2022.
[37]. Zhang W., Yin L., Zhao M., Tan Z., Li G., *Rapid and non-destructive quality verification of epoxy resin product using ATR-FTIR spectroscopy coupled with chemometric methods*, Microchemical Journal, vol. 168, p. 106397, doi: 10.1016/j.microc.2021.106397, sep. 2021.
[38]. Sawicz-Kryniger K., *et al.*, *Performance of FPT, FTIR and DSC methods in cure monitoring of epoxy resins*, European Polymer Journal, vol. 162, p. 110933, doi: 10.1016/j.eurpolymj.2021.110933, ian. 2022.
[39]. Tabatabaeian M., Khaloo A., Khaloo H., *An innovative high performance pervious concrete with polyester and epoxy resins*, Construction and Building Materials, vol. 228, p. 116820, doi: 10.1016/j.conbuildmat.2019.116820, dec. 2019.
[40]. Bhadra S., Nair S., *Tailor-made one-part epoxy resin for tire compound to improve ride and handling and reduce rolling resistance*, Materials Today: Proceedings, vol. 62, p. 7002-7006, doi: 10.1016/j.matpr.2021.12.544, 2022.
[41]. Feng Q.-K., *et al.*, *Particle packing theory guided multiscale alumina filled epoxy resin with excellent thermal and dielectric performances*, Journal of Materiomics, vol. 8, no. 5, p. 1058-1066, doi: 10.1016/j.jmat.2022.02.008, sep. 2022.
[42]. Qian Z., *et al.*, *Bio-based epoxy resins derived from diphenolic acid via amidation showing enhanced performance and unexpected autocatalytic effect on curing*, Chemical Engineering Journal, vol. 435, p. 135022, doi: 10.1016/j.cej.2022.135022, mai 2022.
[43]. Vidil T., Tournilhac F., Musso S., Robisson A., Leibler L., *Control of reactions and network structures of epoxy thermosets*, Progress in Polymer Science, vol. 62, p. 126-179, doi: 10.1016/j.progpolymsci.2016.06.003, nov. 2016.
[44]. Tonozuka Y., Shohji I., Koyama S., Hokazono H., *Degradation Behaviors of Adhesion Strength between Epoxy Resin and Copper Under Aging at High Temperature*, Procedia Engineering, vol. 184, p. 648-654, doi: 10.1016/j.proeng.2017.04.132, 2017.
[45]. Chen J.-H., Lu J.-H., Pu X.-L., Chen L., Wang Y.-Z., *Recyclable, malleable and intrinsically flame-retardant epoxy resin with catalytic transesterification*, Chemosphere, vol. 294, p. 133778, doi: 10.1016/j.chemosphere.2022.133778, mai 2022.
[46]. Gonçalves F. A. M. M., Ferreira P., Alves P., *Synthesis and characterization of itaconic-based epoxy resin: Chemical and thermal properties of partially biobased epoxy resins*, Polymer, vol. 235, p. 124285, doi: 10.1016/j.polymer.2021.124285, nov. 2021.
[47]. Long Y., *et al.*, *Skin-core structure of thermally aged epoxy resin: Roles of oxidation and re-crosslinking*, Polymer Degradation and Stability, vol. 193, p. 109743, doi: 10.1016/j.polymdegradstab.2021.109743, nov. 2021.
[48]. Zhu T., Lu C., Lu X., Zhi J., Song Y., *Curing process optimization and mechanical properties improvement of epoxy resin copolymer modified by epoxy-terminated hyperbranched polyether sulfone*, Polymer, vol. 241, p. 124535, doi: 10.1016/j.polymer.2022.124535, feb. 2022.
[49]. Kishi H., Matsuda S., Imade J., Shimoda Y., Nakagawa T., Furukawa Y., *The effects of the toughening mechanism and the molecular weights between cross-links on the fatigue resistance of epoxy polymer blends*, Polymer, vol. 223, p. 123712, doi: 10.1016/j.polymer.2021.123712, mai 2021.
[50]. Anagnostopoulos C. A., Dimitriadi M., Konstantinidis D., *Static and cyclic behaviour of epoxy resin and bentonite-grouted sands*, Transportation Geotechnics, vol. 33, p. 100725, doi: 10.1016/j.trgeo.2022.100725, mar. 2022.
[51]. Peng Y.-J., He X., Wu Q., Sun P.-C., Wang C.-J., Liu X.-Z., *A new recyclable crosslinked polymer combined polyurethane and epoxy resin*, Polymer, vol. 149, p. 154-163, doi: 10.1016/j.polymer.2018.06.082, aug. 2018.
[52]. Yuksel O., Sandberg M., Baran I., Ersoy N., Hattel J. H., Akkerman R., *Material characterization of a pultrusion specific and highly reactive polyurethane resin system: Elastic modulus, rheology, and reaction kinetics*, Composites Part B: Engineering, vol. 207, p. 108543, doi: 10.1016/j.compositesb.2020.108543, feb. 2021.
[53]. Chen L., Chen S., *Latex interpenetrating networks based on polyurethane, polyacrylate and epoxy resin*, Progress in Organic Coatings, vol. 49, nr. 3, p. 252-258, doi: 10.1016/j.porgcoat.2003.10.010, apr. 2004.
[54]. Malucelli G., Priola A., Ferrero F., Quaglia A., Frigione M., Carfagna C., *Polyurethane resin-based adhesives: curing reaction and properties of cured systems*, International Journal of Adhesion and Adhesives, vol. 25, no. 1, p. 87-91, doi: 10.1016/j.ijadhadh.2004.04.003, feb. 2005.
[55]. Mayer P., Dmitruk A., Kaczmar J. W., *Adhesion of functional layers based on epoxy and polyurethane resins for aluminum substrate*, International Journal of Adhesion and Adhesives, vol. 109, p. 102899, doi: 10.1016/j.ijadhadh.2021.102899, sep. 2021.
[56]. Jia Q., Zheng M., Chen H., Shen R., *Morphologies and properties of polyurethane/epoxy resin interpenetrating network nanocomposites modified with organoclay*, Materials Letters, vol.

60, no. 9-10, p. 1306-1309, doi: 10.1016/j.matlet.2005.11.018, mai 2006.

[57]. Valentino R., Romeo E., Stevanoni D., *An experimental study on the mechanical behaviour of two polyurethane resins used for geotechnical applications*, Mechanics of Materials, vol. 71, p. 101-113, doi: 10.1016/j.mechmat.2014.01.007, apr. 2014.

[58]. Varganici C.-D., Rosu L., Rosu D., Simionescu B. C., *Miscibility studies of some semi-interpenetrating polymer networks based on an aromatic polyurethane and epoxy resin*, Composites Part B: Engineering, vol. 50, p. 273-278, doi: 10.1016/j.compositesb.2013.02.005, iul. 2013.

[59]. Yong Q., Liao B., Huang J., Guo Y., Liang C., Pang H., *Preparation and characterization of a novel low gloss waterborne polyurethane resin*, Surface and Coatings Technology, vol. 341, p. 78-85, doi: 10.1016/j.surfcoat.2018.01.012, mai 2018.

[60]. Peng Y.-J., He X., Wu Q., Sun P.-C., Wang C.-J., Liu X.-Z., *A new recyclable crosslinked polymer combined polyurethane and epoxy resin*, Polymer, vol. 149, p. 154-163, doi: 10.1016/j.polymer.2018.06.082, aug. 2018.

[61]. Verdolotti L., *et al.*, *"Aerogel-like" polysiloxane-polyurethane hybrid foams with enhanced mechanical and thermal-insulating properties*, Composites Science and Technology, vol. 213, p. 108917, doi: 10.1016/j.compscitech.2021.108917, sep. 2021.

[62]. Xu L., Li X., Jiang F., Yu X., Wang J., Xiao F., *Thermosetting characteristics and performances of polyurethane material on airport thin-overlay*, Construction and Building Materials, vol. 344, p. 128252, doi: 10.1016/j.conbuildmat.2022.128252, aug. 2022.

[63]. Banna M. H., Shirokoff J., Molgaard J., *Effects of two aqueous acidic solutions on polyester and bisphenol A epoxy vinyl ester resins*, Materials Science and Engineering: A, vol. 528, no. 4-5, p. 2137-2142, doi: 10.1016/j.msea.2010.11.049, feb. 2011.

[64]. Abral H., *et al.*, *Improving impact, tensile and thermal properties of thermoset unsaturated polyester via mixing with thermoset vinyl ester and methyl methacrylate*, Polymer Testing, vol. 81, p. 106193, doi: 10.1016/j.polymertesting.2019.106193, ian. 2020.

[65]. Ittner Mazali C. A., Felisberti M. I., *Vinyl ester resin modified with silicone-based additives: III. Curing kinetics*, European Polymer Journal, vol. 45, nr. 8, p. 2222-2233, doi: 10.1016/j.eurpolymj.2009.05.022, aug. 2009.

[66]. Gautam V., Kumar A., Sharma A., Kumar A., Kumar D., *Tribological behaviour of hybrid reinforced vinyl ester based functionally graded materials*, Materials Today: Proceedings, vol. 44, p. 4682-4688, doi: 10.1016/j.matpr.2020.11.023, 2021.

[67]. Dev S., Shah P. N., Zhang Y., Ryan D., Hansen C. J., Lee Y., *Synthesis and mechanical properties of flame retardant vinyl ester resin for structural composites*, Polymer, vol. 133, p. 20-29, doi: 10.1016/j.polymer.2017.11.017, dec. 2017.

[68]. Yadav S. K., Schmalbach K. M., Kinaci E., Stanzione J. F., Palmese G. R., *Recent advances in plant-based vinyl ester resins and reactive diluents*, European Polymer Journal, vol. 98, p. 199-215, doi: 10.1016/j.eurpolymj.2017.11.002, ian. 2018.

[69]. Adibzadeh E., Mirabedini S. M., Behzadnasab M., Farnood R. R., *A novel two-component self-healing coating comprising vinyl ester resin-filled microcapsules with prolonged anticorrosion performance*, Progress in Organic Coatings, vol. 154, p. 106220, doi: 10.1016/j.porgcoat.2021.106220, mai 2021.

[70]. Scott T. F., Cook W. D., Forsythe J. S., *Effect of the degree of cure on the viscoelastic properties of vinyl ester resins*, European Polymer Journal, vol. 44, nr. 10, p. 3200-3212, doi: 10.1016/j.eurpolymj.2008.07.009, oct. 2008.

[71]. Sultania M., Rai J. S. P., Srivastava D., *Studies on the synthesis and curing of epoxidized novolac vinyl ester resin from renewable resource material*, European Polymer Journal, vol. 46, nr. 10, p. 2019-2032, doi: 10.1016/j.eurpolymj.2010.07.014, oct. 2010.

[72]. Tu R., Sodano H. A., *Additive manufacturing of high-performance vinyl ester resin via direct ink writing with UV-thermal dual curing*, Additive Manufacturing, vol. 46, p. 102180, doi: 10.1016/j.addma.2021.102180, oct. 2021.

[73]. Arrieta J. S., Richaud E., Fayolle B., Nizeyimana F., *Thermal oxidation of vinyl ester and unsaturated polyester resins*, Polymer Degradation and Stability, vol. 129, p. 142-155, doi: 10.1016/j.polymdegradstab.2016.04.003, iul. 2016.

[74]. Ganesh Gupta K. B. N. V. S., Hiremath M. M., Ray B. C., Prusty R. K., *Improved mechanical responses of GFRP composites with epoxy-vinyl ester interpenetrating polymer network*, Polymer Testing, vol. 93, p. 107008, doi: 10.1016/j.polymertesting.2020.107008, ian. 2021.

[75]. Sousa J. M., Garrido M., Correia J. R., Cabral-Fonseca S., *Hygrothermal ageing of pultruded GFRP profiles: Comparative study of unsaturated polyester and vinyl ester resin matrices*, Composites Part A: Applied Science and Manufacturing, vol. 140, p. 106193, doi: 10.1016/j.compositesa.2020.106193, ian. 2021.

[76]. Wang Y., *et al.*, *Network structure and properties of crosslinked bio-based epoxy resin composite: An in-silico multiscale strategy with dynamic curing reaction process*, Giant, vol. 7, p. 100063, doi: 10.1016/j.giant.2021.100063, aug. 2021.

[77]. Shen Z., Xia Z., Zhang Y., *Characterization and properties of epoxy resin (E-20) modified with silicone intermediate RSN-6018*, Progress in Organic Coatings, vol. 114, p. 115-122, doi: 10.1016/j.porgcoat.2017.10.014, ian. 2018.

[78]. Saludung A., Azeyanagi T., Ogawa Y., Kawai K., *Alkali leaching and mechanical performance of epoxy resin-reinforced geopolymer composite*, Materials Letters, vol. 304, p. 130663, doi: 10.1016/j.matlet.2021.130663, dec. 2021.

[79]. Alia C., Jofre-Reche J. A., Suárez J. C., Arenas J. M., Martín-Martínez J. M., *Characterization of the chemical structure of vinyl ester resin in a climate chamber under different conditions of degradation*, Polymer Degradation and Stability, vol. 153, p. 88-99, doi: 10.1016/j.polymdegradstab.2018.04.014, iul. 2018.

[80]. Yang X., *et al.*, *Fabrication of UV-curable solvent-free epoxy modified silicone resin coating with high transparency and low volume shrinkage*, Progress in Organic Coatings, vol. 129, p. 96-100, doi: 10.1016/j.porgcoat.2019.01.005, apr. 2019.

[81]. Obande W., Gruszka W., Garden J. A., Wurzer C., Ó Brádaigh C. M., Ray D., *Enhancing the solvent resistance and thermomechanical properties of thermoplastic acrylic polymers and composites via reactive hybridisation*", Materials & Design, vol. 206, p. 109804, doi: 10.1016/j.matdes.2021.109804, aug. 2021.

[82]. Luo D., Wu C., Yan M., *Incorporation of the Fe_3O_4 and SiO_2 nanoparticles in epoxy-modified silicone resin as the coating for soft magnetic composites with enhanced performance*", Journal of Magnetism and Magnetic Materials, vol. 452, p. 5-9, doi: 10.1016/j.jmmm.2017.12.005, apr. 2018.

[83]. Wei Y.-Y., An S.-S., Sun S., Jiang Y., *Photo-polymerized and thermal-polymerized silicon hydrogels with different surface microstructure and wettability*, Colloids and Surfaces A: Physicochemical and Engineering Aspects, vol. 618, p. 126284, doi: 10.1016/j.colsurfa.2021.126284, iun. 2021.

[84]. Wang X.-L., *et al.*, *Recycling waste thermosetting unsaturated polyester resins into oligomers for preparing amphiphilic aerogels*, Waste Management, vol. 126, p. 89-96, doi: 10.1016/j.wasman.2021.03.002, mai 2021.

[85]. Zheng C., Wang G., Chu Y., Xu Y., Qiu M., Xu M., *RTV silicone rubber surface modification for cell biocompatibility by negative-ion implantation*, Nuclear Instruments and Methods in Physics Research Section B: Beam Interactions with Materials and Atoms, vol. 370, p. 73-78, doi: 10.1016/j.nimb.2016.01.014, mar. 2016.

[86]. Zhao H., Xu S., Guo A., Li J., Liu D., *The Curing Kinetics Analysis of Four Epoxy Resins Using a Diamine Terminated Polyether as Curing Agent*, Thermochimica Acta, vol. 702, p. 178987, doi: 10.1016/j.tca.2021.178987, aug. 2021.

[87]. Dave P. N., Patel N. N., *Synthesis, properties and applications of interacting blends of acrylated novalac epoxy resin based poly(ester-amide)s and vinyl ester*, Journal of Saudi

Chemical Society, vol. 20, p. S231–S235, doi: 10.1016/j.jscs.2012.10.006, sep. 2016.
[88]. Ling Y., Luo J., Heng Z., Chen Y., Zou H., Liang M., *Synthesis of a comb-like silicone-epoxy co-polymer with high thermal stability and mechanical properties for ablative materials*, Reactive and Functional Polymers, vol. 157, p. 104742, doi: 10.1016/j.reactfunctpolym.2020.104742, dec. 2020.
[89]. Li A., *et al.*, *Study on preparation and properties of superhydrophobic surface of RTV silicone rubber*, Journal of Materials Research and Technology, vol. 11, p. 135-143, doi: 10.1016/j.jmrt.2020.12.074, mar. 2021.
[90]. Hu Q., *et al.*, *Study on Modification of Room Temperature Vulcanized Silicone Rubber by Microencapsulated Phase Change Material*, Journal of Energy Storage, vol. 41, p. 102842, doi: 10.1016/j.est.2021.102842, sep. 2021.
[91]. Gohel G., Bhudolia S. K., Elisetty S. B. S., Leong K. F., Gerard P., *Development and impact characterization of acrylic thermoplastic composite bicycle helmet shell with improved safety and performance*, Composites Part B: Engineering, vol. 221, p. 109008, doi: 10.1016/j.compositesb.2021.109008, sep. 2021.
[92]. Zhu Q., Wang Z., Zeng H., Yang T., Wang X., *Effects of graphene on various properties and applications of silicone rubber and silicone resin*, Composites Part A: Applied Science and Manufacturing, vol. 142, p. 106240, doi: 10.1016/j.compositesa.2020.106240, mar. 2021.
[93]. Joseph V. S., *et al.*, *Silicone/epoxy hybrid resins with tunable mechanical and interfacial properties for additive manufacture of soft robots*, Applied Materials Today, vol. 22, p. 100979, doi: 10.1016/j.apmt.2021.100979, mar. 2021.
[94]. Chen D., *et al.*, *Synthesis and characterization of novel room temperature vulcanized (RTV) silicone rubbers using Vinyl-POSS derivatives as cross linking agents*, Polymer, vol. 51, nr. 17, p. 3867-3878, doi: 10.1016/j.polymer.2010.06.028, aug. 2010.
[95]. Katiyar J. K., Mohammed A. S., *Physical, tribological and mechanical properties of polymer composite coating on silicon wafer*, Tribology International, vol. 165, p. 107307, doi: 10.1016/j.triboint.2021.107307, ian. 2022.
[96]. Guan W., *et al.*, *Novel strategy to improve the tribological property of polymer: In-situ growing amorphous carbon coating on the surface*, Applied Surface Science, vol. 505, p. 144626, doi: 10.1016/j.apsusc.2019.144626, mar. 2020.
[97]. Bharadwaja K., Srinivasa Rao S., Baburao T., *Epoxy/SiO_2 nanocomposite mechanical properties and tribological performance*, Materials Today: Proceedings, p. S2214785321078974, doi: 10.1016/j.matpr.2021.12.172, dec. 2021.
[98]. Shin D.-G., Kim T.-H., Kim D.-E., *Assessment of nano-scale tribological and mechanical properties of flexible transparent polymers based on atomic force microscopy*, CIRP Annals, vol. 68, no. 1, p. 599-602, doi: 10.1016/j.cirp.2019.04.036, 2019.
[99]. Nunez E. E., Gheisari R., Polycarpou A. A., *Tribology review of blended bulk polymers and their coatings for high-load bearing applications*, Tribology International, vol. 129, p. 92-111, doi: 10.1016/j.triboint.2018.08.002, ian. 2019.
[100]. Avalle M., Romanello E., *Tribological characterization of modified polymeric blends*, Procedia Structural Integrity, vol. 8, p. 239-255, doi: 10.1016/j.prostr.2017.12.026, 2018.

THE ANNALS OF "DUNAREA DE JOS" UNIVERSITY OF GALATI
FASCICLE IX. METALLURGY AND MATERIALS SCIENCE
No. 4 - 2022, ISSN 2668-4748; e-ISSN 2668-4756
Article DOI: https://doi.org/10.35219/mms.2022.4.13

EXPERIMENTAL DETERMINATION OF THE KUCZYNSKI EQUATION FOR THE CASE OF CuSn12 ALLOY SINTERING

Petrică ALEXANDRU, Cristian ŞTEFĂNESCU
"Dunarea de Jos" University of Galati, Romania
e-mail: palex@ugal.ro

ABSTRACT

Sintered copper-tin alloys are used to obtain products with numerous applications. Some bronze parts such as filters or bushings for self-lubricating bearings can only be produced by specific powder metallurgy technologies. Metal filters represent an important fraction in the field of sintered products. In the paper, measurements of the intergranular bridges were made on the samples obtained by sintering the spheroidal powder from the CuSn12 alloy. Free casting in graphite moulds followed by sintering was used (9 experiments, 3 temperatures x 3 durations). With these data, the coefficients from the Kuczinski equation were determined. Thus, the correlation between the desired porosity for a filter-type product (expressed by the size of the intergranular bridge) and the sintering technological parameters can be established.

KEYWORDS: Kuczynski equation, CuSn12 powder, sintering intergranular bridge, bronze powder filter

1. Introduction

Metal filters are made of sintered materials with porosity over 30%, with communicating pores used in installations that use fluids. The materials, shapes and sizes of these filter components are very diverse and adapted to applications in numerous fields.

There are the following types of materials used for the production of metal filters: *spherical powders, irregular powders, fabrics and fibres*.

For most metal filters obtained by sintering, spherical powders of: *bronze, brass, nickel, stainless steel, titanium, silver, etc. are generally used*.

1.1. Forming procedures of bronze filter elements

The formation of filter elements obtained from powders can be done: without pressing or by pressing. Press forming processes include: *die pressing, rolling, extrusion, injection moulding, etc*. It should be noted that in order to obtain products with sufficient strength, without using high compaction pressures, additional materials must be used (paraffin, polymers, etc.). Otherwise, by applying high compression pressures, which ensure the mechanical resistance necessary for transport and handling to the sintering furnace, too small porosities can be reached, which disqualifies the product from the category of filters. Non-press forming refers to the processes: *free powder casting, free spreading and smoothing, slip casting, spray deposition, vibration forming, etc*. Each process has several technological variants of application of powder formation.

1.2. The pouring freely in the mould

The powder is poured freely into a mould (form) and then subjected to heating for sintering together with it, (Figure 2.1). It represents the simplest method of forming parts from powders, without compression. The homogenization of the powder distribution in the mould cavity is done by vibrating the mould.

The materials from which the forms are made are relatively expensive (refractory alloys, ceramic materials, graphite, etc.), which is a disadvantage, in addition to a relatively short life cycle (considering the repeated thermal cycles to which they are subjected) [2]. The forms made of metal alloys must be subjected to superficial treatments which form layers of stable chemical compounds at the sintering conditions (temperature and protective atmosphere in the furnace). Thus, welding of the form with the sintered product contained therein is avoided [1].

THE ANNALS OF "DUNAREA DE JOS" UNIVERSITY OF GALATI
FASCICLE IX. METALLURGY AND MATERIALS SCIENCE
Nº. 4 - 2022, ISSN 2668-4748; e-ISSN 2668-4756
Article DOI: https://doi.org/10.35219/mms.2022.4.13

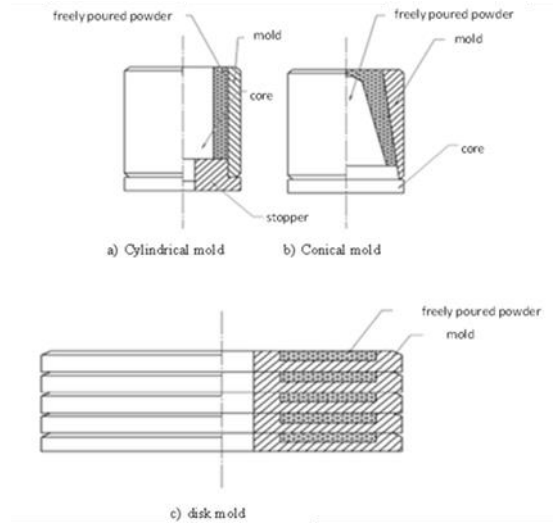

Fig. 1.1. *Powder freely poured into moulds and sintered*

In this work, free casting in graphite moulds was chosen for obtaining the samples, because it is the simplest method, but also because during sintering, graphite provides the protective environment corresponding to the used CuSn12 alloy.

1.3. Kuczinski's equation

The sintering process is governed by the following mechanisms of material transport: diffusion (surface, at grain boundaries, in volume), viscous flow, evaporation-condensation, which develops the formation of sintering bridges (Figure 1.2) [1].

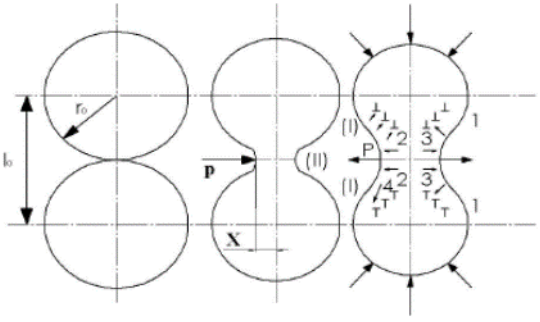

Fig. 1.2. *Principle diagram of the formation of intergranular bridges during sintering*

The studies of the sintering process on regular geometric models of the ball-ball type, led to the establishment of the general form of the law of growth of sintering bridges [1]:

$$\frac{x^n}{r^m} = K(t) \cdot \tau \qquad (1.1)$$

where:

x - half-thickness of the sintering bridge;
r - radius of the powder particle;
τ - sintering time;
K(t) - coefficient depending on the sintering temperature *t*;
m, *n* - constants dependent on the type of material transfer mechanism during sintering.

The constants m and n are presented in the literature, with relatively concordant values, according to various sources, depending on the mechanism of the predominant material transport [2].

1.4. Manufacture of bronze filters

The sintering of bronze filters formed by free pouring is widely used to obtain filter elements with high permeability. The bronze powders used have dimensions between 0.2÷0.8 mm, with a spheroidal shape. Forming vibration is usually applied for controlled compaction.

For powders with spherical particles of the same diameter, a porosity of 26% can be reached, for a theoretically perfect arrangement. In practice, friction between the particles prevents this level of maximum compaction from being reached, and a porosity of 60 or even 70% can be achieved. By using spherical powders with a certain particle size distribution and controlled vibrations, porosity can be reduced to 35-45%.

In industrial practice, bronze filters are sintered at temperatures above 800 ºC, with a maintenance of 20÷60 minutes, in a protective environment.

2. Experimental research on the sintering of CuSn12 alloy powder

2.1. Objectives of experimental research

The purpose of the experiments was to establish the correlation that exists between the parameters of the sintering thermal treatment (sintering temperature, *t* [°C] and holding time at the sintering temperature, *τ* [min]) and the size of the intergranular sintering bridges, *x* [µm] in the case of products with high porosity, such as filters formed by free pouring from CuSn12 powder. We started from the hypothesis of a correlation like the Kuczinski equation, aiming to find the particular form of this expression for the chosen powder.

2.2. Experimental procedure

The samples were formed in a graphite mould. In this way, the conditions of protection during sintering (reducing environment), the simplicity of

THE ANNALS OF "DUNAREA DE JOS" UNIVERSITY OF GALATI
FASCICLE IX. METALLURGY AND MATERIALS SCIENCE
N°. 4 - 2022, ISSN 2668-4748; e-ISSN 2668-4756
Article DOI: https://doi.org/10.35219/mms.2022.4.13

processing the form, but also the avoidance of welding of the powder to it, were ensured. The mould was made up of two semi-cylindrical components. In one of the parts, a parallelepiped cavity with the dimensions: 38 x 4 x 1.5 mm was processed. (Figure 2.1).

Fig. 2.1. *The mould with the two semi-cylindrical components used for the free casting of CuSn12 powder samples*

After pouring the powder into the mould cavity, a slight vibration was made by applying very light blows to the mould and the excess was removed by scraping. The appearance of the powder prepared for sintering, before mounting the "cap" (which closes the mould cavity), can be seen in Figure 2.2.

Fig. 2.2. *The graphite mould with the powder prepared for sintering*

In order to preserve as well as possible during sintering, the reducing environment (generated by the presence of graphite), the shape was inserted into an aluminium tube. The ends of the tube were plugged with ceramic felt plugs (Figure 2.3).

Sintering was done in an electric furnace with a LENTON tubular enclosure, with automatic control of the heating regime.

The analysis and measurement of the powder as well as the sintered samples was done with a stereomicroscope (*Carl Zeiss Jena*), equipped with a *TOUPCAM L3CMOS14000KPA* digital camera. The software used for image acquisition and processing was *ToupCam ToupView*.

Fig. 2.3. *The furnace used for sintering and the aluminium tube (to maintain the reducing environment), plugged with ceramic felt plugs, which contains the graphite form*

Statistical analysis of the data obtained by measuring the powder particles under a microscope led to the results in Table 2.1 and Figure 2.4.

Table 2.1. *Granulometric characterization of CuSn12 powder*

Average diameter, d_m[µm]	348
Standard deviation, [µm]	39

Main sintering parameters: sintering temperature, *t*, [°C] and holding time at sintering temperature, *τ*, [min] were used to establish the experimental program according to Table 2.2.

Table 2.2. *Experimental program for CuSn12 powder sintering*

Temperature, ***t***, [°C]	Time, ***τ***, [min]		
800	20	40	60
900	20	40	60
920	20	40	60

The sintered samples (Figure 2.5) were investigated by optical microscopy in order to determine the dimensions of the intergranular bridges: 2x [µm] and the diameters of the particles joined by them: d1, d2 [µm]. The appearance of one

THE ANNALS OF "DUNAREA DE JOS" UNIVERSITY OF GALATI
FASCICLE IX. METALLURGY AND MATERIALS SCIENCE
No. 4 - 2022, ISSN 2668-4748; e-ISSN 2668-4756
Article DOI: https://doi.org/10.35219/mms.2022.4.13

of the sintered samples (t = 880 °C, τ = 60 min) analysed by optical microscopy is presented in Figure 2.6. For each of the 9 samples, corresponding to the experienced sintering regimes, 38 sets of measurements were made. A set comprises the size of the bridge between two particles and their diameters.

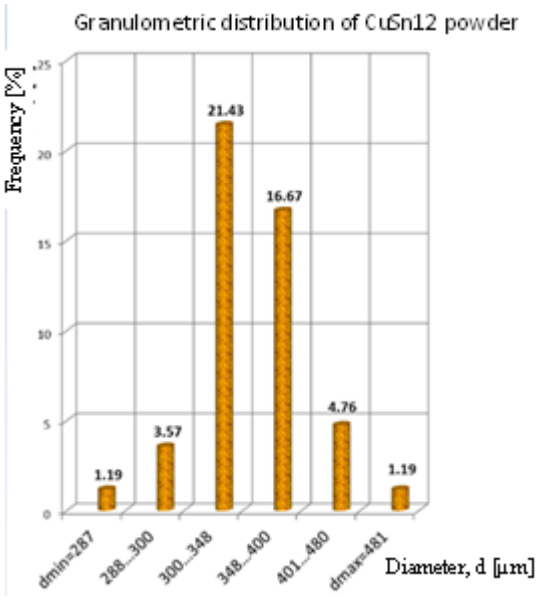

Fig. 2.4. *Granulometric curve of the powder used*

Fig. 2.5. *Appearance of a sintered sample and the mould used for it*

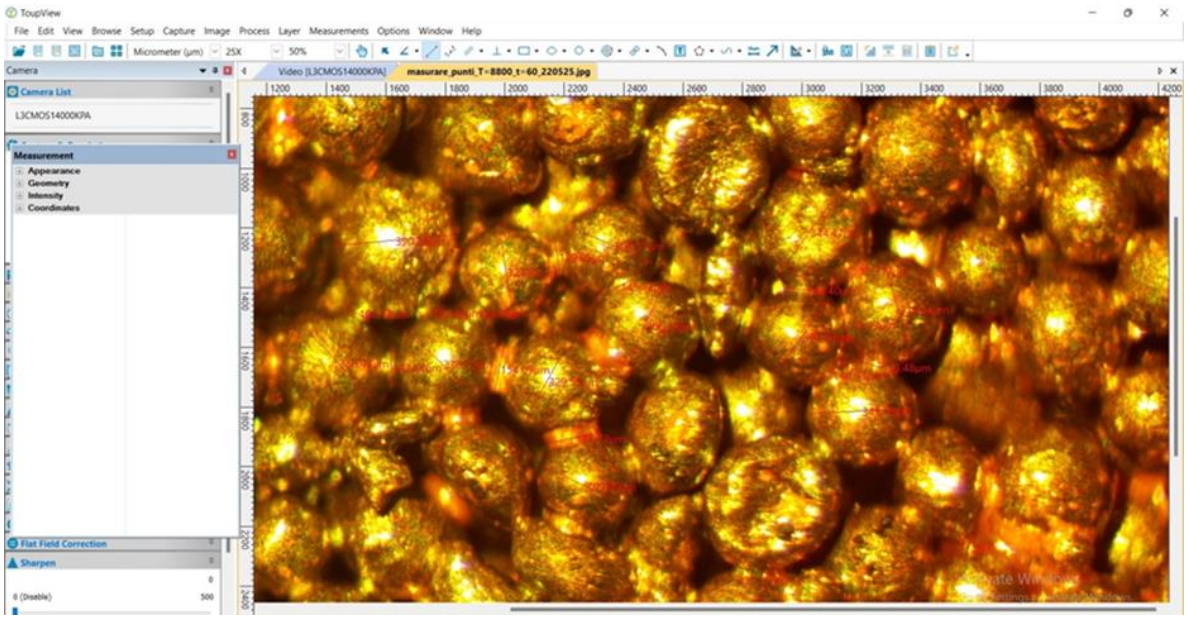

Fig. 2.6. *The appearance of one of the sintered samples (t = 880 °C, τ = 60 min) analyzed by optical microscopy*

2.2. Results obtained

The measurements made on the 9 sintered samples according to the established experimental program (*3 durations x 3 temperatures*) are summarized in Table 3. The r value represents the average of the 76 particles, taken into consideration, in the case of each sample.

THE ANNALS OF "DUNAREA DE JOS" UNIVERSITY OF GALATI
FASCICLE IX. METALLURGY AND MATERIALS SCIENCE
N°. 4 - 2022, ISSN 2668-4748; e-ISSN 2668-4756
Article DOI: https://doi.org/10.35219/mms.2022.4.13

With the data obtained, it is possible to identify the particular forms of the Kuczinski equation (1.1) valid for each level of the sintering temperature used:

$$\frac{x^n}{r^m} = K(t) \cdot \tau$$

Table 2.3. *The average sizes of the intergranular bridges and of the particles joined by them*

Sample	Sintering parameters temperature, ***t*** [°C], time **τ** [min]	Average values (38 bridges, 76 particles)	
		x [μm]	***r*** [μm]
1	**t**=880; **τ**=20	61	165
2	**t**=880; **τ**=40	65	164
3	**t**=880; **τ**=60	67	167
4	**t**=900; **τ**=20	72	168
5	**t**=900; **τ**=40	76	165
6	**t**=900; **τ**=60	82	174
7	**t**=920; **τ**=20	82	207
8	**t**=920; **τ**=40	73	164
9	**t**=920; **τ**=60	84	165

Using the data obtained from the measurements made, on the three samples obtained at the temperature of 880 °C, with the maintenance durations of 20, 40, and 60 minutes, it is possible to formulate, starting from the general form of the relationship, a system of three linear equations where the unknowns are *n*, *m* and *K(t)*.

By applying the logarithm function of the Kuczynski expression can be obtained:

$$lg\left(\frac{x^n}{r^m}\right) = lg\ (K(t) \cdot \tau) \qquad (2.2)$$

After processing:

$$nlgx - mlgr - l\,g\,K(t) = l\,g\,\tau \qquad (2.3)$$

For the sintering holding time of 20 minutes the relationship becomes:

$$nlg0{,}061 - mlg0{,}165 - lgK(t) = lg1200 \qquad (2.4)$$

If we also use the data obtained for the maintenance times of 40 and 60 minutes, we finally obtain the system of three equations, which contains the sought parameters as unknowns:

$$\begin{aligned} nlg0{,}061 - mlg0{,}165 - lgK(t) &= lg1200 \\ nlg0{,}065 - mlg0{,}164 - lgK(t) &= lg2400 \\ nlg0{,}067 - mlg0{,}167 - lgK(t) &= lg3600 \end{aligned} \qquad (2.5)$$

It can be seen that the values for ***r*** and ***x*** have been converted to millimeter and those for ***τ*** durations to seconds

Solving the system of equations allows identifying the coefficients ***n***, ***m*** and ***K(t)*** so that the Kuczynski equation for samples formed by free casting in graphite molds, from CuSn12 powder sintered at 880°C has the form:

$$\frac{x^{12}}{r^6} = (10^{-12{,}92}) \cdot \tau \qquad (2.6)$$

The other two relationships are obtained following the same procedure. Thus for the temperature of 900 °C:

$$\frac{x^{11{,}14}}{r^{7{,}71}} = (10^{-9{,}84}) \cdot \tau \qquad (2.7)$$

and for 920 °C:

$$\frac{x^{3{,}74}}{r^{4{,}431}} = (10^{-4{,}14}) \cdot \tau \qquad (2.8)$$

The three equations 2.6, 2.7, 2.8 can be written in the form:

$$\begin{cases} \boldsymbol{x = 10^{\frac{lg(\tau)+6lg(r)-12{,}92}{12}}}, for\ \mathbf{t = 880°C} \\ \boldsymbol{x = 10^{\frac{lg(\tau)+7{,}71lg(r)-9{,}84}{11.14}}}, for\ \mathbf{t = 900°C} \\ \boldsymbol{x = 10^{\frac{lg(\tau)+4{,}43lg(r)-4{,}14}{3{,}74}}}, for\ \mathbf{t = 920°C} \end{cases} \qquad (2.9)$$

which allows highlighting the more important role of the temperature factor, compared to the one represented by the holding time, regarding the evolution of the size of the intergranular bridges during sintering (***K(t)*** has the maximum value, $10^{-4.14}$, at 920 °C).

3. Conclusions

Based on what is presented in the paper, the following conclusions can be expressed:

1. 9 experiments were programmed, with the parameters of temperature variation and holding time, to identify the coefficients of the Kuczynski relationship, which could describe the evolution of intergranular bridges during the sintering of products formed by free casting, (filter-type products with high porosity) from spherical CuSn12 bronze powder.

2. A set of equations was obtained that describe the evolution, as a function of time, of the intergranular bridge, for a spheroidal powder with a known particle size distribution, sintered at a temperature in the range of 880-920 °C.

THE ANNALS OF "DUNAREA DE JOS" UNIVERSITY OF GALATI
FASCICLE IX. METALLURGY AND MATERIALS SCIENCE
No. 4 - 2022, ISSN 2668-4748; e-ISSN 2668-4756
Article DOI: https://doi.org/10.35219/mms.2022.4.13

3. The Kuczynski equations, customized for the three experimental temperatures, implicitly also include the effects of using a powder with a relatively extensive particle size distribution - the particles of the powder used were spheroidal, with sizes that fall within a relatively wide range, with diameters between 250 and 500 μm.

4. In addition to the dimensional inhomogeneity, the uneven oxidation of the powder particles, which was observed during microscopic analysis, should be noted. The non-homogeneous superficial oxide film in thickness, although it influences the sintering behavior, cannot be taken into account by the Kuczynski equation. That's why the obtained equations should be refined through additional experiments, under the conditions of using a more dimensionally homogeneous spherical powder and with a uniform and as low degree of oxidation.

5. As expected, the obtained equations highlight the much greater influence of the temperature factor, compared to that represented by time, on the evolution of sintering expressed by the variation of the size of the intergranular bridge.

6. It is necessary to establish the quantitative link between the size of the intergranular bridges of the sintered product and its porosity. Thus, it will be possible to correlate the desired porosity with the required sintering regime, based on Kuczynski-type relationships.

References

[1]. Nicoară M., Vida-Simiti I., Demian C., *Esenţial în Metalurgia Pulberilor*, Ed. U.T. PRESS, Cluj-Napoca, 2009.
[2]. Taloi D., Florian E., Bratu C., Berceanu E., *Optimizarea proceselor metalurgice*, Editura Didactică şi Pedagogică, Bucureşti, 1983.

THE ANNALS OF "DUNAREA DE JOS" UNIVERSITY OF GALATI
FASCICLE IX. METALLURGY AND MATERIALS SCIENCE
Nº. 4 - 2022, ISSN 2668-4748; e-ISSN 2668-4756
Article DOI: https://doi.org/10.35219/mms.2022.4.14

DIELECTRIC PMMA THIN LAYERS OBTAINED BY SPIN COATING FOR ELECTRONIC APPLICATIONS

Elena Emanuela HERBEI
Interdisciplinary Research Centre in the Field of Eco-Nano Technology and Advance Materials CC-ITI, Faculty of Engineering, "Dunarea de Jos" University of Galati, 47 Domneasca, 800008 Galati, Romania
e-mail: elena.herbei@ugal.ro

ABSTRACT

Thin polymeric films with dielectric properties become a very important part of today's devices, being indispensable in industry, electrical applications and not only. Nowadays polymeric materials have attracted attention in academic and industrial research due to the miniaturization at the micro and nanoscale of different electronic devices. Polymers in general are used for their light weight, good mechanical strength, dielectric properties, and optical properties, which make them multifunctional materials.

This paper presents research on polymethyl methacrylate (PMMA) thin films obtained by the sol-gel method. The optimization of thin film PMMA layers has been a problem due to the importance of using the polymer in the different electronic domains. Thin films of PMMA with different thicknesses were deposited onto glass and silicon wafers in order to measure dielectric properties. For dielectric properties, the PMMA thin layer was inserted in a metal-insulator-metal structure (MIM). In order to observe the morphology and roughness of thin film, optical microscopy, scanning electron microscopy and atomic force microscopy have proceeded.

The dielectric constant (k) was calculated using the electrical capacitance formula. The I-V and C-V curves showed a dielectric behavior with a leakage current between 10^{-11} and 10^{-8} A and a constant capacitance in the bias range ± 5 V.

KEYWORDS: thin films, polymeric films, dielectric properties, polymethyl methacrylate

1. Introduction

The development of TFTs devices based on thin layers of polymer compounds by sol-gel became a good solution and gain special attention to the low cost obtaining.

Because of its low cost and high output like transparency, thermal stability, electrical insulation, and mechanical resistance, the thin film layer of PMMA has sparked interest for use as an insulator in electronic and optoelectronic devices [1]. It has also good optical properties (transparency in a wide range of wavelengths from near ultraviolet to near-infrared) [2, 3]. For the preparation of polymeric thin films, different types of PMMA in anisole [4] toluene, DMF [5], chloroform [6], benzoyl peroxide (BPO 98%) to start the polymerization of MMA and to obtain PMMA solution at 70 ºC [7] or alcoholic solution [8], or with the value of molecular weight from 495 to 996 Kw were used. There are several methods in order to obtain thin layers of PMMA as ALD [9, 10], ink-jet printing [11] but the most used is sol-gel process due to its versatility and low-cost method [10, 12].

In order to use PMMA as dielectric gate in TFTs requires a lot of conditions to be promising materials.

Transistors parameter depend on the interface formed between dielectric and semiconductor layers, where the trapped charge has a strong influence on the device's electrical behavior [13].

The low leakage current density is highly desirable for the fabrication of stable TFTs for low-power consumption electronic devices [7, 14].

In different papers [3, 15, 16], the capacitance density of the polymeric dielectric layer was measured on the same MIM device in the frequency

THE ANNALS OF "DUNAREA DE JOS" UNIVERSITY OF GALATI
FASCICLE IX. METALLURGY AND MATERIALS SCIENCE
N°. 4 - 2022, ISSN 2668-4748; e-ISSN 2668-4756
Article DOI: https://doi.org/10.35219/mms.2022.4.14

range from 1 kHz to 1 MHz and the results are promising in order to use PMMA gate in TFTs.

In this paper, we have investigated a PMMA anisole solution to prepare thin films by spin coating method, one of the most used sol-gel method, for the simple and low- cost process. We fabricated a MIM device, represented by Al top-electrode/PMMA films/Si/Ta layer substrate, to study the dielectric properties of the obtained polymeric thin films and to calculate their dielectric constant.

2. Experimental

2.1. Preparation of sols and thin films

PMMA (495 kw) in anisole was purchased from MICRO CHEM and used for the preparation of hybrid films. Polymeric solution (25%) was prepared by magnetic stirrer at room temperature. First the solution was deposited on glass substrate to have one and two layers of PMMA with 100-150 nm thickness. The deposition was done by spin-coating method at 2000 rpm for 30 seconds.

After optimisation of the thickness the solution was spin coated for 30 seconds in air, onto the n-doped Si substrates covered with a layer of 100 nm tantalum (Figure 1a). The as-deposed films were thermally treated on hot plate at 120 °C for 30 minutes.

Before film deposition, the substrates were cleaned using the following procedure: washed in water for three times, dipped in isopropanol for 1 minute and cleaned with water, dried with nitrogen stream and hotplate for 5 minutes at 120 °C. To have a MIM structure, after PMMA deposition (Figure 1b), metallic aluminium contacts (Figure 1c) were thermally evaporated through a shadow mask with different areas (180, 320 and 680 μm diameters) resulting a multi-layer structure (Figure 2).

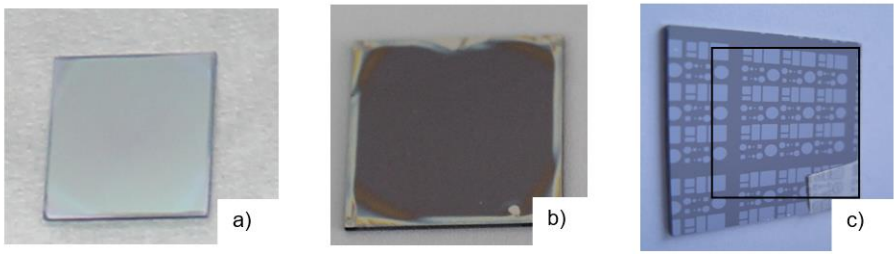

Fig. 1. *a) Si substrate with Ta (100 nm); b) PMMA layers on Si substrate; c) MIM structure*

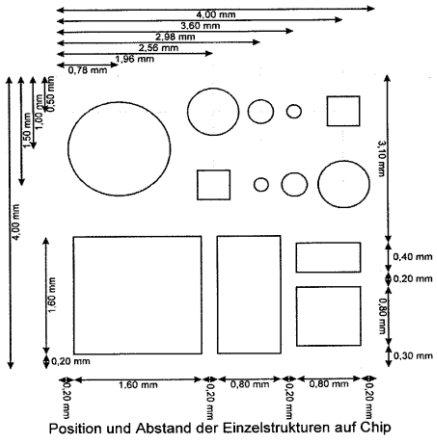

Fig. 2. *Schematic representation of electrodes areas*

2.2. Thin films characterization

The roughness was investigated with atomic force microscopy and for surface and cross-section morphology of the polymeric thin films was used a scanning electron microscopy (SEM) using a EOL JSM-7500F/FA microscope.

The I-V and C-V curves of the hybrid films were measured by including them into a Metal-Insulator-Metal (MIM) structure (Fig. 3), using Agilent 4156 and HP 4277A Analysers, respectively, at 1 MHz.

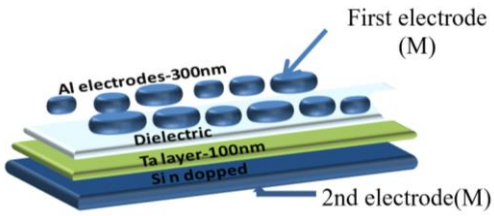

Fig. 3. *Schematic representation (a, b) of MIM structure used for the measurement of I-V and C-V characteristics of thin films*

3. Results and discussion

In Figure 4a and 4b are presented the AFM and SEM images of PMMA layer by comparison. The

THE ANNALS OF "DUNAREA DE JOS" UNIVERSITY OF GALATI
FASCICLE IX. METALLURGY AND MATERIALS SCIENCE
Nº. 4 - 2022, ISSN 2668-4748; e-ISSN 2668-4756
Article DOI: https://doi.org/10.35219/mms.2022.4.14

structure of film is homogenous the entire surface having a specific relief as a honeycomb do to the high molecular weight. The thermal treatment applied for stabilisation is modifying the structure.

From the AFM roughness we can observe that is between 15 to 25 nm (Figure 5).

Figure 6 shows the I–V and C-V characteristics of the investigated films, at gate voltages from 4 to +4 V. The leakage current density is 10^{-6} to 10^{-1} A/cm^2 Further studies are considered to correlate the dielectric behaviour of films with the effect of temperature, number of layers and duration of post-deposition thermal treatment.

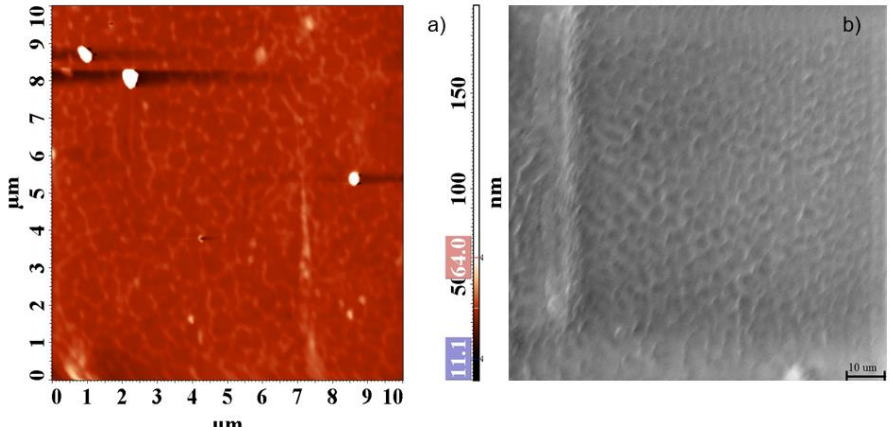

Fig. 4. *a) AFM and b) SEM images of PMMA layer*

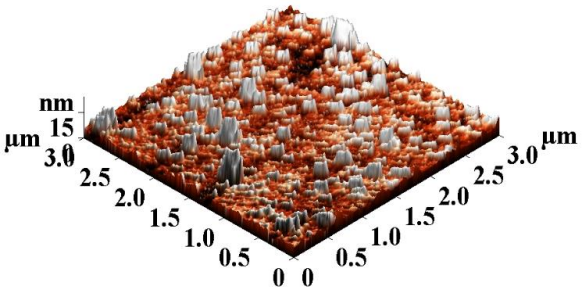

Fig. 5. *AFM image of a central PMMA layer*

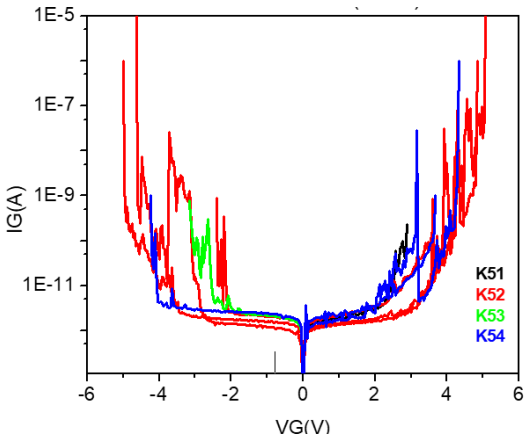

Fig. 6. *I-V characteristics for PMMA layer*

From C–V (Figure 7) curves of the investigated PMMA film, dielectric constant was calculated. The values were determined in the voltage range from -55 to + 55 V, at 1 MHz. The dielectric permittivity of a material is proportional to its electronic polarization.

THE ANNALS OF "DUNAREA DE JOS" UNIVERSITY OF GALATI
FASCICLE IX. METALLURGY AND MATERIALS SCIENCE
Nº. 4 - 2022, ISSN 2668-4748; e-ISSN 2668-4756
Article DOI: https://doi.org/10.35219/mms.2022.4.14

The measurements showed a dielectric behaviour enough homogenous without breakdown leakage. The values of dielectric constant measured on different electrodes area varied from 3 to 4 as in Table 1.

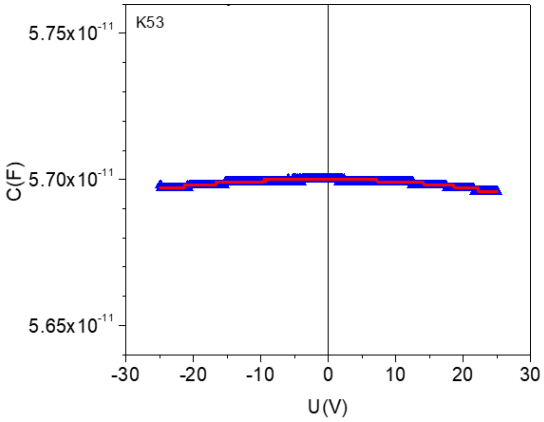

Fig. 7. *C-V characteristics for PMMA layer*

Table 1. *Electrical capacitance and dielectric values of PMMA layer for different electrodes area*

Electrode area *10^{-4} cm^2	Electrical capacitance C (F) *10^{-11}			ε_r
	Area 1	Area 2	Area 3	
2.054 (K1)	42.32	42.04	40.67	3
8.043 (K2)	1.536	1.464	1.504	3.2
32.17 (K3)	5.511	5.295	5.291	3.8
128.7 (K4)	0.2049	0.1972	0.1971	4

4. Conclusions

PMMA dielectric thin films for flexible electronics were successfully prepared by sol-gel methods below 200 ºC. The I-V curves show a leakage current between 10^{-11} and 10^{-8} A and a constant capacitance in bias range ± 4 V. Dielectric constant varying from 3 to 4 was obtained for different electrodes area films. Further investigation will be continued to establish the variation of dielectric constant on different point of thin film of the sample.

References

[1]. Nassier L. F., Shinen M. H., *Study of the optical properties of poly (methyl methacrylate) (PMMA) by using spin coating method*, Mater. Today Proc., vol. 60, p. 1660-1664, doi: 10.1016/j.matpr.2021.12.213, 2022.

[2]. Valcu E. E., Musat V., Jank M., Oertel S., *Sol-gel preparation of ZrO2-PMMA for thin films transistors*, Rev. Chim., vol. 65, no. 5, p. 574-577, 2014.

[3]. Mușat V., *et al.*, *Low-Temperature and UV Irradiation Effect on Transformation of Zirconia-MPS nBBs-Based Gels into Hybrid Transparent Dielectric Thin Films*, Gels, vol. 8, no. 2, doi: 10.3390/gels8020068, 2022.

[4]. Shekar B. C., Sathish S., Sengoden R., *Spin coated nano scale PMMA films for organic thin film transistors*, Phys. Procedia, vol. 49, no. 0, p. 145-157, doi: 10.1016/j.phpro.2013.10.021, 2013.

[5]. Tippo T., Thanachayanont C., Muthitamongkol P., Junin C., Hietschold M., Thanachayanont A., *The effects of solvents on the properties of ultra-thin poly (methyl methacrylate) films prepared by spin coating*, Thin Solid Films, vol. 546, p. 180-184, doi: 10.1016/j.tsf.2013.05.022, 2013.

[6]. Mohajerani E., Farajollahi F., Mahzoon R., Baghery S., *Morphological and thickness analysis for PMMA spin coated films*, J. Optoelectron. Adv. Mater., vol. 9, no. 12, p. 3901-3906, 2007.

[7]. Syamala Rao M. G., *et al.*, *ZrHfO2-PMMA hybrid dielectric layers for high-performance all solution-processed In_2O_3-based TFTs*, Mater. Res. Bull., vol. 150, no. December 2021, doi: 10.1016/j.materresbull.2022.111768, 2022.

[8]. Emanuela E., Herbei V., Musat V., Oertel S., Jank M., *High-k dielectric inorganic-organic hybrid thin films for field effect transistors (FETFT)*, p. 64-68, 2013.

[9]. Schröder S., Strunskus T., Ababii N., Lupan O., Magariu N., Faupel F., *New vapor deposited dielectric polymer thin films for electronic applications*, p. 94-96, doi: 10.52326/ic-ecco.2021/el.02, 2022.

[10]. Forte M. A., Silva R. M., Tavares C. J., Silva R. F. E., *Is poly(Methyl methacrylate) (PMMA) a suitable substrate for ALD?: A review*, Polymers, vol. 13, no. 8, doi: 10.3390/polym13081346, 2021.

[11]. Buchheit R., Kuttich B., González-García L., Kraus T., *Hybrid Dielectric Films of Inkjet-Printable Core–Shell Nanoparticles*, Advanced Materials, vol. 33, no. 41, doi: 10.1002/adma.202103087, 2021.

[12]. Sathish S., Shekar B. C., *Dip and spin coated nanoscale transparent PMMA thin films for field effect thin film transistors*

and optoelectronic devices, J. Optoelectron. Adv. Mater., vol. 15, no. 3-4, p. 139-144, 2013.

[13]. Morales-Acosta M. D., Quevedo-Lopez M. A., Alshareef H. N., Gnade B., Ramirez-Bon R., *Dielectric properties of PMMA-SiO_2 hybrid films*, Mater. Sci. Forum, vol. 644, no. March, p. 25-28, doi: 10.4028/www.scientific.net/MSF.644.25, 2010.

[14]. Herbei E. E., Busila M., Alexandru P., Epure S., Musat V., *Dielectric Behaviour of PVP 360 and PVA for Thin Flexible Transistors Application*, Mater. Plast., vol. 59, no. 1, p. 1-7, doi: 10.37358/MP.22.1.5554, 2022.

[15]. Pantano M. F., Pavlou C., Pastore Carbone M. G., Galiotis C., Pugno N. M., Speranza G., *Highly Deformable, Ultrathin Large-Area Poly(methyl methacrylate) Films*, ACS Omega, vol. 6, no. 12, p. 8308-8312, doi: 10.1021/acsomega.1c00016, 2021.

[16]. Aras G., Orhan E., Selçuk A. B., Ocak S. B., Ertuğrul M., *Dielectric Properties of Al/Poly (methyl methacrylate) (PMMA)/p-Si Structures at Temperatures Below 300 K*, Procedia - Soc. Behav. Sci., vol. 195, p. 1740-1745, doi: 10.1016/j.sbspro.2015.06.295, 2015.

THE ANNALS OF "DUNAREA DE JOS" UNIVERSITY OF GALATI
FASCICLE IX. METALLURGY AND MATERIALS SCIENCE
Nº. 4 - 2022, ISSN 2668-4748; e-ISSN 2668-4756
Article DOI: https://doi.org/10.35219/mms.2022.4.15

REAL-TIME ASSEMBLY OPERATION RECOGNITION

Florin-Bogdan MARIN, Gheorghe GURĂU, Mihaela MARIN
"Dunarea de Jos" University of Galati, Romania
e-mail: flmarin@ugal.ro

ABSTRACT

This research is concerned to propose a computer vision algorithm to track manual assembly task. Manual assembly in case of electronics parts are used largely in automotive industry. The phases tracking of assembly could also be used for learning purposes such in case showed in this research, checking the assembly of an electronic educational board. The algorithms used for detection of different components are CNN (Convolutional Neuronal Network) as well as blob detection.

KEYWORDS: computer vision, assembly operation, recognition

1. Introduction

Manual assembly in case of electronics parts are used largely in automotive industry. The tracking of phases of assembly could also be used for learning purposes such in case showed in this research, checking the assembly of an electronic educational board. There are authors that used cameras such as Kinect® to investigate the position in 3D space of assembly line in order to assess there are minimum errors. Though robotics has advantages in industry, however manual assembly work cannot be avoided.

Recently concept in manufacturing Industry 4.0 underline the benefits using sensors on large scale and process in a "BIG DATA" set in order to extract best optimization for the industrial process. The data processed is used to eventually improve to maximum the manufacturing processes.

Nowadays, computer processing capabilities, as long with the computer vision algorithm available, allows the introduction of surveillance camera to be used on extensive scale in order to assess phases of assembly. There are previous works [1-6] attempted to utilize visual sensors to predict the pose in robotics task in assembly. Several researchers considered reconstructing 3D parts [7-10] in order to control the assembly process. At first glance, object recognition is very known topic in manufacturing with few challenges not solved. However, in case of assembly the identification and recognition of correct position of wires and parts with limited visibility while the operator is continuing the assembly process is a challenge. Object recognition is used in industry for decades for automated machine and robot to recognize parts and manipulate to certain position. The assembly process of electronic components such as in case of automotive electric parts, we well as in case of surveillance for educational purposes showed important challenges. Many approaches of assembly surveillance are taking into account of identifying parts using features such as colour, specific shape and of course using artificial intelligence algorithm such as CNN (Convolutional neural networks) versus manual assembly task on a production line [11-13].

This research is concerned to propose a computer vision algorithm to track manual assembly task.

2. Experimental procedure

We considered that the camera is located 1.5 meters above the scene. The table height position allows a good estimation of proportion taking into account that electronic boards have low height. The illumination is variable, as in case of a school class, influenced by outdoor luminosity. The CNN network has trained with 50 images for each category: sensor, pin location (with the number written on the board) and electronic board.

We manually cropped every pin component along with the number written on the board. These specific classes cannot be found on public trained data base, except the electronic board.

Input images are resized to 224 × 224 × 3 for matching the convolutional layer. Convolutional neuronal network identification is used for electronic board, pin location and sensor. The algorithm is depicted in Fig.1.

In order to identify the wire, we used blob identification considering the specific colours of the wires and shape. Several challenges occur in this stage in case the wire positioning is overlapping. The

THE ANNALS OF "DUNAREA DE JOS" UNIVERSITY OF GALATI
FASCICLE IX. METALLURGY AND MATERIALS SCIENCE
Nº. 4 - 2022, ISSN 2668-4748; e-ISSN 2668-4756
Article DOI: https://doi.org/10.35219/mms.2022.4.15

task is composed of three steps, the wire connection of a sensor to the electronic board. Each step is assed at the end of each step (Fig. 2). The position of the hands is in a specific position as showed in Fig. 5. The recognition of this position triggers the computer vision assessment in order to determine the correct wiring. In this case there are specific ports where wiring should be done.

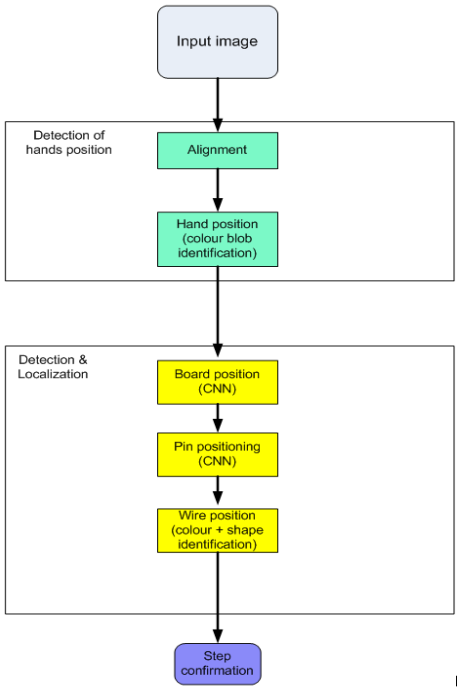

Fig. 1. *Algorithm for scene understanding of assembly operation*

When the hands are in a specific position the software processes the scene. We need to stress some limitation in the proposed algorithm. Firstly, the algorithm is not considering important illumination variation. Secondly, for the educational application real cases, the input data could vary in an important manner concerning illumination.

3. Results and discussions

As discussed above, the proposed approach can be used in many domains, such as industry or for educational surveillance purposes. We show a proof-of-concept application utilizing simple testing case (Fig. 4). This research used a single web camera to assess assembly operations on an electronic board by recognition of wires position connection to specific pins. Each step of the assembly is processed only after the hands are allowing the camera to see the entire scene. Also, the background might be with variation of patterns. In case of industry, illumination could be maintained constant as well as the background. We used one single electronic board for training while the real case scenario should include different models.

Currently, the proof-of-concept application developed is tested with a limited data for the described specific assembly task.

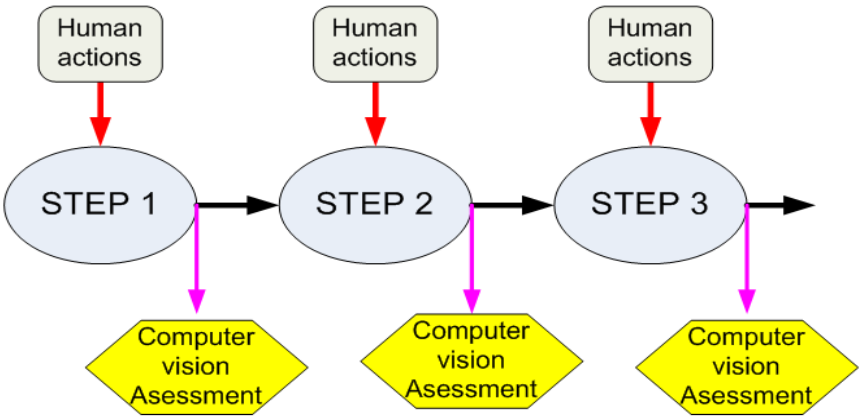

Fig. 2. *The assembly steps surveillance*

THE ANNALS OF "DUNAREA DE JOS" UNIVERSITY OF GALATI
FASCICLE IX. METALLURGY AND MATERIALS SCIENCE
Nº. 4 - 2022, ISSN 2668-4748; e-ISSN 2668-4756
Article DOI: https://doi.org/10.35219/mms.2022.4.15

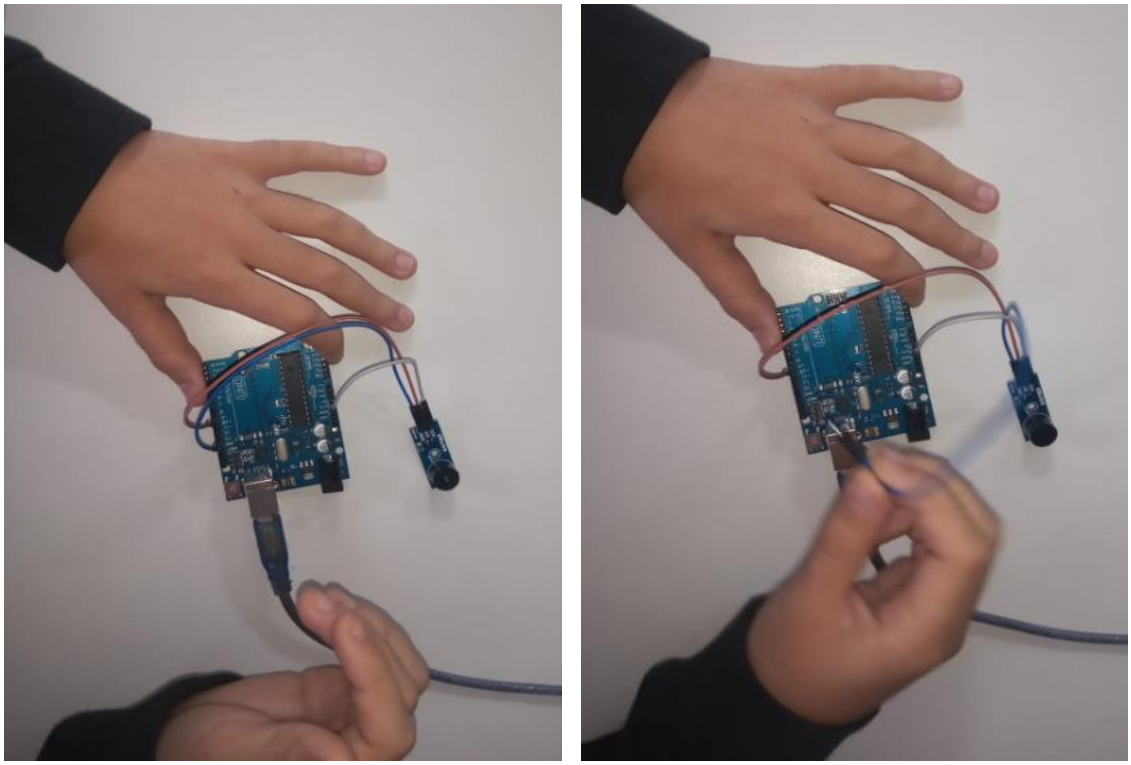

Fig. 3. *Operation of assembly*

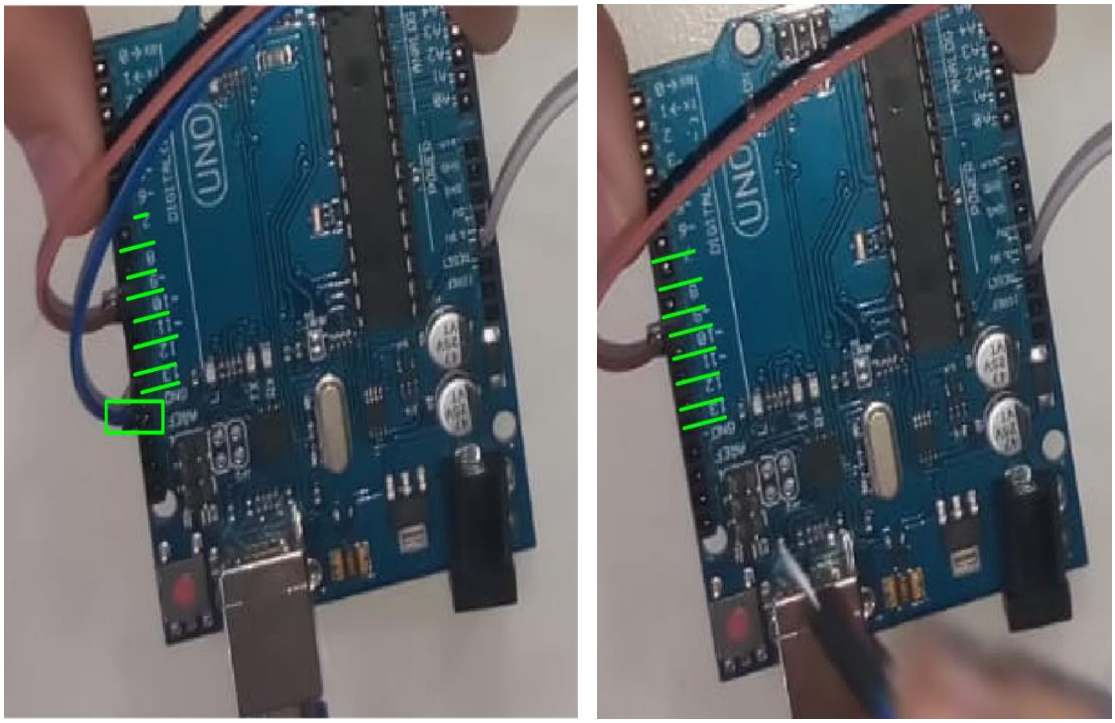

Fig. 4. *Visualization of the pins location and wire connection*

THE ANNALS OF "DUNAREA DE JOS" UNIVERSITY OF GALATI
FASCICLE IX. METALLURGY AND MATERIALS SCIENCE
Nº. 4 - 2022, ISSN 2668-4748; e-ISSN 2668-4756
Article DOI: https://doi.org/10.35219/mms.2022.4.15

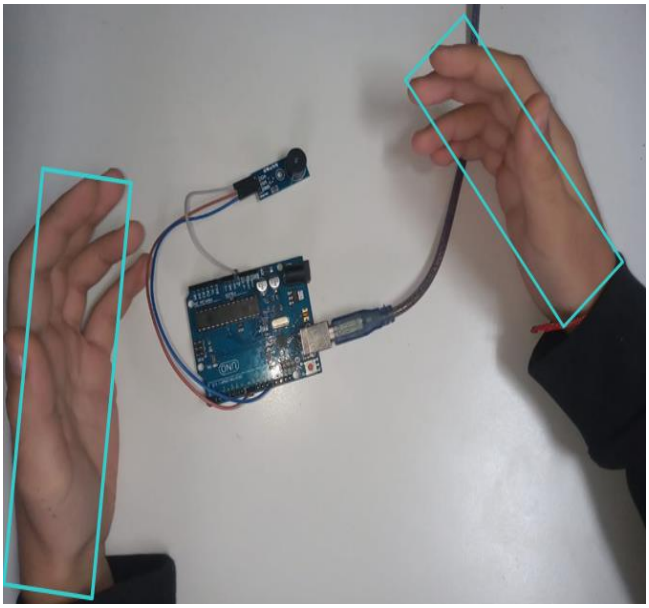

Fig. 5. *Identification of hand position*

4. Conclusions

The proposed algorithm is able to recognize position, no matter the rotation or position of the boards in the scene. It has been shown that it is possible to identify position of wires connected to specific pins on the boards. This was achieved by using shape identification using CNN to be carried our using different colour parts, such as in case of educational applications. Though only 2D image processing was used, the algorithm shows to be robust. Colour recognition of board was used as this is not subject to changes, such in case of industrial applications. Several advancements should be made for future development:

1) The algorithm capabilities should be tested by using a stereo vision;

2) Detection precision can be increased incorporating 3D part estimation rate.

References

[1]. Alzubaidi L., Zhang J., Humaidi A. J., *et al.*, *Review of deep learning: concepts, CNN architectures, challenges, applications, future directions*, J Big Data, 8, 53, 2021.

[2]. Zhang Z., Peng G., Wang W., Chen Y., Jia Y., Liu S., *Prediction-Based Human-Robot Collaboration in Assembly Tasks Using a Learning from Demonstration Model*, Sensors, 22, (11), 4279, 2022.

[3]. Wenjin T., Md Al-Amin Haodong C., Ming C. L., Zhaozheng Y., Ruwen Q., *Real-Time Assembly Operation Recognition with Fog Computing and Transfer Learning for Human-Centered Intelligent Manufacturing*, Procedia Manufacturing, vol. 48, p. 926-931, ISSN 2351-9789, 2020.

[4]. Nottensteiner K., Sachtler A., Albu-Schäffer A., *Towards Autonomous Robotic Assembly: Using Combined Visual and Tactile Sensing for Adaptive Task Execution*, J Intell Robot Syst 101, 49, 2021.

[5]. Levine S., Pastor P., Krizhevsky A., Ibarz J., Quillen D., *Learning hand-eye coordination for robotic grasping with deep learning and large-scale data collection*, Int J Robotics Res., vol. 37, p. 421-436, 2018.

[6]. Tobin J., Fong R., Ray A., Schneider J., Zaremba W., Abbeel P., *Domain randomization for transferring deep neural networks from simulation to the real world*, Intelligent Robots and Systems (IROS), 2017.

[7]. Hennersperger C., Fuerst B., Virga S., Zettinig O., Frisch B., Neff T., Navab N., *Towards MRI-based autonomous robotic US acquisitions: a first feasibility study*, IEEE Transactions on Medical Imaging, 36, (2), p. 538-548. 2017.

[8]. Ganin Y., Ustinova E., Ajakan H., Germain P., Larochelle H., Laviolette F., Marchand M., Lempitsky V., *Domain-adversarial training of neural networks*, JMLR, 2016.

[9]. Ren S., He K., Girshick R., Sun J., *Faster R-CNN: Towards realtime object detection with region proposal networks*, Advances in Neural Information Processing Systems, 2015.

[10]. Ping L., Ji L., Zeng Y., Chen B., Zhang X., *Real-time monitoring for manual operations with machine vision in smart manufacturing*, Journal of Manufacturing Systems, vol.65, p. 709-719, ISSN 0278-6125, 2022.

[11]. Howard A., Andrew G., Menglong Z., Bo C., Kalenichenko D., Weijun W., Weyand T., Andreetto M., Hartwig A., *MobileNets: Efficient Convolutional Neural Networks for Mobile Vision Applications*, arXiv abs/1704.04861, 2017.

[12]. Teng X., Yu Q., Luo J., Wang G., Zhang X., *Aircraft Pose Estimation Based on Geometry Structure Features and Line Correspondences*, Sensors, 19, 2165, 2019.

[13]. Yang H., Jiang P., Wang F., *Multi-View-Based Pose Estimation and Its Applications on Intelligent Manufacturing*, Sensors (Basel), 20, (18), 5072, 2020.

THE ANNALS OF "DUNAREA DE JOS" UNIVERSITY OF GALATI
FASCICLE IX. METALLURGY AND MATERIALS SCIENCE
Nº. 4 - 2022, ISSN 2668-4748; e-ISSN 2668-4756
Article DOI: https://doi.org/10.35219/mms.2022.4.16

CFD MODELING AND SIMULATION OF A TINY HOUSE IN EXTREME WEATHER CONDITIONS

Florin-Bogdan MARIN, Mihaela MARIN
"Dunarea de Jos" University of Galati, Romania
e-mail: flmarin@ugal.ro, mihaela.marin@ugal.ro

ABSTRACT

The subject of this research is the use of CFD techniques to identify the impact of using shutters in case of tiny house. Low temperatures and the aim to use as less energy amount as possible need solution. The composites shells allow designing efficient shutters that is isolating in an important manner windows. The CFD software allows to identify the air currents and the areas where heat is lost due to the extreme weather conditions.

KEYWORDS: CFD, modeling, simulation, house

1. Introduction

Nowadays energy crisis is concerning not only about the price of energy but also about its availability. It is publicly available information that different countries announced the possibility of blackout scenario. A lot of total energy consumption is concerning the heating of residential buildings. House design was previously taken into account relative low price of energy available on the market. However, nowadays reality show that this calculus should be updated [1-4].

The windows are causing a high amount of heat losses for most houses due to their relatively large area and thin dimension. These elements are thereby an important factor in insulation for tiny houses, for their specific characteristics such as the fact a small volume in a single room building [5-6]. All the walls are exposed to the elements. Their direct contact with the outdoor conditions makes one of the most important parts of the house, as the source of heat loss.

While the comfort means a wider surface of window to allow the owner a great view to nature, the thermal restrictions indicate to minimize the windows surface. Also, the natural light need translates to a wider surface condition to design.

Computational fluid dynamics (CFD) deals with the mechanics of fluids by using numerical models that is simulating the real case scenarios to estimate fluid flow and thermal transfer [7-9].

The principle of finite element simulation is that a structure, both fluid and part, is divided in multiple sub-parts called "finite element" and the model allows studying the interaction between these elements. The operation of separating or partitioning the part or the fluid domain is called "discretization" and is an important phase of simulation as the complicated parts, such in case of complex surface objects often cannot be completed by automated algorithm but manual operation should act [10-12].

When a building is heated, and this can be seen in case of extreme weather condition, the heat can be stored in its thermal mass, which is advantageous for buildings made of bricks or other materials that store heat. However, in case of tiny house made of composite panel is not an advantage over the classical buildings.

The best way to optimize window surface is to use store in order to be used during night, when the low temperature occurs or in case of low temperature during the entire day. This improves heat transfer between space outside taking into account glass thickened and thermal characteristics. In addition, insulation could be applied to the outer surface of the wall to keep the heat stored in the building.

2. Experimental procedure

In this research we aim to show the importance of the outer window shutters. The simulation of a tiny house heating is performed to calculate the thermal efficiency in extreme winter scenario to establish if shutters are efficient. The parameters are average mesh size 100 mm for fluid and 10 mm for parts. We considered the real dimensions of a tiny house 2000 x 10000 mm. The tiny houses are made of SIP sandwich composite made of 50 mm. We considered

THE ANNALS OF "DUNAREA DE JOS" UNIVERSITY OF GALATI
FASCICLE IX. METALLURGY AND MATERIALS SCIENCE
N°. 4 - 2022, ISSN 2668-4748; e-ISSN 2668-4756
Article DOI: https://doi.org/10.35219/mms.2022.4.16

heating system and outside temperature of 20 Celsius degrees.

3. Results and discussions

Following the numerical experiments performed, the trajectories of the air currents are that described in Fig.1 We observed that there is a movement of the air currents from the heat source to the ceiling, where the air mass is colder. There is also a disordered and non-optimized motion in 3D space. Fig. 2 shows that there is a fairly good movement of the air mass in the vertical section in the sense that there is an upward rotational movement between the connecting sources.

The simulation was performed transiently and the situation represented in Figures 1, 2 and 3 is 20 minutes after the heating system has been switched on. We can note there are an important amount of thermal energy that is lost in the window area and also this is affecting the current in the tiny house in the sense that the currents are transferring the heat to the window. We also compared with the case of using shutters composed of 130 mm of 20 cm wood 80 foam and 20 cm wood the effect of insulation means 30% less heat loss. We considered that the shutters are in contact with the wall and is perfect contact allowing 50 mm of air insulation.

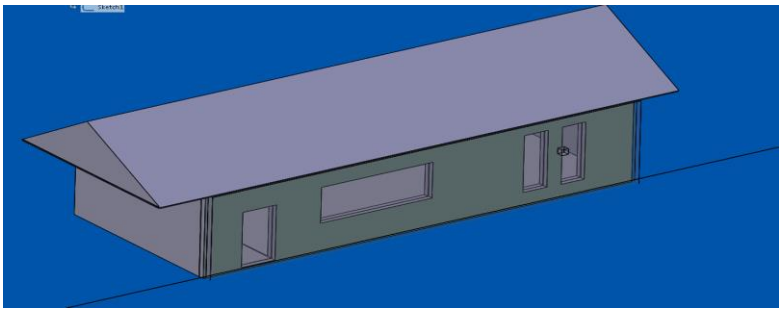

Fig. 1. *3D model of the tiny house design*

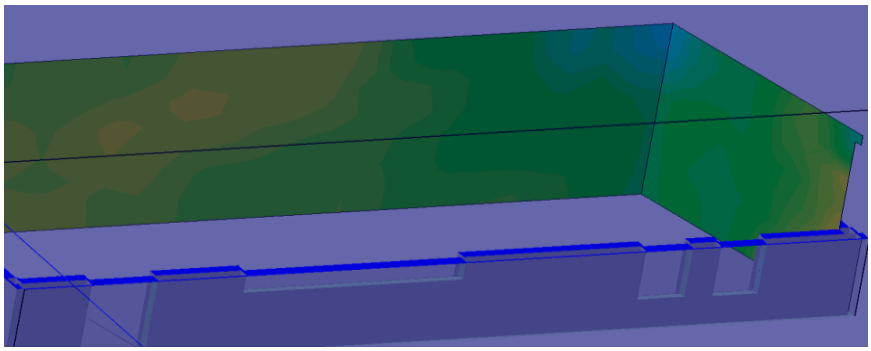

Fig. 2. *Wall temperature of the tiny house*

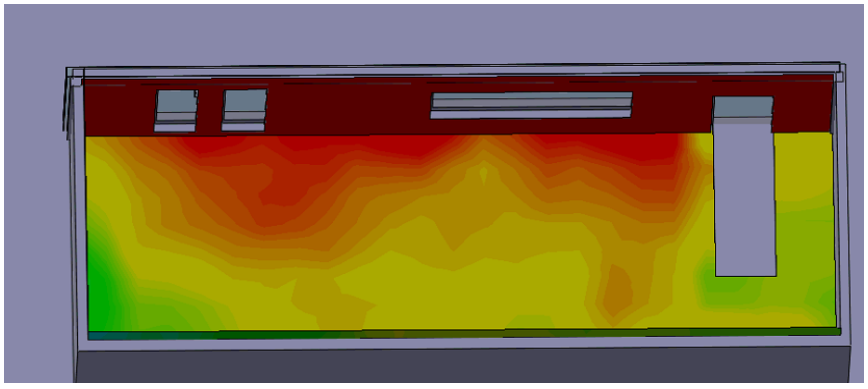

Fig. 3. *Air temperature variation at a height of 50 cm to the ground in the tiny house*

THE ANNALS OF "DUNAREA DE JOS" UNIVERSITY OF GALATI
FASCICLE IX. METALLURGY AND MATERIALS SCIENCE
Nº. 4 - 2022, ISSN 2668-4748; e-ISSN 2668-4756
Article DOI: https://doi.org/10.35219/mms.2022.4.16

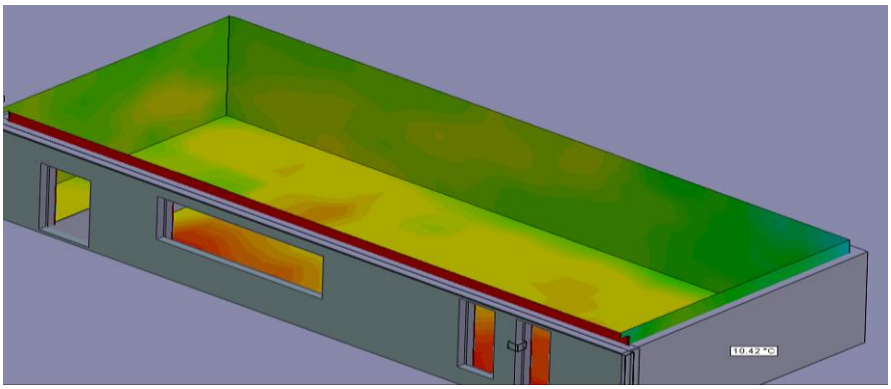

Fig. 4. *Air fluid temperature in a horizontal plane of the tiny house*

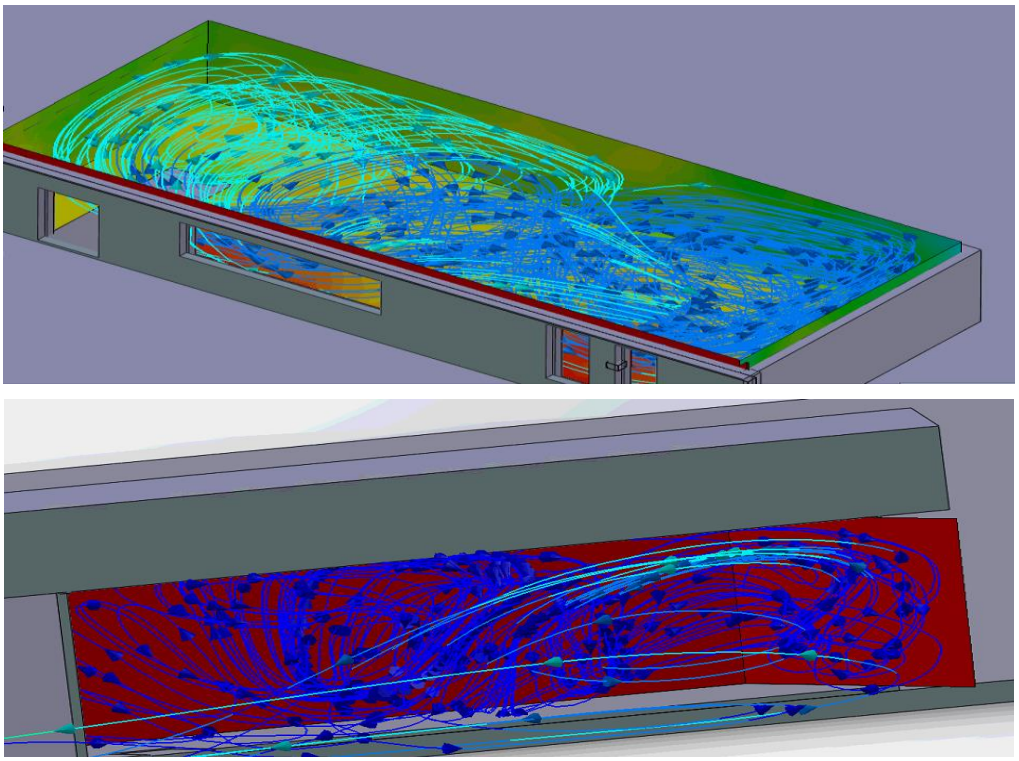

Fig. 5. *Fluid trajectories in the tiny house and the temperature associated with each trajectory line*

4. Conclusions

- CFD techniques allow the simulation of heating/cooling/ventilation of houses;
- The shutter allows improving 30% heating efficiency;
- The simulation for the solar input depending on the geographical positioning and the season should be further taken into account for the location of a tiny house;
- Tiny houses have some particularities that mean special restrictions in relation to their design.

References

[1]. Balali A., Hakimelahi A., Valipour A., *Identification and prioritization of passive energy consumption optimization measures in the building industry: An Iranian case study*, Journal of Building Engineering, 30, p. 101239, 2020.
[2]. Ma L., Shao N., Zhang J., Zhao T., *The Influence of Doors and Windows on the Indoor Temperature in Rural House*, Procedia Engineering, 121, p. 621-627, 2015.
[3]. Zschaeck G., Frank T., Burns A., *CFD modelling and validation of wall condensation in the presence of non-condensable gases*, Nuclear Engineering and Design, vol. 279, p. 137-146, 2014.
[4]. Abdoly N. S., Haghparast F., Singery M., Sattari Sarbangholi H., *Providing an Optimal Execution Model for Windows Based on Glazing to Reduce Fossil Fuel Consumption (Case Study: Asman Residential Complex of Tabriz)*, Iranian

Journal (Iranica) of Energy and Environment, 11(4), p. 260-270, 2020.
[5]. Lechowska A. A., Schnotale J. A., Baldinelli G., *Window frame thermal transmittance improvements without frame geometry variations: An experimentally validated CFD analysis*, Energy and Buildings, 145, p. 188-199, 2017.
[6]. Huang J., Zhang J., Wang L., *Review of vapor condensation heat and mass transfer in the presence of non-condensable gas*, Applied Thermal Engineering, no. 89, p. 469-484, 2015.
[7]. Shankar V., Hagentoft C.-E., *Influence of natural convection on the thermal properties of insulating porous medium with air cavity*, Proceedings, Indoor Air '99, The international society of indoor air quality and climate, Edinburgh, Scotland, 1999.
[8]. Shankar V., Davidson L., Olsson E., *Numerical Investigation of Turbulent Plumes in both Ambient and Stratified Surroundings*, Journal of indoor air, Denmark, 2019.
[9]. Hellsvik R., *Transient Simulation of Ventilation Rate and Moister load for Cold Attic Constructions*, Master Thesis, Chalmers University of Technology, Gothenburg, 2015.
[10]. Horikiri K., Yao Y., Yao J., *Numerical simulation of convective airflow in an empty room*, International Journal of Energy and Environment, vol. 5, p. 574-581, 2011.
[11]. Kuhn S. Z., *An investigation of condensation from steam–gas mixtures flowing downward in a vertical tube*, Nuclear Engineering and Design, p. 53-69, 1997.
[12]. Kwon-Yeong L., Moo Hwan K., *Experimental and empirical study of steam condensation heat transfer with a noncondensable gas in a small-diameter vertical tube*, Nuclear Engineering and Design, vol. 238, p. 207-216, 2008.

THE ANNALS OF "DUNAREA DE JOS" UNIVERSITY OF GALATI
FASCICLE IX. METALLURGY AND MATERIALS SCIENCE
Nº. 4 - 2022, ISSN 2668-4748; e-ISSN 2668-4756
Article DOI: https://doi.org/10.35219/mms.2022.4.17

THE INVESTIGATION ON DIMENSIONAL STABILITY IN SOME SINTERED POWDER METALLURGY ALLOYS

Mihaela MARIN, Florin-Bogdan MARIN
"Dunarea de Jos" University of Galati, Romania
e-mail: mihaela.marin@ugal.ro

ABSTRACT

The subject of this research was to study the effect of sintering time on the dimensional characteristics of some powder metallurgy (PM) materials. The powders used in this study are prealloyed iron-based powders with Cu, Ni and Mo. The powders were single pressed at 600 MPa and the disc specimens have the dimensions of 8-6 mm. The green compacts were sintering in a laboratory furnace at 1150 ºC for 60, 75 and 90 minutes and air-cooled to room temperature. The density of green and sintered specimens, the porosity and the dimensional changes were evaluated.

KEYWORDS: powder, sintering, dimensional stability

1. Introduction

Powder metallurgy (PM) has been regarded as a green manufacturing technology for producing high quality technical components. The conventional PM method (Fig. 1) entails creating a formulated mixture of metal powders, pressing the mixture into appropriate shapes, and then heating (sintering) the compacted powder at a temperature to achieve the desired density and strength [1-3]. The dimensional changes are critical in the production of PM components. An important goal is to manage the dimensional change that occurs during the sintering treatment in order to achieve the required part dimensions. The dimensional changes are influenced by both the powder properties and the process parameters. Several factors influence the dimensional changes of PM products, including particle size, alloying element addition, compaction density, sintering time and temperature [4-6]. The temperature and time sintering process have an impact on the shrinkage of the specimens.

The alloying elements have a significant influence in the chemical composition of the powders, which helps to improve the mechanical properties of sintered parts [7-9]. In theory, sintered steels and conventional steels are both affected in the same way by the alloying elements. In general, all the alloying components increase hardenability. For example, due to its relatively minor impact on compressibility, molybdenum (Mo) is one of the primary pre-alloyed elements utilized in powder metallurgy [10, 11]. Nickel (Ni), as an alloying element, raises the sintered density due to the fact that during sintering, nickel is in solid state and forms the as-called Ni-rich areas in the sintered microstructure, which provide a local ductility [12]. Copper (Cu), increases the strength and hardness when the typical amounts of copper used as an alloying element are 1.5-3 wt.%; any more can cause iron to expand [13, 14]. An investigation regarding the dimensional changes in some iron-based P/M alloys were investigated in this paper.

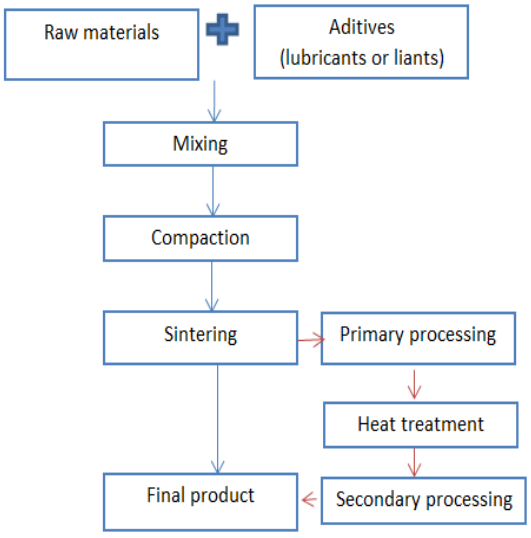

Fig. 1. *Process flow diagram of powder metallurgy*

THE ANNALS OF "DUNAREA DE JOS" UNIVERSITY OF GALATI
FASCICLE IX. METALLURGY AND MATERIALS SCIENCE
No. 4 - 2022, ISSN 2668-4748; e-ISSN 2668-4756
Article DOI: https://doi.org/10.35219/mms.2022.4.17

2. Experimental procedure

The analysed specimens in this paper were prepared from pre-alloyed iron base powders. In Table 1 is showed the chemical composition of the analysed powders and Fig. 2 provided the particle size distribution of analysed powders. The analysed powders were mixed with zinc stearate 1% as a lubricant. In the next step, the homogenous powders were cold compacted at 600 MPa in cylindrical specimens with ϕ8 x 6 mm dimensions using a uniaxial steel matrix.

Table 1. *Chemical composition of analysed powders*

Powder type	Cu	Mo	Ni	C
P_1	1.50	0.50	1.75	<0.01
P_2	1.50	0.50	4.00	<0.01

After the compaction step, the green samples were sintered in a laboratory furnace at 1150 °C for 60, 75 and 90 minutes (Fig. 3). The density of green, sintered specimens, the porosity and the dimensional changes were evaluated. The sintered compacts' volumetric dimensional change was calculated, which were accurate to within ±0.01 g and ± 0.001 mm, respectively. All the test results were the average of three experiments.

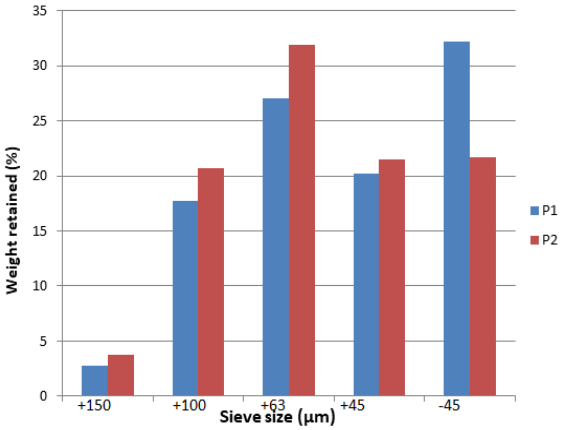

Fig. 2. *Particle size distribution of analyzed powders*

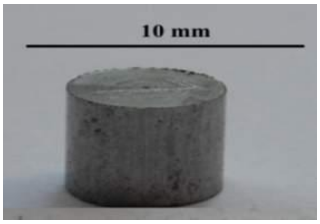

Fig. 3. *The aspect of sintered sample*

3. Results and discussions

The density and dimensional changes of compacted, green, and sintered specimens were calculated. Table 2 displays the green and sintered density and represents the average values for each set of three samples.

A micrometre with a digital display was used to measure the dimensions of the pressed and sintered samples. The total porosity is defined as the percentage ratio of void spaces to total bulk volume of the material. The conventional method from density technique was used to calculate porosity.

The total porosity of the compact, in volume percent, is calculated using the following equation:

$$P_t = 100\,(1 - \rho_s/\rho_t)\ [\%] \qquad (1)$$

where ρ_s, ρ_t and ρ_t are the sintered density and theoretical density. In Table 3 are detailed the porosity values of the sintered specimens. The processing parameters such as: powder particle size distribution, alloying elements, green density, sintering temperature and time have influence in the porosity of P/M parts [15, 16].

The dimensional change (ΔLDGs) in % for sintered specimens were calculated using the following relation:

$$\Delta LDGs = [(L_S - L_P) / L_P] \times 100\ \% \qquad (2)$$

where: LS is the length of sintered sample and LP is the length of pressed sample, in mm.

The dimensional change analysis (Table 4) shows that the sample P_2 has a smaller dimensional change from die size than P_1. The powder type is the major contributor to the final dimensional change values in this case.

It is critical in powder metallurgy that the dimensional changes of structural parts during sintering be as small as possible. Copper alone can cause dimensional growth when is added to iron, whereas nickel alone can cause contraction [17]. Green density and compaction also have a strong influence. The green densities of two powders mixture compositions are found to be highly related to the applied pressure during compaction, the green density rapidly increasing as the compaction pressure increases.

THE ANNALS OF "DUNAREA DE JOS" UNIVERSITY OF GALATI
FASCICLE IX. METALLURGY AND MATERIALS SCIENCE
No. 4 - 2022, ISSN 2668-4748; e-ISSN 2668-4756
Article DOI: https://doi.org/10.35219/mms.2022.4.17

Table 2. *Green and sintered density of analysed alloys*

Powder type	**Green density, (g/cm^3), ρg**	**Sintered density, (g/cm^3), ρs**		
	pressed at 600 MPa	**sintered at 1150 °C and 60 minutes**	**sintered at 1150 °C and 75 minutes**	**sintered at 1150 ° C and 90 minutes**
P_1	6.72	6.91	7.03	7.08
P_2	6.80	6.98	7.07	7.11

Table 3. *The total porosity of analysed alloys*

State	**Powder type**	**Porosity, (%)**
Sintered state (at 1150 °C and 60 minutes)	P_1	12.31
	P_2	12.11
Sintered state (at 1150 °C and 75 minutes)	P_1	11.76
	P_2	11.43
Sintered state (at 1150 °C and 90 minutes)	P_1	10.95
	P_2	10.31

Table 4. *The dimensional change analysis*

State	**Powder type**	**Dimensional change in sintered state (%)**
sintered (at 1150 °C and 60 minutes)	P_1	-0.06
	P_2	-0.05
sintered (at 1150 °C and 75 minutes)	P_1	-0.06
	P_2	-0.04
sintered (at 1150 °C and 90 minutes)	P_1	-0.04
	P_2	-0.02

4. Conclusions

- When manufacturing PM parts, dimensional accuracy is crucial, especially for parts with near-net shapes;

- Densities in sintered state are ranging from 6.91 to 7.08 g/cm^3 for sample P_1 and 6.98 to 7.11 g/cm^3 for sample P_2. A good compression behavior is observed for samples P_2;

- Sintering does not completely eliminate porosity; rather, it changes it. In comparison to sample P_1, sample P_2 had lower porosity for all sintering times of 60, 75 and 90 minutes;

- The porosity is decreasing with increasing sintering time. The samples with the lower porosity are in the sintered state with a high sintering time of 90 minute and 4% Ni, of 10.31% for P_2 and 10.95% for P_1;

- The shrinkage of the specimen is affected by parameters such as sintering time, but the sintering temperature has a greater influence.

References

[1]. Jang G. B., Hur M. D., Kang S. S., *A study on the development of a substitution process by powder metallurgy in automobile parts*, Journal of Materials Processing Technology, p. 110-115, 2000.

[2]. Narasimhan K. S., *Sintering of powder mixtures and the growth of ferrous powder metallurgy*, Materials Chemistry and Physics, vol. 67, p. 56-65, 2001.

[3]. Chagnon F., Gelinas C., Trudel Y., *Development of high density materials for P/M applications*, Advances in P/M & Particulate Materials, 3, p. 199-206, 2004.

[4]. Rathore S. S., Dabhade V. V., *Dimensional Change During Sintering of Fe–Cu–C Alloys: A Comparative Study*, Trans Indian Inst Met, 69: 991, doi:10.1007/s12666-015-0596-7, 2016.

[5]. Lindsley B., Murphy T., *Dimensional Control in Cu-Ni Containing Ferrous PM Alloys*, Proceedings of the 2006 International Conference on Powder Metallurgy and Particulate Materials. Compiled by W.R. Gasbarre, J.W von Arx, Metal Powder Industry Federation. Princeton, NJ, 10, p.140-153, 2006.

[6]. Cristofolini I., Pilla M., Rao A., *et al.*, *Dimensional and geometrical precision of powder metallurgy parts sintered and sinterhardened at high temperature*, Int. J. Precis. Eng. Manuf., 14, p. 1735-1742, 2013.

[7]. Wu M. W., Tsao L. C., Shu G. J., Lin B. H., *The effects of alloying elements and microstructure on the impact toughness of*

powder metal steels, Materials Science and Engineering, vol. A 538, p. 135-144, 2010.

[8]. Barbosa A., Bobrovnitchii G., Diegues Skury A. L., Guimaraes R. S., Filgueira M., *Structure, microstructure and mechanical properties of PM Fe–Cu–Co alloys*, Materials & Design, vol. 31, p. 522-526, 2010.

[9]. Sulowski M., *Sintered Structural steels containing Mn, Cr and Mo, The summary of the investigations*, Powder Metallurgy Progress, vol. 16, no. 2, p. 59-85, 2016.

[10]. Ramazan Y., Azim G., Hakan K., *Effect of FerroMolybdenum Addition on the Microstructure and Mechanical Properties of Sintered Steel*, Advanced Materials Research, 23, p. 71-74, 1, 2007.

[11]. Sanjay S. R., Milind M. S., Vikram V. D., *Effect of molybdenum addition on the mechanical properties of sinter-forged Fe Cu C alloys*, Journal of Alloys and Compounds 649, p. 988-995, 2015.

[12]. Chawla N., Babic D., Williams J. J., Polasik S. J., *Effect of copper and nickel alloying additions on the tensile and fatigue behavior of sintered steels*, Advances in powder metallurgy & particulate materials, part 5, 104, Princeton, NJ: MPIF, 2002.

[13]. Angel W. D., Tellez L., Alcala J. F., Martinez E., Cedeno V. F., *Effect of copper on the mechanical properties of alloys formed by powder metallurgy*, Materials and Design, vol. 58, p. 12-18, 2014.

[14]. Marucci M. L., Hanejko F. G., *Effect of copper alloy addition method on the dimensional response of sintered Fe-Cu-C steels*, Advances in Powder Metallurgy and Particulate Materials, MPIF, p. 1-11, 2010.

[15]. Ramabulana K., *et al.*, *Effect of particle size distribution on green properties and sintering of Ti-6Al-4V*, IOP Conf. Ser., Mater. Sci. Eng., 655, 012020, 2019.

[16]. Bolzoni L., Ruiz-Navas E. M., Gordo E., *Influence of Sintering Parameters on the Properties of Powder Metallurgy Ti-3Al-2.5V Alloy*, Materials Characterization, vol. 84, p. 48-57, 2013.

[17]. Singh T., Stephenson T. F., Cambell S. T., *Nickel-copper interactions in P/M steels*, Advances in Powder Metallurgy and Particulate Materials, compiled by James W. B. and Chernenkoff R. A., Metal Powder Industries Federation, Princeton, NJ, 7, p. 7-93, 2004.

THE ANNALS OF "DUNAREA DE JOS" UNIVERSITY OF GALATI
FASCICLE IX. METALLURGY AND MATERIALS SCIENCE
N°. 4 - 2022, ISSN 2668-4748; e-ISSN 2668-4756
Article DOI: https://doi.org/10.35219/mms.2022.4.18

STUDIES ON THE POSSIBILITIES OF IMPROVING PLASTIC MANAGEMENT SERVICES

Nicoleta BOGATU[a,b], Marius MOCANU[b,*], Viorica GHISMAN[a,b], Daniela-Laura BURUIANA[a,b,*]

[a]Interdisciplinary Research Centre in the Field of Eco-Nano Technology and Advance Materials CC-ITI, Faculty of Engineering, "Dunarea de Jos" University of Galati, 47 Domneasca, 800008 Galati, Romania
[b]Department of Materials and Environmental Engineering, Faculty of Engineering, "Dunarea de Jos" University of Galati, 47 Domneasca, 800008 Galati, Romania
e-mail: daniela.buruiana@ugal.ro, marius.mocanu100@yahoo.ro

ABSTRACT

Waste management is seen as a filter between the anthroposphere and the environment. Therefore, these substances must be eliminated from the products' life cycle and managed in a way that does not harm the environment or human health.

At the same time, into consideration it must be taken that a significant part of plastic products belongs to the group of long-life goods and accumulates in the anthroposphere for years. Even if some dangerous additives are forbidden or replaced with more ecological alternatives, years or decades after the manufactured goods have been produced for various application sectors, plastics that contain these kinds of substances appear in the waste streams of the above-mentioned long-life goods.

Therefore, the knowledge regarding the plastic waste quantity, the level of information of the population, as well as the citizens' attitude towards selective waste management are important aspects for the efficient design of the future action plan for plastic waste management.

This study tries to analyse the attitudes that the citizens of the "Plantelor" neighbourhood of Braila Municipality have regarding the environment and their ecological behaviour.

At the same time, we propose to obtain a perspective upon the citizen's knowledge from that area regarding the actual environmental problems and the way in which they adopt sustainable behaviours in a circular economy in order to issue a warning. This is necessary in order to create some educational programs in partnership with public institutions and to be informed about the 3R philosophy.

KEYWORDS: plastic recycling, circular economy, waste management, pollution risks, action plan

1. Introduction

In the last 30 years, plastic materials became one of the most frequently used materials for the manufacturing of a wide range of products that are used in different industrial sectors. They are usually used in the packaging industry, for manufacturing automobile parts or electronics, but also for furniture and sports equipment [1-4].

Their characteristics, like durability, strength, lightness and low price, contributed to the replacement of many products made out of traditional materials, like wood, but it also allowed creating various innovative products [1-4].

As a consequence of continuous consumption that is also rising due to the pandemic context, the increasing amounts of generated waste have drawn the attention of several environmental institutions or associations at national and international level [5-8]. Taking into consideration that the consumption per citizen is constantly increasing, the necessity of developing some population awareness campaigns regarding the environmental benefits brought by the selective collection of waste is imperative [5-8].

THE ANNALS OF "DUNAREA DE JOS" UNIVERSITY OF GALATI
FASCICLE IX. METALLURGY AND MATERIALS SCIENCE
Nº. 4 - 2022, ISSN 2668-4748; e-ISSN 2668-4756
Article DOI: https://doi.org/10.35219/mms.2022.4.18

Plastic waste, produced mainly out of products of petroleum processing, that is from non-renewable resources, is perceived as valuable from the point of view of material recovery [5-9].

Generally, recycling is the most used solution for solving plastic waste problems [5-9]. However, when recycling is not the most feasible solution due to its high thermal power, plastic waste is seen as a potential alternative energy source of interest [5-9].

Moreover, because plastic decomposes very slowly, it takes a lot of space in landfills to dispose of it. All of these aspects contribute to debates regarding the most efficient treatment of this waste fraction from an environmental and economic point of view [1-8].

Another important problem related to plastic products is the fact that various auxiliary substances and additives are used during polymer production and product manufacturing. [5, 6].

Among them, there are stabilizers, antioxidants, flame retardants, etc. Some of them contain or contained dangerous substances, for example, toxic heavy metals or toxic organic compounds that may cause endocrine disruption among consumers [5, 6].

After adhering to the European Union (EU), Romania had to adapt its legal regulations to EU standards, including those of environmental policy. The need to implement these standards, among others, the Directive of Packaging and Waste Packaging [10], to the Romanian law, has increased the awareness of decision-makers in Romania regarding the issue of planning and adequate development of waste management systems [9].

The recovery of material and energy from waste is seen as feasible solutions to the problem of the increasing amounts of waste, also perceived as a step towards sustainable development in modern societies [9].

However, the problems of using some dangerous substances in production and manufacturing processes, the limits regarding collecting and the quality of waste contribute to the complexity of designing an adequate managing process of plastic material waste [9].

Romania is still at the beginning of developing its own management system. Therefore, the analysis of the current situation in eliminating waste, estimating the waste quantity generated and investigating environmental problems and resource conservation issues related to plastic waste management is important in this regard [3].

Industrialization and the rise of the living standard have brought impressive amounts of waste that, unfortunately, affect the environment through climate change, have a negative impact on the fauna and flora, and last but not least, upon our health [3].

By decomposition, waste from landfills releases methane, a gas that is over 80 times stronger than carbon dioxide and when they are illegally burnt, they release high levels of carbon dioxide into the atmosphere. Both are greenhouse gases that warm the planet and change the climate [3].

It was observed that open landfills release 91% of all methane emissions from landfills and about 40% of the world's waste is burned in this way. Moreover, these gases are unseen long-term dangers for the population that cause diseases, like asthma, cancer, cardiovascular diseases, genetic disorders in new-borns, low birth weight, infectious diseases, etc [3, 5, 6].

Last but not least, due to ingesting plastic and garbage, many species of animals, birds and marine mammals are affected. Their stomach is not capable of digesting the ingested objects [3, 5-6]. The United States Environmental Protection Agency calculated that in 2017 the total municipal waste generated was 267.8 million tons. This figure increased by 5.7 million compared to 2015, while in 2019, in the European Union, 225 million tons of municipal waste were generated, that is 502 kg per person, slightly more than in 2018 (495 kg). Per capita, Denmark (844 kg) was the country that generated the most important amount of municipal waste in 2019, while Romania ranked last (280 kg) [3].

In the EU, environmental efforts have been intensified by implementing initiatives that may lead to a climate neutral Europe by 2050. Particular attention is paid to the circular economy that aims to reduce waste and ultimately reduce its impact on the environment, production and consumption, thus bringing benefits to both society and people [11].

Even if the circular economy, the latest research subject both for theoreticians and for practitioners, has different definitions, the most used one refers to reduction, reuse and recycling activities for economic prosperity and environmental quality [11].

Circular economy transforms goods and products that are no longer used in future resources for other people, thus, minimizing waste [12], and having environmental, economic and social implications for both the industry and consumers [8].

In March 2022, the European Commission presented a new Action Plan to support Circular Economy that focuses on preventing and managing waste and its purpose is to stimulate economic growth and competitiveness, as well as maintain the leading position of the Union in this field [3].

The fact is that the base policy for good waste management should be centered on the 3R principle (reduce, reuse and recycle). Attention should be paid to reducing the amount of waste before it is generated and then trying to reuse it or, if this is not possible, selectively collect it for recycling [3].

THE ANNALS OF "DUNAREA DE JOS" UNIVERSITY OF GALATI
FASCICLE IX. METALLURGY AND MATERIALS SCIENCE
N°. 4 - 2022, ISSN 2668-4748; e-ISSN 2668-4756
Article DOI: https://doi.org/10.35219/mms.2022.4.18

Things are not looking too good for Romania. In May 2020, our country was threatened with the beginning of an infringement procedure by the European Commission because it did not make any progress since 2014 regarding municipal waste management. It did not comply with the decision of the Court of Justice of October 18, 2018, to close 48 illegal landfills, besides the original 68, in important cities of Romania, that represent real dangers to the population's health [3].

According to the Report of the European Commission of 2022, Romania is still struggling with waste management, having low municipal waste recycling (14%) and high waste deposit rates (70%). At the moment, Romania recycles only 15% of the collected waste, with a target of 50%, which is highly unlikely to be achieved by 2050 [3].

According to the Revised Framework Directive on Waste, that established more ambitious recycling objectives until 2035, the authorities must assure that the quantity of municipal waste from landfills is reduced to 10% or less until 2035 [3].

Measures that could lead to an improvement of the actual situation are absolutely necessary, and for this to happen people should be aware of the impact that waste can have on the environment and also the importance of reducing the waste quantity that is generated and the benefits of reusing and recycling it. It was reported that in the top European pollution-related deaths, Romania is in third place, with 19%, after Bosnia Herzegovina and Albania [3].

The transition to a circular economy depends on the way in which people and organizations adopt values and behaviours that aim to reach the "zero waste" objective and to make consumers aware of the environment, as well as the importance of sustainability at local, national and international levels [3].

But to reach this element, these practices must be known so that people understand the way in which their behavior damages the environment. The starting point for achieving education in the circular economy is represented by environmental education initiatives that ensure the development of knowledge, values and attitudes that lead to actions in this sense [3].

In order to protect the environment, reduce pollution and save natural resources, it is necessary to reduce, reuse and recycle waste. These actions are also known as the 3R, Reduce, Reuse, and Recycle, and from a simple marketing motto, it became a lifestyle for many people [3]. According to the Web of Science database, a search on the topic "plastic recycling management" presents 1921 publications between 1990-2022 with a significant increase in articles between 2017-2022 (1305 publications) [13]. However, for the topic "selective behaviour of plastic recycling", 25 publications between 2001-2022 resulted [13]. In Romania, 3 case studies were published regarding the topic of selective waste collection [3, 14, 15]. The purpose of this study is to increase public understanding and shape the community's perceptions of the dangers of plastic pollution and available solutions. Thereby, giving more power to people and organizations to take action.

Everyday plastic waste has a negative impact on the ecosystem, habitats, human health and sustainable development in the entire world. Despite the vast scale of the problem, the general public and other important stakeholders have not been adequately involved and educated about how they can become part of the solution [3].

Mass public awareness can help the way in which plastic is viewed, used and managed as waste. Education and involvement are part of the strategic action plan of the city and can include consumer awareness campaigns, business awareness campaigns, documentaries, school initiatives and clean-up activities among others [3].

The purpose is to increase the public's understanding and to form the community's perceptions regarding the dangers of plastic pollution and the solutions available, in order to give power to take action to more organizations and people. Actions community can include changes in purchasing habits and individual attitudes, increased recycling behavior and sorting, responsible practices and business processes.

2. Materials and Methods

2.1. Description of the selected location

Braila, as a county, is located in a plain area, in the South-East of Romania. It occupies small portions of Salcioara and Buzau Plain and part of Baraganul Plain and a part of the inferior meadow of Siret. To the East, Braila includes the Great Braila Island and it is a county that represents 2% of the entire country's surface. Braila's neighbours are Galati to the North, Tulcea to the East, Ialomita to the South and Buzau to the West [16]. The Braila municipality is formed of 41 neighbourhoods and it has a total number of residents of 201 414 [17, 18].

"Plantelor" neighbourhood is located in the East part of Braila and it is the last set of blocks before the city's exit to the Municipality of Galati. It is delimited in the North by Str. Plantelor, in the East by Str. Abatorului, in the South by Blvd. Dorobantilor and to the West by the Str. Calea Galati. It is formed of 9 blocks and 6 houses (1022 residents).

According to Braila's County Waste Management Plan 2020-2025 (CWMP), in Braila, the

THE ANNALS OF "DUNAREA DE JOS" UNIVERSITY OF GALATI
FASCICLE IX. METALLURGY AND MATERIALS SCIENCE
Nº. 4 - 2022, ISSN 2668-4748; e-ISSN 2668-4756
Article DOI: https://doi.org/10.35219/mms.2022.4.18

economic operators who carry out the activity of collecting household waste and similar to them are: AD ECO, BRAI CATA and RER ECOLOGIC SERVICE [16].

After collecting, the waste is deposited within the municipality of Braila, at the Muchea deposit. TRACON SRL is the operator that administrates this deposit until 2028. The capacity of this deposit is 2,130,710 m^3 with a number of 4 storage cells. The current occupied capacity is 1.033.857 m^3. Separate collection of usable fractions (paper, cardboard, plastic, metal) is done at the Vadeni sorting station with a projected capacity of 30,000 t/year and the recovery is done at Eco Metal Recycling SRL Galati [16].

In Braila, operators have set up platforms for separate collection of recyclable waste, equipped with 58 bell containers of 2.5 m^3 / 278 containers of 1.1 m^3 or 116 big/bag pens of 1.5 m^3, which are insufficient compared to the total number of inhabitants. This is basically where the problem starts: the fact that most of the time the population does not selectively collect. According to the CWMP, the municipal waste generation index is permanently increasing. If in 2014 the index was 280 kg/inhabitant x year, in 2018 it increased to 382 kg/inhabitant x year. Another problem is the amount of household waste collected separately. If in 2014 the amount was 3080 kg/inhabitant x year, in 2018 it increased very little to 3,299 kg/inhabitant x year [16]. According to the 2020 European Commission's Report, Romania still struggles with waste management and it has low municipal waste recycling (14%) and high landfill rates (70%). At the moment, Romania recycles only 15% of collected waste, with a target of 50% that is highly unlikely to be achieved by 2050 [3].

2.2. Description of the method

In order to carry out the research and collect data, a questionnaire was applied, in order to observe the attitude of citizens regarding the selective management of waste. The target population was the citizens that live in Plantelor neighbourhood of Braila city. The data was gathered between May-July 2022. Initially, a classical approach was attempted of distributing questionnaires among the population, but without any success, because people are mostly reserved and politely decline saying that they do not have time to answer our questions. As a result of the citizens' attitude and following the premise that people spend quite a lot of time in the online environment, I made this questionnaire with the help of https://docs.google.com/. The questionnaire was anonymous and its average completion time was a maximum of 15 minutes. Completing the questionnaire was voluntary and citizens could withdraw at any time from completing it. Also, no rewards were given for this activity. For reasons of anonymity and confidentiality, the respondents' e-mail addresses or other personal data were not collected. Plantelor neighbourhood is quite small and it has approximately 1022 inhabitants. The total number of respondents was 100 people.

The questionnaire was designed with a number of 17 questions in order to reveal the citizens' knowledge and their behavior regarding the selective collection, if they are involved in green campaigns and if they know the environmental benefits brought by selective collection.

3. Results and discussion

The results of the answers given by the citizens of Plantelor neighbourhood (Braila Municipality) are presented in Figures 1 to 17. The first questions from the questionnaire were to find the person's sex, age and level of studies of the people who completed this questionnaire. In Figure 1 (a-c), the charts are shown in the form of bars with the distribution of the answer and their percentage.

From Figure 1(a), it can be observed that people who have completed this questionnaire are 63% women and 37% men. From the analysis of Figure 1(b), it appears that 53% of the surveyed people belong to the age category of 20-40 years, 41% to the category of 40-60 years, 4% to the < 20 years category and 2% to the > 60 years category. From Figure 1(c), it can be observed that most respondents have higher studies (60.8%), 34.2% secondary studies and 5% have graduated vocational school. The second question of the questionnaire was designed to find out if the population understands what selective collection means (Figure 2).

From Figure 2, it can be observed that 51% of the questioned persons answered that the meaning is to protect the environment, 19% answered that it means recycling different types of materials, 18% answered "to contribute to the health of the population", 10% to make a civic action for the area where they live and 2% that they "do not know".

The third question is likely to find out if the population knows the meaning of the 3Rs (Reuse, Recycle, Reduce).

From the analysis of Figure 3, it turns out that 52% of the questioned people know the meaning of the 3R, 38% do not know and 10% have never heard of this terminology.

The fourth question of the questionnaire is designed to find out which are the fractions that citizens selectively collect most often (Figure 4).

THE ANNALS OF "DUNAREA DE JOS" UNIVERSITY OF GALATI
FASCICLE IX. METALLURGY AND MATERIALS SCIENCE
N°. 4 - 2022, ISSN 2668-4748; e-ISSN 2668-4756
Article DOI: https://doi.org/10.35219/mms.2022.4.18

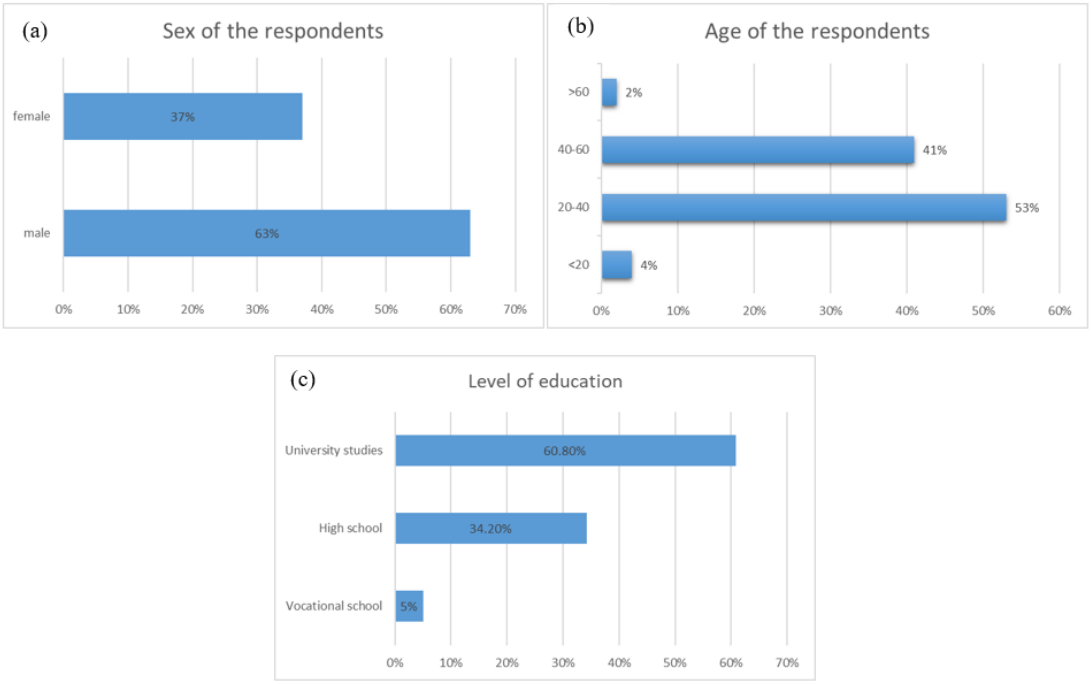

Fig. 1. *Distribution of answers for a) respondents' gender, b) respondents' age, and c) level of education*

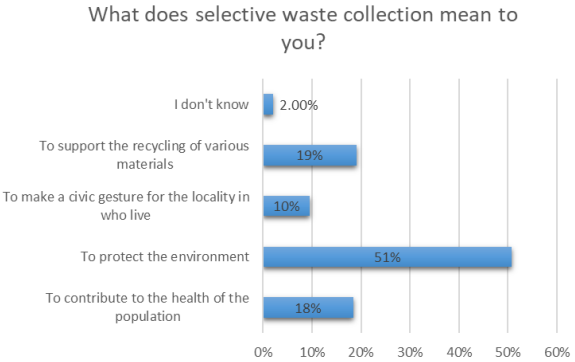

Fig. 2. *Distribution of answers for "What does selective waste collection mean to you?"*

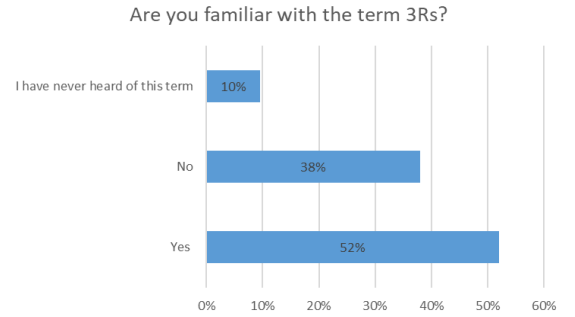

Fig. 3. *Distribution of answers for "knowing the meaning of the 3R terminology (Reuse, Recycle, Reduce)?"*

Figure 4 shows that the fraction most often collected is the fraction of plastic materials with a percentage of 50%, followed by paper, glass, organic waste and metal.

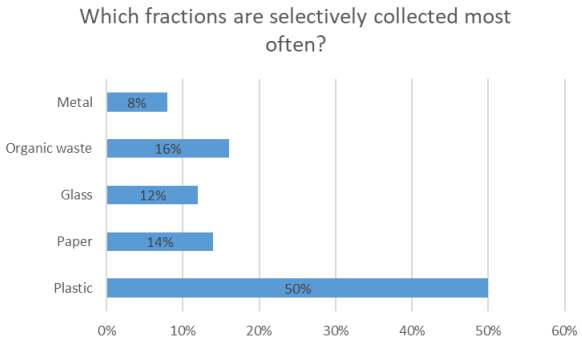

Fig. 4. *Distribution of answers for "Which fraction are selectively collected most often?"*

The fifth question is to designed to find at what time interval they do selective collection (Figure 5).

The frequency that they do this selective collection is 2-3 times per week with a rate of 41%, but it is worrying that 14% of the respondents admit that they never do this action. The sixth question is to find the people's reason who answered "Never" to question number 5 (Figure 6).

Figure 6 shows that 16% have answered "that they are not interested in this aspect", 38% answered that "they do not have where to do this thing", 29%

THE ANNALS OF "DUNAREA DE JOS" UNIVERSITY OF GALATI
FASCICLE IX. METALLURGY AND MATERIALS SCIENCE
Nº. 4 - 2022, ISSN 2668-4748; e-ISSN 2668-4756
Article DOI: https://doi.org/10.35219/mms.2022.4.18

that "they do not have the necessary information for this collecting system" and 17% have answered that there are no necessary conditions for selective collection at any time. These answers are worrying but they reflect reality. As mentioned before in the materials and methods section of this article, the number of bins is insufficient and the distance between houses and the collecting points is too long, thus making citizens give up the selective collection.

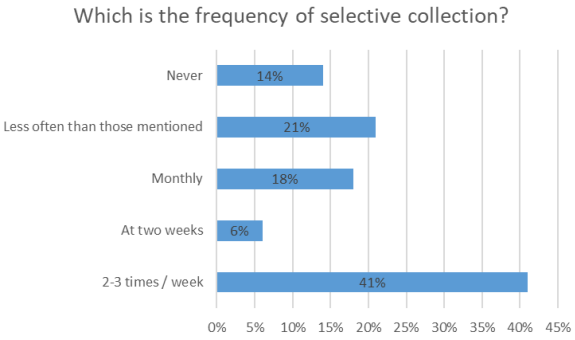

Fig. 5. *Distribution of answers for "Frequency of selective collection?"*

The seventh question is meant to clarify which of the people are in charge of waste disposal in their homes (Figure 7).

Figure 7 points out the fact that 59% of respondents say that the wife is the one who takes care of this matter, taking into consideration the fact that the highest frequency of completing the questionnaire was female. We can understand this because they are more concerned with household chores than the opposite sex.

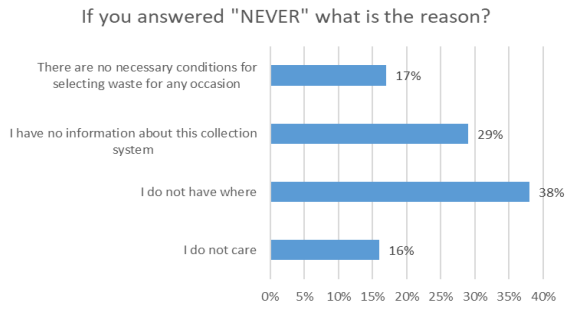

Fig. 6. *Distribution of answers for "The reason for non-selective collection?"*

The eighth question is about the fact that citizens are interested to find out what happens with their waste after it has been collected from them. This is quite an important question because knowing the route of waste makes the population aware of environmental risks and benefits, as well as appreciating the people who often deal with sorting them manually.

As we can correlate certain answers presented in Figure 8, this question confirms the population's lack of interest towards this problem. Henceforth, the high number of people who answered that they "never" do selective collection.

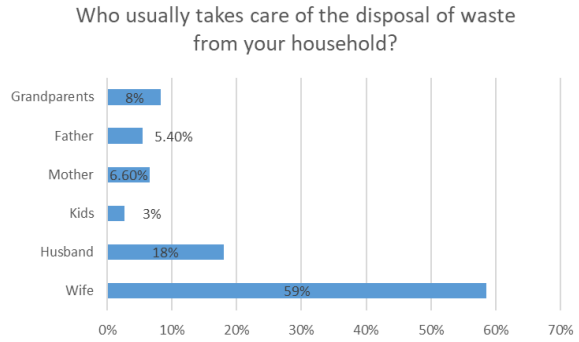

Fig. 7. *Distribution of answers for "Who takes care of waste disposal most often?"*

The ninth question is to find out if citizens know the containers' colour code (Figure 9).

Figure 9 shows that 51% of respondents have knowledge about the significance of each colour and know what type of waste must be thrown in that container. 16% answered that they do not know the colour code and 33% answered that they know some of them.

The tenth question was conceived with the purpose to find out if citizens from the chosen area for this study are aware of the risks of non-selective collection.

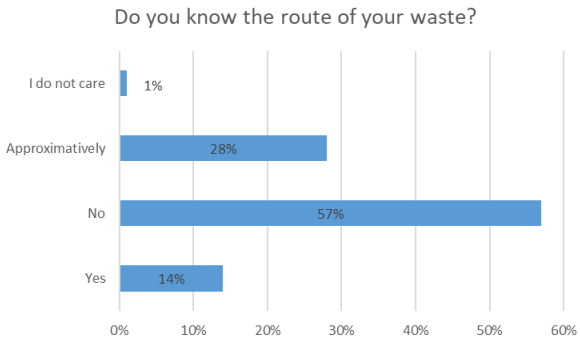

Fig. 8. *Distribution of answers for "Do you know the route of your waste?"*

Figure 10 shows that 86% of respondents answered with "yes", 13% answered with "I do not know" and 1% with no.

Until this question, we can conclude that most of the respondents to this questionnaire were females and the age category is between 20-40 years, relatively young persons, with higher education. Most people know what selective collection means, they often do it for many types of materials, but they do

THE ANNALS OF "DUNAREA DE JOS" UNIVERSITY OF GALATI
FASCICLE IX. METALLURGY AND MATERIALS SCIENCE
N°. 4 - 2022, ISSN 2668-4748; e-ISSN 2668-4756
Article DOI: https://doi.org/10.35219/mms.2022.4.18

not know what happens to their waste after it has been sorted. Special attention must be given to people who do not know about this system. After the analysis of this questionnaire, 14% of respondents answered that they never did selective collection. The situation in the field (waste thrown near the bins, fractions thrown into other types of containers than the ones they should be, etc.) is much more worrying because the number of those who do not do this thing is greater.

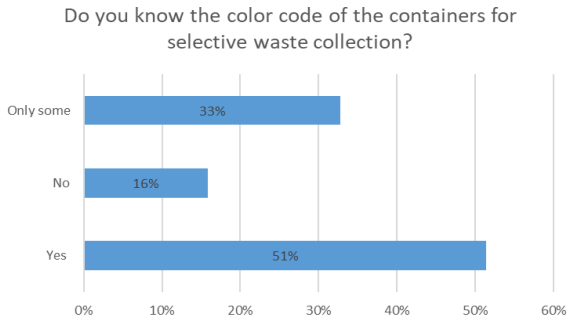

Fig. 9. *Distribution of answers for "Do you know the colour code of the containers for selective waste collection?"*

Question number 11 asked under what conditions they would accept to do selective collection. The distribution of the answers is presented in Figure 11.

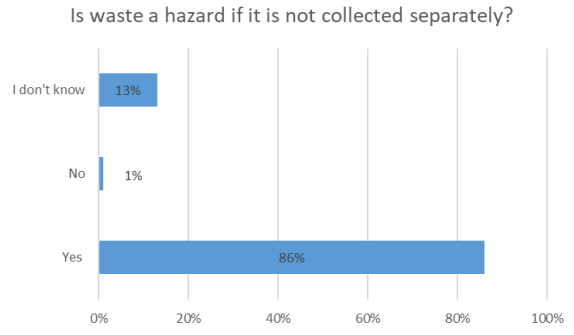

Fig. 10. *Distribution of answers for "Is waste a hazard if it is not collected separately?"*

From the analysis of Figure 11, it appears that 45% of the questioned people answered: "if there were suitable spaces arranged". This is an actual problem, as mentioned in the materials and method section. The containers distributed at the level of Braila municipality for selective collection are not enough in relation to the total number of inhabitants. A proportion of 29% answered that "if there were more collection points near their home" and a proportion of 16% answered, "if there were information campaigns on what happens after the recycled waste is collected". Is it worth noting that to this question 6% of respondents said that being penalized by an additional tax would lead them to do so and 5% answered that they would do so if recycling also had a direct social purpose.

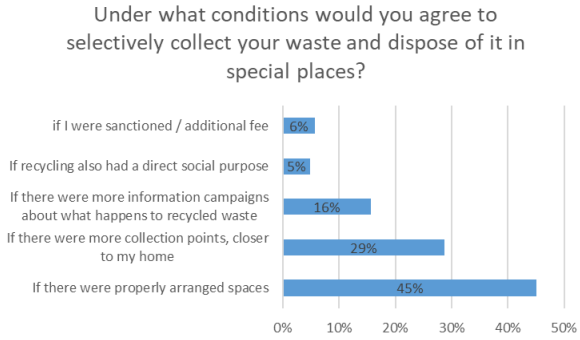

Fig. 11. *Distribution of answers for "Under what conditions would you agree to selectively collect your waste and dispose of it in special places?"*

Asked if they know the environmental benefits brought by selective collection (Figure 12), people answered 54% with "yes", 33% with "approximately" and 13% with "no".

When asked about the sources from where they found about the environmental benefits brought by selective collection (Figure 13), 45% of the respondents said the main source was the internet.

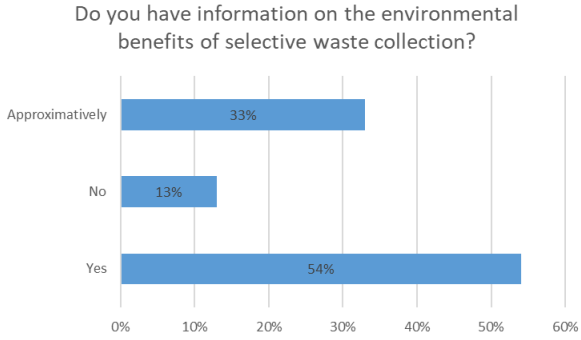

Fig. 12. *Distribution of answers for "Do you have information on the environmental benefits of selective waste collection?"*

Question fourteen (Figure 14) regarding in what way the authorities should determine the population to selectively collect, 32% answered that more bins should be available for the inhabitants, 31% answered more information programs, 19% said that those who do not selectively collect should be fined and 14% consider that the school, church and NGOs should do more information campaigns. 3% of respondents answered with "I do not know what authorities should

THE ANNALS OF "DUNAREA DE JOS" UNIVERSITY OF GALATI
FASCICLE IX. METALLURGY AND MATERIALS SCIENCE
Nº. 4 - 2022, ISSN 2668-4748; e-ISSN 2668-4756
Article DOI: https://doi.org/10.35219/mms.2022.4.18

do" and 1% consider that all answers should be applied in order to determine citizens to selectively collect.

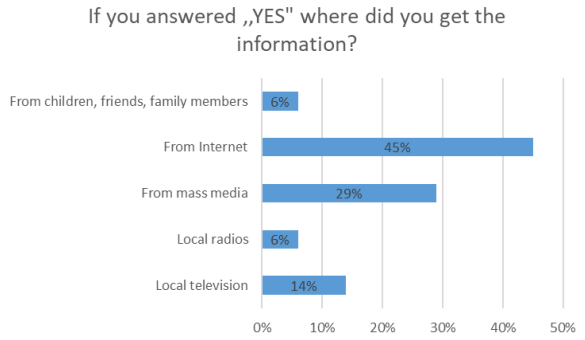

Fig. 13. *Distribution of answers for "Where did they receive information about the benefits of selective collection?"*

The statistics for the answer to question number fifteen "Are you involved in greening activities?" are given in Figure 15.

From Figure 15, it can be seen that around 55% answered that they are little involved, 22% with "no", 22 with "yes" and 1% with "I do not care". The lack of involvement from the authorities, the neglect of the citizens and other considerations only make us take a step back in the fight against our country's poor waste management and how to dispose of it. The fact is that all these actions will be reflected in the increase in product prices and sanitation fees.

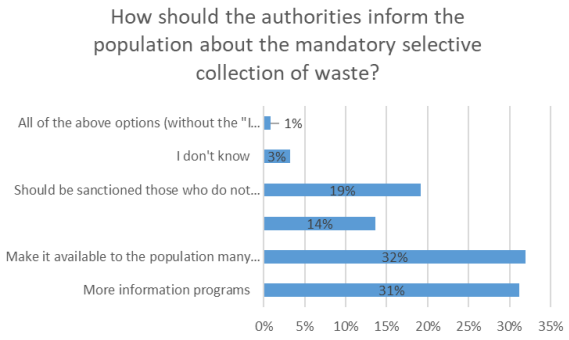

Fig. 14. *Distribution of answers for "How should the authorities inform the population about the mandatory selective collection of waste?"*

For question number 16: "From which source of information would you prefer to find out more information about the environmental projects carried out by the authorities" (Figure 16), 10% answered that they would prefer local television stations and 40% that they prefer the Internet as a communication method.

Question 17: "Would you agree that the waste collection tax be calculated according to the amount of waste you generate?" (Figure 17).

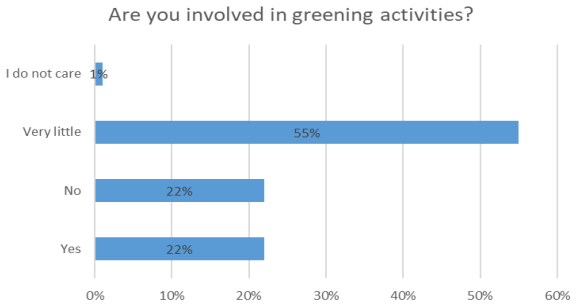

Fig. 15. *Distribution of answers for "Are you involved in greening activities?"*

Like many EU countries that have the "polluter pays" principle, this question is meant to find the citizens' opinion on this principle. From the statistical analysis of the answers presented in Figure 17, it can be seen that 54% of respondents agree with the increase of the waste collection tax according to the amount of waste they generate, 29% do not agree and 17% answered: "I do not know".

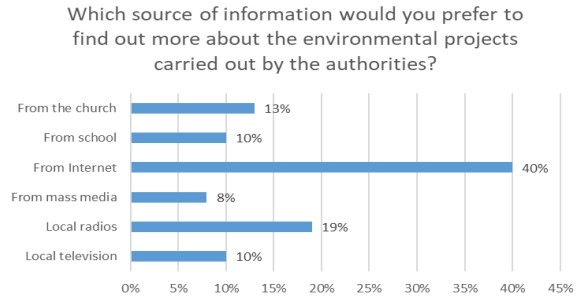

Fig. 16. *Distribution of answers for "From which source of information would you prefer to find out more about the environmental projects carried out by the authorities?"*

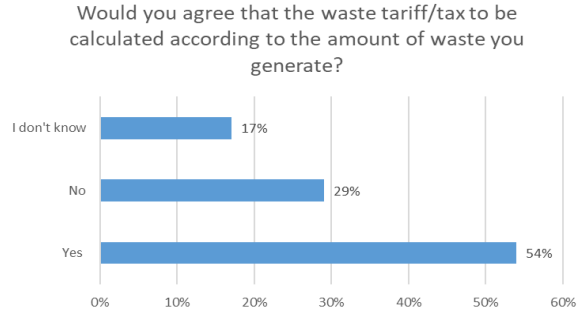

Fig. 17. *Distribution of answers for "Would you agree that the waste tariff/tax be calculated according to the amount of waste you generate?"*

THE ANNALS OF "DUNAREA DE JOS" UNIVERSITY OF GALATI
FASCICLE IX. METALLURGY AND MATERIALS SCIENCE
Nº. 4 - 2022, ISSN 2668-4748; e-ISSN 2668-4756
Article DOI: https://doi.org/10.35219/mms.2022.4.18

We consider that by applying this principle, citizens would be more aware/pay more attention to the amount of waste that they generate/to the way of collecting, as long as their incomes are affected.

4. Conclusions

Research on global production of plastic materials and environmental pollution showed that plastic waste is a major environmental problem. The effect of plastic waste on marine organisms, people and the environment are of public concern and calls for the need to save ecosystems and the lives within them. Despite the fact that plastic materials are used in daily life, toxic chemical substances used in production must be carefully monitored in order to ensure environmental and health safety. Reducing the community's exposure to toxic substances from plastic waste will increase the chances of a clean environment and a healthy society. There is an urgent need for government agencies and health authorities to adopt and apply environmental laws that will monitor the production, usage and elimination of plastic materials. Moreover, some harmful chemical constituents used in the production of plastics (for example phthalates, BPA, etc.) must be forbidden in consumer goods and in plastic products that are in direct contact with food, beverages and children.

From the statistical analysis of the study case, we can conclude that most of the questionnaire respondents are females. Even though the study identified gender differences through the fact that women are more aware and involved in environmental protection activities, regardless of gender, the young generation should harness their knowledge in this field and adopt these behaviours that may lead to a sustainable future. The age category is between 20-40 years, relatively young people, with higher education. Most people know what selective collection means and they usually do it for several types of materials, but they do not know what happens to their waste after it has been sorted.

Special attention must be given to people who do not have knowledge about this system. From the analysis of this questionnaire, 14% of people answered that they never do selective collection.

The situation in the field (waste thrown near the bins, fractions thrown into other types of containers than the ones they should be, etc.) is much more worrying because the number of those who do not do this thing is greater.

Although a large part of the population does selective collection only for certain fractions, it can be observed that the lack of information regarding what happens with their waste after it is collected, makes the citizens' attitude hostile towards greening activities.

For the question of how they would prefer to be informed regarding the environmental benefits of selective collection and the obligation of selective collection, respondents consider that the involvement of local authorities should be by television, Internet, churches, schools and installing more available bins for the citizens would help and improve the system.

Moreover, by raising awareness and assessing the impact of our behaviours towards the environment through education, by adopting a sustainable lifestyle, production and consumption practices, we will be able to reduce the pressure on the planet's resources.

Taking into consideration that Romania still has a lot of problems in the field of environmental protection, it is possible that this solution provided by blockchain technology, which is still in full development, will help solve these problems quickly. This technology has the potential to change social behaviours, involving more interested parties, especially citizens, and can stimulate the waste management process and lead to the ultimate goal of "zero pollution" cities.

We consider that in order to fight and reduce the persistent environmental pollution with plastic materials, we need tougher laws that must be respected and applied accordingly. This should include the need for a global convention on plastic pollution that forces plastic manufacturers to declare all the ingredients in their products and warn consumers about the potential health effects of these constituents.

Another measure would be adequate management of plastic waste through well implemented environmental management. Moreover, an emphasis should be put on educational and public awareness campaigns. And last but not least, the use of bioplastic as an alternative.

Even though the study offers some answers regarding the environmental problems that Romania faces, it is important to identify the people responsible for solving them. There are also limitations of the undertaken study, taking into consideration that the perspective of only a part of the population was questioned.

Therefore, in order to fix the deficiencies, the first solution to the waste problem is to organize awareness and educational campaigns for the population. By providing theoretical knowledge and by organizing extracurricular activities, universities, high schools, kindergartens, churches can contribute to cultivate environmentally responsible mentalities that will lead to the adoption of sustainable habits.

From this point of view, it would be necessary to carry out additional studies on the questioning of more citizens from several geographical areas and on different categories of the public. There are other variables that can influence attitudes towards

environmental protection and reuse and recycling behaviours (background, place of origin, how the legislation in the field is applied, living standard, economic status, local culture and beliefs, details about living conditions, etc.) and that can be inserted. This objective could be realized by performing subsequent qualitative and quantitative analyses that will surely lead to a better understanding of the citizens' behavior.

Acknowledgments

The work of Nicoleta Bogatu was supported by the project "PROINVENT", Contract no. 62487/03.06.2022 - POCU/993/6/13 - Code 153299, financed by the Human Capital Operational Programme 2014-2020 (POCU), Romania.

References

[1]. Abukasim S. M., Zuhria F., Saing Z., *Alternative management of plastic waste*, Journal of Physics: Conference Series, 1517, 012041, doi:10.1088/1742-6596/1517/1/012041, 2020.
[2]. Massarutto A., *Economic Analysis of Waste Management Systems in Europe*, Sustainable Development and Environmental Management Experiences and Case Studies, Clini C., Musu, I., Gullino, M. L., (Ed), Springer Netherlands, p. 171-186, 2008.
[3]. Gherhes V., Farcasiu M. A., Para I., *Environmental Problems: An Analysis of Students'Perceptions Towards Selective Waste Collection*, Front. Psychol., 12:803211, doi: 10.3389/fpsyg.2021.803211, 2022.
[4]. Munteanu R. A., *Innovative Solutions for Local Public Administration in the Process of the Waste Collection*, International Conference Innovative Business Management & Global Entrepreneurship, IBMAGE 2020, p. 140-156, Iasi, Romania: LUMEN Publishing House. https://doi.org/10.18662/lumproc/ibmage2020/11, 2020.
[5]. Alabi O. A., Ologbonjaye K. I., Awosolu O., Alalade O. E., *Public and Environmental Health Effects of Plastic Wastes Disposal: A Review*, J Toxicol Risk Assess, 5:021, doi.org/10.23937/2572-4061.1510021, 2019.
[6]. Proshad R., Islam M. S., Kormoker T., Haque M. A., Mahfuzur Rahman M. D., *et al.*, *Toxic effects of plastic on human health and environment: A consequences of health risk assessment in Bangladesh*, Inter J Hlth, 6, p. 1-5, 2018.
[7]. Hopewell J., Dvorak R., Kosior E., *Plastics recycling: Challenges and opportunities*, Philos Trans R Soc Lond B Biol Sci, 364, p. 2115-2126, 2009.
[8]. Meseguer-Sánchez V., Gálvez-Sánchez F. J., Molina-Moreno V., Wandosell-Fernández-de-Bobadilla G., *The main research characteristics of the development of the concept of the circular economy concept: a global analysis and the future agenda*, Front. Environ. Sci., 304, 704387, 2021.
[9]. Alassali A., Picuno C., Chong Z. K., Guo J., Maletz R., Kuchta K., *Towards Higher Quality of Recycled Plastics: Limitations from the Material's Perspective*, Sustainability, 13, 13266. https://doi.org/10.3390/su132313266, 2021.
[10]. ***, https://leap.unep.org/countries/eu/national-legislation/european-parliament-and-council-directive-9462ec-packaging-and.
[11]. Kirchherr J., Reike D., Hekkert M., *Conceptualizing the circular economy: an analysis of 114 definitions*, Resour. Conserv. Recycl., 127, p. 221-232, doi: 10.1016/j.resconrec.2017.09.005, 2017.
[12]. Stahel W. R., *The circular economy*, Nat. News, 531, 435, 2016.
[13]. ***, https://www.webofscience.com/wos/woscc/basic-search.
[14]. Jigani A.-I., Delcea C., Ioanăș C., *Consumers' Behavior in Selective Waste Collection: A Case Study Regarding the Determinants from Romania*, Sustainability, 12(16), 6527, doi:10.3390/su12166527, 2020.
[15]. Delcea C., Crăciun L., Ioanăs C., Ferruzzi G., Cotfas L.-A., *Determinants of Individuals' E-Waste Recycling Decision: A Case Study from Romania*, Sustainability, 12, 2753, 2020.
[16]. ***. https://cjbraila.ro/dm/portal.nsf/E8B6C36F006708DEC225857C003A92DB/$FILE/PJGD%20Braila_2019_Varianta_2_2020%20-%202025.pdf.
[17]. ***, https://ro.wikipedia.org/wiki/Lista_cartierelor_din_Br%C4%83ila
[18]. ***, https://braila.insse.ro/wp-content/uploads/2020/03/Populа%C5%A3ia-dup%C4%83-domiciliu2019l.pdf.

THE ANNALS OF "DUNAREA DE JOS" UNIVERSITY OF GALATI
FASCICLE IX. METALLURGY AND MATERIALS SCIENCE
Nº. 4 - 2022, ISSN 2668-4748; e-ISSN 2668-4756
Article DOI: https://doi.org/10.35219/mms.2022.4.19

A REVIEW ON MODIFIED POLYMERS AND THEIR COMPOSITES

Irina DĂNĂILĂ (ȚÎCĂU), Tamara APARECI (GÎRNEȚ), Sebastian Marian DRĂGHICI, Iulian PĂDURARU, Gabriel SĂRACU, Adrian CÎRCIUMARU, Mihaela-Claudia GOROVEI*

"Dunarea de Jos" University of Galati, Romania
e-mail: *mihaela_gorovei@yahoo.com

ABSTRACT

The main objective of this paper is to realise a review on fundamental research regarding the development of new and efficient methods to determine the mechanical, thermal, tribological, and thermo-mechanical properties of composite materials, analysing the results obtained through various graphs and diagrams accompanied by demonstrations and explanations from the specialized literature. Developing new materials or improving the properties of existing materials has been and is a concern of researchers. The chemistry of complex combinations represents one of the most important fields of scientific research, both in terms of theoretical investigations and practical applications. The interest shown towards complex combinations is justified by the contribution brought by the accumulation of knowledge about inorganic chemicals, polymers as well as about epoxy resins and polyvinyl ester, of course also about the design, formation and analysis through mechanical tests (compression, tension, three-point bending), thermal, tribological of composite materials modified with various modifying agents.

KEYWORDS: modified polymers, composites, complex combinations, epoxy resins

1. Introduction

Many current industrial fields are in continuous development, both in terms of products and the materials used to make them. This fact has recently led to the replacement of classic (heavy) materials with modern materials, often plastics or composites [1-6]. Due to some of their higher characteristics, the applications of composite materials are numerous in fields such as: electronics, chemistry, medicine, optics, construction, sports, cars, agricultural machines, automobiles, electrotechnics, etc. Composite materials have some physical and chemical characteristics clearly superior to conventional materials (metals, wood, plastic, concrete), but they also have weak points. Despite the fact that there are factors that could stop the wide use of composite materials such as: high costs, elaborated research, lack of testing standards, the advantages of using these materials, in the long term, will establish, worldwide, a considerable increase in applications created from composite materials. Composite materials became the first to allow researchers to modify their internal structure, both by combining them at the molecular level and in preferential directions with the aim of obtaining clearly superior properties to the original materials [7-9]. Thus, the diversity of composite materials, their properties and behaviours are limited only by the imagination of human nature, giving a multitude of possibilities, of associations, of course, taking into account the performances and costs defined as research objectives [10-12]. Starting with the second half of the 19th century, the chemical modification of natural materials had generated a really boom of the diversity of polymers produced in the laboratory [13-15]. It is difficult to list what exactly around us does not contain polymers, starting with the surrounding objects and ending with aerospace applications [16, 17].

Tuttle M. E., in his work [18], claims that the function of a matrix, of a composite material, is to provide a relatively rigid environment that is able to transfer the effort to the fibrous components of the material. The function of the reinforcement in a composite material is to take the loading stress transferred through the matrix. The load must thus be distributed between the matrix and the reinforcement [19]. The reinforcement is included in the matrix

THE ANNALS OF "DUNAREA DE JOS" UNIVERSITY OF GALATI
FASCICLE IX. METALLURGY AND MATERIALS SCIENCE
Nº. 4 - 2022, ISSN 2668-4748; e-ISSN 2668-4756
Article DOI: https://doi.org/10.35219/mms.2022.4.19

material (via interphase bonds) [20]. In the formation of composites, an important aspect regarding with the choice of matrix and reinforcement is the provision of a high-quality interphase that ensures the transfer of stresses from the matrix to the reinforcement without being directly affected. Technological additions have the role of catalyst, accelerator, flame retardant agents, protection against ultraviolet rays [21]. According to studies, both the matrix and the reinforcement of a composite material can be obtained from different types of materials [22]. The classification of composite materials can be done according to the type of matrix material, reinforcement material, how the composite is made, use, mechanical, physical or chemical properties, etc [23].

2. Polymer matrix

To make the composites, the most common matrices used are metallic, ceramic or polymeric, of which, due to the very low prices, the polymeric ones are the most common, however, the remarkable properties of the ceramic matrix composites (especially those related to thermal resistance) make them preferred for aerospace applications [24]. On the other hand, metal matrix composites are preferred for underwater applications because metals are much easier to treat in terms of corrosion resistance, by painting, coating with various protective layers or chemical passivation, etc. [25]. Regarding polymer matrices, at present, the trends are especially related to obtaining polymers or modified polymers with properties as close as possible to those of metals [26]. The matrix defines the shape of the landmark, protects the reinforcement from the action of external factors and keeps its geometry predefined in the design, so that the functionality of the part is ensured [27]. The choice of matrix type is made according to the technology of forming composite materials [28, 29].

Depending on the type of polymer, composite materials can be formed with thermoplastic or thermoset matrices [30]. If, in the case of thermoplastic materials, all technologies involve bringing the raw material into the melting phase followed by injection, the polymerization being ensured by cooling the material in the mould, in the case of thermoset polymers, the polymerization or polycondensation is ensured by use of catalytic agents, usually called hardeners [31]. Composite materials with a thermoplastic matrix are relatively easy to separate, while composites with a thermoset matrix are extremely stable and the reinforcement or additive can no longer be extracted from the matrix [32].

The molecular configurations, and the properties manifested by polymers at the macroscopic level, in the liquid or solid phase, depend on the configurations of the molecular chains, and this dependence can be explained on the basis of the low or high mobility of the polymer molecules under the conditions of heating the material, or the external mechanical loading of it [33-35]. If in the case of thermosetting polymers, the chemical bonds that are made between the polymer chains are covalent bonds, in the case of thermoplastic polymers the bonds between the polymer chains are hydrogen bonds or van der Waals bonds [36]. In the case of thermosetting polymers, heating leads at most to the breaking of covalent bonds, which leads to the oxidation of the material and its destruction [37]. The most important difference between thermosetting polymers and thermoplastic polymers is their behavior at temperature and pressure. Thermosetting polymer matrices are hydrothermally sensitive and can degrade at moderately high temperatures (70 °C – 80 °C in the presence of water) by absorbing moisture [17, 38]. An increase in temperature leads to gradual softening of the polymer, up to a certain point, indicating a transition from a glassy behavior to an elastic or elasto-plastic behavior. The temperature at which this transition occurs is called the glass transition temperature Tg, which decreases with increasing humidity [39]. An increase in temperature beyond this transition point causes the polymer to undergo a rapid transition from rigid solid behavior to elasto-plastic or elastic solid behavior. As a result, the dominant properties of the matrix (shear strength and stiffness) are reduced and the material becomes too soft for use as a structural material [40-42].

3. Thermoset matrix

Thermosetting matrices are characterized in particular by: limited life time, long formation cycle – due to the cross-linking times necessary to reach the degree of hardening, the hardening process in the matrix can lead to the appearance of products with small molecules, which causes the appearance of bubbles and pores in the final product, processing waste is not recyclable [43]. The most commonly used thermoset polymers are epoxy, polyester and vinylester resins, and all of them can be single-component systems or two-component systems and are in the liquid phase at room temperature. Resins are heat treated at high temperatures (or sometimes just at room temperature) to obtain the final shape [44]. The formation of composite materials with thermosetting matrix offers the following advantages: very easy processing, because in the initial phase the resin systems are in a liquid state, the wetting of fibres or particles with thermosets is relatively easy,

THE ANNALS OF "DUNAREA DE JOS" UNIVERSITY OF GALATI
FASCICLE IX. METALLURGY AND MATERIALS SCIENCE
Nº. 4 - 2022, ISSN 2668-4748; e-ISSN 2668-4756
Article DOI: https://doi.org/10.35219/mms.2022.4.19

thereby avoiding voids, porosity and dry areas in formed composite materials, the heat and pressure required in the processing of thermosets show lower values than those required in the processing of thermoplastics [45].

Unsaturated polyester resins – properties depend on molecular weight and chemical composition. The increase in molecular mass determines the improvement of the main mechanical properties, the increase in hardness, resistance to temperature and chemical agents [46]. The specific properties of unsaturated polyester resins are [47]: easy acquisition and quick access to raw materials, fast solidification, no production of secondary elements, dimensional durability and positive mechanical properties of the reinforced form, multiple colouring characteristics as well as transparency, high chemical resistance to the action of different non-oxidized acids and alcohols [48]. It is also present the following disadvantages: high shrinkage during the forming process, poor flame behavior, low resistance to hot water and alkalis [49].

Vinylester resins – the mechanical properties of the hardened resins, especially the tensile and flexural strengths, depend on the molecular mass of the epoxy resin used in the synthesis (they are obtained by acid or acrylic reactions with the reactive oxiranic groups in crosslinked epoxy resins under the action of UV radiation), have good dielectric properties, those based on epoxy resins with methacryloid end groups show particular chemical resistance to the action of acids, bases and solvents [50-52].

Epoxy resins – are generally more expensive than polyester or phenolic resins, but have very good mechanical, chemical and electrical characteristics, forming at temperatures between 50 °C and 130 °C, hard materials and dimensionally stable during curing, have structure that ensures good adhesion to most of the reinforcement materials, they are resistant to the action of acids and solvents, very resistant to the action of alkaline substances, very good electrical insulating materials, thermally stable at temperatures up to 260 °C and very little hygroscopic [53-55]. They have mechanical properties dependent on the loading or reinforcing agent, the thermal properties depend on the chemical structure and the hardening method [56]. In the case of epoxy resins, the cross-linking of polymer chains is very important, and leads to improved mechanical performance. This process is carried out by using chemical cross-linking agents, which also contribute to the polymerization and hardening of resins [57]. In the case of an epoxy resin, the polymerization is due to the specific groups (epoxy), the cross-linking of the chains being a consequence of the use of hardeners, for this the mixture recipe must be extremely balanced. Thus, if the hardening-crosslinking agent is a primary or secondary amine, it is necessary that the ratio between the number of mobile hydrogen atoms in the respective amine and the number of epoxy groups has to be 1:1 [58]. This aspect leads to the possibility of controlling the reaction by establishing the amount of the strengthening-crosslinking agent [59]. Most studies of polymer composites are focused on epoxy matrices due to this polymer's versatility and ease of handling. In general, manufacturers deliver it in liquid form (bi-component), they recommend it for use in additive strategies with various agents – especially carbon nanotubes [60].

4. Composites with polymer matrices

Polymer matrix composites contain a wide variety of long, short fibres and powders fused through and within a polymer matrix. Unlike ceramic matrix composites, in which reinforcements are used to increase fracture resistance, in the case of polymer composites reinforcements are used to increase mechanical strength and material persistence [61]. Composites with a polymer matrix are created so that the mechanical loads of the structures exposed to the loads are taken over by the reinforcements, and the role of the matrix is to bind the fibres or other reinforcing elements and to transfer the loads between them [62-64]. Polymer matrix composites are often grouped into two broad categories: reinforced plastics and advanced composite materials [65]. Here the difference is made based on the level of mechanical properties (e.g., strength and stiffness), although this is not a sufficient criterion for the delimitation process of these materials [66]. The most used properties of composite materials with polymer matrix are: low density, high mechanical strength along the reinforcement (long, ordered reinforcing fibres) [67].

Recently, these materials have been studied with increased attention that can be applied to the construction of structures for the aircraft industry (military, at first, and civil). Their cost, often very high, still remains an important obstacle in expanding the area of use in commercial fields [68]. The most advanced polymer composites are created by a complicated way of adding layer by layer (lay-up) [69]. Ceramic composites, compared to polymer composites, show performance results in production (especially military aircraft) [70]. In some cases, it could even be concluded that technology has surpassed the scientific understanding of these materials and their behavior [71].

In order to create more efficient versions of materials and for an effective design, studies are needed in the field [72]:

THE ANNALS OF "DUNAREA DE JOS" UNIVERSITY OF GALATI
FASCICLE IX. METALLURGY AND MATERIALS SCIENCE
N°. 4 - 2022, ISSN 2668-4748; e-ISSN 2668-4756
Article DOI: https://doi.org/10.35219/mms.2022.4.19

1. Materials processing - new cheaper ways like, cost and knowledge of how the forming method adjusts the final characteristics of the materials;

2. Increasing the impact resistance of polymer composite materials in order to ensure the effectiveness and durability in service of the structures [73];

3. Increasing the resistance to the delamination process, the studies that have already been carried out confirm the conclusion that this process is the only one that can lead to the destruction of these materials [74].

5. Nanomaterials and nanostructures

Nanotechnology is the science of designing, manufacturing and applying nanostructures or nanomaterials. Also, nanotechnology studies the relationships between the physical properties and dimensions of materials [75]. Nanotechnology operates with materials or structures of nanometric scalar order [76]. We call nanotechnology any technology that results in a nanometric product: fine particles, microlithography [77]. If we take into account the increasingly close collaboration between engineering and medicine in the nanotechnological field, we inevitably come to the conclusion that nanotechnology represents an important link in the development process of humanity in the years to come [78].

Among the main components of the science of nanomaterials and nanotechnology, the following can be highlighted: fundamental studies of the properties of materials at the nanoscale level, the development of nanotechnology both for the intentional creation of nanomaterials [79], as well as the search for the use of natural objects with nanostructured elements [80], the creation of finished products using nanomaterials and the integration of nanomaterials and nanotechnologies in various branches of industry and science, the development of tools and methods for studying the structure and properties of nanomaterials, as well as methods of control and certification of semi-finished products for nanotechnology [81]. The term nanotechnology was first proposed by N. Taniguchi in 1974 [82].

6. Applications of composite materials

Mishra *et al.* [83], stated that many researches are ongoing to improve the mechanical and tribological properties of these engineered biocomposites by filling the appropriate amount of inorganic nanoparticles such as ZrO_2, SiO_2, CuS, ZnO, CuO and TiO_2 in polymer matrices. The analysis revealed that the incorporation of inorganic nanoparticles into a natural fiber reinforced polymer composite improved the mechanical and tribological properties, also improved the thermal stability and flame resistance, and reduced the water absorption capacity of the biocomposites.

Chuan Li, *et al.* and his work [9], fabricated phase change composite materials using inorganic salts for thermal energy storage at medium and high temperatures. It was concluded that the performance of the selected salts in various aspects directly influences the thermal loading/discharging behavior and also the thermal energy storage capacity of the composite. In cases where heat transfer is viewed as a restriction, thermal conductivity additives are required to improve heat transfer in salt-based composites.

In [84], a new type of functionalized silicone polymer was designed and synthesized. The DMA test showed that the functionalized silicon polymer preserved the heat resistance of the epoxy composite material to a certain extent while strengthening the epoxy. SEM images of the fracture surface of the composites confirm that the novel silicone polymer PSOL-(N-TMSPrVaC) is uniformly dispersed in the epoxy resin. The impact resistance reaches the highest value with 3.0 phr PSOL-(N-TMSPrVaC), the percentage was increased by 18.2% compared to pure epoxy resin.

Polymer matrix composites were produced from type I collagen fibers as reinforcement and epoxy matrices with varying fiber volume fractions, namely 10%, 20%, 30% and 40% [85]. The obtained results were tabulated and the following conclusions were drawn: the specific wear rate of the composites decreased as the percentage content of fibers increased, from the investigation the minimum wear rate for collagen reinforced composites of 30% volume loading was observed of 15 N, collagen fibers embedded in epoxies can considerably reduce abrasive wear losses. At a fiber composition of 30% volume fraction, the best wear resistance property was obtained.

In the paper [86], materials based on Multicast polyurethane resin and ISO 2 hardener and copper wires were designed. Based on the results of the experimental tests, in the case of the characteristic curves for the specimens reinforced with three copper wires, an increase in the maximum force can be observed, compared to the unreinforced specimens, by 17.51% and a significant increase in the maximum elongation, by 42.25% compared to of the unreinforced specimens. Glass fiber reinforced polymer (GFRP) laminates, a range of thermosetting resins and an infusible thermoplastic resin were used. SEM showed a transition from matrix-dominated failure in the dry state to failure at the fiber-matrix interface in wet and organic-wet specimens. The

THE ANNALS OF "DUNAREA DE JOS" UNIVERSITY OF GALATI
FASCICLE IX. METALLURGY AND MATERIALS SCIENCE
Nº. 4 - 2022, ISSN 2668-4748; e-ISSN 2668-4756
Article DOI: https://doi.org/10.35219/mms.2022.4.19

overall performance of the infusible thermoplastic was good compared to marine resin systems, however, environmental performance could be improved if the thermoplastic resin is used in conjunction with a fiber size that is tailored for use with acrylic resin systems.

Researchers [87], used vinyl ester (VE) resin for additive manufacturing of high-performance vinyl ester resin by direct writing with UV-thermal dual curing ink. The printed and dual-cured VE nanocomposites achieved a Young's modulus of 3.7 GPa and a tensile strength of about 80 MPa, which exceeds by about 10% conventionally cast pure VE cured with methyl ethyl ketone peroxide (MEKP) and, by also indistinguishable from the tensile properties of cast VE nanocomposites with the same composition. The fracture toughness of dual-imprinted and reinforced VE nanocomposites was 16% higher than MEKP-reinforced neat cast VE.

The influence of resin-based bonding agents loaded with different inorganic filler content, with or without adhesive, on the micro tensile strength, biaxial bending strength and adhesive interface morphology of bonded ceramic specimens were investigated [88]. It was shown that increasing inorganic filler content of experimental resin-based bonding agents strengthened bonded feldspathic ceramics. The bonding agent with high filler content produced significantly higher viscosity and film thickness. In contrast, bond strength was lower and structural reliability decreased if no adhesive was used.

The role of heat diffusion on the occurrence of instabilities during the frontal polymerization of an adiabatic channel of neat DCPD resin and unidirectional carbon/DCPD composites was investigated [89], through a numerical analysis based on a thermo-chemical reaction-diffusion model. Numerical study performed on the neat resin showed how these FP-driven instabilities diminish and the wavelength and amplitude of the thermal peak present at the front decrease as the initial monomer temperature increase, leading to an increasingly the most stable of the front. Although these thermal instabilities can influence the quality of the manufactured polymer component, they do not affect the speed of the polymerization front.

Micro fluidization [90], has been proposed as a very promising method to prepare low MWCNT modified epoxy suspensions with improved thermal properties. Sonication was performed for the same purpose for performance comparison. Micro fluidization was found to have the ability to disperse MWCNTs more homogeneously compared to sonication, thus improving the final thermal properties of the composite. The time to prepare the suspension by micro fluidization was shown to be approximately 9.3 times less than the processing time required to prepare the same suspension by sonication. In short, given the characteristics of the near-spontaneous flow field, micro fluidization can be used to various applications of any nano filled modified thermosetting polymers that require very high-quality requirements in terms of particle size of the dispersed phase, particle size distribution and stability of the resulting suspension.

In [91], fast remote response cross-linked recycled polyurea nanocomposites were synthesized by a two-step method involving in situ photo-induced polymerization and hot compression. The dynamic nanocomposites exhibited excellent and fast photo-induced self-healing abilities and regained their mechanical properties after damage. This aspect can be attributed to the synergistic effect of the dynamic exchange reactions in the CPU matrix and the efficient photo-thermal effect of the filler materials. The nanocomposite prepared using 1% CNT exhibited excellent toughness, high elasticity, high tensile strength, efficient photo-thermal shape, memory effect and good recyclability.

Radiation-synthesized inorganic-organic hybrid nanoparticles of inorganic nanoparticles (Ag and CeO_2) in aqueous dispersions containing radiation-synthesized poly(N-vinylpyrrolidone) (PVP) nanogels (NG) were obtained [92]. The experiments showed that there are strong interactions between the inorganic precursors (Ag^+ and Ce^{3+}) and the nanogel before irradiation. The two hybrid systems (Ag/NG and CeO_2/NG) were characterized using X-ray diffraction (XRD) and transmission electron microscopy (TEM). XRD confirmed the formation of crystalline Ag and CeO_2. TEM proved that the inorganic nanoparticles are uniformly distributed in/on the nanogel. Both XRD and TEM confirmed that the inorganic particle size is controlled by the nanogel.

An extrinsic welding method using interfacial covalent bond exchange reactions (CBER) has been investigated to enable strong and repeatable welding of conventional thermosetting composites [93]. Dip treatment and welding time have been shown to significantly affect joint strength. By choosing appropriate immersion and welding conditions, appreciable bond strength has been achieved for epoxy composites. Also, higher resistance could be available for longer welding time.

Researchers [94], made a completely bio-based heat-resistant epoxy network by curing a renewable luteolin-derived epoxy resin (DGELU) with a furan-derived hardener, 5,5′-methylenedifurfurylamine(DFA), anti-flammable and non-toxic for coating applications fire retardant. For comparison, a control sample was prepared by curing commercial petroleum-based epoxydiglycidyl ether of

THE ANNALS OF "DUNAREA DE JOS" UNIVERSITY OF GALATI
FASCICLE IX. METALLURGY AND MATERIALS SCIENCE
Nº. 4 - 2022, ISSN 2668-4748; e-ISSN 2668-4756
Article DOI: https://doi.org/10.35219/mms.2022.4.19

bisphenol A (DGEBA) with a petroleum-based hardener, 4,4′-diaminodiphenylmethane (DDM). The storage modulus at 30 °C and tensile strength of cured DGELU/DFA were 82.5% and 23.2% higher than those of cured DGEBA/DDM. The benzopyrone unit of the luteolin structure led to exceptional carbonization, and the carbon yield for thermal decomposition in nitrogen cured DGELU/DFA was 3.2 times higher than that of cured DGEBA/DDM. The results proved that a bio-derived, anti-flammable, high-strength, and non-toxic heat-resistant epoxy network was successfully developed for highly safe epoxy coating applications.

Polyurea has been used as a reinforcing filler for anti-corrosion and wear-resistant application of epoxy resin [95]. The polyurea nanofiber-reinforced composite layer mainly improved the anti-corrosion performance from three aspects: (a) the polyurea nanofibers were arranged in a staggered arrangement and acted as an excellent barrier for corrosive solutions, the physical barrier effect of the filler was fully applied in coverage; (b) reduction of coating defects resulted in less corrosive environmental infiltration; (c) polyurea nanofibers can evenly distribute the internal stress caused by the expansion of corrosion products and reduce blistering in the coating.

In this paper [96], a new visco-plastic model was developed to predict the rate-dependent nonlinear mechanical behavior of an epoxy resin. The presented model was based on a potential function in which a combination of the second and third invariants of the deviatoric stress tensor as well as the first invariant of the stress tensor was realized. A set of tensile and shear tests at different constant strain rates were performed to investigate the rate dependence of the resin and derive model parameters. Under shear loading, the nonlinearity of the resin stress-strain curve was significantly more evident than that under tensile loading, even at low strain rates. The initial modulus and strength of the resin increased with strain rate under both tensile and shear loads, however this was more significant under shear loading.

A multiscale model was developed and it can simulate the influence of synthetic conditions (such as molar ratio) on the structure and physical properties of thermoset resins (e.g., phenolic resin) by introducing a comprehensive reaction model that includes the addition reaction [97]. The effectiveness of the model was validated by verifying the influence of primary synthetic index, i.e., molar ratio, on the physical and thermal properties (i.e., density and glass transition temperature) of Resol resins. This model can help to develop more efficient and suitable synthetic conditions to obtain products exhibiting the desired material properties.

A new class of high-performance resins based on dicyanoimidazole (DCI) reactive group with flexible structural modification has been developed [98]. This work first introduced a new type of high-performance thermosetting resin with flexible molecular modification capability based on DCI cross-linking groups. Preliminary studies have shown that the synthesized aliphatic-containing DCI model compound (PDBDCI) has higher curing reactivity than phthalonitrile and benzonitrile, and its cured products also exhibit better thermal properties than most thermosetting resins, including phthalonitrile resins containing aliphatic compounds. In conclusion, due to flexible molecular modification, high reactivity, unique aromatic heterocyclic structures, excellent thermal and thermomechanical properties, and easy industrialization, DCI resins present a wide range of application prospects in the field of high-performance thermosetting resins and even functional polymers.

The authors [99], of a new flexible binder with improved mechanical properties for bridge deck applications. This research studied the preparation process, microstructural morphology and mechanical properties of a newly developed thermosetting polyurethane (TPUA) modified asphalt binder. The results showed that the viscosity of TPUA was greatly affected by the preparation temperature and the rate of viscosity increases with the increase of the preparation temperature. The curing time was determined by the change in the absorption peak of the infrared spectra of the NCO groups. When the PU modifier content exceeded 30% by mass, the polyurethane resin (PU) formed a continuous polymer network in the asphalt binder, and the PU had relatively good compatibility with the asphalt binder. In general, the mechanical properties of asphalt binder were substantially improved by incorporating PU resin, generating a flexible binder with favourable application prospects, and PU had relatively good compatibility with asphalt binder. TPUA still showed the characteristics of a viscoelastic material at medium and low temperatures.

Waste thermoset unsaturated polyester resins (WTUPR), potassium carbonate, glycol, and polyvinyl alcohol were used to obtain styrene-maleic acid copolymer (SMC) [100]. The hydrophilic carboxylate/hydroxyl groups and the hydrophobic benzene ring structure of SMC endowed the airgel with amphiphilic properties after physical cross-linking with PVA. The concentration of SMC-K has a significant impact on the performance of AAs, and AAs with SMC-K/PVA ratios of 1:1 or 2:1 exhibited hierarchical pore structures, low densities, good mechanical properties, and affinity/high absorption for water and organic liquids. The good comprehensive performance makes AA a candidate

THE ANNALS OF "DUNAREA DE JOS" UNIVERSITY OF GALATI
FASCICLE IX. METALLURGY AND MATERIALS SCIENCE
Nº. 4 - 2022, ISSN 2668-4748; e-ISSN 2668-4756
Article DOI: https://doi.org/10.35219/mms.2022.4.19

for fast and efficient absorbents. This study provides a new route for high value-added reuse of waste thermosetting polymers.

In [101], the rational design of a functionalized silicone polymer for the modification of epoxy-based composites was carried out. The tensile strength of PSOL-(N-TMSPrVaC)/EP composites was improved by 8.9% compared to pure epoxy resin when the content of PSOL-(N-TMSPrVaC) was 0.5 phr. The impact strength of PSOL-(N-TMSPrVaC)/EP composite reaches the highest value with 3.0 phr PSOL-(NTMSPrVaC). It was increased by 18.2% compared to pure epoxy resin. SEM images of the fracture surface of the composites confirmed that the novel silicone polymer PSOL-(N-TMSPrVaC) was uniformly dispersed in the epoxy resin. In addition, the DMA results showed that the thermal stability of the composites was preserved, while the hardness is improved.

Studies have been conducted on composites based on HTV and RTV silicone rubber and carbon nanotubes for sensors and actuators [102]. HTV and RTV silicone rubber were used as rubber matrix and CNT as nanofiller. This study showed that the incorporation of CNT nanofillers significantly improves the mechanical and electrical properties of rubber nanocomposites. TEM investigations showed that the CNTs had 1-D morphology, diameters of 12–15 nm, and aspect ratios of 70-75. The compressive modulus after incorporating CNTs into HTV rubber nanocomposites at 3 phr was improved by 65% and the tensile modulus was improved by 96%. Similarly, the compressive modulus in RTV rubber nanocomposites at 3 phr improved by 110% and the tensile modulus improved by 105%. Addition of 3phr of CNTs in HTV and RTV rubber nanocomposites led to decreases in electrical resistance to 13 kΩ and 0.3 kΩ. Similarly, the actuation displacement was 2.3 mm (a 920% increase) for RTV silicone and 1.55 mm for HTV silicone rubber (a 1025% increase) from 2 to 12 kV. In addition, strain sensors showed a higher measurement factor for RTV silicone rubber than HTV rubber. The flexible piezoresistive strain sensor showed >100% stretch.

Silicone rubber, silica nanoparticles, benzoyl peroxide, and europium nitrate were used to study the effect of fluorescence labelling on the mechanical properties of silica-filled silicone rubber [103]. It has been shown that when the filler loading reaches 30 phr, especially 40 phr, fluorescence labelling rarely affects the mechanical performance of filled silicone rubber. Therefore, the optimal filler loading is 40 phr for investigating the properties of silicone rubber filled by fluorescent labelling of the SiO_2 filler.

An electrically conductive carbon fiber reinforced plastic (CFRP) was developed for lightning protection by infusing the carbon fiber (CF) fabric with a thermoset resin [104]. The new CFRP fabrication method used a liquid dispersion of heat-resistant resin based on styrene derivatives, including micron-sized polyaniline (PANI)/dodecyl benzene sulfonic acid (DBSA) composite particles. The results indicated a non-uniform distribution of PANI-CP particles between the CF fabric layers and the presence of very small particles on the surface of the CFs inside the bundles, which contributed to high electrical conductivity. Non-uniform particle size distribution was found to increase the density of CFs in bundles.

Sprayed polyurea (SPUA) was used to develop a nonlinear visco-hyperelastic tensile constitutive model over the wide strain rate range [105]. The mechanical properties of SPUA were shown to be strain rate sensitive, i.e., the elastic modulus and tensile stress increase with increasing strain rate, while the strain at fracture is linearly negatively correlated with the logarithm of the strain rate. SPUA is a material sensitive to strain rate, dynamic elastic modulus dependencies, tensile stress.

In [106], an effective strategy for improving the interfacial adhesion of immiscible methylvinyl silicone elastomer/thermoplastic polyurethane blends were addressed by developing a hybrid Janus particle with an amphiphilic brush. According to SEM and AFM analyses, the modified Janus particles were stably located and ordered at the polymer blend interface due to the asymmetry structure of the particles and the interaction between the polymer matrix and similar short polymer chains on the particles. Furthermore, the elongation at break, 300% strain and tensile strength of the blends were also significantly increased due to the compatibilizing effect of the modified Janus particles.

Three types of epoxy systems and glass-coated cobalt-based microwires (GCM) were used to predict the interfacial shear strength before use for fiber-reinforced thermosetting composites based on the impedance-stress effect of ferromagnetic microwires [107]. The local interfacial stress induced by the resin microdroplets significantly improved the microwire impedance, but the stress concentration reduces this improvement effect. The increase in impedance has a non-monotonic linear relationship with the total embedded length, and the absolute value of the slope for the descending side shows the same trend as the IFSS of the GCM-3/resin composites. The proposed IFSS prediction method using Co-based microwires can dramatically simplify the testing process and reduce industrial costs, facilitating the performance optimization and application of advanced fiber-reinforced polymer composites.

A novel healing kinetics modeling methodology was established to facilitate matrix formulation [108]. The proposed kinetic curing methodology established

an explicit link between material chemistry and material modeling overcoming the traditional limitations of standard curing kinetics phenomenological techniques and reducing experimental effort and development time for resin formulation. The Formulation Ratio Superposition (FRS) approach has been shown to satisfactorily approximate the kinetics of ternary mixtures on a wide variety of amine/epoxide systems. Matrix formulations can be tailored to specific design requirements controlling reaction intensity and reaction time by changing the constituent functional group fraction. Characterization of the curing kinetics of the binary blend and matrix parameterization of the constituent functional groups provided greater design flexibility, as complex matrix formulations can be tailored to improve hardness, damage tolerance, and environmental stability.

This paper [109] is an overview of manufacturing defects in fiber-reinforced resin matrix composites, including: resin defects, fiber defects, interface defects, and processing defects. To characterize the defects of composites, the authors synthesize the non-contact detection of composite defects and prospect the development of composite defects in the future. This article analyses and discusses the generation mechanism, distribution, and optimization methods of manufacturing defects in hot press moulding, resin transfer moulding, and additive manufacturing moulding. The main manifestations of defects produced by the carbon fiber reinforced composites processing process are: delamination; rupture; burrs. Delamination is the most serious machining defect, which results in many engineering application problems such as decreased strength and short lifetime in composite structures.

The static and dynamic compressive and tensile response of highly elastic polyurea was investigated in [110]. Curing of thermoset resin and thermoplastic resin, resin infiltration process in hot pressing, resin transfer moulding and 3D printing were described in this article. The formation mechanism of fiber reinforcement defects such as fiber puckering and curling in composites was introduced, and the influence of these defects on the bending and compression properties of the composites was analysed, and showed that fiber misalignment defects would seriously reduce modulus, strength. and the stability of the supporting structures. The main manifestations were delamination, breakage and burrs, which seriously affected the strength and reliability of the connection between components.

7. Conclusions

As a conclusion, efforts to develop nanostructured polymeric materials have attracted attention due to the increasing importance of these materials in the engineering industry, aerospace industry, food industry or biomedical applications. Also, in this paper, the deepening of some aspects regarding the influence of modifying agents as well as their concentrations on the mechanical behavior of the formed materials intended for the study was sought.

Following the analysis of the obtained experimental results, the following conclusions can be displayed: internal properties of materials such as solubility, polymer-payload interactions, polymer chain flexibility, surface charge, stereochemistry, surface chemistry, molecular weight and crystallization ability, etc. They must be considered for choosing the appropriate preparation method and for the appropriate processing.

From the review, it follows that controlling the nanostructure of polymers and adding nanoparticles has led to improvements in structural and functional properties in a number of polymer systems in response to the continuous demands of advanced industrial sectors.

Acknowledgements

This work has been funded by the European Social Fund from the Sectoral Operational Programme Human Capital 2014-2020, through the Financial Agreement with the title "Training of PhD students and postdoctoral researchers in order to acquire applied research skills - SMART", Contract no. 13530/16.06.2022 - SMIS code: 153734.

References

[1]. Gay D., *Matériaux composites, 6e éd. revue et augmentee*, Paris: Lavoisier Hermès, 2015.
[2]. Yao D., *et al.*, *Composition regulation of composite materials in laser powder bed fusion additive manufacturing*, Powder Technology, vol. 408, p. 117795, doi: 10.1016/j.powtec.2022.117795, aug. 2022.
[3]. Mohd Nasir N. H., Usman F., Saggaf A. Saloma, *Development of composite material from Recycled Polyethylene Terephthalate and fly ash: Four decades progress review*, Current Research in Green and Sustainable Chemistry, vol. 5, p. 100280, doi: 10.1016/j.crgsc.2022.100280, 2022.
[4]. Yurrita N., *et al.*, *Composite material incorporating protective coatings for photovoltaic cell encapsulation*, Solar Energy Materials and Solar Cells, vol. 245, p. 111879, doi: 10.1016/j.solmat.2022.111879, sep. 2022.
[5]. Soni A., Chakraborty S., Kumar Das P., Kumar Saha A., *Materials selection of reinforced sustainable composites by recycling waste plastics and agro-waste: An integrated multi-criteria decision making approach*, Construction and Building Materials, vol. 348, p. 128608, doi: 10.1016/j.conbuildmat.2022.128608, sep. 2022.
[6]. Ambaye T. G., Vaccari M., Prasad S., van Hullebusch E. D., Rtimi S., *Preparation and applications of chitosan and cellulose composite materials*, Journal of Environmental Management, vol. 301, p. 113850, doi: 10.1016/j.jenvman.2021.113850, ian. 2022.

THE ANNALS OF "DUNAREA DE JOS" UNIVERSITY OF GALATI
FASCICLE IX. METALLURGY AND MATERIALS SCIENCE
Nº. 4 - 2022, ISSN 2668-4748; e-ISSN 2668-4756
Article DOI: https://doi.org/10.35219/mms.2022.4.19

[7]. Liu M., Chen B., Zhang D., Wang Y., Kan P., *Numerical studies on effective thermal conductivities of the glass/polyimide composite materials under the conditions of conduction & radiation*, International Journal of Heat and Mass Transfer, vol. 180, p. 121764, doi: 10.1016/j.ijheatmasstransfer.2021.121764, dec. 2021.
[8]. Karem M. R., Salih A. I., *Synthesis and characterization of epoxy and natural fiber composite material*, Materials Today: Proceedings, vol. 61, p. 925-929, doi: 10.1016/j.matpr.2021.10.101, 2022.
[9]. Li C., Li Q., Lu X., Ge R., Du Y., Xiong Y., *Inorganic salt based shape-stabilized composite phase change materials for medium and high temperature thermal energy storage: Ingredients selection, fabrication, microstructural characteristics and development, and applications*, Journal of Energy Storage, vol. 55, p. 105252, doi: 10.1016/j.est.2022.105252, nov. 2022.
[10]. Chellamuthu K., Sivakumar M., Parthiban N., *Simulations of composite material blended with thermoplasitc and jute fabric*, Materials Today: Proceedings, p. S221478532204891X, doi: 10.1016/j.matpr.2022.07.268, iul. 2022.
[11]. Januszewski R., Orwat B., Dutkiewicz M., Kownacki I., *Structurally-unique polymeric materials obtained through catalytic post-polymerization protocols*, Materials Today Chemistry, vol. 26, p. 101073, doi: 10.1016/j.mtchem.2022.101073, dec. 2022.
[12]. Allen N. S., Edge M., Hussain S., *Perspectives on yellowing in the degradation of polymer materials: inter-relationship of structure, mechanisms and modes of stabilisation*, Polymer Degradation and Stability, vol. 201, p. 109977, doi: 10.1016/j.polymdegradstab.2022.109977, iul. 2022.
[13]. Zhang J., *et al.*, *A review of epoxy-based composite materials: Synthesis, structure and application for electromagnetic wave absorption*, Journal of Alloys and Compounds, vol. 922, p. 166096, doi: 10.1016/j.jallcom.2022.166096, nov. 2022.
[14]. Sun P., Qin B., Xu J.-F., Zhang X., *Supramonomers for controllable supramolecular polymerization and renewable supramolecular polymeric materials*, Progress in Polymer Science, vol. 124, p. 101486, doi: 10.1016/j.progpolymsci.2021.101486, ian. 2022.
[15]. Chae K., *et al.*, *Mechanical failures of Two-Dimensional materials on polymer substrates*, Applied Surface Science, vol. 605, p. 154736, doi: 10.1016/j.apsusc.2022.154736, dec. 2022.
[16]. Banu K. S., Dutta T., Majumdar G., *Effect of Contamination on Characteristics of Plastic and Polymeric Materials*, Encyclopedia of Materials: Plastics and Polymers, Elsevier, p. 623-636, doi: 10.1016/B978-0-12-820352-1.00210-8, 2022.
[17]. Naito M., *et al.*, *Applicability of composite materials for space radiation shielding of spacecraft*, Life Sciences in Space Research, vol. 31, p. 71-79, doi: 10.1016/j.lssr.2021.08.004, nov. 2021.
[18]. Tuttle M. E., *Structural analysis of polymeric composite materials*, New York: Marcel Dekker, 2004.
[19]. Vijay Kumar V., Ramakrishna S., Rajendran S., Surendran S., *Enhancing the material properties of carbon fiber epoxy composite by incorporating electrospun polyacrylonitrile nanofibers*, Materials Today: Proceedings, p. S2214785322029959, doi: 10.1016/j.matpr.2022.04.818, mai 2022.
[20]. Rana S., Singh V., Singh B., *Recent trends in 2D materials and their polymer composites for effectively harnessing mechanical energy*, iScience, vol. 25, nr. 2, p. 103748, doi: 10.1016/j.isci.2022.103748, feb. 2022.
[21]. Solazzi L., Vaccari M., *Reliability design of a pressure vessel made of composite materials*, Composite Structures, vol. 279, p. 114726, doi: 10.1016/j.compstruct.2021.114726, 2022.
[22]. Ahsan Feroz A., Harshit D. Chawla, Kumar R., *To study and analyze the design of drive shafts for automobiles using composite material through empirical review on literature*, Materials Today: Proceedings, vol. 56, p. 3820-3822, doi: 10.1016/j.matpr.2022.01.309, 2022.
[23]. Yurkov G. Y., *et al.*, *Composite materials based on a ceramic matrix of polycarbosilane and iron-containing nanoparticles*, Ceramics International, p. S0272884222032722, doi: 10.1016/j.ceramint.2022.09.096, sep. 2022.
[24]. Blachowicz T., Grzybowski J., Ehrmann A., *Influence of agglomerations on magnetic properties of polymer matrices filled with magnetic nanoparticles*, Materials Today: Proceedings, p. S2214785322050039, doi: 10.1016/j.matpr.2022.07.362, 2022.
[25]. Arkas M., *et al.*, *Investigation of two bioinspired reaction mechanisms for the optimization of nano catalysts generated from hyperbranched polymer matrices*, Reactive and Functional Polymers, vol. 174, p. 105238, doi: 10.1016/j.reactfunctpolym.2022.105238, 2022.
[26]. Apryatina K. V., Salomatina E. V., Sologubov S. S., Markin A. V., Smirnova L. A., *Specific features of thermal properties of polymer composites containing conductive nanoparticles in non-conductive polymer matrices*, Thermochimica Acta, vol. 705, p. 179036, doi: 10.1016/j.tca.2021.179036, 2021.
[27]. Shakeel A., *et al.*, *Polymer based nanocomposites: A strategic tool for detection of toxic pollutants in environmental matrices*, Chemosphere, vol. 303, p. 134923, doi: 10.1016/j.chemosphere.2022.134923, sep. 2022.
[28]. Brandner S., Becker T., Jekle M., *Impact of the particle-polymer interface on small- and large-scale deformation response in protein- and carbohydrate-based food matrices*, International Journal of Biological Macromolecules, vol. 191, p. 51-59, doi: 10.1016/j.ijbiomac.2021.09.048, nov. 2021.
[29]. Ventura-Cruz S., Tecante A., *Nanocellulose and microcrystalline cellulose from agricultural waste: Review on isolation and application as reinforcement in polymeric matrices*, Food Hydrocolloids, vol. 118, p. 106771, doi: 10.1016/j.foodhyd.2021.106771, sep. 2021.
[30]. Bokka S., Chowdhury A., *Reviewing the Potential of Novel Nanofillers in Polymer Matrices for Advanced Technological Applications*, Encyclopedia of Materials: Plastics and Polymers, Elsevier, p. 662-698, doi: 10.1016/B978-0-12-820352-1.00132-2, 2022.
[31]. Amulya K., Katakojwala R., Ramakrishna S., Venkata Mohan S., *Low carbon biodegradable polymer matrices for sustainable future*, Composites Part C: Open Access, vol. 4, p. 100111, doi: 10.1016/j.jcomc.2021.100111, mar. 2021.
[32]. Vom Saal F. S., Nagel S. C., Coe B. L., Angle B. M., Taylor J. A., *The estrogenic endocrine disrupting chemical bisphenol A (BPA) and obesity*, Mol Cell Endocrinol, vol. 354, no. 1-2, p. 74-84, doi: 10.1016/j.mce.2012.01.001, 2012.
[33]. Idumah C. I., *Progress in polymer nanocomposites for bone regeneration and engineering*, Polymers and Polymer Composites, vol. 29, no. 5, p. 509-527, doi: 10.1177/0967391120913658, 2021.
[34]. Pradeep S. A., Iyer R. K., Kazan H., Pilla S., *Automotive Applications of Plastics: Past, Present, and Future*, Applied Plastics Engineering Handbook, Elsevier, p. 651-673, doi: 10.1016/B978-0-323-39040-8.00031-6, 2017.
[35]. Brydson J. A., *Plastics materials*, 7th ed., Oxford,; Boston: Butterworth-Heinemann, 1999.
[36]. Xu G., Wang Q., *Chemically recyclable polymer materials: polymerization and depolymerization cycles*, Green Chem., vol. 24, no. 6, p. 2321-2346, doi: 10.1039/D1GC03901F, 2022.
[37]. Loganathan N. N., Perumal V., Pandian B. R., Atchudan R., Edison T. N. J. I., Ovinis M., *Recent studies on polymeric materials for supercapacitor development*, Journal of Energy Storage, vol. 49, p. 104149, doi: 10.1016/j.est.2022.104149, 2022.
[38]. García-Collado A., Blanco J. M., Gupta M. K., Dorado-Vicente R., *Advances in polymers based Multi-Material Additive-Manufacturing Techniques: State-of-art review on properties and applications*, Additive Manufacturing, vol. 50, p. 102577, doi: 10.1016/j.addma.2021.102577, feb. 2022.
[39]. Olaitan Ayeleru O., Apata Olubambi P., *Concept of self-healing in polymeric materials*, Materials Today: Proceedings, vol. 62, p. S158-S162, doi: 10.1016/j.matpr.2022.04.811, 2022.
[40]. Maqbool M., Aftab W., Bashir A., Usman A., Guo H., Bai S., *Engineering of polymer-based materials for thermal management solutions*, Composites Communications, vol. 29, p. 101048, doi: 10.1016/j.coco.2021.101048, 2022.

THE ANNALS OF "DUNAREA DE JOS" UNIVERSITY OF GALATI
FASCICLE IX. METALLURGY AND MATERIALS SCIENCE
Nº. 4 - 2022, ISSN 2668-4748; e-ISSN 2668-4756
Article DOI: https://doi.org/10.35219/mms.2022.4.19

[41]. Holkem A. P., Iop G. D., Bitencourt G. R., Flores E. M. M., Mesko M. F., Mello P. A., *Combining microwave and ultraviolet energy for sample preparation of polymer-based materials for further halogen determination*, Advances in Sample Preparation, vol. 4, p. 100038, doi: 10.1016/j.sampre.2022.100038, oct. 2022.
[42]. Rasheed T., Naveed A., Chen J., Raza B., Wang J., *Revisiting the role of polymers as renewable and flexible materials for advanced batteries*, Energy Storage Materials, vol. 45, p. 1012-1039, doi: 10.1016/j.ensm.2021.10.037, 2022.
[43]. Marieta C., Remiro P. M., Garmendia G., Harismendy I., Mondragon I., *AFM approach toward understanding morphologies in toughened thermosetting matrices*, European Polymer Journal, vol. 39, nr. 10, p. 1965-1973, doi: 10.1016/S0014-3057(03)00113-7, oct. 2003.
[44]. Gnädinger F., Middendorf P., Fox B., *Interfacial shear strength studies of experimental carbon fibres, novel thermosetting polyurethane and epoxy matrices and bespoke sizing agents*, Composites Science and Technology, vol. 133, p. 104-110, doi: 10.1016/j.compscitech.2016.07.029, sep. 2016.
[45]. Gebhardt M., Manolakis I., Kalinka G., Deubener J., Chakraborty S., Meiners D., *Re-use potential of carbon fibre fabric recovered from infusible thermoplastic CFRPs in 2nd generation thermosetting-matrix composites*, Composites Communications, vol. 28, p. 100974, doi: 10.1016/j.coco.2021.100974, dec. 2021.
[46]. John B., Reghunadhan Nair C. P., *Thermosetting polymer based syntactic foams: an overview*, Handbook of Thermoset Plastics, Elsevier, p. 801-832, doi: 10.1016/B978-0-12-821632-3.00020-8, 2022.
[47]. Çakir M., Akin E., *Characterization of carbon fiber-reinforced thermoplastic and thermosetting polyimide matrix composites manufactured by using various synthesized PI precursor resins*, Composites Part B: Engineering, vol. 231, p. 109559, doi: 10.1016/j.compositesb.2021.109559, feb. 2022.
[48]. Restaino A. J., James D. B., Ko F. K., Beaumont P. W. R., Wells J. K., *Thermosetting Resin Matrices*, Concise Encyclopedia of Composite Materials, Elsevier, p. 289-309, doi: 10.1016/B978-0-08-042300-5.50028-5, 1994.
[49]. Wippl J., Schmidt H.-W., Giesa R., *High Temperature Thermosets with a Low Coefficient of Thermal Expansion*, Macromol. Mater. Eng., vol. 290, no. 7, p. 657-668, doi: 10.1002/mame.200500120, 2005.
[50]. Yang S., *et al.*, *Synthesis of tung oil-based vinyl ester resin and its application for anti-corrosion coatings*, Progress in Organic Coatings, vol. 170, p. 106967, doi: 10.1016/j.porgcoat.2022.106967, sep. 2022.
[51]. Zhang X., Zhang W., Pan Y.-T., Qian L., Qin Z., Zhang W., *Synthesis and performance of intrinsically flame-retardant, low-smoke biobased vinyl ester resin*, Reactive and Functional Polymers, vol. 171, p. 105158, doi: 10.1016/j.reactfunctpolym.2021.105158, feb. 2022.
[52]. Huang Z., Deng Z., Dong C., Fan J., Ren Y., *A closed-loop recycling process for carbon fiber reinforced vinyl ester resin composite*, Chemical Engineering Journal, vol. 446, p. 137254, doi: 10.1016/j.cej.2022.137254, oct. 2022.
[53]. Chen B., *et al.*, *A universal strategy toward flame retardant epoxy resin with ultra-tough and transparent properties*, Polymer Degradation and Stability, p. 110132, doi: 10.1016/j.polymdegradstab.2022.110132, sep. 2022.
[54]. Sun Q., Feng Y., Guo J., Wang C., *High performance epoxy resin with ultralow coefficient of thermal expansion cured by conformation-switchable multi-functional agent*, Chemical Engineering Journal, vol. 450, p. 138295, doi: 10.1016/j.cej.2022.138295, dec. 2022.
[55]. Wang Y., Wang C., Zhou S., Liu K., *Effect of amination rate and neutralization degree of cationic epoxy resin on the repair effect of electrophoretic deposition*, Progress in Organic Coatings, vol. 172, p. 107069, doi: 10.1016/j.porgcoat.2022.107069, nov. 2022.
[56]. Yu D., *et al.*, *Preparation and performance of pervious concrete with wood tar-formaldehyde-modified epoxy resins*, Construction and Building Materials, vol. 350, p. 128819, doi: 10.1016/j.conbuildmat.2022.128819, oct. 2022.
[57]. Zhao Y., Kikugawa G., Kawagoe Y., Shirasu K., Okabe T., *Molecular-scale investigation on relationship between thermal conductivity and the structure of crosslinked epoxy resin*, International Journal of Heat and Mass Transfer, vol. 198, p. 123429, doi: 10.1016/j.ijheatmasstransfer.2022.123429, dec. 2022.
[58]. Zhi M., *et al.*, *A comprehensive review of reactive flame-retardant epoxy resin: fundamentals, recent developments, and perspectives*, Polymer Degradation and Stability, vol. 201, p. 109976, doi: 10.1016/j.polymdegradstab.2022.109976, 2022.
[59]. Jia C., Li J., Wang Q., Li Z., Pu L., *Analysis of low-energy impact damage to epoxy resin film based on surface damage characteristics*, Progress in Organic Coatings, vol. 172, p. 107147, doi: 10.1016/j.porgcoat.2022.107147, 2022.
[60]. Fiore V., Valenza A., *Epoxy resins as a matrix material in advanced fiber-reinforced polymer (FRP) composites*, Advanced Fibre-Reinforced Polymer (FRP) Composites for Structural Applications, Elsevier, p. 88-121, doi: 10.1533/9780857098641.1.88, 2013.
[61]. Bachchan A. A., Das P. P., Chaudhary V., *Effect of moisture absorption on the properties of natural fiber reinforced polymer composites: A review*, Materials Today: Proceedings, p. S2214785321019751, doi: 10.1016/j.matpr.2021.02.812, 2021.
[62]. Ascione F., Lamberti M., Napoli A., Razaqpur G., Realfonzo R., *An experimental investigation on the bond behavior of steel reinforced polymers on concrete substrate*, Composite Structures, vol. 181, p. 58-72, doi: 10.1016/j.compstruct.2017.08.063, 2017.
[63]. Andrew J. J., Srinivasan S. M., Arockiarajan A., Dhakal H. N., *Parameters influencing the impact response of fiber-reinforced polymer matrix composite materials: A critical review*, Composite Structures, vol. 224, p. 111007, doi: 10.1016/j.compstruct.2019.111007, sep. 2019.
[64]. Azimpour-Shishevan F., Akbulut H., Mohtadi-Bonab M. A., *Synergetic effects of carbon nanotube and graphene addition on thermo-mechanical properties and vibrational behavior of twill carbon fiber reinforced polymer composites*, Polymer Testing, vol. 90, p. 106745, doi: 10.1016/j.polymertesting.2020.106745, 2020.
[65]. Birsan I. G., Bria V., Bunea M., Circiumaru A., *An Experimental Investigation of Thermal Properties of Fabric Reinforced Epoxy Composites*, Mater. Plast., vol. 57, no. 2, p. 159-168, doi: 10.37358/MP.20.2.5362, 2019.
[66]. Bedi H. S., Kumar S., Agnihotri P. K., *Wettability of thermoplastic and thermoset polymers with carbon nanotube grafted carbon fiber*, Materials Today: Proceedings, vol. 41, p. 838-842, doi: 10.1016/j.matpr.2020.09.162, 2021.
[67]. Benin S. R., Kannan S., Bright R. J., Jacob Moses A., *A review on mechanical characterization of polymer matrix composites & its effects reinforced with various natural fibres*, Materials Today: Proceedings, vol. 33, p. 798-805, doi: 10.1016/j.matpr.2020.06.259, 2020.
[68]. Das P., Banerjee S., Das N. C., *Polymer-graphene composite in aerospace engineering*, Polymer Nanocomposites Containing Graphene, Elsevier, p. 683-711, doi: 10.1016/B978-0-12-821639-2.00001-X, 2022.
[69]. Fanteria D., Lazzeri L., Panettieri E., Mariani U., Rigamonti M., *Experimental characterization of the interlaminar fracture toughness of a woven and a unidirectional carbon/epoxy composite*, Composites Science and Technology, vol. 142, p. 20-29, doi: 10.1016/j.compscitech.2017.01.028, apr. 2017.
[70]. Forintos N., Czigany T., *Multifunctional application of carbon fiber reinforced polymer composites: Electrical properties of the reinforcing carbon fibers – A short review*, Composites Part B: Engineering, vol. 162, p. 331-343, doi: 10.1016/j.compositesb.2018.10.098, apr. 2019.
[71]. Cao Y., *et al.*, *Computational parameter identification of strongest influence on the shear resistance of reinforced concrete*

beams by fiber reinforcement polymer, Structures, vol. 27, p. 118-127, doi: 10.1016/j.istruc.2020.05.031, oct. 2020.

[72]. Gabriel Andrei, Dumitru Dima, Bîrsan I. G., Laurenția Andrei, Adrian Cîrciumaru, *Effect of Ferrite Particles on Mechanical Behaviour of Glass Fibers Reinforced Polymer Composite*, Materiale Plastice, vol. 46, no. 3, p. 284-287, 2009.

[73]. Green S. D., Matveev M. Y., Long A. C., Ivanov D., Hallett S. R., *Mechanical modelling of 3D woven composites considering realistic unit cell geometry*, Composite Structures, vol. 118, p. 284-293, doi: 10.1016/j.compstruct.2014.07.005, 2014.

[74]. Goli E., *et al.*, *Frontal polymerization of unidirectional carbon-fiber-reinforced composites*, Composites Part A: Applied Science and Manufacturing, vol. 130, p. 105689, doi: 10.1016/j.compositesa.2019.105689, mar. 2020.

[75]. Waltham, M. A., *Design and applications of nanostructured polymer blends and nanocomposite systems*, 1st edition, Elsevier, 2015.

[76]. Zavyalov S., *Formation and characterization of metal-polymer nanostructured composites*, Solid State Ionics, vol. 147, no. 3-4, p. 415-419, doi: 10.1016/S0167-2738(02)00038-3, 2002.

[77]. Yang P., Ren M., Chen K., Liang Y., Lü Q.-F., Zhang T., *Synthesis of a novel silicon-containing epoxy resin and its effect on flame retardancy, thermal, and mechanical properties of thermosetting resins*, Materials Today Communications, vol. 19, p. 186-195, doi: 10.1016/j.mtcomm.2019.01.014, 2019.

[78]. Whang S. H., *Nanostructured metals and alloys: processing, microstructure, mechanical properties and applications*, Oxford: WP, Woodhead Publ, 2011.

[79]. Teran A. A., Tang M. H., Mullin S. A., Balsara N. P., *Effect of molecular weight on conductivity of polymer electrolytes*, Solid State Ionics, vol. 203, no. 1, p. 18-21, doi: 10.1016/j.ssi.2011.09.021, 2011.

[80]. ter Horst B., Moiemen N. S., Grover L. M., *Natural polymers*, Biomaterials for Skin Repair and Regeneration, Elsevier, p. 151-192, doi: 10.1016/B978-0-08-102546-8.00006-6, 2019.

[81]. Thakur T., Jaswal S., Parihar S., Gaur B., Singha A. S., *Bio-based epoxy thermosets with rosin derived imidoamine curing agents and their structure-property relationships*, Express Polym. Lett., vol. 14, no. 6, p. 512-529, doi: 10.3144/expresspolymlett.2020.42, 2020.

[82]. Mehnath S., Das A. K., Verma S. K., Jeyaraj M., *Biosynthesized/green-synthesized nanomaterials as potential vehicles for delivery of antibiotics/drugs*, Comprehensive Analytical Chemistry, vol. 94, Elsevier, p. 363-432, doi: 10.1016/bs.coac.2020.12.011, 2021.

[83]. Mishra T., Mandal P., Rout A. K., Sahoo D., *A state-of-the-art review on potential applications of natural fiber-reinforced polymer composite filled with inorganic nanoparticle*, Composites Part C: Open Access, vol. 9, p. 100298, doi: 10.1016/j.jcomc.2022.100298, oct. 2022.

[84]. Shi Y.-C., *et al.*, *Rational design of a functionalized silicone polymer for modifying epoxy-based composites*, Journal of Materials Research and Technology, vol. 19, p. 3867-3876, doi: 10.1016/j.jmrt.2022.06.086, 2022.

[85]. Hemanth B., Hanumantharaju H. G., Prashanth K. P., Venkatesha B. K., *Investigation of wear characteristics of collagen fiber reinforced polymer matrix composites used for orthopaedic implants*, Materials Today: Proceedings, vol. 54, p. 498-501, doi: 10.1016/j.matpr.2021.11.429, 2022.

[86]. Petrașcu O.-L., Manole R., Pascu A.-M., *The behavior of composite materials based on polyurethan resin subjected to uniaxial tensile test*, Materials Today: Proceedings, vol. 62, p. 2673-2678, doi: 10.1016/j.matpr.2022.05.308, 2022.

[87]. Tu R., Sodano H. A., *Additive manufacturing of high-performance vinyl ester resin via direct ink writing with UV-thermal dual curing*, Additive Manufacturing, vol. 46, p. 102180, doi: 10.1016/j.addma.2021.102180, oct. 2021.

[88]. Barbon F. J., Moraes R. R., Isolan C. P., Spazzin A. O., Boscato N., *Influence of inorganic filler content of resin luting agents and use of adhesive on the performance of bonded ceramic*, The Journal of Prosthetic Dentistry, vol. 122, no. 6, p. 566.e1-566.e11, doi: 10.1016/j.prosdent.2019.09.013, dec. 2019.

[89]. Goli E., Peterson S. R., Geubelle P. H., *Instabilities driven by frontal polymerization in thermosetting polymers and composites*, Composites Part B: Engineering, vol. 199, p. 108306, doi: 10.1016/j.compositesb.2020.108306, oct. 2020.

[90]. Durukan O., Kahraman I., Parlevliet P., Geistbeck M., Seyhan A. T., *Microfluidization, time-effective and solvent free processing of nanoparticle containing thermosetting matrix resin suspensions for producing composites with enhanced thermal properties*, European Polymer Journal, vol. 85, p. 575-587, doi: 10.1016/j.eurpolymj.2016.11.012, dec. 2016.

[91]. Zhou Z., *et al.*, *Remotely fast response healing crosslinked polyurea nanocomposites with recyclability via two-step method*, Composites Science and Technology, vol. 224, p. 109462, doi: 10.1016/j.compscitech.2022.109462, 2022.

[92]. Li Z., *et al.*, *Inorganic/organic hybrid nanoparticles synthesized in a two-step radiation-driven process*, Radiation Physics and Chemistry, vol. 197, p. 110166, doi: 10.1016/j.radphyschem.2022.110166, aug. 2022.

[93]. An L., Li X., Jin C., Zhao W., Shi Q., *An extrinsic welding method for thermosetting composites: Strong and repeatable*, Composites Part B: Engineering, vol. 245, p. 110224, doi: 10.1016/j.compositesb.2022.110224, oct. 2022.

[94]. Wang X., Nabipour H., Kan Y.-C., Song L., Hu Y., *A fully bio-based, anti-flammable and non-toxic epoxy thermosetting network for flame-retardant coating applications*, Progress in Organic Coatings, vol. 172, p. 107095, doi: 10.1016/j.porgcoat.2022.107095, nov. 2022.

[95]. Huang Y., *et al.*, *Polyurea as a reinforcing filler for the anti-corrosion and wear-resistant application of epoxy resin*, Progress in Organic Coatings, vol. 171, p. 107049, doi: 10.1016/j.porgcoat.2022.107049, oct. 2022.

[96]. Shafiei E., Kiasat M. S., *A new viscoplastic model and experimental characterization for thermosetting resins*, Polymer Testing, vol. 84, p. 106389, doi: 10.1016/j.polymertesting.2020.106389, apr. 2020.

[97]. Li J., *et al.*, *A multiscale model for the synthesis of thermosetting resins: From the addition reaction to cross-linked network formation*, Chemical Physics Letters, vol. 720, p. 64-69, doi: 10.1016/j.cplett.2019.02.012, apr. 2019.

[98]. Hu J., *et al.*, *A novel development route for cyano-based high performance thermosetting resins via the strategy of functional group design-dicyanoimidazole resins*, Polymer, vol. 203, p. 122823, doi: 10.1016/j.polymer.2020.122823, aug. 2020.

[99]. Yang F., Cong L., Li Z., Yuan J., Guo G., Tan L., *Study on preparation and performance of a thermosetting polyurethane modified asphalt binder for bridge deck pavements*, Construction and Building Materials, vol. 326, p. 126784, doi: 10.1016/j.conbuildmat.2022.126784, 2022.

[100]. Wang X.-L., *et al.*, *Recycling waste thermosetting unsaturated polyester resins into oligomers for preparing amphiphilic aerogels*, Waste Management, vol. 126, p. 89-96, doi: 10.1016/j.wasman.2021.03.002, 2021.

[101]. Shi Y.-C., *et al.*, *Rational design of a functionalized silicone polymer for modifying epoxy-based composites*, Journal of Materials Research and Technology, vol. 19, p. 3867-3876, doi: 10.1016/j.jmrt.2022.06.086, 2022.

[102]. Kumar V., Lee G. Monika, Choi J., Lee D.-J., *Studies on composites based on HTV and RTV silicone rubber and carbon nanotubes for sensors and actuators*, Polymer, vol. 190, p. 122221, doi: 10.1016/j.polymer.2020.122221, 2020.

[103]. Xiong Y., Shen S., Kang M., Wang Z., Lu A., *Effect of fluorescence labeling on mechanical properties of silica filled silicone rubber*, Polymer, vol. 208, p. 122904, doi: 10.1016/j.polymer.2020.122904, 2020.

[104]. Takahashi K., Yaginuma K., Goto T., Yokozeki T., Okada T., Takahashi T., *Electrically conductive carbon fiber reinforced plastics induced by uneven distribution of polyaniline composite micron-sized particles in thermosetting matrix*,

Composites Science and Technology, vol. 228, p. 109642, doi: 10.1016/j.compscitech.2022.109642, 2022.

[105]. Chen D., Wu H., Wei J. S., Xu S. L., Fang Q., *Nonlinear visco-hyperelastic tensile constitutive model of spray polyurea within wide strain-rate range*, International Journal of Impact Engineering, vol. 163, p. 104184, doi: 10.1016/j.ijimpeng.2022.104184, 2022.

[106]. Hu J., Song Y., Ning N., Zhang L., Yu B., Tian M., *An effective strategy for improving the interface adhesion of the immiscible methyl vinyl silicone elastomer/thermoplastic polyurethane blends via developing a hybrid janus particle with amphiphilic brush*", Polymer, vol. 214, p. 123375, doi: 10.1016/j.polymer.2020.123375, feb. 2021.

[107]. Xu P., *et al.*, *Pre-use interfacial shear strength prediction for fiber-reinforced thermosetting composites based on stress-impedance effect of ferromagnetic microwires*, Composites Part A: Applied Science and Manufacturing, vol. 152, p. 106684, doi: 10.1016/j.compositesa.2021.106684, 2022.

[108]. Voto G., Sequeira L., Skordos A. A., *Formulation based predictive cure kinetics modelling of epoxy resins*, Polymer, vol. 236, p. 124304, doi: 10.1016/j.polymer.2021.124304, 2021.

[109]. Fu Y., Yao X., *A review on manufacturing defects and their detection of fiber reinforced resin matrix composites*", Composites Part C: Open Access, vol. 8, p. 100276, doi: 10.1016/j.jcomc.2022.100276, 2022.

[110]. Wang X., *et al.*, *Static and dynamic compressive and tensile response of highly stretchable polyurea*, International Journal of Impact Engineering, vol. 166, p. 104250, doi: 10.1016/j.ijimpeng.2022.104250, 2022.

THE ANNALS OF "DUNAREA DE JOS" UNIVERSITY OF GALATI
FASCICLE IX. METALLURGY AND MATERIALS SCIENCE
Nº. 4 - 2022, ISSN 2668-4748; e-ISSN 2668-4756
Article DOI: https://doi.org/10.35219/mms.2022.4.20

MATERIAL RECOGNITION USING CNN APPROACH FOR GARBAGE COLLECTION SYSTEM

Florin-Bogdan MARIN, Mihaela MARIN, Gheorghe GURĂU
"Dunarea de Jos" University of Galati, Romania
e-mail: flmarin@ugal.ro

ABSTRACT

Material identification has been proved to be of important interest for different fields such as industrial automation, autonomous robots The autonomous robots for garbage collection, such as aquatic-cleaning [3] or garbage gathering [6] need the algorithm for identification of materials. Automatic conveyer identification for garbage collection and segregation also use algorithm for material identification. In this paper is proposed an algorithm based on Convolutional Neural Network.

KEYWORDS: material identification, waste management, convolutional neural network

1. Introduction

Material identification has been proved to be of important interest for different fields such as industrial automation, autonomous robots, autonomous navigation or autonomous car. In case of industrial application material identification resumes to find the exceptional cases where the material structure indicates there is the correct part selected. In recent years, using the latest computer vision algorithms, semantic description of the scene is taken in to account, where all the objects in the scene, such as tree, car, street, buildings are identified in order to identify the road and dangerous situation for driving. One of the components of the scene identification could be also the material identification of objects. For autonomous navigation, such in case of delivery autonomous robots already available for public use, the identification of an area with snow is very important, as this might cause blocking the robot. Researchers use classic computer vision algorithms, such as image filters and conduct quantitatively analyse of the material. For instance, a Canny algorithm filter followed by contour identification might indicate by the amount of certain dimension of contours a certain material.

Concerning Artificial intelligence there are various initiative for to develop different material databases: CUReT database or Flicker Material Database. Databases contain different material samples taken at different illumination levels. OpenSurfaces data base has more than 110,000 segmented materials. Understanding of the material composition of a scene is paramount in the scene understanding problem, such in case of automated system to collect garbage.

Fig. 1. *Example of material identification problem* [1]

The autonomous robots for garbage collection, such as aquatic-cleaning [3] or garbage gathering [6] need the algorithm for identification of materials. Automatic conveyer identification for garbage collection and segregation (Fig. 2) also use algorithm for material identification. While the shape detection is one of the phases of identification, there are objects that have the same shape but different material. In such a garbage collector system a robotic-like arm or actuator collects garbage automatically through a conveyer transporting different objects. For which we are designing an arena for the machine. The actuator is controlled by a software that is processing image from a camera located above the conveyer. The software send command to the robotic arm to collect the stationary waste [3].

THE ANNALS OF "DUNAREA DE JOS" UNIVERSITY OF GALATI
FASCICLE IX. METALLURGY AND MATERIALS SCIENCE
Nº. 4 - 2022, ISSN 2668-4748; e-ISSN 2668-4756
Article DOI: https://doi.org/10.35219/mms.2022.4.20

HDPE	Aluminum	PET Transparent	PET Dark	PET Green	PET Blue	PET Teal	PET Multicolor	Other	**Total**
4978	3411	1749	1477	511	1041	309	52	1007	14 535

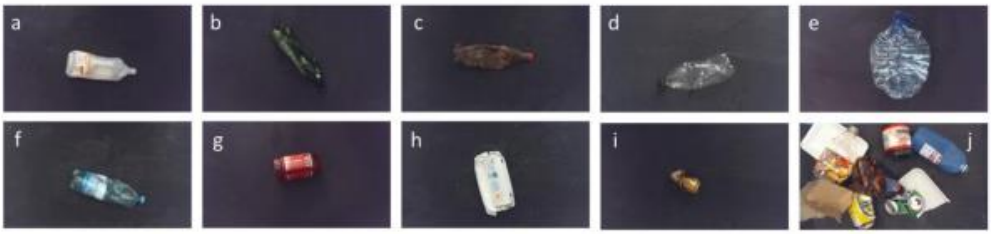

Fig. 2. *Examples of waste objects images from the created database: a) HDPE; b) PET green; c) PET dark; d) PET transparent; e) PET blue; f) PET teal; g) PET multicolour; h) 'other'; i) aluminium can; j) multiple objects scene*

2. Experimental procedure

We considered that different objects representing garbage, as in case of a garbage conveyer, are located 600 mm above the scene. The conveyer is transporting the garbage with the speed of 0.3 meters/s. Though the speed might produce a distorted image the algorithm is correctly identified the objects.

The algorithm is described in Fig. 3 The image is filtered in order to obtain blob analysis to identify parts in image with the same characteristics. The algorithm is using CNN (Convolutional Neural Network) to identify 3 types of material, namely paper, fabric and plastics. The test images consisted of 30 different images containing the 3 types of materials. As seen in Fig. 7 the false positive identification produces the identification the object made of metal as one in the three classes indicated.

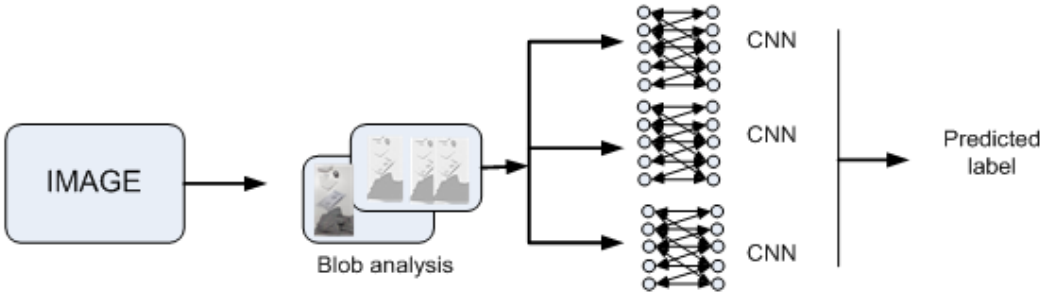

Fig. 3. *Algorithm for material recognition*

3. Results and discussions

We used own set for training of 100 images for each type. The recognition rate is about 80% and the false positive detection rate is 15%. The trained set included objects that are different from the testing test set. The trained set was obtained using different illumination. The algorithm needs lower computer resources. We used an i5-11260H processor on a computer with 16 Gb. The image is acquired with a Logitech C505 webcam. The resolution used is 1200 X 800 pixels. The processing speed is in the range 200-300 ms. We note that not all images acquired in the video stream is processed as some are blurred and are not processed. We used own algorithm to detect blurred images, with a speed of 20-30 ms per frame. In case a blurred image is detected the algorithm for detection of material is not used and we skip to the next image. The blob analysis is applied to each image in 5 different filters in order to identify materials with the same texture. The texture with many information is quite hard to detect. Using blob analysis followed by CNN network we obtain satisfying results. However further development needs to use several filters in order to obtain better results. Also, better results should be obtained using a higher number of images to be trained. In figure 6 is depicted the scene acquired by the camera to be processed by computer. Several materials are on the scene. In Figure 7 is shown the identification results. In this picture is shown a false positive identification, the software identifies as plastic the metal part on the conveyer.

THE ANNALS OF "DUNAREA DE JOS" UNIVERSITY OF GALATI
FASCICLE IX. METALLURGY AND MATERIALS SCIENCE
Nº. 4 - 2022, ISSN 2668-4748; e-ISSN 2668-4756
Article DOI: https://doi.org/10.35219/mms.2022.4.20

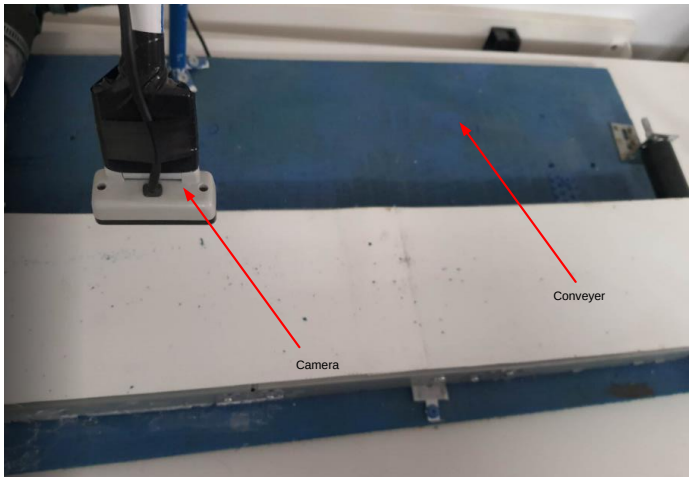

Fig. 4. *Conveyer used for material identification*

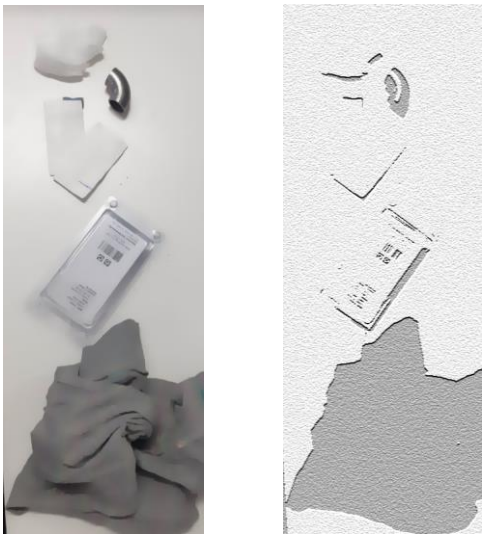

Fig. 5. *Blob analysis result of the image*

Fig. 6. *Detection of different materials*

Fig. 7. *Detection of different materials*

THE ANNALS OF "DUNAREA DE JOS" UNIVERSITY OF GALATI
FASCICLE IX. METALLURGY AND MATERIALS SCIENCE
N°. 4 - 2022, ISSN 2668-4748; e-ISSN 2668-4756
Article DOI: https://doi.org/10.35219/mms.2022.4.20

4. Conclusions

The study of material detection for garbage collection shows that the task of identifying materials in garbage is a challenging task. Using blob analysis followed by CNN network we obtain satisfying results. However further development needs to use several filters in order to obtain better results. Also, better results should be obtained using a higher number of images to be trained.

References

[1]. ***, *Raport tehnic, etapa I*, proiectul PN-III-P2-2.1-PTE-2019-0085.
[2]. Seredkin A. V., *et al.*, *Development of a method of detection and classification of waste objects on a conveyor for a robotic sorting system*, J. Phys., Conf. Ser., 1359, 012127, 2019.
[3]. ***, *Automated Garbage Collector*, Technomentis, https://www.instructables.com/id/Automated-Garbage-Collector/, accessed on April 10, 2019.
[4]. Bai J., Lian S., Liu Z., Wang K., Liu D., *Deep Learning Based Robot for Picking up Garbage on the Grass Automatically*, Proc. IEEE Transaction on Consumer Electronics, TCE, 2859629, 2018.
[5]. Zhihong C., Hebin Z., Yan W., Yanbo W., Binyan L., *Multi-task Detection System for Garbage Sorting base on High-order Fusion of Convolutional Feature Hierarchical Representation*, Proc. 37th Chinese Control Conference, 2018.
[6]. Ren S., He K., Girshick R., Sun J., *Faster r-cnn: Towards real-time object detection with region proposal networks*, Proc. NIPS, 2015.
[7]. Huang J., Rathod V., Sun C., Zhu M., Korattikara A., Fathi A., Fischer I., Wojna Z., Song Y., Guadarrama S., Murphy K., arXiv arXiv:1611.10012v, 2017.
[8]. Chen S., Wang D., Liu T., Ren W., Zhong Y., *An autonomous ship for cleaning the garbage floating on a lake*, 2nd Int. Conf. Intell. Comput. Technol. Autom., Changsha, p. 471-474, 2009.
[5]. Zhang H., Zhang J., Zong G., Wang W., Liu R., *Sky Cleaner 3: a real pneumatic climbing robot for glass-wall cleaning*, IEEE Robot. Autom. Mag., vol. 13, no. 1, p. 32-41, Mar. 2006.

MANUSCRISELE, CĂRŢILE ŞI REVISTELE PENTRU SCHIMB, PRECUM ŞI ORICE CORESPONDENŢE SE VOR TRIMITE PE ADRESA:

MANUSCRIPTS, REVIEWS AND BOOKS FOR EXCHANGE COOPERATION, AS WELL AS ANY CORRESPONDANCE WILL BE MAILED TO:

LES MANUSCRIPTS, LES REVUES ET LES LIVRES POUR L'ECHANGE, TOUT AUSSI QUE LA CORRESPONDANCE SERONT ENVOYES A L'ADRESSE:

MANUSCKRIPTEN, ZIETSCHRITFTEN UND BUCHER FUR AUSTAUCH SOWIE DIE KORRESPONDENZ SID AN FOLGENDE ANSCHRIFT ZU SEDEN:

After the latest evaluation of the journals by the National Center for Science Policy and Scientometrics (**CENAPOSS**), in recognition of its quality and impact at national level, the journal will be included in the B^+ category, 215 code (http://cncsis.gov.ro/userfiles/file/CENAPOSS/Bplus_2011.pdf).

The journal is already indexed in:

DOAJ: https://doaj.org/

SCIPIO-RO: http://www.scipio.ro/web/182206

EBSCO: http://www.ebscohost.com/titleLists/a9h-journals.pdf

Google Academic: https://scholar.google.ro

Index Copernicus: https://journals.indexcopernicus.com

Crossref: https://search.crossref.org/

The papers published in this journal can be viewed on the website: http://www.gup.ugal.ro/ugaljournals/index.php/mms

Name and Address of Publisher:
Contact person: Prof. Dr. Eng. Elena MEREUȚĂ
Galati University Press - GUP
47 Domneasca St., 800008 - Galati, Romania
Phone: +40 336 130139
Fax: +40 236 461353
Email: gup@ugal.ro

Name and Address of Editor:
Ș. L. Dr. Eng. Marius BODOR
"Dunarea de Jos" University of Galati, Faculty of Engineering
111 Domneasca St., 800201 - Galati, Romania
Phone: +40 336 130208
Phone/Fax: +40 336 130283
Email: marius.bodor@ugal.ro

AFFILIATED WITH:

- THE ROMANIAN SOCIETY FOR METALLURGY
- THE ROMANIAN SOCIETY FOR CHEMISTRY
- THE ROMANIAN SOCIETY FOR BIOMATERIALS
- THE ROMANIAN TECHNICAL FOUNDRY SOCIETY
- THE MATERIALS INFORMATION SOCIETY (ASM INTERNATIONAL)

Edited under the care of the FACULTY OF ENGINEERING

Annual subscription (4 issues per year)

Fascicle DOI: https://doi.org/10.35219/mms

Volume DOI: https://doi.org/10.35219/mms.2022.4

Editing date: 15.12.2022
Number of issues: 200
Printed by Galati University Press (accredited by CNCSIS)
47 Domneasca Street, 800008, Galati, Romania